AD-A012 551

ANALYTICAL AND DESIGN STUDY FOR A HIGH-PRESSURE, HIGH-ENTHALPY CONSTRICTED ARC HEATER

W. E. Nicolet, et al

Acurex Corporation

Prepared for:

Arnold Engineering Development Center

July 1975

DISCLAIMER NOTICE

THIS DOCUMENT IS BEST QUALITY PRACTICABLE. THE COPY FURNISHED TO DTIC CONTAINED A SIGNIFICANT NUMBER OF PAGES WHICH DO NOT REPRODUCE LEGIBLY.

AEDC-TR-75-47

211117

ANALYTICAL AND DESIGN STUDY FOR A HIGH-PRESSURE, HIGH-ENTHALPY CONSTRICTED ARC HEATER

AD A012551

AEROTHERM DIVISION/ACUREX CORPORATION
MOUNTAIN VIEW, CALIFORNIA

July 1975

Final Report for Period April – December 1974

Prepared for

ARNOLD ENGINEERING DEVELOPMENT CENTER (DY)
AIR FORCE SYSTEMS COMMAND
ARNOLD AIR FORCE STATION, TENNESSEE 37389

NOTICES

When U. S. Government drawings, specifications, or other data are used for any purpose other than a definitely related Government procurement operation, the Government thereby incurs no responsibility nor any obligation whatsoever, and the fact that the Government may have formulated, furnished, or in any way supplied the said drawings, specifications, or other data, is not to be regarded by implication or otherwise, or in any manner licensing the holder or any other person or corporation, or conveying any rights or permission to manufacture, use, or sell any patented invention that may in any way be related thereto.

Qualified users may obtain copies of this report from the Defense Documentation Center.

References to named commercial products in this report are not to be considered in any sense as an endorsement of the product by the United States Air Force or the Government.

APPROVAL STATEMENT

This technical report has been reviewed and is approved for publication.

FOR THE COMMANDER

Ules L. Barnwell Jr.

ULES L. BARNWELL, JR.
Major, USAF
Research & Development Division
Directorate of Technology

Robert C. Dietz

ROBERT C. DIETZ
Director of Technology

UNCLASSIFIED

REPORT DOCUMENTATION PAGE

1. REPORT NUMBER AEDC-TR-75-47	3. RECIPIENT'S CATALOG NUMBER
4. TITLE ANALYTICAL AND DESIGN STUDY FOR A HIGH-PRESSURE, HIGH-ENTHALPY CONSTRICTED ARC HEATER	5. TYPE OF REPORT & PERIOD COVERED Final Report - April 1974 to December 1974
	6. PERFORMING ORG. REPORT NUMBER Aerotherm 74-125
7. AUTHOR(s) W. E. Nicolet, C. E. Shepard, K. J. Clark, A. Balakrishnan, J. P. Kesselring, K. E. Suchsland, and J. J. Reese, Jr	8. CONTRACT OR GRANT NUMBER(s) F40600-74-C-0015
9. PERFORMING ORGANIZATION NAME AND ADDRESS Aerotherm Division/Acurex Corporation 485 Clyde Ave. Mountain View, California 94042	10. PROGRAM ELEMENT, PROJECT, TASK AREA & WORK UNIT NUMBERS 65802F
11. CONTROLLING OFFICE NAME AND ADDRESS Arnold Engineering Development Center (DYFS) Arnold Air Force Station, Tennessee 37389	12. REPORT DATE July 1975
	13. NUMBER OF PAGES 207
14. MONITORING AGENCY NAME & ADDRESS	15. SECURITY CLASS. UNCLASSIFIED
	15a. DECLASSIFICATION/DOWNGRADING SCHEDULE N/A

16. DISTRIBUTION STATEMENT (of this Report)

Approved for public release; distribution unlimited.

17. DISTRIBUTION STATEMENT (of the abstract entered in Block 20, if different from Report)

18. SUPPLEMENTARY NOTES

Available in DDC

19. KEY WORDS

arc heaters	enthalpy
ablation	thermodynamic properties
segmented arc	transport properties
ARCFLO	

20. ABSTRACT

This report presents a prediction method for high-pressure, high-enthalpy constrictor arc heater performance, the conceptual design of 5 MW and 40 MW arc heaters, and supporting documentation. An existing computer code for arc heater performance was modified by upgrading the radiation model, the thermodynamic and transport properties, and the turbulence model. The radiation properties model was modified to include visible and infrared

PRICES SUBJECT TO CHANGE

DD FORM 1473 EDITION OF 1 NOV 65 IS OBSOLETE

UNCLASSIFIED

20. ABSTRACT (Continued)

atomic lines, the ultraviolet continuum, ultraviolet bands and band systems, and ultraviolet atomic lines, while the radiation transport model was modified for an absorbing and emitting gaseous medium. Thermodynamic and transport properties for air covering the pressure range from 1 to 200 atmospheres and the temperature range from 1000°K to 30,000°K were calculated, and a turbulence model that has been shown to be applicable for developing flows, and that satisfies both wall and centerline boundary conditions, was included. The revised computer code was validated by comparison with existing high-pressure arc heater data. A scaling study using the modified computer code was conducted to determine the relation between arc heater performance and arc design parameters, and this information was used in the design of 5 MW and 40 MW constrictor arc heaters for operation in the 150-200 atmosphere pressure range, with mass-average enthalpies of 6000-8000 Btu/lbm.

PREFACE

This report was prepared by the Acurex Corporation, Aerotherm Division, Mountain View, California under USAF Contract F40600-74-C-0015. The work was sponsored by the Arnold Engineering Development Center (AEDC), Air Force Systems Command (AFSC), Arnold Air Force Station, Tennessee 37389. AEDC technical monitor for this work was Maj Ules L. Barnwell, AEDC/DYR.

The authors of this report were M. E. Nicolet, C. E. Shepard, K. J. Clark, A. Balakrishnan, J. P. Kesselring, K. E. Suchsland, and J. J. Reese, Jr.

TABLE OF CONTENTS

LIST OF FIGURES

LIST OF FIGURES (Concluded)

LIST OF TABLES

SECTION 1

INTRODUCTION

Realistic simulation of reentry heating conditions experienced by high performance reentry vehicles requires the combination of high test stream enthalpy and high stagnation pressure. Arc heaters offer the potential for achieving these required conditions. The presently available Huels-type arc heater provides the required pressure capability but cannot match flight enthalpies. The segmented constrictor arc heater has been employed extensively in low-to-moderate pressure, high enthalpy reentry simulation but has not been employed at high pressure. Recent low-to-moderate power tests at AEDC and preliminary analyses at Aerotherm have demonstrated significantly improved enthalpy capability at high pressure for the constrictor arc as compared to the Huels-type arc. The necessary analysis techniques to allow the performance and design optimization of a high power, high pressure constrictor arc heater are not available, however. Such techniques are necessary to eliminate or at least minimize the very costly (both financial and schedule) design and hardware iterations associated with the empirical development of such an arc heater.

This report presents the development of the necessary accurate analysis technique for predicting the performance and operating characteristics of constrictor arc heaters. Proper physical models which are applicable for the complete range of pressures (to over 200 atm) and other conditions of interest were incorporated into an existing computer code which was also further modified for improved capabilities. The resultant computer code was validated through comparisons of predictions with available experimental data. The validated code was then employed to determine the relation of performance capabilities to the various design and operating parameters. Finally, the conceptual design including basic geometric and operating variables was developed for moderate and high power operation. The performance goal on which the designs were based was simultaneous operation in the 150 to 200 atmospheres total pressure range and the 6000 to 9000 Btu/lb bulk enthalpy range.

The following briefly describes the report content. Information about predictive procedures is discussed in Sections 2 to 5 in terms of previously available prediction techniques, improved phenomenology modeling for the radiation

losses, the thermodynamic and transport properties, and the turbulent model, respectively. These are followed by Section 6 which describes the validation of the computer code predictive procedure, and Section 7, which presents the results of the scaling study. These sections summarize essential details of the technical work. In most cases, additional details are given in a series of supporting appendices. Section 8 presents the conceptual designs for the 5 MW and 40 MW constrictor arc units. Finally, the conclusions of the study are presented in Section 9. The supporting appendices then follow, the last being a user's manual for the ARCFLO Version 2 code which was developed in part in the present study and represents an automated version of the predictive procedure.

SECTION 2

PREVIOUS PREDICTIVE CODES

Two existing predictive procedures were reviewed for possible use in the present study. The Watson and Pegot (Reference 1) procedure was developed for the analysis of constrictor arcs operating at low pressures and, consequently, does not consider phenomenological events which are important at high pressures, as discussed below. This procedure offers the advantage of sound numerics which are suitable for extension to analysis of flows in high pressure arcs. In addition, the procedure offers the advantage of familiarity and has been used extensively in previous studies to generate predictions which can be used in the present study as baseline data for the evaluation of changes in the phenomenological modeling. For instance, the Watson and Pegot code with empirical corrections has been used by Aerotherm since 1969 for all arc heater design activities. The Graves and Wells (Reference 2) procedure has the same shortcomings with regard to modeling and the same strengths with regard to the numerics, but it does not offer the advantage of high familiarity or an existing body of predictions of flows in high pressure arcs. Based on these considerations the Watson and Pegot (Reference 1) predictive procedure was selected as the baseline for the present study.

For high pressure predictions, the phenomenological modeling employed by Watson and Pegot (Reference 1) is inadequate for accurate predictions of radiation flux. It also includes only low pressure thermodynamic and transport properties, and incorporates a somewhat simplistic turbulent model. The radiation properties model does not include the following:

- Visible and infrared atomic lines
- Ultraviolet continuum
- Ultraviolet bands and band systems
- Ultraviolet atomic lines

while the radiation transport model employs the optically thin approximation which does not allow self-absorption. The properties model will cause the radiative loss predictions to be low, while the transport model will cause these

predictions to be high. At times the two approximations will compensate; however, one cannot depend on such good fortune when the radiation flux is the dominant loss mechanism (which it is for high pressure conditions).

The Watson and Pegot thermodynamic and transport properties are subject to the following approximations and constraints:

- Air is approximated as N_2, dissociated and ionized
- The pressure is limited to $1 \leq p \leq 10$ atm
- Thermodynamic properties are not state-of-the-art
- Transport properties do not employ the most recent cross sections

and their turbulent model employs the following idealizations:

- A mixing length obtained from the work of Nikuradse (Reference 3) and divided by 2
- A unity turbulent Prandtl number
- An oversimplified treatment of the effects of constrictor wall roughness

The thermodynamic and transport property data can be expected to be in substantial error because they are both out of date and subject to extrapolation errors. The turbulent model is not valid for non-fully developed flows or the flow near the centerline of the constrictor tube or the immediate vicinity of the wall.

The development of more accurate radiation, thermodynamic and transport, and turbulence models and data for inclusion in an upgraded computer code is presented in the following three sections.

SECTION 3

THE RADIANT FLUX IN A CONSTRICTOR ARC

RADIANT TRANSPORT

The accurate calculation of radiation transport within a constrictor arc requires consideration of the geometry; namely, a right circular cylinder of high length-to-diameter ratio as shown in Figure 1. It also requires consideration of the spectral absorption and emission from the gaseous media. To obtain the present transport formulation, these features were combined with the following key assumptions:

- Media is nonscattering
- Constrictor walls are black and maintained at constant temperature
- Cylinder is of infinite length
- Temperature does not vary axially
- Exponential kernel approximation is valid

These assumptions restrict the applicability of the analysis to arc flows which do not have appreciable particulate concentrations, which do not have important end wall effects, which have gradients in the radial direction much larger than those in the axial direction and which do not have walls made of or coated with reflective materials. None of those are viewed as serious restrictions for the applications envisioned in the present study.

Consider a unit area at Point C (Figure 1) situated at an axial distance z and a radial distance r. Let A-C-B represent a ray having spectral intensity I_ν at Point C directed toward A. For this system, the spectral flux in the radial direction is obtained by integrating over all the rays passing through C, i.e.,

$$q_\nu(r) = \int_\Omega I_\nu \cos \quad d\Omega \tag{1}$$

Equation (1) can be written in terms of exponential integral functions $D_2(x)$ and $D_3(x)$ (see Appendix A), which can be approximated by an exponential kernel:

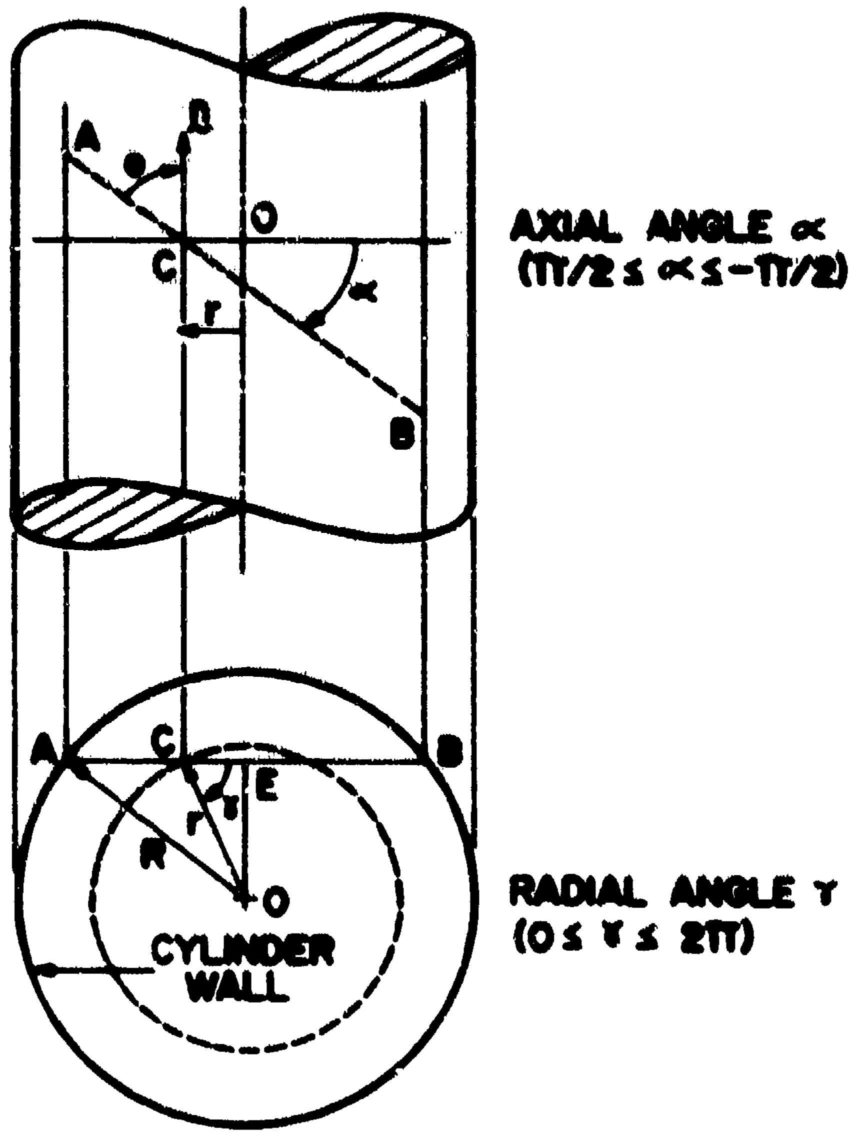

Figure 1. Cylindrical geometry and coordinate system.

$$D_2(x) = a \exp(-bx) \tag{2}$$

This approximation allows an analytic integration of Equation (1) over the θ variable and results in

$$q_\nu(r) = q_\nu^+(r) - q_\nu^-(r) \tag{3}$$

where

$$q_\nu^\pm(r) = \int_0^{\pi/2} \cos\gamma \; G^\pm(r,\gamma)\, d\gamma \tag{4}$$

and where the angular directional fluxes $G^\pm(r,\gamma)$ are given in Appendix A.

Let any of the N discrete values of the radial coordinate be singled out with the subscript i. The wall is located at $r_{i=N} = R$ and the axis of the constrictor tube at $r_{i=N} = 0$. Consider, as shown in Figure 2, the plane perpendicular to the axis of the constrictor tube, and let j be the index on the radial mesh points perpendicular to the axis. Finite difference relations can be obtained (and are given in Appendix A) by assuming logrithmic variations for μ with r and for E with τ. The angular directional flux can be represented by a recursion formula which allows significant simplification, i.e.,

$$G^\pm_{i,j} = e^{-\Delta\tau_{i,i\mp1,j}} \left\{ G^\pm_{i\mp1,j} + \frac{E_{i,j}\, e^{\Delta\tau_{i,i\mp1,j}} - E_{i\mp1,j}}{1 + \dfrac{1}{\Delta\tau_{i,i\mp1}} \ln \dfrac{E_{i,j}}{E_{i\mp1,j}}} \right\} \tag{5}$$

where the $\Delta\tau_{i,i\mp1,j}$ are the optical depth increments. Equation (5) includes the effect of self-absorption explicitly.

With known values of spectral absorption coefficients $\mu(y_{i,j})$, the optical depth increments $\Delta\tau_{i,i-1,j}$ are generated. Starting at the wall, i=N, from the known or assumed wall boundary condition, values of $G^-_{i,j}$ are calculated. Due to the symmetry in the geometry, we have $G^-_{i,j} = G^+_{i,j}$. Invoking this symmetry condition, the $G^+_{i,j}$ are then computed starting at the axis of the constrictor, i=1. With these calculated quantities, the local spectral radiative flux $q_\nu^\pm(r_i)$ may be found from Equation (3) cast into proper computational form (Appendix A).

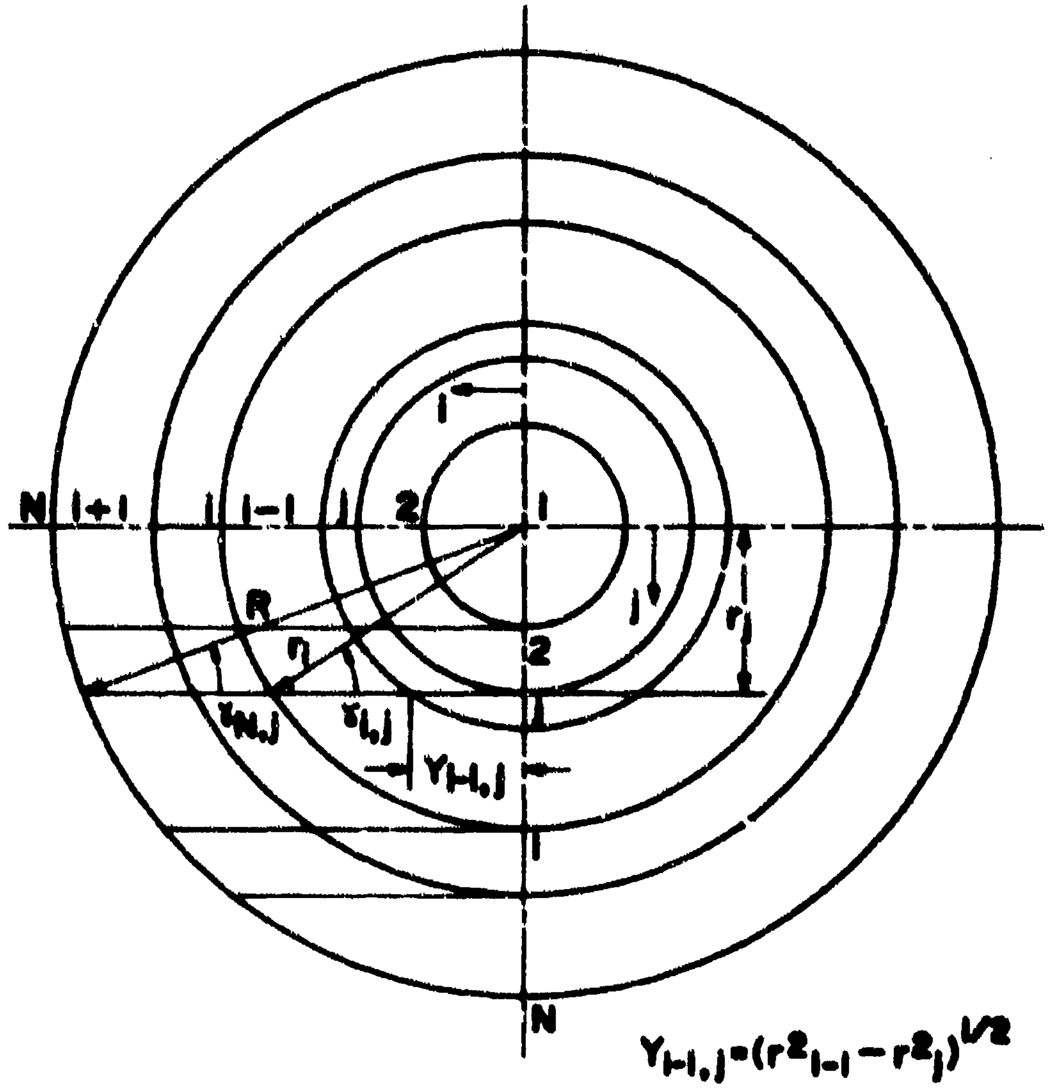

Figure 2. Radial mesh distribution.

To allow assessment of the exponential kernel approximation, calculated radiant flux profiles are presented in Figure 3 for a gray gas in a cylindrical geometry. The temperature distribution is assumed to be linear with the radius, and the absorption coefficient of the medium is assumed to be constant. The calculated radial radiant heat flux distributions are compared with exact calculations of Keston (Reference 4) and approximate calculations of Chiba (Reference 5). Keston employed a numerical integration scheme to evaluate the exponential integral functions $D_3(x)$ and $D_2(x)$, whereas, Chiba and the present method used an approximation. Chiba (Reference 5) used a value of a = 1 and b = 5/4 in the exponential approximation for $D_2(x)$, whereas, the values a = $5\pi/16$ and b = 5/4 were selected for the present study because they allow additional simplification in the analysis. It is seen from Figure 3 that the results obtained by the present calculational method compare excellently with the approximate results of Chiba, and the results are in good agreement with the exact calculations of Keston.

RADIATIVE PROPERTIES

The radiative properties of high temperature air were treated on a band-model basis. The spectrum was divided into two gray bands as shown in Figure 4. Absorption coefficient data for various pressures (1-200 atm) and temperatures (1000°K - 30,000°K) were obtained from several sources and are given in Appendix A. Rosseland mean opacities were used for the low frequency band, which is consistent with the present interest in a self-absorbing gas. The absorption coefficients selected for the high frequency band were selected to correspond to the nitrogen ground state photo-ionization threshold.

COMPARISON WITH WATSON AND PEGOT

The formulation used in the present study includes the effects of self-absorption. This requires consideration of a specific geometry (right circular cylinder of infinite length) and consideration of the spectral nature of the radiation. In contrast, the optically thin approximation of Watson and Pegot (Reference 1) allows great simplification in the analysis, in that radiation losses need be treated only as a heat loss term in the energy equations. Unfortunately, the optically thin model is not appropriate for the high pressure constrictor arc environment and should lead to unacceptably high predictions (for a given set of radiation properties).

On the other hand, the Watson and Pegot (Reference 1) values of the radiation properties are not state-of-the-art and are also viewed as being incomplete in that all the important contributions were not included. This should

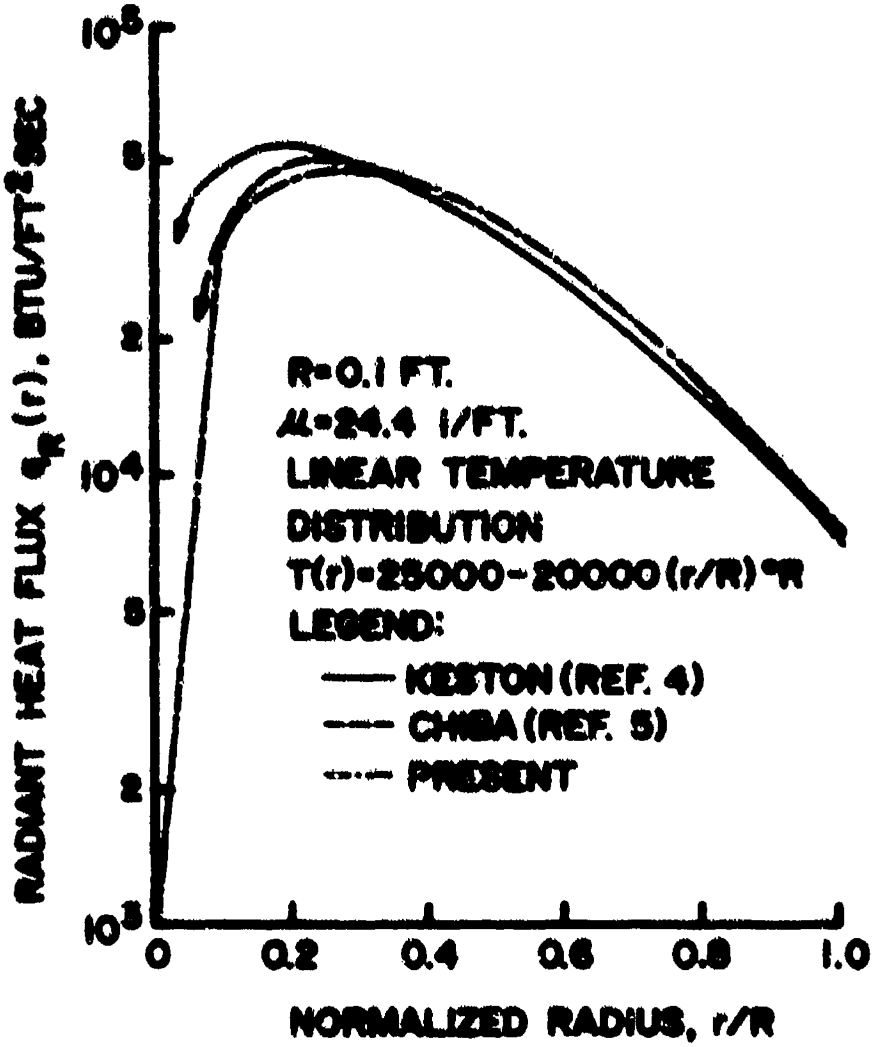

Figure 3. Comparison of radiant flux profiles, R = 0.1 ft.

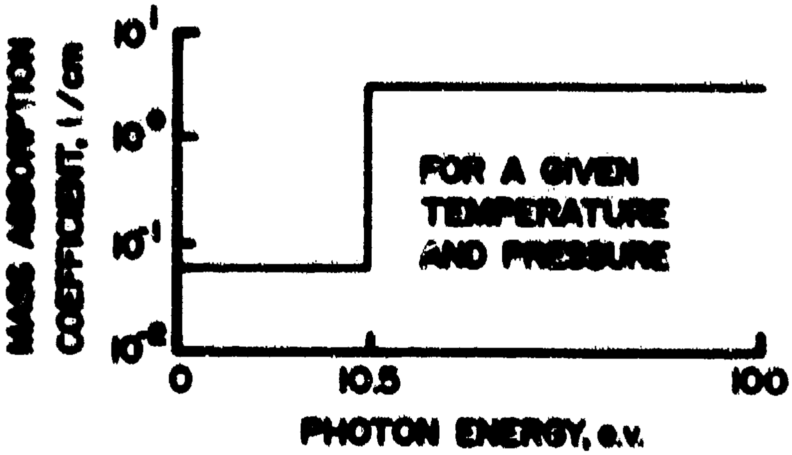

Figure 6. Schematic diagram of a two-gray-band absorption coefficient model.

cause the present predictions to be higher than theirs (for a given transport formulation) by factors which can be as high as 4.

The substantial differences in both the transport and properties models precludes any general statement with regard to which approach gives the higher predictions. Indeed, the comparisons which have been made show that the differences can go either way. For the important cases of asymptotic flows in constrictor tubes of 1-1/2 to 2 inches in diameter and in the 100 to 200 atmosphere pressure range, the present predictions tend to be about a factor of 2 higher than those made with the Watson and Pegot (Reference 1) method.

SECTION 4

THERMODYNAMIC AND TRANSPORT PROPERTIES

To solve the flow field equations applicable to a constricted arc, the following properties are required in table format for use in the computational procedure:

Thermodynamic - ρ, T, X_i

Transport - μ, K, σ

In this work, the property tables must cover a pressure range of $1 \le p \le 200$ atm and a temperature range of $1000°K \le T \le 30{,}000°K$. The primary weakness of the property tables used by Watson and Pegot (Reference 1) is that they extend up to only 10 atm. Also, nitrogen properties were used to approximate those of air, and the nitrogen transport properties used are based upon collision cross-sections which are not state-of-the-art. Due to these deficiencies, a complete updating of the property tables was a prerequisite to carrying out the high-pressure flow field analyses.

Hilsenrath, et al. (Reference 6) and Gilmore (Reference 7) provide tabular and graphical values of thermodynamic properties for air under the conditions of interest. These data were awkward to use here because of difficulties associated with making accurate interpolations of the graphical data for species mole fractions. In addition, much of these data are presented with temperature and density as the independent variables; however, pressure and enthalpy are the desired independent variables. Therefore, to permit calculating ρ, T, and X_i for arbitrary values of the independent variables p and h, the calculational procedure described below was developed and employed.

With regard to the transport properties, a calculational procedure was also developed even though there are some experimental data available. In particular, a reasonable amount of experimental data are available for the electrical and thermal conductivities of a nitrogen plasma (References 8-11), while only limited experimental data are available for the viscosity (Reference 12). For air, there are only a few experimental values of thermal and electrical conductivity available (References 11, 13), and air viscosity data appear to be nonexistent. All of these data have been acquired at atmospheric pressure, so that the data can be used to validate transport property calculational

procedures but cannot be used as input to solve the flow field equations in the 200 atm pressure range of interest. A calculational procedure is therefore necessary.

A number of kinetic theory calculations have been carried out for both nitrogen (References 14-16) and air (References 16-18) plasmas. The calculation of nitrogen properties by Capitelli and DeVoto (Reference 14) uses the best available collision cross-sections and is the most recent and most accurate; however, only atmospheric pressure was considered. The heavily referenced calculations of air transport properties by Yos (Reference 16), Peng and Pindroh (Reference 17), and Hansen (Reference 18) have been available for some time, and it now appears that certain collision cross-sections used in these treatments are in serious error. Furthermore, the maximum pressure considered by Yos was 30 atm, while the other two air property calculations are limited to temperatures below 15,000°K. For these reasons, the air transport properties were recalculated with the updated model described below. This model was validated through extensive comparisons with the one-atmosphere experimental data for air and nitrogen plasmas. It should be noted that all of the experimental data considered are very recent, 1970 or later, and are viewed as being the state-of-the-art.

THERMODYNAMIC PROPERTIES

A chemical equilibrium computational procedure (the ACE computer program (References 19, 20)) was used to calculate the mixture density, enthalpy, and species mole fractions for air under the conditions $1 \leq p \leq 200$ atm and $1000°K \leq T \leq 30,000°K$. The ACE code was modified to include the Debye-Hückel correction. (The details of this modification are discussed in Appendix B.) The Debye-Hückel correction is required when ionization is significant to account for the storage of potential energy associated with the Coulomb interaction between charged particles. The net effect of these Coulomb interactions is to reduce the ionization potential, the thermal pressure, and the various mixture properties including enthalpy, entropy, density, and internal energy (References 21, 22). Under the conditions of interest, the only significant effect is the reduction in the ionization potential, which leads to shifts in the predicted values of charged-particle mole fractions of up to 25 percent.

The predictions of air thermodynamic properties provided by the modified ACE code were compared with the values given by Hilsenrath, et al. (Reference 6) and Gilmore (Reference 7) (see Appendix B). Agreement on predicted values of ρ and h was within 1 percent, while agreement was always within 5 percent for the mole fractions of the significant species.

The new calculations of ρ and h were also compared with the values at 1 and 10 atm used in the Watson and Pegot procedure (see Appendix B). At temperatures below 8000°K, the Watson and Pegot (old) values of h are 30-40 percent lower than the new values, while at higher temperatures, they are 10-15 percent higher. At the same two pressures, there is close agreement between the old and new values of density. Of course, when higher pressures were considered by the Watson and Pegot procedure, the property values were obtained from extrapolations of the 1 and 10 atm values. It follows that high-pressure properties determined in this manner can be in substantial error, especially when the 1 and 10 atm properties are in error to begin with.

TRANSPORT PROPERTIES

The transport properties were calculated using the mixture rules of Yos (Reference 16), which are summarized in Appendix B. These expressions reduce to the results of rigorous kinetic theory in the limit of a one-specie gas. For mixtures, they are approximate in that they exclude the higher order terms in the first Chapman-Enskog approximation (Reference 23). However, calculations based on the simple mixture rules rarely differ from the more exact first approximation by more than a few percent (Reference 16).

In the Yos formulation, the total thermal conductivity K is the sum of translational, internal, and reactive contributions. The internal contribution is computed with the Eucken correction (Reference 23), and the reactive thermal conductivity is based upon the Butler-Brokaw formulation (Reference 24) for multicomponent neutral mixtures which also has been shown to be valid for partially-ionized gases in equilibrium (Reference 25).

All of the collision integrals (cross-sections) used in the work by Yos were carefully examined and in many cases updated, based on collision integrals from References 14, 15, 16, 17, 26, 27, and 28. The details of this investigation are discussed in Appendix B. For the sake of consistency, the Yos collision integral for a given collision was always used when it appeared to be as valid as that from any of the other sources considered. The Yos collision integrals for charge exchange, which make important contributions to the reactive thermal conductivity, appeared to be too high by a factor of up to four. Therefore, the charge exchange collision integral for nitrogen was taken from Capitelli and DeVoto (Reference 14) and that for oxygen was taken from Knof, et al. (Reference 28).

The Yos collision integrals for Coulomb collisions were based on the Gvosdover cross-section multiplied by factors ranging from 0.3 to 12.8, depending on the particular pair of charged particles. The multiplicative factors were obtained through comparison with the electrical and thermal conductivities of a fully-ionized gas predicted by Spitzer and Härm (Reference 29), but these latter results have been found to be low relative to experimental data (Reference 14). Thus, in this work Coulomb collision integrals, based upon an unscreened Coulomb potential with Debye-length cutoff, were taken from Liboff (Reference 27). The Debye length was computed based upon screening by electrons only, as recommended by Capitelli and DeVoto (Reference 14). A single multiplicative factor of 0.6, obtained through the comparisons with experimental data for electrical conductivity discussed below, was applied to all Coulomb collisions involving an electron.

The theoretical model for transport properties described above was compared critically with the available experimental data and theories. This comparison is discussed in detail in Appendix B. Because experimental data for the nitrogen plasma are more extensive than those for air, the former were used as a standard for comparison. Specifically, the calculations were compared with the one-atmosphere nitrogen electrical conductivity data, and it was found that multiplying the collision integrals for Coulomb collisions involving electrons by a factor of 0.6 gave optimum agreement over the entire temperature range up to 24,000°K. The new model then agreed well with the one-atmosphere results of Capitelli and DeVoto (Reference 14). Comparisons were also made with the 100 atm results of Sherman (Reference 15) for $T \leq 15,000$°K, and good agreement was obtained.

The new model with modified Coulomb collision integrals was then compared with the available data and theories for the air plasma. This comparison is summarized in Figures 5, 6, and 7. The present calculations compared with the experimental data as well as or better than the other available theories in all cases. They are also in good agreement with the one-atmosphere results of Peng and Pindroh up to $T = 15,000$°K, where the latter calculation was terminated. For electrical conductivity, the present calculations are 20 percent higher than the results of Yos (Reference 16) at temperatures in the vicinity of 20,000°K, due to the different Coulomb collision integrals. The total thermal conductivity of Yos is up to 30 percent lower than present calculations at temperatures in the range $9000°K \leq T \leq 20,000°K$, due to the erroneously high charge exchange collision integrals used by Yos. Both the viscosity and the total thermal conductivity predicted by Hansen (Reference 18) are in poor agreement with the present calculations, due most likely to the outdated cross

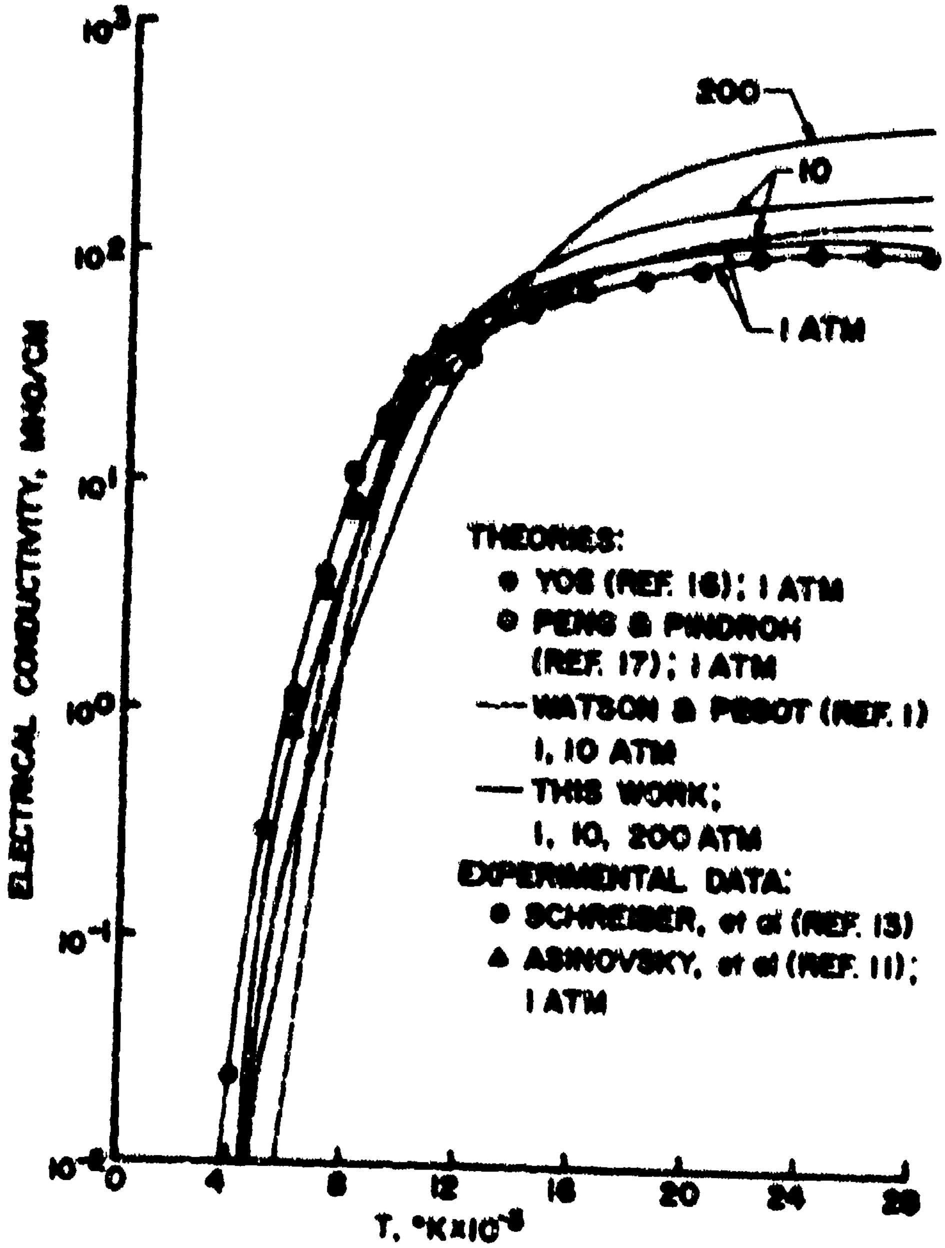

Figure 5. Air electrical conductivity.

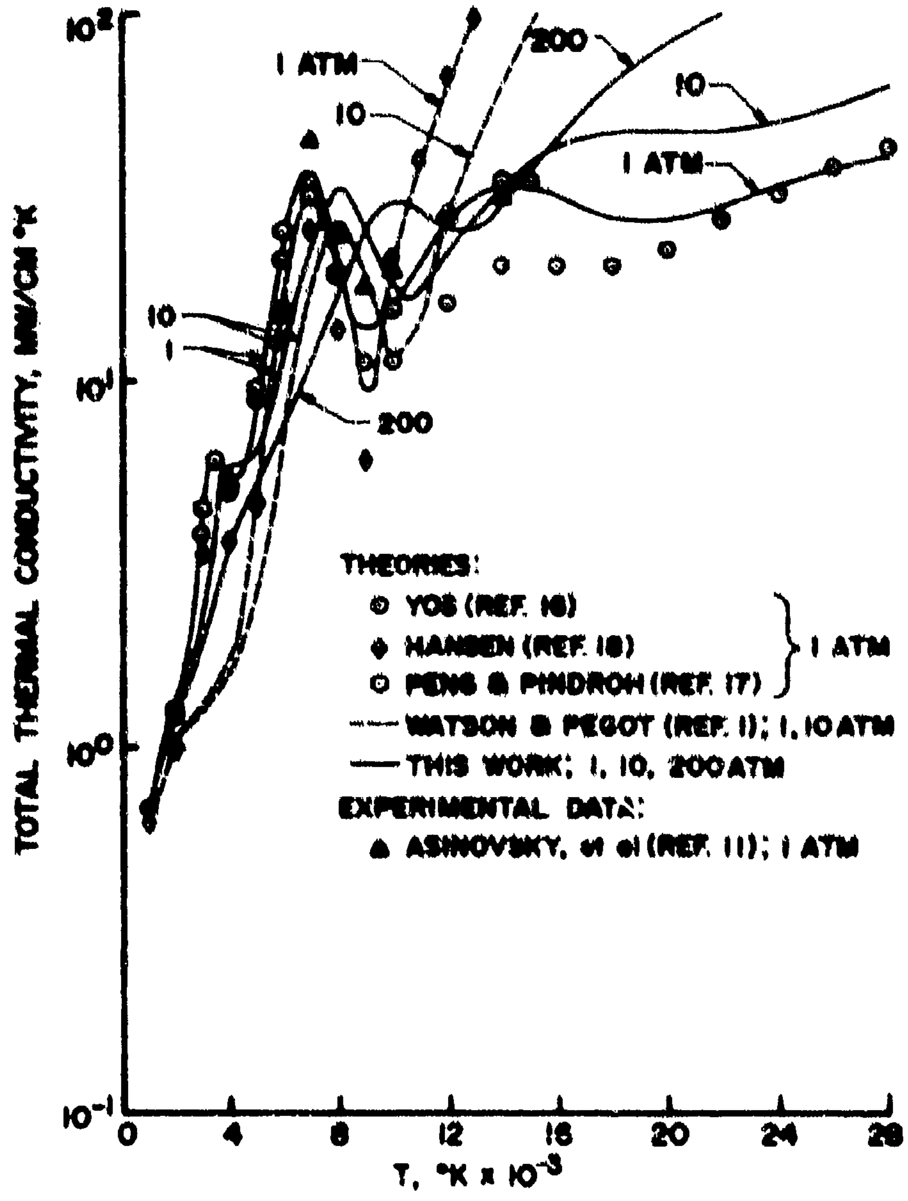

Figure 6. Air total thermal conductivity.

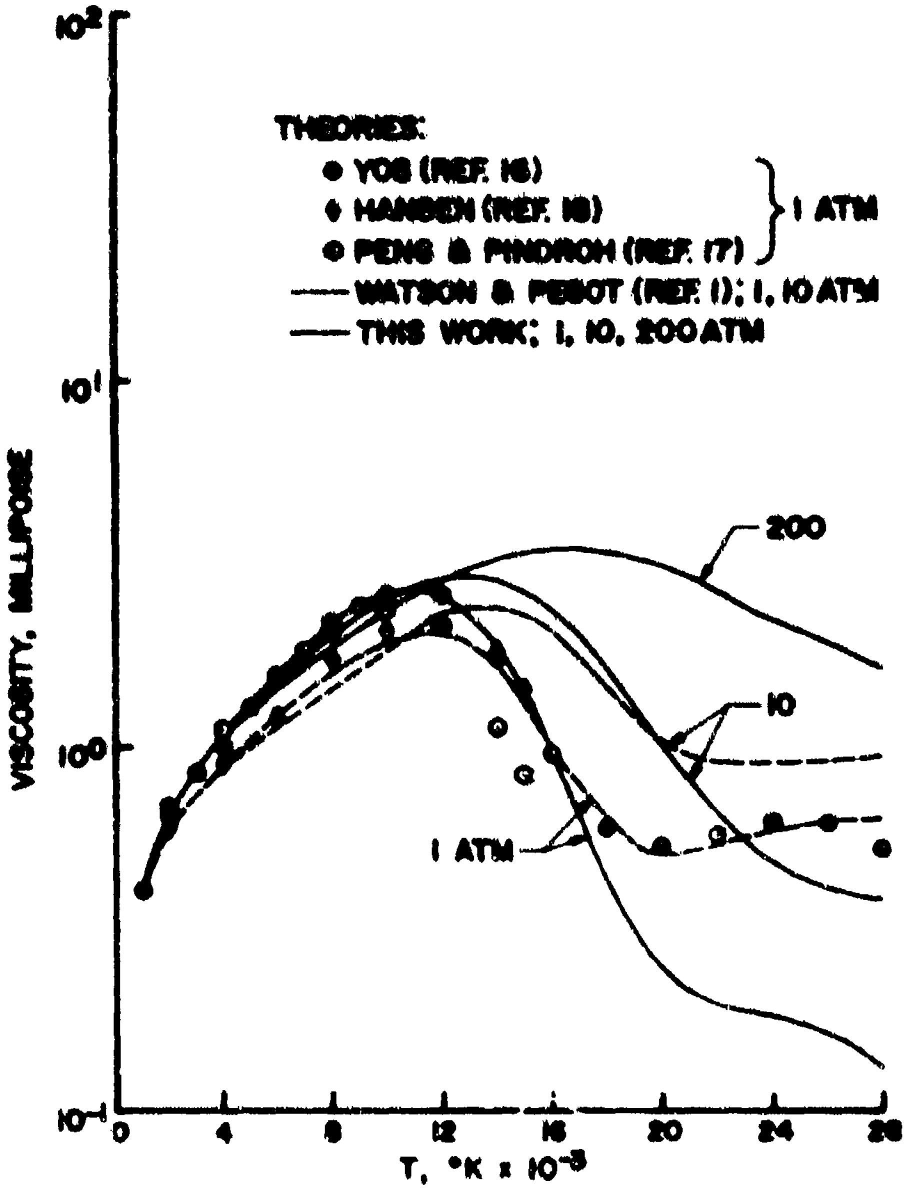

Figure 7. Air viscosity.

sections used in the former work. Although not shown on the figures, calculations were also compared with the 100 atm predictions of Peng and Pindroh, and good agreement was obtained (see Appendix B).

Figures 5, 6, and 7 also present comparisons between the new properties and those used by Watson and Pegot (Reference 1) at both 1 and 10 atm. The Watson and Pegot properties are based partially upon the work of Yos for electrical conductivity and the work of Hansen for viscosity and total thermal conductivity, and are in substantial error under many conditions. Consequently, the new properties should lead to significant improvements in the accuracy of the predictions of flow fields within constricted arcs.

SECTION 5

TURBULENT FLOW MODEL

For the arc conditions of interest in this study, it is expected that the flow will be turbulent. The Reynolds number based on cold flow properties and tube diameter is approximately 2×10^5, a value which far exceeds the usual transition value of 3×10^3.

By using an eddy viscosity model for turbulent flow, the equations for shear stress, τ, and heat flux, q, can be written as

$$\tau = \rho(\nu + \varepsilon)\,\frac{d\bar{u}}{dy} \tag{6}$$

$$q = -\left(\frac{k}{c_p} + \frac{\rho\varepsilon}{P_t}\right)\frac{d\bar{h}}{dy} \tag{7}$$

The eddy viscosity, ε, is given by

$$\varepsilon = \ell^2 \left|\frac{d\bar{u}}{dy}\right| , \tag{8}$$

where ℓ is the mixing length. At the wall, the mixing length should satisfy the boundary conditions (Reference 30)

$$\lim_{y \to 0} \ell = 0$$

and (9)

$$\lim_{y \to 0} \frac{\Delta \ell}{\Delta y} = 0$$

In the Watson and Pegot study (Reference 1) a modified form of Nikuradse's mixing length equation (Reference 3) was employed (see Appendix E) which satisfies the first boundary condition but gives $d\ell/dy \to 0.2$ as $y \to 0$. A more suitable equation for the mixing length in the wall region is the van Driest (Reference 31) "law of the wall" model, given by:

$$\ell = 0.4\, y \left[1 - \exp\left(\frac{-y\sqrt{\tau_w g_c/\rho_w}}{26\ \nu_w}\right)\right] \tag{10}$$

This model of the mixing length satisfies both wall boundary conditions stated previously, and has been proven effective by other investigators (References 32, 33).

All information on the distribution of the mixing length across the tube radius comes from experimental data (e.g., Reference 34) and supports separating the flow into two regions: an inner region, where a wall model for the mixing length is applicable, and an outer region, where the mixing length is proportional to the tube radius. Therefore, the following expression for mixing length was adopted:

$$\begin{aligned} \ell_i &= 0.4\, y \left[1 - \exp\left(\frac{-y\sqrt{\tau_w g_c/\rho_w}}{26\ \nu_w}\right)\right] && \text{for} \quad y_o \le y \le y_c \\ \ell_o &= 0.075\, R && \text{for} \quad y_c \le y \le R \end{aligned} \tag{11}$$

where y_o is a small distance from the wall and y_c is obtained from the continuity of ℓ. A comparison of the mixing lengths due to Nikuradse, Watson and Pegot, van Driest, and the one given in Equation (11) is shown in Figure 8 for a typical case.

In addition to changing the mixing length, the turbulent Prandtl number used by Watson and Pegot needs modification. Watson and Pegot assume a turbulent Prandtl number of unity throughout, which is close to the value often adopted for boundary layer calculations. Rotta (Reference 35) has proposed the turbulent Prandtl number for flow in ducts be given by

$$P_t = 0.95 - 0.45 \left(\frac{y}{R}\right)^2 \, , \tag{12}$$

which allows significant deviations from unity near the axis. This value has been used in other recent investigations of duct flows (Reference 36) and was adopted in the present study.

Changing the mixing length model and the turbulent Prandtl number can have a significant effect on wall heat flux calculations, as shown in Figure 9. Here it is seen that the principal heat transfer mode has been changed from radiation to convection for the low-pressure case being studied. At a distance

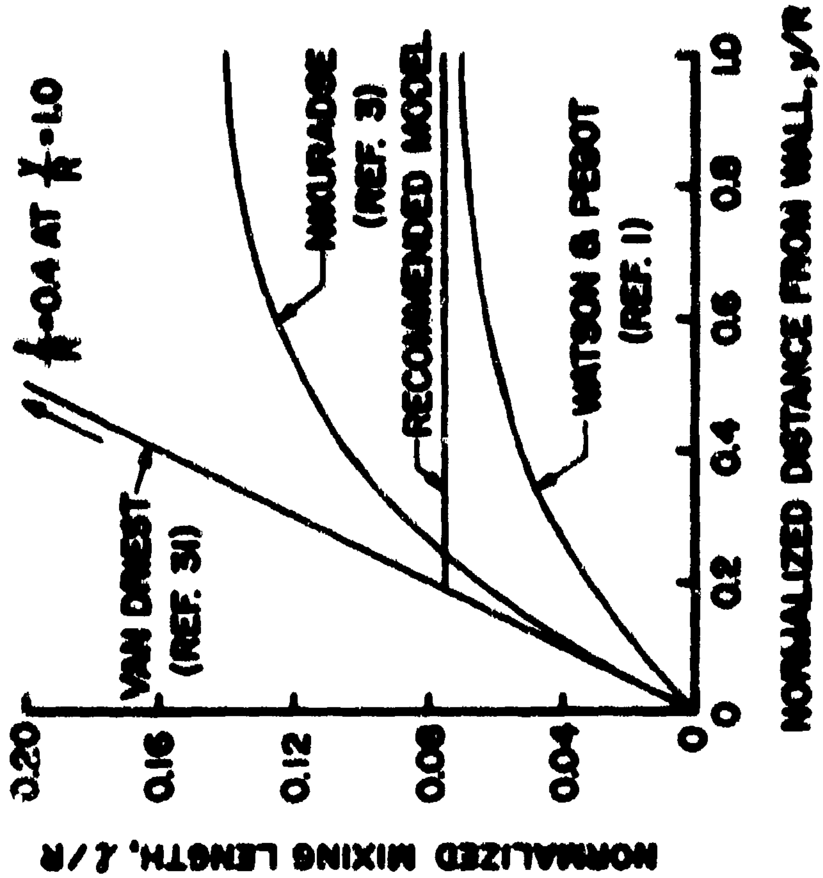

Figure 6. Comparison of several mixing lengths.

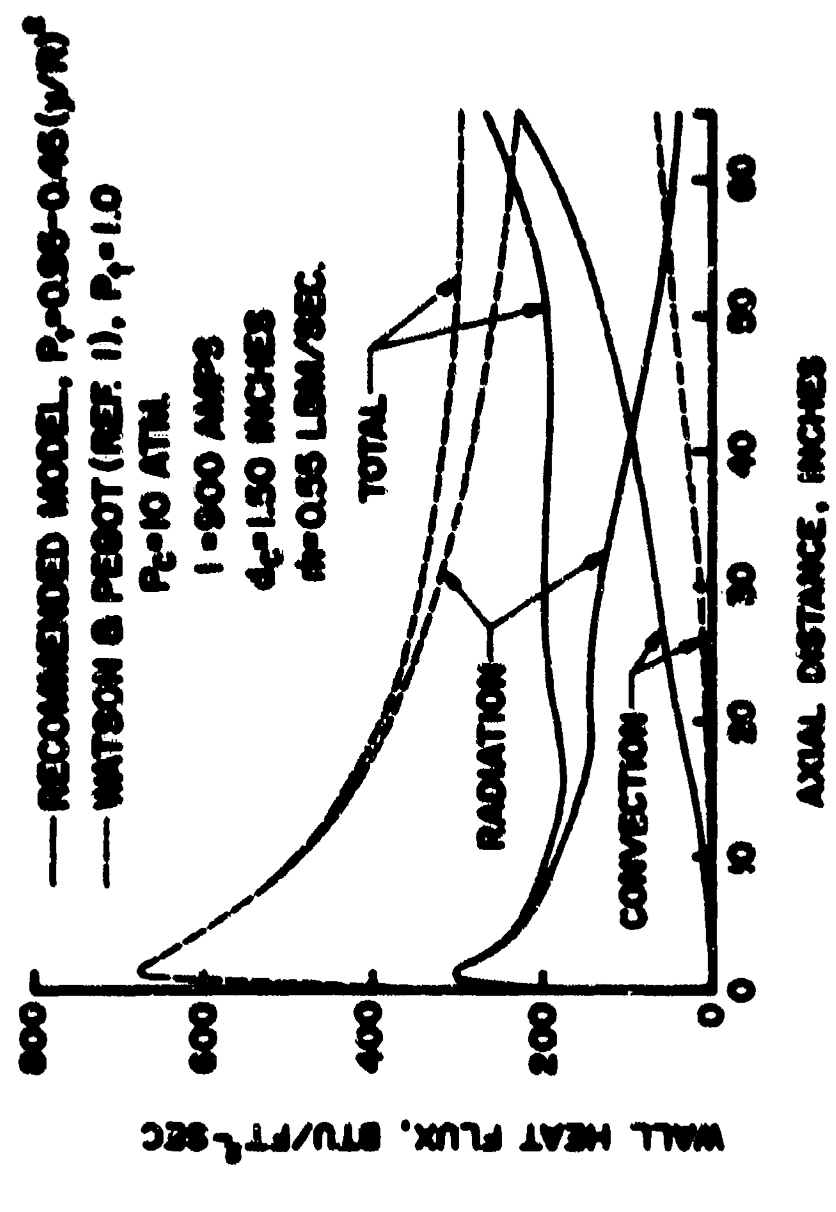

Figure 9. Results for different turbulence models in ARCFLO.

of 45 inches in axial length, the mass-average enthalpy was changed from 5200 Btu/lbm (Watson and Pegot turbulent model) to 7200 Btu/lbm (present turbulent model). It should be emphasized that the only differences between the two calculations presented in Figure 9 are the mixing length and turbulent Prandtl number calculations; all other aspects of the two flow field models are the same.

Up to this point, the discussion of turbulence has assumed the presence of a smooth wall. In reality, the constrictor wall is rough, due to both the segmented nature of the wall and the existence of an oxide scale on the exposed segment surfaces (particularly in an air arc). In both the above formulation and that of Watson and Pegot, for a smooth wall the mixing length ℓ and, hence, the eddy viscosity ϵ are zero at the wall. In contrast, for a rough wall Watson and Pegot assumed the mixing length at the wall was finite and equal to 0.010 inch for all flow conditions and constrictor configurations. However, this was felt to be too restrictive in this work. Furthermore, the roughness associated with constrictor segments of interest in the present study has been measured at Aerotherm and found to rarely exceed 0.005 inch in equivalent sand grain roughness height.

In this work, wall roughness is modeled by evaluating Equation (11) above at "$y + K_s$" rather than "y", where K_s is the equivalent sand grain roughness height. This means that at the wall, $y = 0$, the mixing length ℓ will be finite and $\ell_w \leq 0.4\ K_s$. It follows that turbulent components of wall shear and convection heat flux will exist since $\epsilon(0) > 0$. See Appendix C for further discussion.

Wall roughness also influences the turbulent Prandtl number in the wall region. It has been found that roughness augments wall shear more than it augments wall heat transfer, suggesting that P_t in the wall region can exceed unity. In this work, P_{t_w} was varied parametrically and the optimum value was determined to be $P_{t_w} = 3.0$ (see Appendix C).

SECTION 6

CODE VALIDATION

The improved models for radiation properties and transport, thermodynamic and transport properties, and turbulence have been incorporated into the original version of the flow field computational procedure developed by Watson and Pegot (Reference 1) designated here as ARCFLO Version 1. In addition, further minor code modifications were performed to improve the iteration technique used to determine the pressure drop for each axial step. The updated code is designated here as ARCFLO Version 2. A series of predictions of constrictor arc performance was then made for operating conditions where experimental data were available.

CRITERIA FOR DATA SOURCE SELECTION

The sources of the data available for this purpose are listed in Table 1 together with the range of constrictor diameter and constrictor lengths and pressures. A listing of all the data is given in Appendix D for the 270 data points that were collected.

The following factors were considered in choosing the best source of experimental data:

- High pressure, high enthalpy levels
- Consistency with other experimental data
- Self-consistency

Maximum values of mass-average enthalpy and pressure are shown in Figure 10 for the various experimental data. Lines of constant $H/\sqrt{p}$ are also shown in Figure 10. The AEDC constricted-arc data is superior to all of the other sources because it more closely approaches the design goal of 6000-8000 Btu/lb at 150-200 atmospheres pressure.

A power law correlation of all of the experimental data was formulated in order to judge the consistency of the enthalpy and voltage data. Both mass-average enthalpy and arc voltage were assumed to vary with current, air mass flow rate, pressure, constrictor length and constrictor diameter to some power. A multiple regression computer routine was used to calculate the exponents. The following equations were obtained:

TABLE 1

CONSTRICTOR ARC DATA SOURCES

Data Source	Constrictor Diameter (inches)	Constrictor Length (inches)	Pressure (atm)
Arnold Engineering Development Center, (AEDC), Tullahoma, Tennessee	0.934	17	26-102
Air Force Flight Dynamics Laboratory, (AFFDL), Wright-Patterson Air Force Base, Ohio	3.000	45-96	25-107
Sandia Laboratories, (Sandia), Albuquerque, New Mexico	1.000	37	7-15
National Aeronautics and Space Administration - Johnson Space Center, (NASA-JSC), Houston, Texas	1.5000	36-122	1-7.5
National Aeronautics and Space Administration - Ames Research Center, (NASA-Ames, 6 cm), Moffett Field, California	2.362	47-94	1-9
Martin-Marietta Corporation, Denver Division, (MMC), Denver, Colorado	1.000	7-66	0.06-30

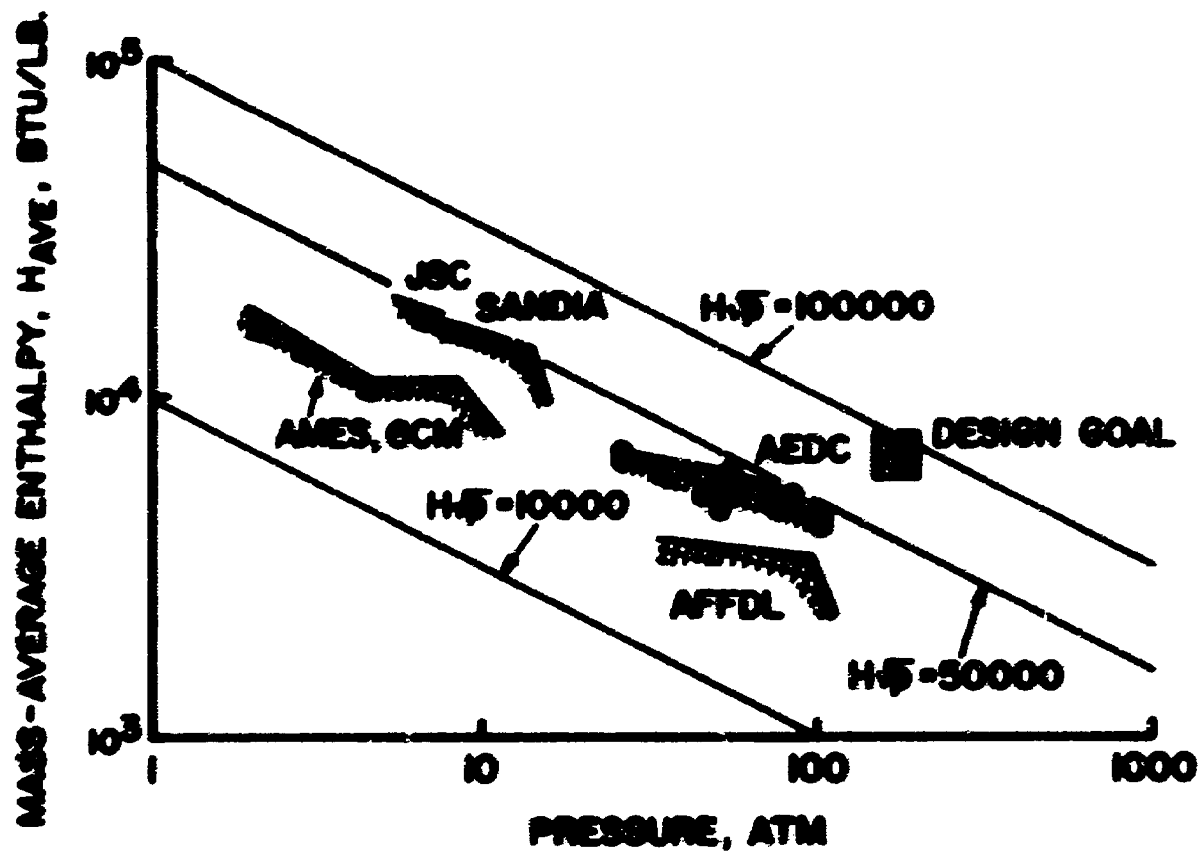

Figure 10. Maximum values of mass-average enthalpy for various arc heaters.

$$H_{corr} = 4.818 \left(\frac{I}{\dot{m}}\right)^{\text{[illegible]}} \left(\frac{L}{D}\right)^{\text{[illegible]}} p^{\text{[illegible]}} \text{, Btu/lb} \qquad (13)$$

$$V_{corr} = 294\ \dot{m}^{\text{[illegible]}} \left(\frac{L}{D}\right)^{\text{[illegible]}} p^{\text{[illegible]}} \text{, volts} \qquad (14)$$

These equations were used to calculate values of enthalpy and voltage for data evaluation. Equations (13) and (14), while based on extensive data correlations, should be used only for interpolations between given data ranges. They can lead to erroneous results when extrapolated beyond the defining data base.

Another data test involved the "sonic-flow enthalpy" as calculated by the Winovich formula (Reference 37):

$$H_{sf} = 280 \left(\frac{\dot{m}}{A^{*}p}\right)^{\text{[illegible]}} \text{, Btu/lb} \qquad (15)$$

where A^{*} is the sonic throat area in square feet.

RESULTS OF DATA EVALUATION

The data were first compared with enthalpies and voltages that were calculated by means of the correlation equations. Of all the data, the AEDC constricted arc enthalpy data, shown in Figure 11, were the best, although excellent correlations were also achieved by the Sandia data. The small amount of scatter in the AEDC data indicates good self-consistency.

The voltage comparison of Figure 12 shows that the AEDC constricted arc voltage is about 50 percent higher than predicted by the correlation formula. This discrepancy is apparently due to the fact that the electrode voltage drops are a larger fraction of the total arc voltage for the relatively short AEDC arc heater. Again, the small amount of scatter in the voltage data indicates good self-consistency.

The final test of the data from all sources is a plot of mass-average enthalpy versus the "sonic-flow enthalpy". Figure 13 shows this correlation for the AEDC enthalpy where the sonic flow enthalpy is calculated using Equation (15). When Figure 13 is compared with other such sonic flow enthalpy correlations, the AEDC constricted arc enthalpy is superior to all of the others.

As a result of the above data comparisons, runs were selected from the AEDC data and from the Martin Marietta Corporation data for the code validation. These data, designated as Runs 1-16, are listed in Table 2; the final

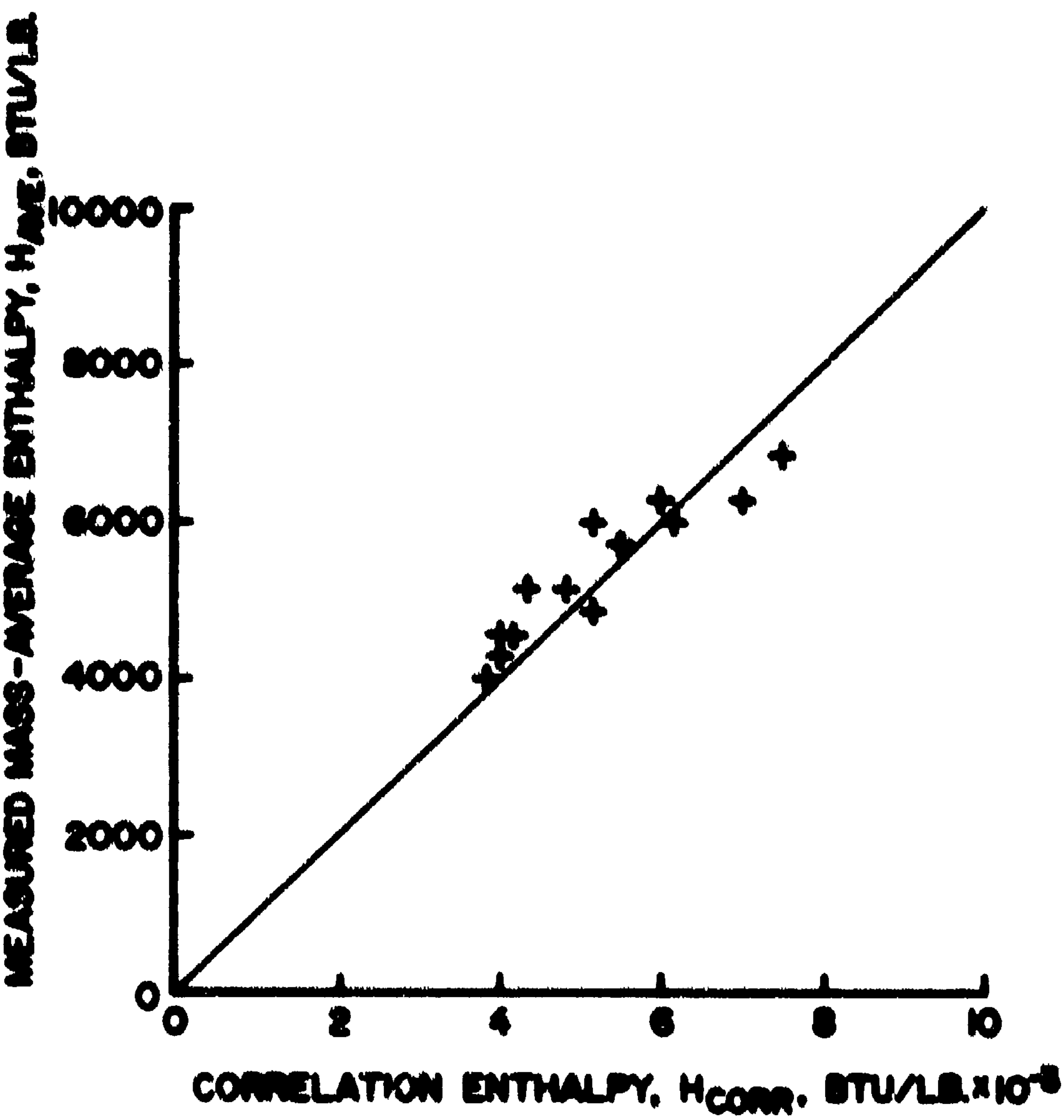

Figure 11. AEDC constricted arc enthalpy data.

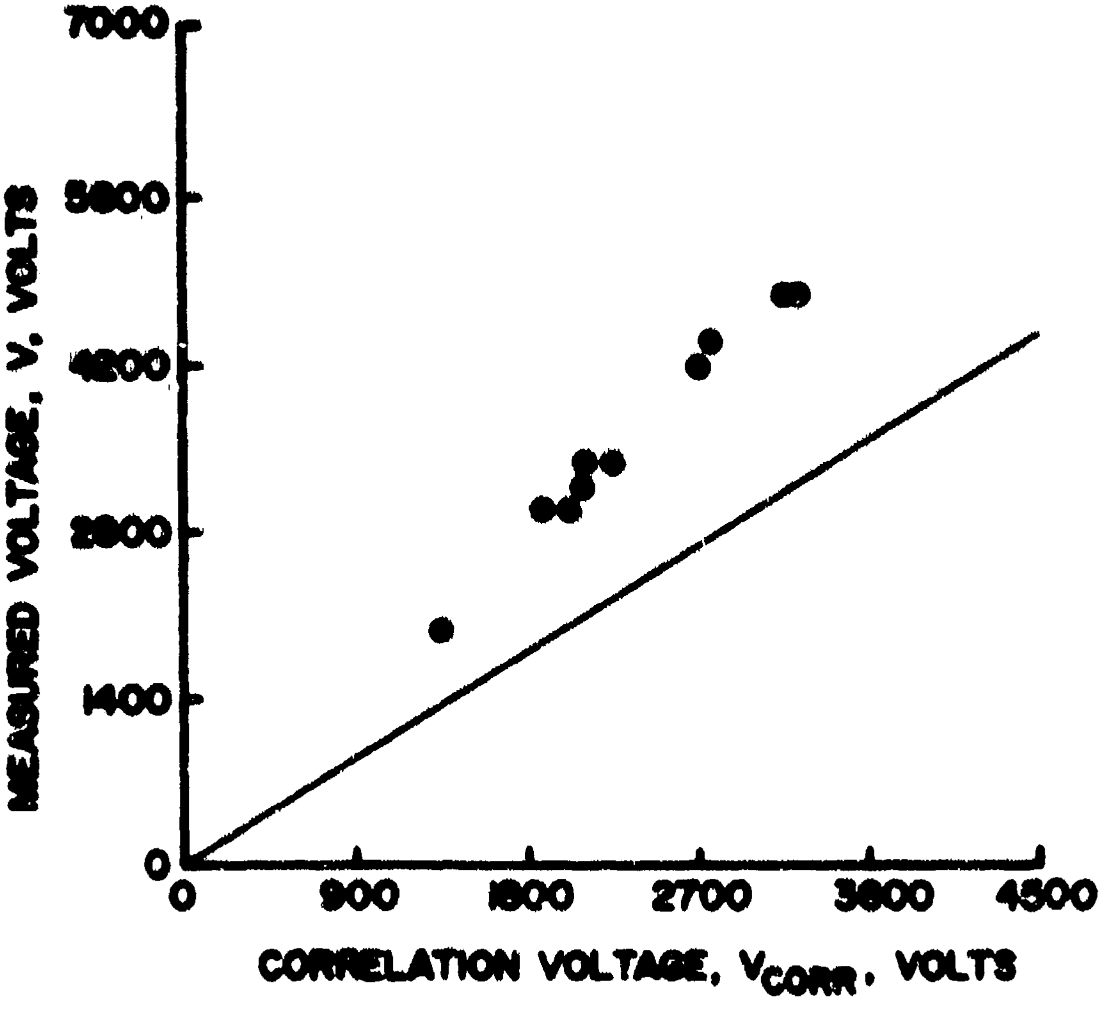

Figure 12 AEDC constricted arc voltage data.

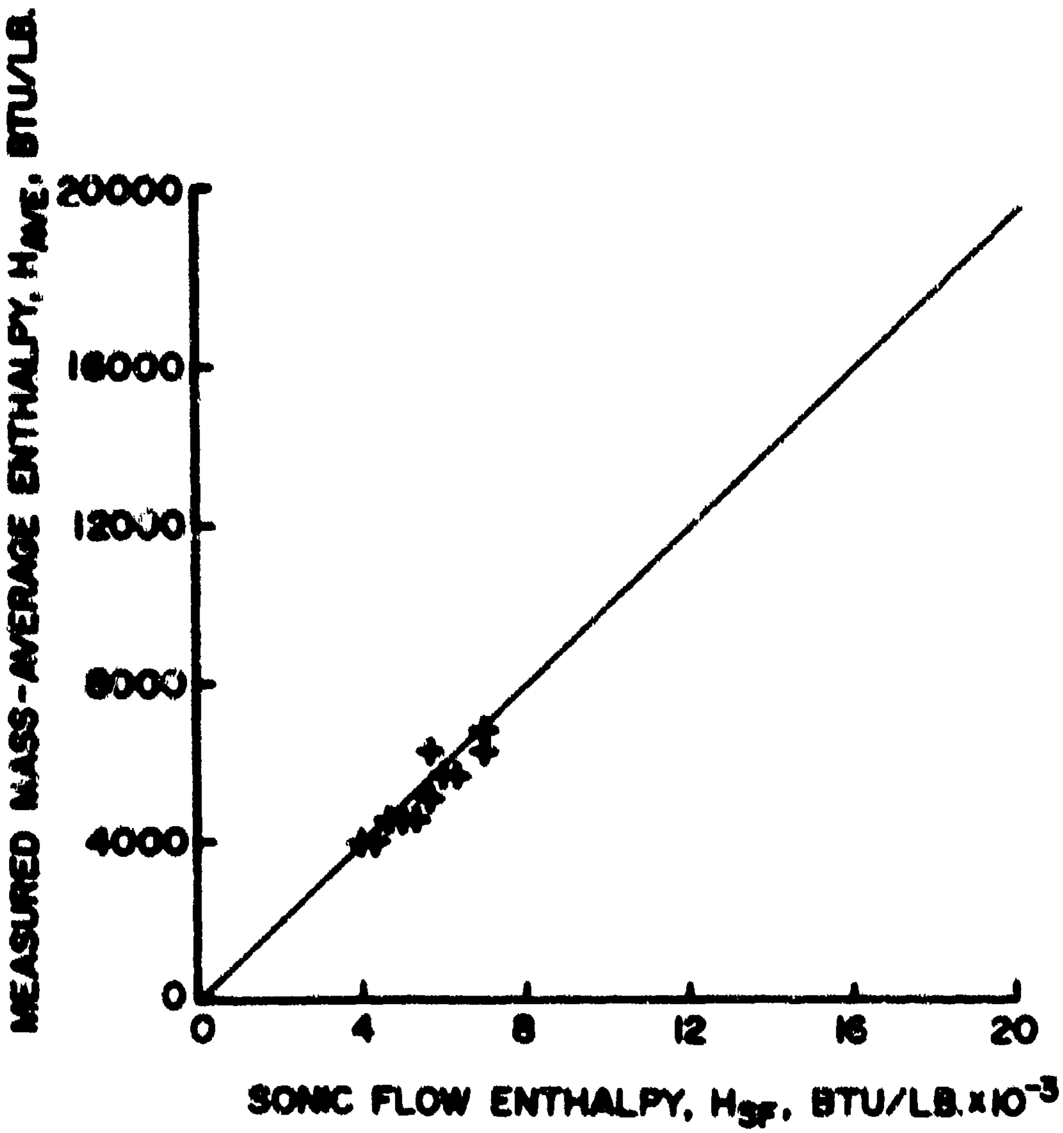

Figure 11. AEDC enthalpy data correlation with sonic flow enthalpy.

TABLE 2

EXPERIMENTAL DATA FOR CODE VALIDATION

Run	Amps	Volts	Dia. inch	Length inch	Flow lbm/sec	$\bar{H}$ Btu/lbm	Pressure atm
1	521	2080	0.934	17.00	0.055	6,403	26.3
2	427	2080	0.934	17.00	0.058	6,024	26.0
3	591	2120	0.934	17.00	0.055	6,989	26.2
4	475	3300	0.934	17.00	0.120	5,326	53.2
5	370	3360	0.934	17.00	0.121	4,508	51.0
6	575	3300	0.943	17.00	0.116	5,963	53.7
7	477	4230	0.934	17.00	0.187	4,663	77.6
8	561	4465	0.934	17.00	0.192	5,270	84.4
9	602	4830	0.934	17.00	0.260	4,448	102.0
10	682	3544	0.934	17.00	0.136	5,886	64.0
11	529	3016	0.934	17.00	0.112	5,140	46.0
12	543	3295	0.934	17.00	0.123	5,084	52.9
13	635	3050	0.934	17.00	0.100	6,340	43.9
14	525	3460	0.934	17.00	0.120	6,025	55.4
15	554	4980	0.934	17.00	0.253	4,256	101.5
16	900	6176	1.030	65.00	0.147	10,037	24.9

data set selected for code validation were Runs 3, 4, 5, 8, 15, and 16. The first five runs include data acquired at the AEDC constricted arc heater facility where pressures reached 100 atm in a relatively short arc, L/d ≈ 20. The Martin Marietta Corporation data for Run 16 were included to exercise the code's prediction capability for long arcs, L/d ≈ 65, where fully-developed or asymptotic flow is obtained.

RESULTS OF CODE VALIDATION

Table 3 summarizes the comparisons between experimental data and the ARCFLOW Version 2 predictions for both bulk enthalpy and voltage drop at the constrictor exit. The comparisons indicate that the discrepancy between the Version 2 prediction of bulk enthalpy and the corresponding experiental value for a developing arc exceeds 10 percent in only one case, while in several cases it is less than 5 percent. This agreement is viewed as being within the uncertainty of the experimental data. The single comparison with a fully developed arc is within 2 percent. The predictions of voltage drop for the AEDC test conditions are consistently below the measured values. This is most likely due to the fact that the flow field model does not treat the anode and cathode fall regions. For the short AEDC arc, the voltage drops in the electrode fall regions can be a significant portion of the total measured voltage drop.

For the MMC arc (Run 16), the wall roughness parameter K_s was parametrically varied from 0.0 to 0.010 inch, and K_s = 0.0035 inch was found to provide the best combined prediction of ΔV and $\bar{H}$ when compared to the experimental values. This value of K_s agrees with measurements and estimates made at Aerotherm. For the AEDC arc, K_s = 0.005 inch was used since the insulator width in this arc is somewhat larger than that for the MMC arc.

The bulk enthalpies are presented in Figure 14 to allow comparisons between the Version 1 and Version 2 predictions and the experiental data.* In every case, the Version 2 predictions are superior to the Version 1 predictions. Considering only the AEDC data, it is observed that the Version 1 predictions are lower than the measured values, and the deviations increase with increasing pressure, while the much smaller deviations associated with the Version 2 predictions show no particular trend. Further, the Version 2 predictions for the long arc considered in Case 16 are in good agreement with experimental data, while the Version 1 predictions are substantially too high. In general, the Version 2 predictions compare with the Version 1 predictions as follows:

- The Version 2 predictions indicate that a given enthalpy will be reached in a shorter axial distance

*The Watson and Pegot version of ARCFLO would not operate for Run 15 due to an extrapolation of the 1 and 10 atm property tables to negative property values.

TABLE 3

SUMMARY OF COMPARISONS BETWEEN ARCFLO VERSION 2 PREDICTIONS AND EXPERIMENTAL DATA

Run No.	Measured		ARCFLO Version 2 Prediction	
	ΔV (volts)	$\bar{H}$ (Btu/lbm)	ΔV (volts)	$\bar{H}$ (Btu/lbm)
3	2120	6,980	1722 -18.8%	6201 -11.3%
4	3300	5,326	2596 -21.3%	4791 -10.0%
5	3360	4,500	2642 -21.4%	4304 - 4.4%
8	4465	5,270	3565 -20.2%	4574 -13.2%
15	4980	4,256	4176 -16.1%	4380 + 2.9%
16	6176	10,037	6253 + 1.2%	9850 - 1.9%

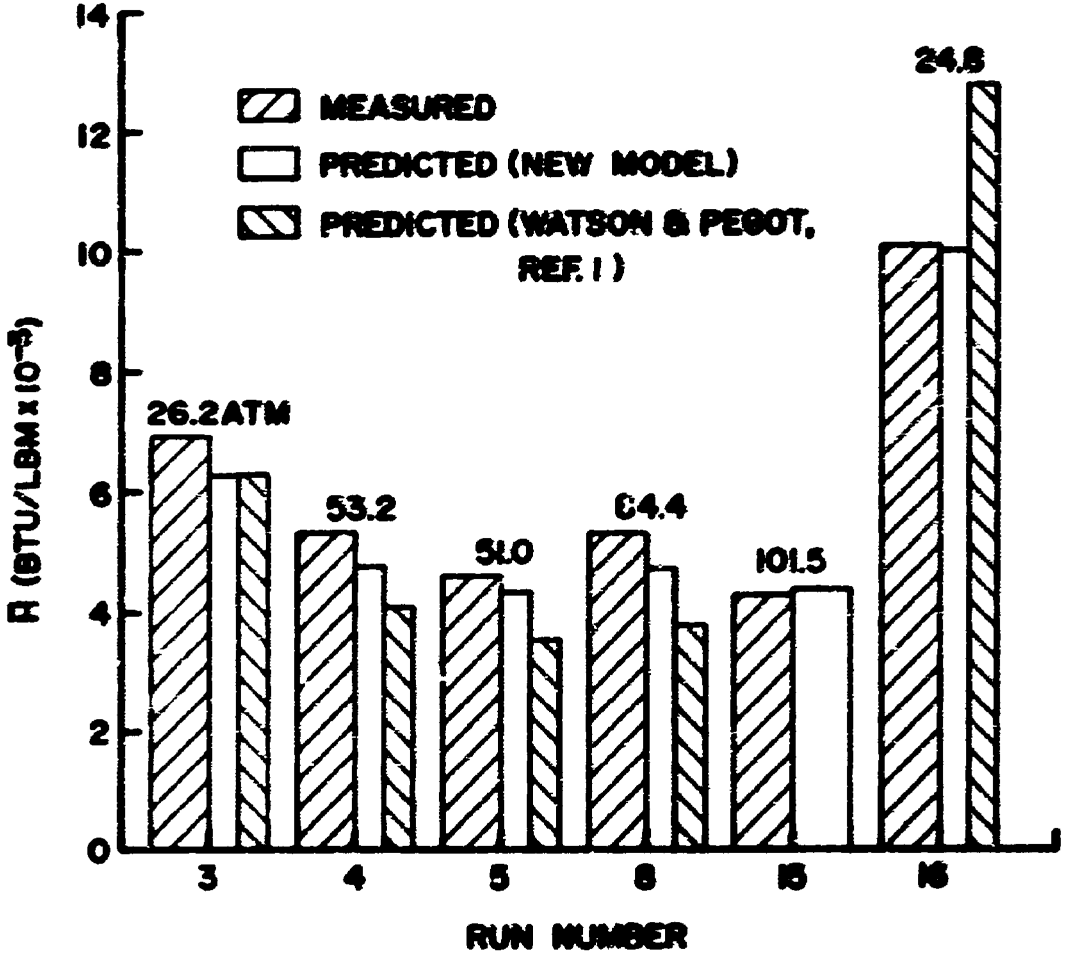

Figure 14. Comparison of Version 1 and Version 2 ARCFLO predictions for bulk enthalpy with experimental data.

- The Version 2 predictions indicate that a lower asymptotic enthalpy will be reached.

A discussion of these code comparisons follows.

Flows in short arcs are characterized by enthalpy profiles which are sharply peaked near the center of the constrictor tube. Energy events in this type of flow tend to be dominated by the mixing of the hot core with the surrounding cold gases, with turbulent diffusion being the primary transport mechanism. Consequently, the selection for the Version 2 analysis of a turbulent Prandtl number which goes to 0.5 at the center of the constrictor tube has the effect of significantly increasing both the predicted transport of energy and the predicted axial rate of growth of the bulk enthalpy.

Run 16 corresponds to a constrictor length for which fully developed or asymptotic conditions are approached. In this particular case, the Version 2 code calculation predicts twice as much total wall heat flux as that of Version 1. With the much lower losses, the Version 1 prediction of $\bar{H}$ is correspondingly higher. As discussed in Section 3, the lower prediction of radiative losses by ARCFLO Version 1 is due to the fact that the visible, infrared, and ultraviolet lines and the ultraviolet continuum are not included in the Watson and Pegot model.

In conclusion it is felt that ARCFLO Version 2 provides significantly more accurate predictions in high-pressure applications as demonstrated by the good agreement between measured values of $\bar{H}$ and those predicted by ARCFLO Version 2 and the large degree of improvement relative to the predictions of Version 1. The remainder of this section is devoted to a brief discussion of several physical phenomena predicted by the upgraded version of ARCFLO.

Figures 15 and 16 present the ARCFLO Version 2 predictions of axial distributions for Runs 8 and 16, respectively. The axial gradient of $\bar{H}$ is large at the exit of the AEDC constrictor, while for the much longer NWC constrictor it is nearly zero. This means that higher bulk enthalpies could be achieved in the AEDC facility if the constrictor were lengthened and the total voltage drop increased while holding mass flow and current constant. In contrast, further increases in $\bar{H}$ in the NWC facility cannot be realized by simply lengthening the constrictor.

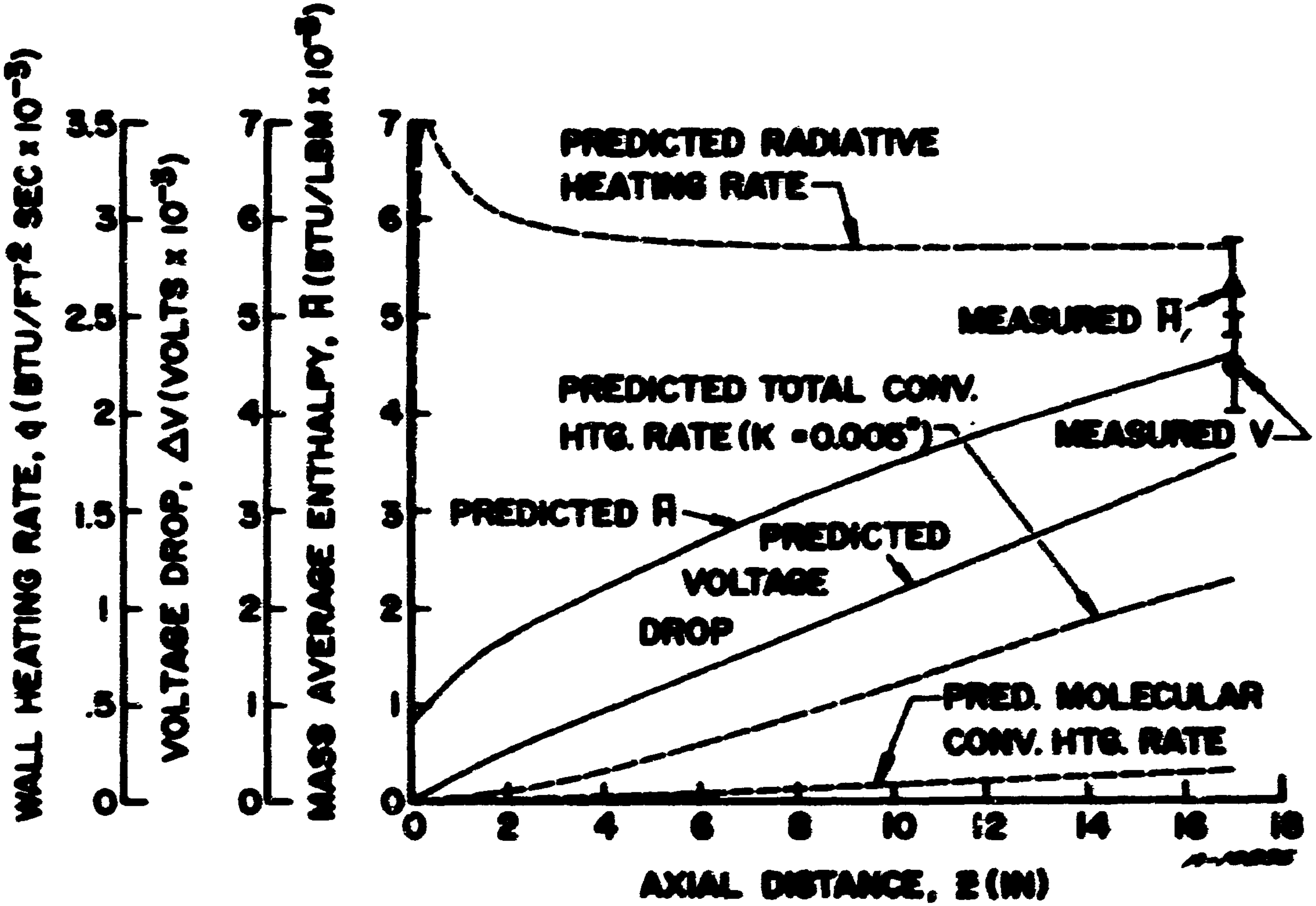

Figure 15. Axial distributions predicted by ARCFLO Version 2 for Run No. 8.

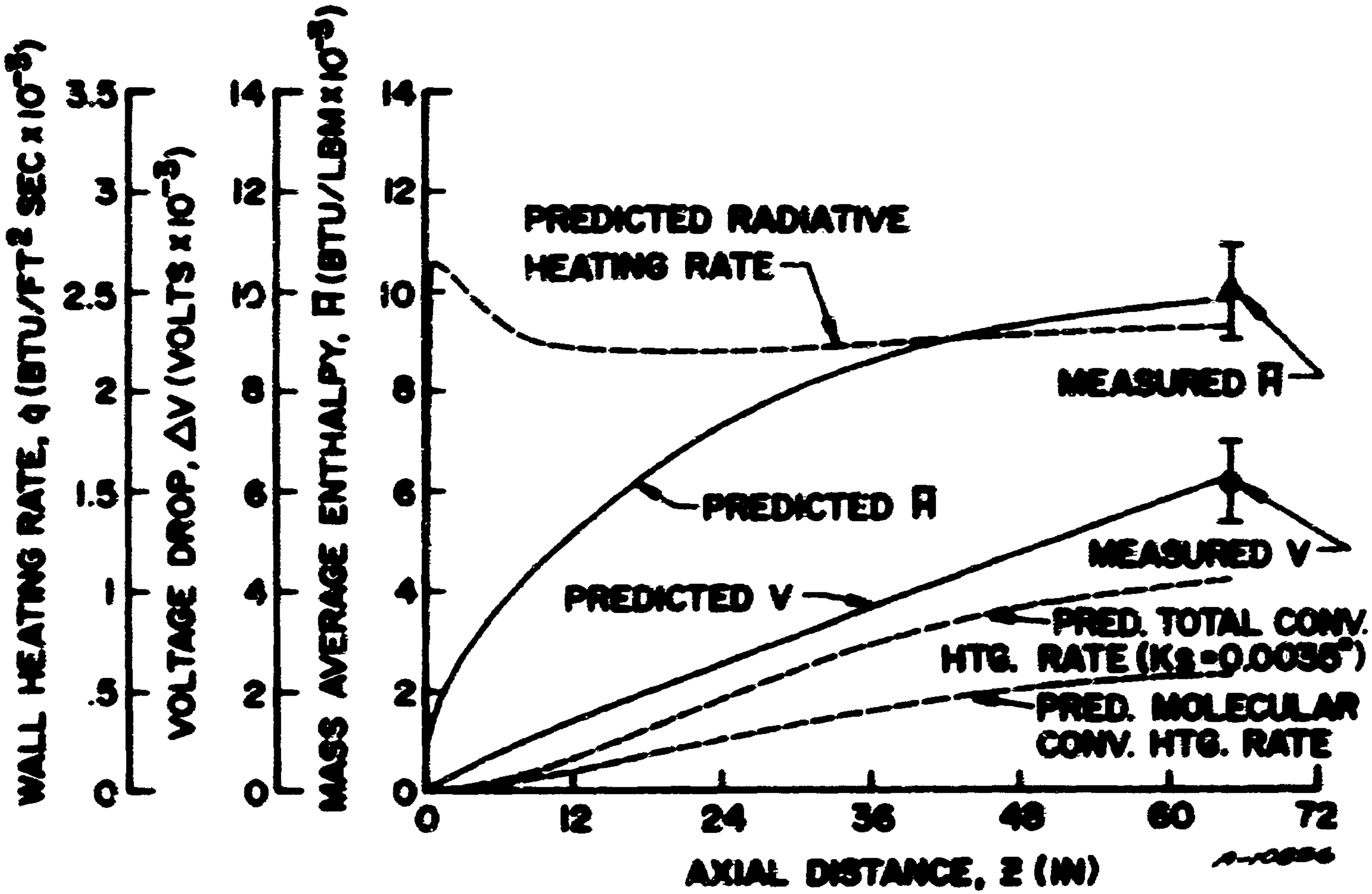

Figure 16. Axial distributions predicted by ARCFLO Version 2 for Run No. 16.

Figures 15 and 16 also indicate that in the thermally developing portion of the flow field, the wall heat flux is dominated by radiation. The convective heat flux becomes significant only after asymptotic conditions are approached. Even at this point, convection is typically no more than 30 percent of the total wall heat flux for the elevated operating pressures considered. For the AEDC constrictor, the wall convection is dominated by the turbulent contribution due to wall roughness. In contrast, for the MMC case where both bulk Reynolds number and wall roughness are smaller, the wall convection is approximately equally divided between the molecular and turbulent contributions. The nature of the radiative and convective wall heat flux predictions in the entrance region is a direct result of the entrance profiles considered. The entrance profiles used in the calculations are discussed below.

Figures 17 and 18 illustrate the radial temperature profiles predicted by ARCFLO Version 2 for Runs 8 and 16, respectively. In each case, the assumed starting enthalpy profile is essentially the same. The bulk enthalpy corresponding to the entrance temperature profile is low, being approximately 800 Btu/lbm. The low energy content of the flow at this point is assumed to be concentrated in the core; that is, the arc column, where significant ionization is present, resides in a small region of the center of the flow field. A short distance downstream of the entrance a large temperature spike is generated because the Ohmic heating is confined to the narrow conducting core of the flow field. In both runs, this temperature spike persists past the 17-inch axial position. When the temperature spike is present, the wall temperature gradient is relatively low. As a result, radiation from the core is the major contributor to the wall heat flux. However, as indicated for Run 16, if the flow is allowed to develop, the high-energy core will tend to spread to the confining walls of the constrictor, and the classical flat profile characteristic of turbulent pipe flow is approached. Radiation continues to be dominant in the fully-developed regime, but the steep wall gradients also cause convection to be significant.

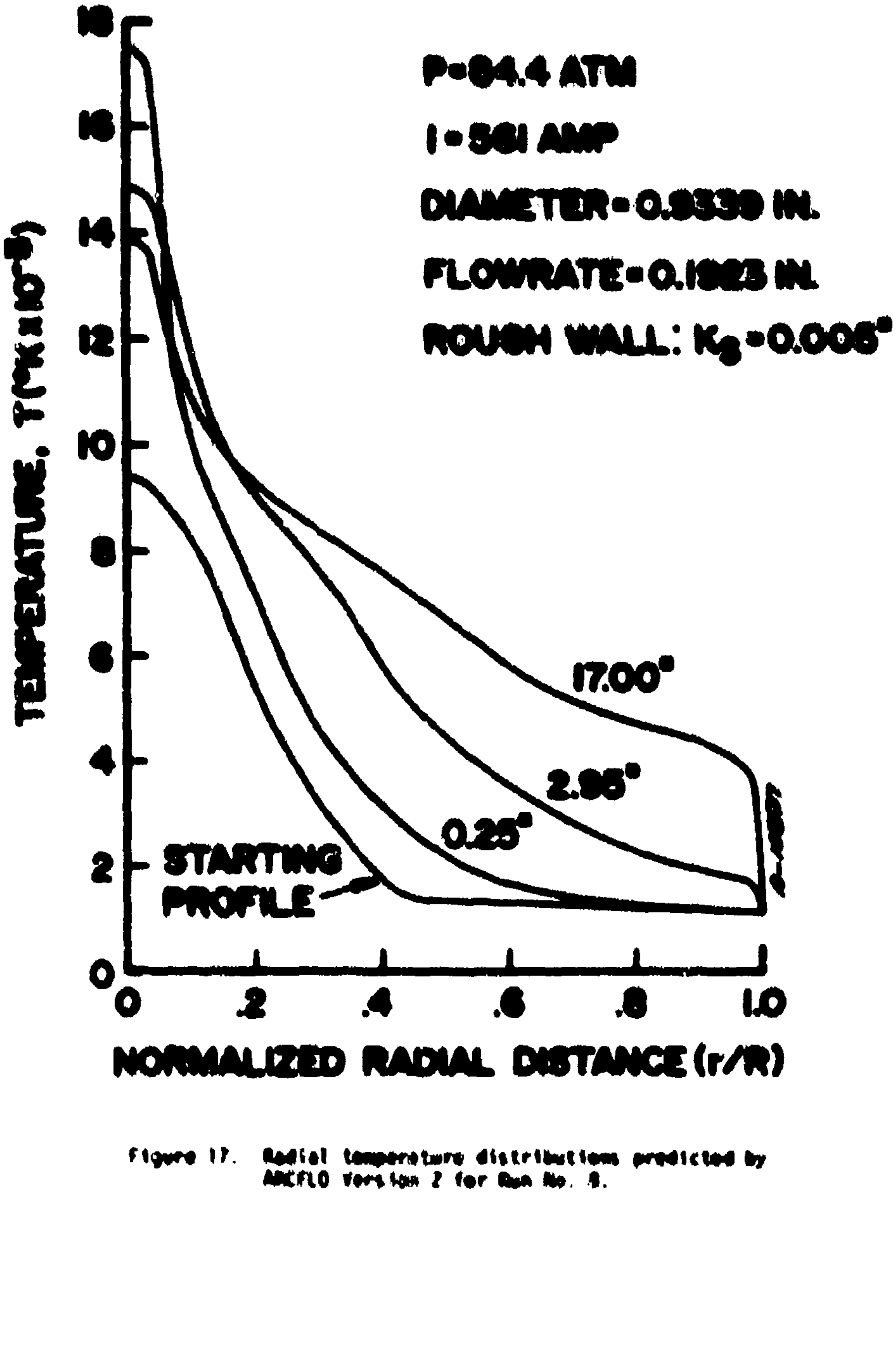

Figure 17. Radial temperature distributions predicted by ARCFLO Version 2 for Run No. 8.

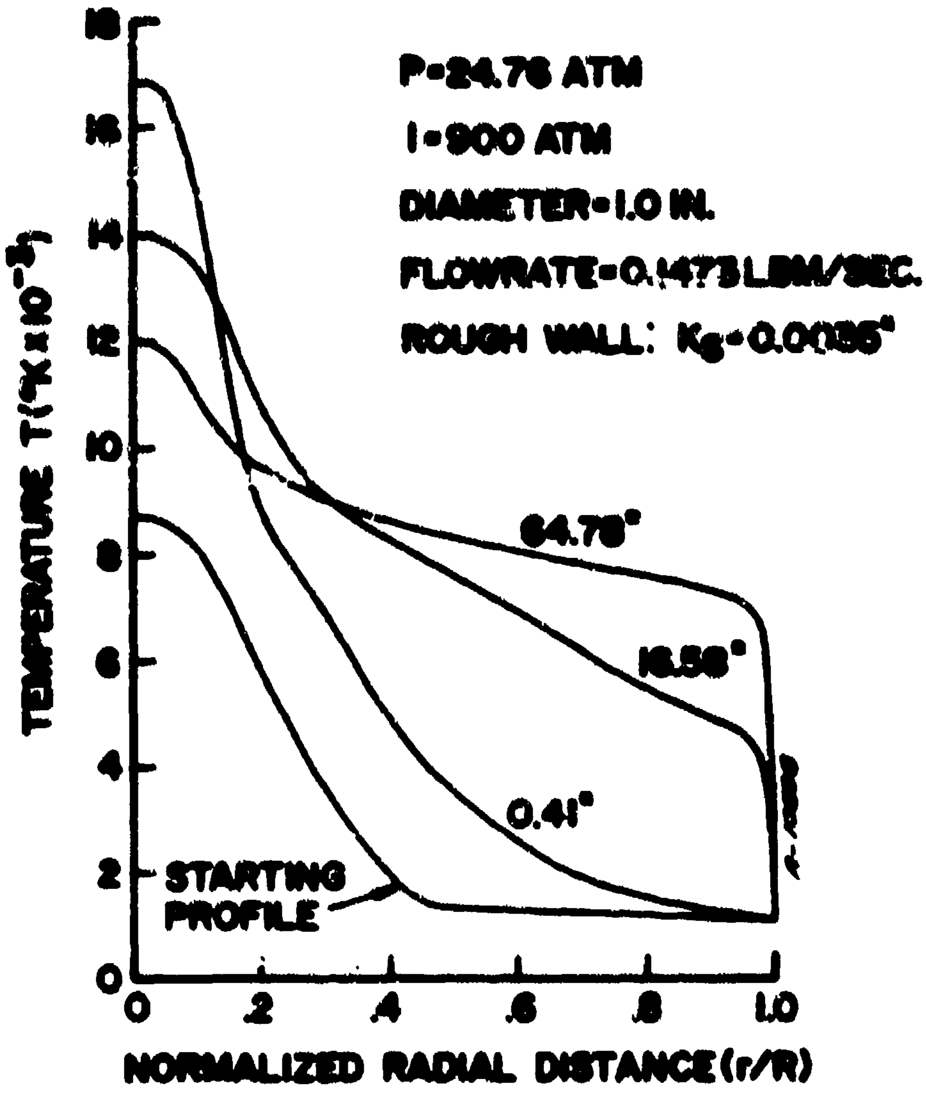

Figure 18. Radial temperature distributions predicted by ARCFLO Version 2 for Run No. 16.

SECTION 7

SCALING STUDY

The purpose of the scaling study was to characterize and optimize the performance of high pressure arc heaters. Specifically, the important parameters were identified and their effect on performance established. One of the primary results obtained was a curve relating the maximum mass-average enthalpy to pressure for given values of maximum permissible constrictor wall heat transfer rate. Additional constraints such as those imposed by the power supplies and the test stream requirements are discussed in Section 8.

The data used for the scaling study were obtained from a series of ARCFLO Version 2 computer code calculations. A matrix of 32 cases was identified; this matrix is given in Table 4. The input data covers the following range:

- Pressure: 82 to 300 atmospheres
- Current: 500 to 2500 amperes
- Air Mass Flow Rate: 0.125 to 4.0 lbm/sec
- Diameter: 0.75 to 2.939 inches
- Length: 0 to 90 inches

As shown in Table 4, all cases were successfully computed in the first attempt except Case 27. The initial starting assumptions for this case caused the solution to blow up early in the computation and since the conditions were not of primary interest a second attempt was not made.

In order to describe the important trends in the ARCFLO Version 2 performance data, equations were sought relating mass-average enthalpy, constrictor wall heat-transfer rate, voltage, and efficiency. These equations are viewed as useful correlation and interpolation formulae for use in the design optimization presented in Section 8. They should not, however, be used to extrapolate results beyond data ranges given above.

RESULTS OF SCALING STUDY

The mass-average enthalpy was found to increase with axial distance at a relatively rapid rate to an asymptotic level as shown in Figure 19.

TABLE 4

ARCFLO VERSION 2 CALCULATION MATRIX

Case No.	Current amps	Air Flow lb/sec	Pressure atm	Diameter inches	Comments
1	1500	3	150	1.75	
2	2000				
3	1000				
4	1500	4			
5		2			
6		3	200		
7			80		
8			150	1.544	
9	2000			2.032	
10	1000	4		1.75	
11	2000	2			
12	2500	3			
13	600	0.5		0.934	
14	700				
15	500				
16	600	1.0			
17		0.25			
18		0.50	200		
19			80		
20			150	1.25	
21	2500	3	80	1.75	
22			200		
23			150	1.50	
24				2.00	
25	2000			1.50	
26				1.25	
27			80		• Did not run
28			200		
29		2	150		
30	600	0.25		0.75	
31		0.125		0.934	
32	1500	2 to 3		1.75	• Distributed flow injection

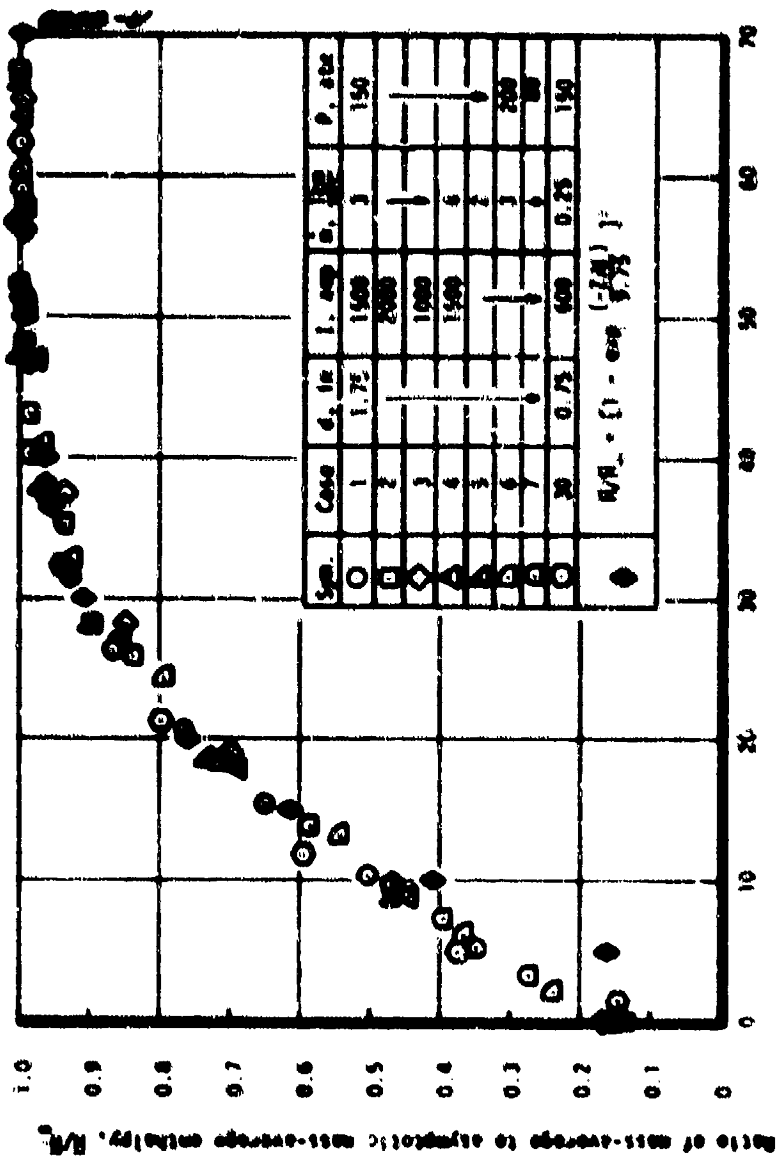

Figure 19. Increase of mass-average enthalpy to asymptotic value as function of axial distance.

Once the mass-average enthalpy had reached its asymptotic value, further increases in constrictor length caused the radial enthalpy profile to become flatter, but did not change the value of the mass-average enthalpy. Further, when the ratio of local to asymptotic mass-average enthalpy was examined, it was found to be primarily a function of the ratio of axial distance to constrictor diameter, Z/d, and relatively independent of constrictor diameter, pressure, air mass flow rate, or current (Figure 19). For values of Z/d greater than 15, the enthalpy-length curve can be approximated by

$$\frac{\bar{H}}{\bar{H}_\infty} = \left[1 - \exp\left(-\frac{z}{9.75d}\right)\right]^2 \qquad (16)$$

A summary of the ARCFLO Version 2 values of mass-average enthalpy, constrictor-wall heat transfer rate, voltage, and current is given in Table 5 for a value of Z/d of 31. At this length, $\bar{H}/\bar{H}_\infty$ [illegible] 0.99.

Correlation equations of the ARCFLO Version 2 results were obtained using a multiple regression statistical technique for mass-average enthalpy, constrictor wall heat-transfer rate, arc voltage, and efficiency. The equations, for a given value of Z/d, are:

$$\bar{H} = \left(\frac{I}{d}\right)^{[illegible]}\left(\frac{\dot{m}}{p}\right)^{[illegible]} \times \text{const}\ ,\ \text{Btu/lbm} \qquad (17)$$

$$\dot{q} = \left(\frac{I}{d}\right)\left(\frac{\dot{m}}{d^2}\right)^{-[illegible]} p^{[illegible]} \times \text{const}\ ,\ \text{Btu/ft}^2\text{-sec} \qquad (18)$$

$$V = \left(\frac{I}{d}\right)^{[illegible]} \dot{m}^{[illegible]} p^{[illegible]} \times \text{const}\ ,\ \text{volts} \qquad (19)$$

$$\eta = \left(\frac{I}{d}\right)^{-[illegible]}\left(\frac{\dot{m}}{d^2}\right)^{[illegible]} p^{-[illegible]} \times \text{const} \qquad (20)$$

An alternate approximate expression for mass-average enthalpy can be obtained in terms of constrictor wall heat-transfer rate, rather than current:

$$\bar{H} = d^{[illegible]}\left(\frac{\dot{q}}{p}\right)^{[illegible]} \times \text{const}\ ,\ \text{Btu/lbm} \qquad (21)$$

TABLE 5

SUMMARY OF ARCFLO VERSION 2 CALCULATIONS AT Z/d = 51

Case No.	$\bar{H}$ (Btu/lbm)	$\dot{q}_{wall}$ (Btu/ft^{2}sec)	Voltage (kV)	Current (amps)
1	5275	5,441	33.4	1500
2	5960	7,648	27.8	2000
3	4677	3,854	32.8	1000
4	5149	5,119	33.6	1500
5	6509	6,796	26.3	
6	5189	6,670	32.1	
7	5658	3,290	25.4	
8	5568	5,962	29.4	
9	5684	6,963	29.2	2000
10	4499	3,763	37.9	1000
11	6141	8,406	24.7	2000
12	6434	9,537	26.5	2500
13	5500	4,672	17.6	600
14	5650	5,440	17.0	700
15	5100	3,800	18.5	500
16	5000	3,580	23.9	600
17	5850	5,500	14.4	
18	5325	5,900	18.9	
19	5900	2,646	14.9	
20	4850	4,000	11.97	
21	6981	5,822	22.2	2500
22	6325	11,239	23.7	
23	6888	10,042	25.8	
24	6073	8,869	23.3	
25	6260	8,063	27.2	2000
26	6610	7,704	27.3	
27	--	--	--	--
28	6421	10,098	28.6	2000
29	6999	9,421	23.1	
30	6480	6,337	13.1	600
31	6310	6,000	12.7	
32	4730	5,300	20.0	1500

Equation (21) shows that, for a given pressure and wall heat transfer rate, the mass-average enthalpy is solely a function of constrictor diameter. Curves of maximum enthalpy versus pressure are shown in Figure 20 for several constrictor diameters and an assumed constrictor wall heat-transfer rate of 10,000 Btu/ft^{2}sec. Thus, it should be possible to attain the "average" design goal of 7000 Btu/lbm at 175 atmospheres, providing the constrictor diameter is less than one inch.*

*Practical considerations, as discussed in Section 8, limit the general application of this conclusion. For instance, a 40 MW arc heater should have a constrictor diameter larger than one inch.

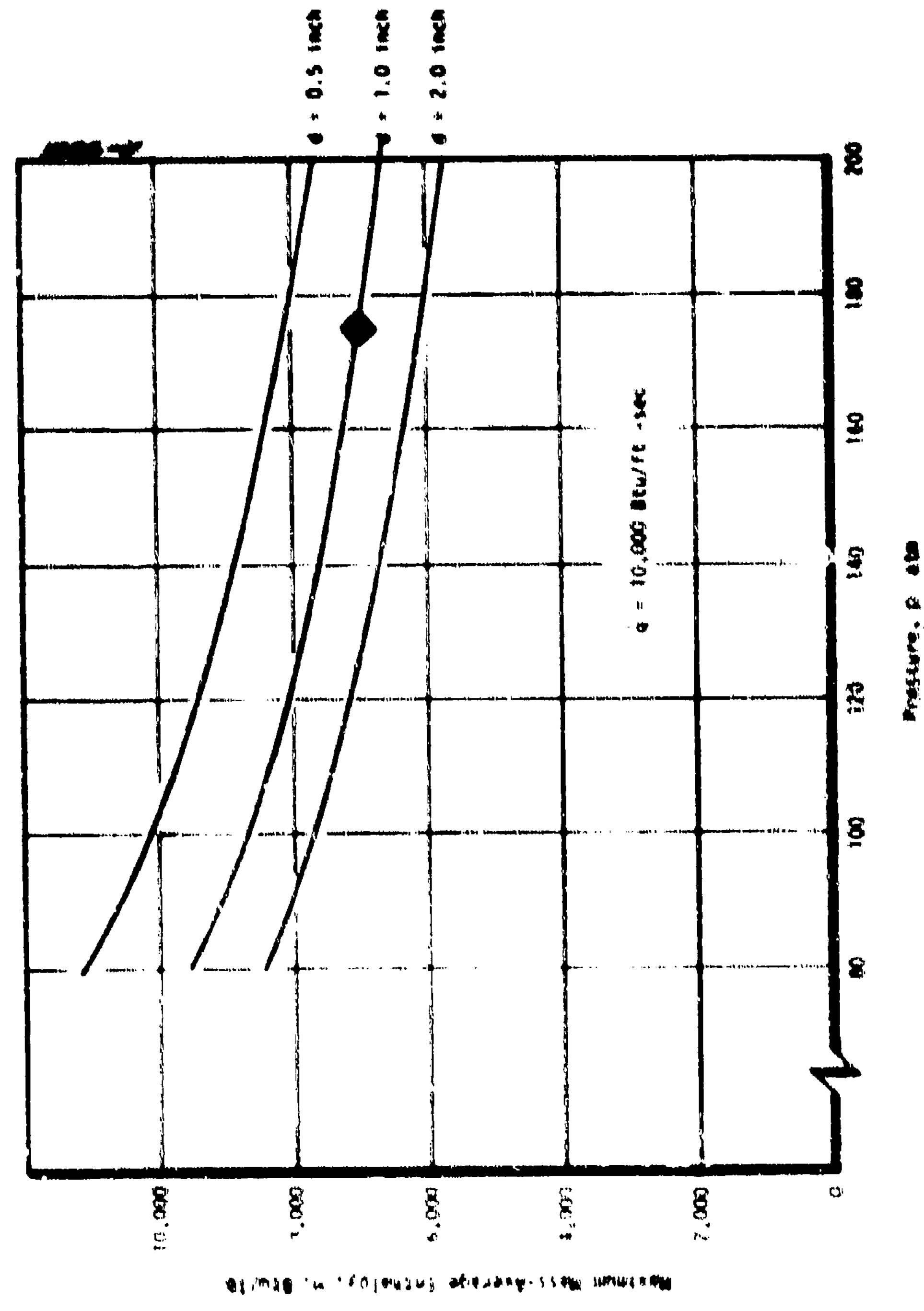

Figure 20. Maximum mass-average enthalpy as a function of pressure for different constrictor diameters.

SECTION 8

CONCEPTUAL ARC HEATER DESIGNS

The scaling study discussed in Section 7 provides the basis for development of conceptual designs for the 5 and 40 MW high pressure, high enthalpy constrictor arc heaters. Specific design goals for the arc units are as follows:

- Total mass-average enthalpy: 6000-8000 Btu/lbm
- Chamber pressure: 150-200 atm
- Minimum operating time: 10 sec
- Nozzle exit Mach number: 1.7 - 2.3

A nominal Mach 2 nozzle corresponding to an area ratio of 1.79 was chosen for design purposes. The maximum levels of current, voltage and input power allowed for the design are as follows:

Parameter	5 MW	40 MW
• Arc current, amps	750	2000
• Arc voltage, kilovolts	10	30
• Input power, MW	5	40

DESIGN GUIDELINES

The above performance and operating parameters provide the constraints for the designs; there are also a number of operating and geometric parameters which provide some further design guidelines. Maximum values of these guideline parameters achieved in operational arc heaters serve at least as indicators of design constraints. The important guideline parameters are:

- Enthalpy-pressure parameter, $H\sqrt{\bar{p}}$ - an indicator of overall arc heater performance
- Constrictor wall heat flux, $\dot{q}$ - an indicator of the cooling requirements
- Arc current-constrictor diameter parameter, I/d - an indicator of overall losses and constrictor heat load

- Axial voltage gradient, $\mathcal{E}$ - an indicator of the maximum constrictor disk thickness which is defined by the allowable voltage difference between adjacent disks, ΔV
- Input power per unit length, $\mathcal{E}I$ - an indicator of the local constrictor column energy loading
- Input power per unit volume, $VI/(\pi d^2 L/4)$ - an indicator of the overall constrictor column energy loading
- Constrictor mass flux, $(\rho u)_{ave}$ - an indicator of the constrictor column aerodynamics and ratio of constrictor diameter to throat diameter

Maximum values of these parameters are presented in Table 6 for the high pressure experimental data of the AEDC constricted arc heater and the AFFDL Huels-type arc heater, and for all of the data for the actively cooled arc heaters of Table 1. Consideration of these results yielded the following maximum and recommended values of these guideline parameters for the conceptual designs:

Parameter	Maximum from Table 6	Conceptual Design Maximum	Conceptual Design Recommended
$H/\sqrt{p}$, Btu-atm$^{1/2}$/lbm	52,800	*	*
$\dot{q}$, Btu/ft^{2}sec	4,620	10,000	5,000
I/d, amp/cm	638	638	638
$\mathcal{E}$, volts/cm	115	175	115
ΔV, volts	79	100	100
$\mathcal{E}I$, kw/cm	210	210	210
$VI/(\pi d^2 L/4)$, kw/cm^3	15.2	40	15
$(\rho u)_{ave}$, lb/ft^{2}sec	167	250	200

Even the minimum performance goal of 6000 Btu/lbm at 150 atm requires an increase of about 50 percent over previously achieved performance. This requires in turn an extension of demonstrated capability for some of the other parameters:

- Constrictor wall heat flux, $\dot{q}$ - requires high efficiency cooling, optimum design constrictor disks
- Axial voltage gradient, $\mathcal{E}$ - requires thinner constrictor disks to maintain the voltage gradient between adjacent disks, ΔV, at acceptable levels

*Minimum design goal 74,000 (6000 Btu/lbm at 150 atm); maximum design goal 113,000 (8000 Btu/lbm at 200 atm).

TABLE 6

OBSERVED OPERATIONAL LIMITS OF VARIOUS ARC HEATERS

	$H/\sqrt{p}$ Btu-atm$^{1/2}$/lbm	$\dot{q}$ Btu/ft^{2}sec	I/d amp/cm	E volt/cm	ΔV_{ave} cm^3	EI kW/cm	$VI/\frac{\pi d^2 L}{4}$ kw/cm^3	$(\rho u)_{ave}$ lb/ft^{2}sec
AEDC Constrictor Arc	48,400	4620	250	115	79	64	15.2	55
AFFDL	33,200	3900	740	--	--	210	4.4	167
ALL	52,800	4620	638	115	79	210	15.2	167

- Input power per unit volume, $VI/(\pi d^2 L/4)$ - requires high efficiency cooling, optimum design constrictor disks
- Constrictor mass flux, $(\rho u)_{ave}$ - small departure from demonstrated acceptable value; results in the requirement for a smaller ratio of constrictor diameter to nozzle throat diameter

BASIC DESIGN SELECTION

The above guidelines together with the scaling study results of Section 7 allowed the selection of the optimum conceptual designs. Many computations were required to develop this optimum design that satisfied the constraints and guidelines presented above. In order to facilitate these computations, a simple computer code which represented the correlation equations for the ARCFLO Version 2 results of Section 7 was therefore developed.* The results of these computations, consistent with the performance goals and operating guidelines, were arc heaters with the following basic configurations:

Configuration Variable	Arc Heater 5 MW	Arc Heater 40 MW
Constrictor diameter, in.	0.70	1.75
Constrictor length, in.	25.5	75.0
Constrictor disk thickness, in.	0.12	0.20
Constrictor disk spacing (center-to-center), in.	0.17	0.25

Note that the design includes a 0.05-inch gap between constrictor disks. The following paragraphs present predicted performance.

PREDICTED PERFORMANCE

The predicted performance of the conceptual designs defined above is presented in Figures 21 through 25 and Tables 8 and 9. The mass-average enthalpy as a function of pressure for both the maximum conditions ($\dot{q}$ = 10,000 Btu/ft^{2}sec) and the recommended conditions ($\dot{q}$ = 5000 Btu/ft^{2}sec) is presented

*A listing of the extended BASIC language code utilized is presented in Table 7 (M 11-ARCFLO). The code applies only to the results of the ARCFLO Version 2 code presented in Section 7; it should not be utilized for performance predictions outside the range of parameters of the scaling study matrix presented in Table 4.

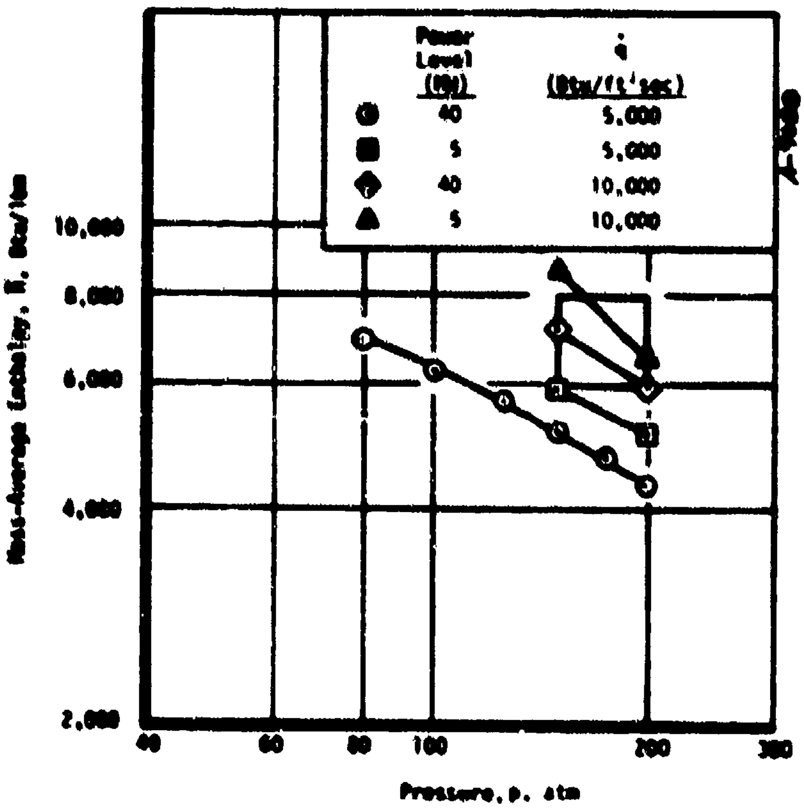

Figure 21. Mass-average enthalpy as a function of chamber pressure for 5 MW and 40 MW arc heater designs.

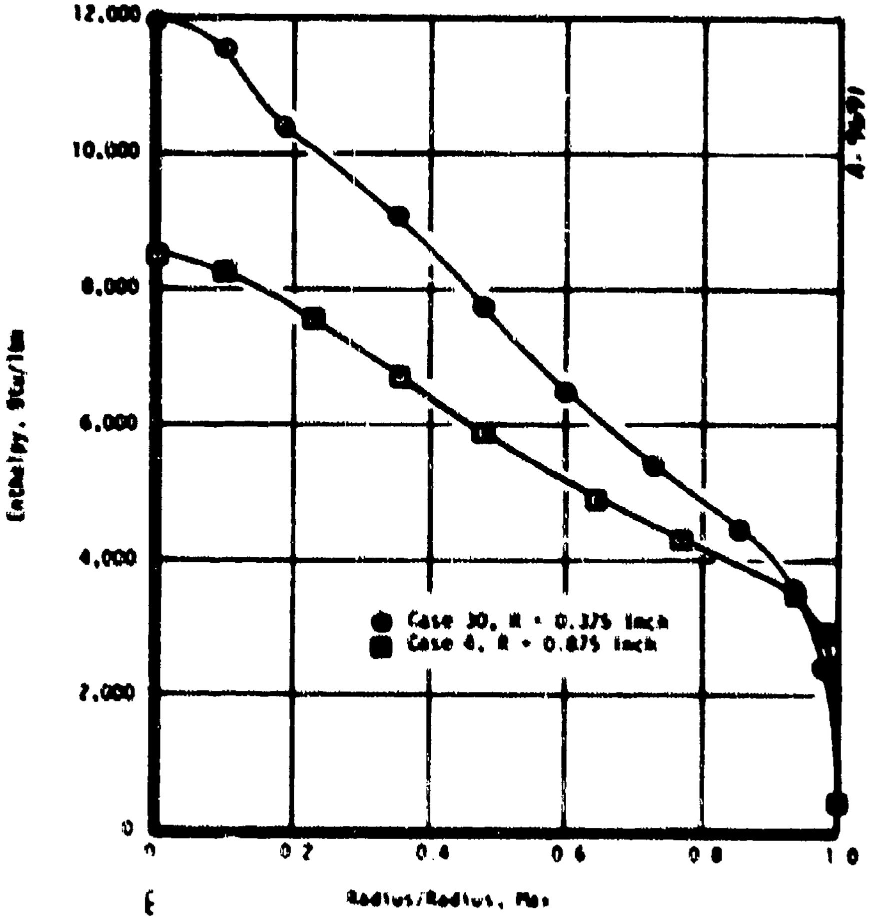

Figure 22. Radial enthalpy distributions

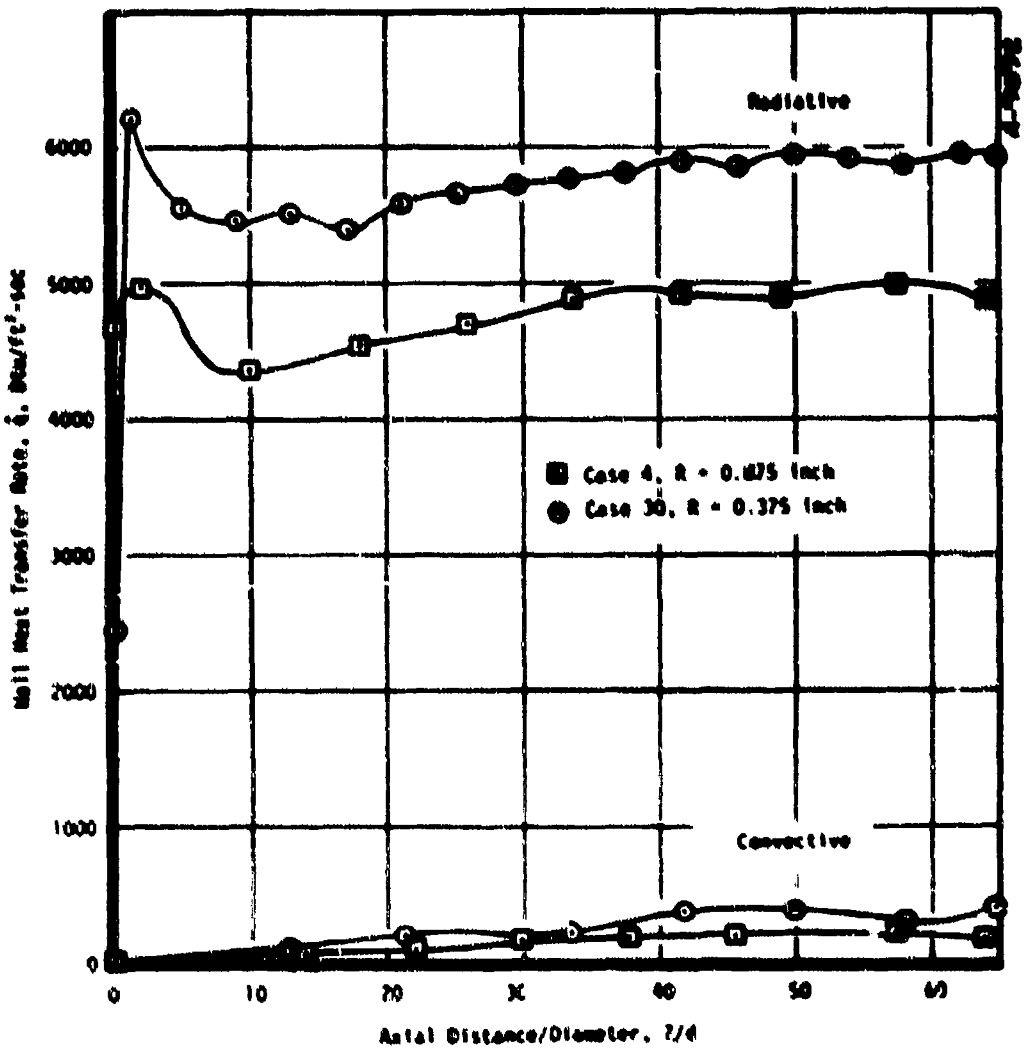

Figure 23. Wall heat transfer distributions

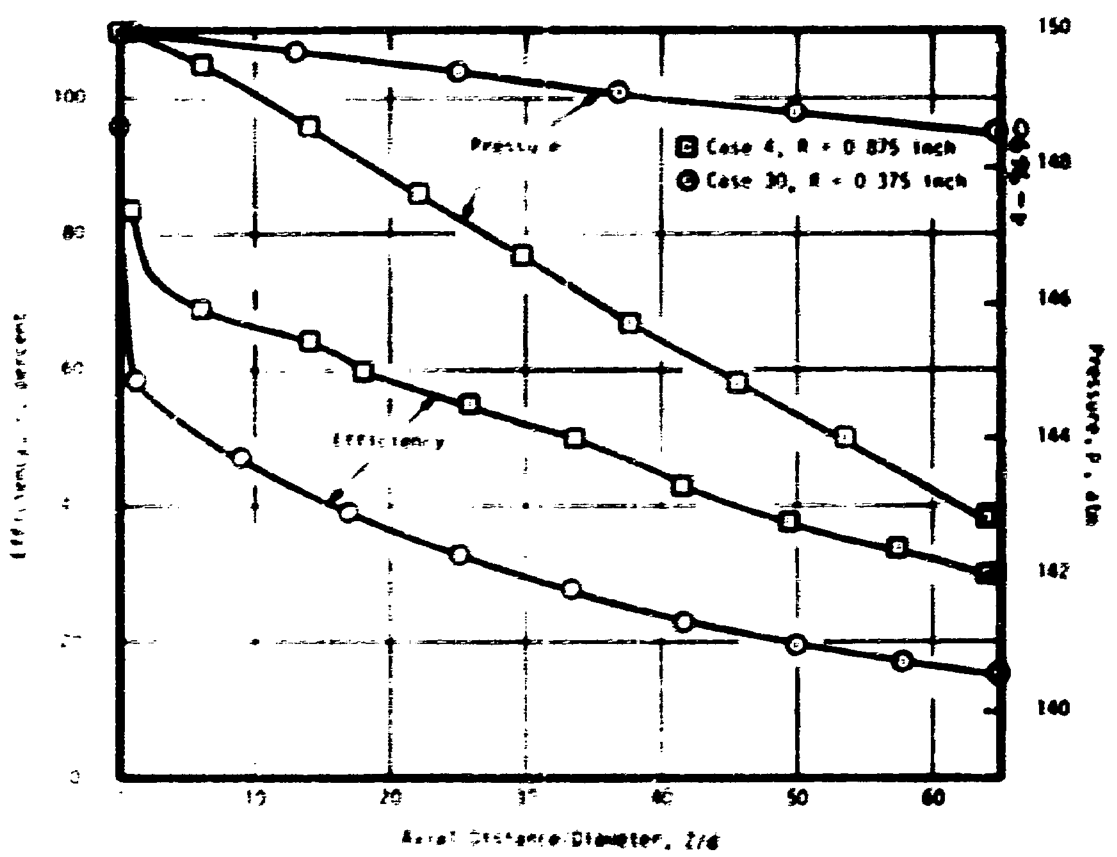

Figure 24 Constrictor pressure drop and efficiency

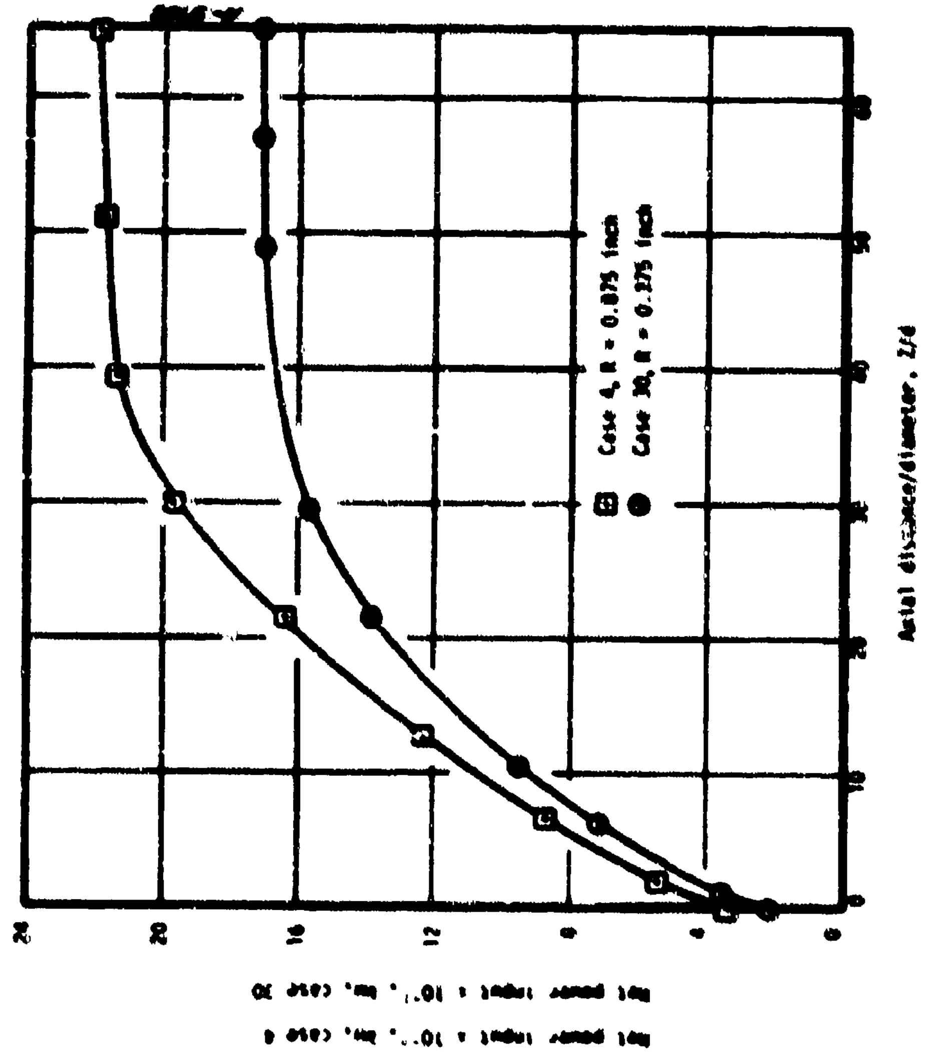

Figure 25. Net power input as function of axial distance

TABLE 7

MIKI-ARCFLO PROGRAM LISTING

TABLE 8

ARCFLO VERSION 2 RESULTS - CASE 38

AXIAL STATION DATA — NC THERMAL ARC WITH AXIAL GAS FLOW

AXIAL DIST	= [illegible] METERS [illegible] INCHES	STARTED	= [illegible] METERS [illegible] INCHES
VOLTAGE GRAD	= [illegible] VOLTS/M [illegible] VOLTS/INCH	CURRENT	= [illegible] AMPS
WALL HEAT FLUX	= [illegible] WATTS/M2 [illegible] BTU/FT2-SEC	FLOW RATE	= [illegible] KG/SEC [illegible] LB/SEC
RADIATION LOSS=	[illegible] PERCENT	TOTAL EFFIC.	= [illegible]
PRESSURE	= [illegible] ATMS	WALL ENTHALPY	= [illegible] JOULES/KG [illegible] BTU/LB
LTE	= 1		= 25
B	= [illegible]	TTF	= [illegible]
Z'LE	= [illegible]	EPS	= [illegible]
THETA	= [illegible] SEC	EF	= [illegible]
		ETT	= [illegible]

BULK AVERAGE ENTHALPY =	[illegible] JOULES/KG	OR	[illegible] BTU/LB
FLOW AVERAGE ENTHALPY =	[illegible] JOULES/KG	OR	[illegible] BTU/LB
AVERAGE ENERGY DENSITY =	[illegible] JOULES/M3	OR	[illegible] BTU/INCH3
TOTAL ENTHALPY FLUX =	[illegible] JOULES/KG	OR	[illegible] BTU/LB

RADIUS METERS	RADIUS INCH	ENTHALPY JOULES/KG	ENTHALPY BTU/LB	VELOCITY M/S	VELOCITY FT/SEC	MASS FLUX KG/S M2	MASS FLUX LB/FT2-SEC
0.	0.	[illegible]	[illegible]	[illegible]	[illegible]	[illegible]	[illegible]
[illegible]	[illegible]	[illegible]	[illegible]	[illegible]	[illegible]	[illegible]	[illegible]
[illegible]	[illegible]	[illegible]	[illegible]	[illegible]	[illegible]	[illegible]	[illegible]
[illegible]	[illegible]	[illegible]	[illegible]	[illegible]	[illegible]	[illegible]	[illegible]
[illegible]	[illegible]	[illegible]	[illegible]	[illegible]	[illegible]	[illegible]	[illegible]
[illegible]	[illegible]	[illegible]	[illegible]	[illegible]	[illegible]	[illegible]	[illegible]
[illegible]	[illegible]	[illegible]	[illegible]	[illegible]	[illegible]	[illegible]	[illegible]
[illegible]	[illegible]	[illegible]	[illegible]	[illegible]	[illegible]	[illegible]	[illegible]
[illegible]	[illegible]	[illegible]	[illegible]	[illegible]	[illegible]	[illegible]	[illegible]
[illegible]	[illegible]	[illegible]	[illegible]	[illegible]	[illegible]	[illegible]	[illegible]
[illegible]	[illegible]	[illegible]	[illegible]	[illegible]	[illegible]	[illegible]	[illegible]
[illegible]	[illegible]	[illegible]	[illegible]	[illegible]	[illegible]	[illegible]	[illegible]
[illegible]	[illegible]	[illegible]	[illegible]	[illegible]	[illegible]	[illegible]	[illegible]
[illegible]	[illegible]	[illegible]	[illegible]	[illegible]	[illegible]	[illegible]	[illegible]
[illegible]	[illegible]	[illegible]	[illegible]	[illegible]	[illegible]	[illegible]	[illegible]
[illegible]	[illegible]	[illegible]	[illegible]	[illegible]	[illegible]	[illegible]	[illegible]
[illegible]	[illegible]	[illegible]	[illegible]	[illegible]	[illegible]	[illegible]	[illegible]
[illegible]	[illegible]	[illegible]	[illegible]	[illegible]	[illegible]	[illegible]	[illegible]
[illegible]	[illegible]	[illegible]	[illegible]	[illegible]	[illegible]	[illegible]	[illegible]
[illegible]	[illegible]	[illegible]	[illegible]	[illegible]	[illegible]	[illegible]	[illegible]
[illegible]	[illegible]	[illegible]	[illegible]	[illegible]	[illegible]	[illegible]	[illegible]
[illegible]	[illegible]	[illegible]	[illegible]	[illegible]	[illegible]	[illegible]	[illegible]
[illegible]	[illegible]	[illegible]	[illegible]	[illegible]	[illegible]	[illegible]	[illegible]
[illegible]	[illegible]	[illegible]	[illegible]	[illegible]	[illegible]	[illegible]	[illegible]
[illegible]	[illegible]	[illegible]	[illegible]	[illegible]	[illegible]	[illegible]	[illegible]
[illegible]	[illegible]	[illegible]	[illegible]	0.	0.	0.	0.

AXIAL DIST METER	AXIAL DIST INCH	AVERAGE ENTHALPY JOULES/KG	AVERAGE ENTHALPY BTU/LB	HTR = CENE WATTS/METER	HTR = CENE BTU/FT-SEC	HTR = RAD WATTS/METER	HTR = RAD BTU/FT-SEC	VOLTAGE VOLTS	EFF
[illegible]	[illegible]	[illegible]	[illegible]	[illegible]	[illegible]	[illegible]	[illegible]	[illegible]	[illegible]

[illegible]

TABLE 9

ARCFLO VERSION 2 RESULTS - CASE 4

AXIAL STATION [illegible] — [illegible] THERMAL ARC WITH AXIAL GAS FLOW

AXIAL DIST	= [illegible] METERS [illegible] INCHES	DIAMETER	= [illegible] METERS [illegible] INCHES
VOLTAGE GRAD	= [illegible] VOLTS/M [illegible] VOLTS/INCH	CURRENT	= [illegible] AMPS
WALL HEAT FLUX	= [illegible] WATTS/M**2 [illegible] BTU/FT2-SEC	FLOW RATE	= [illegible] KG/SEC [illegible] LB/SEC
RADIATION LOSS	= [illegible] PERCENT	TRANS COEFFICIENT	= [illegible] KG/SEC-M**2 [illegible] LB/FT2-SEC
		WALL ENTHALPY	= [illegible] JOULES/KG [illegible] BTU/LB
PRESSURE	= [illegible] ATMS	[illegible]	= [illegible]
[illegible]	= 1	[illegible]	= [illegible]
[illegible]	= [illegible]	[illegible]	= [illegible]
[illegible]	= [illegible]	[illegible]	= [illegible]
[illegible]	= [illegible] DEG	[illegible]	= [illegible]

SPACE AVERAGE ENTHALPY =	[illegible] JOULES/KG	OR	[illegible] BTU/LB
MASS AVERAGE ENTHALPY =	[illegible] JOULES/KG	OR	[illegible] BTU/LB
AVERAGE [illegible] DENSITY =	[illegible] JOULES/M**3	OR	[illegible] BTU/FT**3
TOTAL ENTHALPY [illegible] =	[illegible] JOULES/KG	OR	[illegible] BTU/LB

RADIUS METERS	RADIUS INCH	ENTHALPY JOULES/KG	ENTHALPY BTU/LB	VELOCITY M/S	VELOCITY FT/SEC	MASS FLUX KG/S M**2	MASS FLUX LB/FT2-SEC
0.	0.	[illegible]	[illegible]	[illegible]	[illegible]	[illegible]	[illegible]
[illegible]	[illegible]	[illegible]	[illegible]	[illegible]	[illegible]	[illegible]	[illegible]
[illegible]	[illegible]	[illegible]	[illegible]	[illegible]	[illegible]	[illegible]	[illegible]
[illegible]	[illegible]	[illegible]	[illegible]	[illegible]	[illegible]	[illegible]	[illegible]
[illegible]	[illegible]	[illegible]	[illegible]	[illegible]	[illegible]	[illegible]	[illegible]
[illegible]	[illegible]	[illegible]	[illegible]	[illegible]	[illegible]	[illegible]	[illegible]
[illegible]	[illegible]	[illegible]	[illegible]	[illegible]	[illegible]	[illegible]	[illegible]
[illegible]	[illegible]	[illegible]	[illegible]	[illegible]	[illegible]	[illegible]	[illegible]
[illegible]	[illegible]	[illegible]	[illegible]	[illegible]	[illegible]	[illegible]	[illegible]
[illegible]	[illegible]	[illegible]	[illegible]	[illegible]	[illegible]	[illegible]	[illegible]
[illegible]	[illegible]	[illegible]	[illegible]	[illegible]	[illegible]	[illegible]	[illegible]
[illegible]	[illegible]	[illegible]	[illegible]	[illegible]	[illegible]	[illegible]	[illegible]
[illegible]	[illegible]	[illegible]	[illegible]	[illegible]	[illegible]	[illegible]	[illegible]
[illegible]	[illegible]	[illegible]	[illegible]	[illegible]	[illegible]	[illegible]	[illegible]
[illegible]	[illegible]	[illegible]	[illegible]	[illegible]	[illegible]	[illegible]	[illegible]
[illegible]	[illegible]	[illegible]	[illegible]	[illegible]	[illegible]	[illegible]	[illegible]
[illegible]	[illegible]	[illegible]	[illegible]	[illegible]	[illegible]	[illegible]	[illegible]
[illegible]	[illegible]	[illegible]	[illegible]	[illegible]	[illegible]	[illegible]	[illegible]
[illegible]	[illegible]	[illegible]	[illegible]	[illegible]	[illegible]	[illegible]	[illegible]
[illegible]	[illegible]	[illegible]	[illegible]	[illegible]	[illegible]	[illegible]	[illegible]
[illegible]	[illegible]	[illegible]	[illegible]	[illegible]	[illegible]	[illegible]	[illegible]
[illegible]	[illegible]	[illegible]	[illegible]	[illegible]	[illegible]	[illegible]	[illegible]
[illegible]	[illegible]	[illegible]	[illegible]	[illegible]	[illegible]	[illegible]	[illegible]
[illegible]	[illegible]	[illegible]	[illegible]	[illegible]	[illegible]	[illegible]	[illegible]
[illegible]	[illegible]	[illegible]	[illegible]	[illegible]	[illegible]	[illegible]	[illegible]
[illegible]	[illegible]	[illegible]	[illegible]	0.	0.	0.	0.

AXIAL DIST METER	AXIAL DIST INCH	AVERAGE ENTHALPY JOULE/KG	AVERAGE ENTHALPY BTU/LB	HTR - CONS WATTS/M**2	HTR - CONS BTU/FT2-SEC	HTR - RAD WATTS/M**2	HTR - RAD BTU/FT2-SEC	VOLTAGE VOLTS	EFF
[illegible]	[illegible]	[illegible]	[illegible]	[illegible]	[illegible]	[illegible]	[illegible]	[illegible]	[illegible]

[illegible]

in Figure 21. (These results are from the correlation code which accurately characterizes the ARCFLO Version 2 code over the range of conditions of interest; all other results are directly from the ARCFLO Version 2 code at conditions and geometries close to those of the conceptual design.) From Figure 21, the performance goal can only be achieved at the maximum conditions, and the 5 MW performance at a given constrictor heat flux level is better than that of the 40 MW.

Typical results from the ARCFLO Version 2 code for a location near the downstream end of the constrictor are presented in Tables 8 and 9, respectively. These results are from ARCFLO Version 2 computation Cases 30 and 4 which were used as examples of the radial and axial distribution of properties as presented in Figures 22 through 25. Note that the 5 MW case represents a more severe condition than the 40 MW case (e.g., $\dot{q}$ = 6200 Btu/ft^{2}sec vs. 5100 Btu/ft^{2}sec) and therefore no conclusions from quantitative comparisons are possible.

The radial distributions of enthalpy for both the 5 MW and 40 MW configurations are presented in Figure 22. The centerline enthalpy is almost a factor of two higher than the mass-average enthalpy, and this factor increases with increasing constrictor wall heat flux and decreasing constrictor length.

The axial distribution of radiative and convective constrictor heat flux is presented in Figure 23. The radiative flux is by far the dominant flux, the convective flux being less than 5 percent of the total.

The constrictor pressure drop and efficiency are presented in Figure 24. The efficiency is lower for the 5 MW condition (Case 30) due to the higher constrictor heat flux and the less-than-optimum air flow rate required by the limited voltage capability of the AEDC 5 MW power supply. The smaller pressure drop for the 5 MW case is also due to the lower flow rate and therefore lower mass flux.

The net power input - the power to the gas, $\dot{m}H$ - is presented in Figure 25 as a function of axial distance. The curve shape is the same as that for mass-average enthalpy since concentrated gas injection at the upstream end of the constrictor was assumed for the computations.

A summary of the performance, operating, geometric, and guideline parameters for both arc heaters at the recommended conditions ($\dot{q}$ = 5000 Btu/ft^{2}sec and 150 atm) is presented below:

Parameter	5 MW	40 MW	Design Goal, Constraint, or Recommended/Maximum
$\bar{H}$, Btu/lbm	5,900	5,150	6000 to 8000
p, atm	150	150	150 to 200
$\dot{m}$, lbm/sec	0.25	4.0	--
$\dot{q}$, Btu/ft^{2}sec	5,000	5,000	5000, 10,000
V, kv	9.9	26.3	10 or 30
I, amps	690	3,500	740 or 2000
d, in.	0.70	1.75	--
L, in.	25.5	75.0	--
$\mathcal{E}$, volts/cm	131	133	115/175
ΔV, volts	66	88	100/300
$H\sqrt{p}$, Btu-atm$^{1/2}$/lbm	72,300	63,100	--
I/d, amps/cm	338	338	650
$\mathcal{E}$I, kw/cm	79	399	210/210
VI/($\pi d^2 L/4$), kw/cm^3	37	13	15/40
$(\rho u)_{ave}$, lbm/ft^{2}sec	94	240	200/250

For reference, those 5 MW and 40 MW conditions correspond to throat diameters of 0.19 and 0.75 inches and to exit diameters of 0.25 and 1.00 inches for the exit Mach number of 2, respectively. Note that none of the maximum guideline parameters presented previously are exceeded. Also, operation at the conditions presented in Figure 26 up to flux levels of 10,000 Btu/ft^{2}sec and 200 atm yields acceptable (but in some cases maximum) values of the guideline parameters.

SECTION 9

CONCLUSIONS

The conclusions derived from the program and the recommendations for additional effort are summarized below.

__CONCLUSIONS__

- Accurate characterization of the performance and operating characteristics of constrictor arc heaters, particularly at high pressure, requires proper state-of-the-art modeling of radiation, thermodynamic and transport properties, and turbulence.
- Radiation properties must include contributions from continuum, lines, and bands for the complete spectrum, and radiation transport must consider self-absorption; thermodynamic and transport models must include proper treatment of charged particles; and the turbulent transport model must adequately characterize physical events, including the effects of constrictor wall roughness.
- Valid approximations and techniques are available to reduce computational complexity for radiation without compromise in accuracy; these include a two-band radiation properties model, exponential approximation of radiation transport, and the use of recursion formulas.
- A new computer code, ARCFLO Version 2, which incorporates these proper models and is based on the procedure of Watson and Pegot (Reference 1) has been developed and validated for high pressure (as well as low and moderate pressure) constrictor arc heater applications.
- This new code, relative to the original procedure, predicts that the bulk enthalpy increases at a more rapid rate with axial distance, but reaches a lower value of the asymptotic bulk enthalpy; the maximum practical constrictor length was found to be defined by a constrictor length-to-diameter ratio of 40.
- Radiation is by far the dominant thermal loss mechanism at high pressure.
- For the high Reynolds numbers typical of high-pressure arcs, wall roughness significantly affects wall shear and heat transfer; further characterization is required.

REFERENCES

1. Watson, V. R. and Pegot, E. B., "Numerical Calculations for the Characteristics of a Gas Flowing Axially Through a Constricted Arc," NASA Technical Note D-4042, June 1967.

2. Graves, R. A. and Wells, W. L., "Preliminary Study of a Wall-Stabilized Constricted Arc," NASA Technical Memorandum X-2700, February 1973.

3. Nikuradse, J., "Gesetzmässigkeit der turbulenten Strömung in glatten Rohren." Forschungsheft 356 (1932).

4. Keston, A. S., "Radiant Heat Flux Distribution in a Cylindrically Symmetric Nonisothermal Gas with Temperature Dependent Absorption Coefficient," Journal of Quantitative Spectroscopic and Radiative Transfer, Vol. 8, 1963, pp. 419-434.

5. Chiba, Z., The Study of Heat Transfer with Radiation to Gases in Turbulent Flow Within Tubes, Ph.D. Thesis in Engineering, University of California, Berkeley, September 1972.

6. Hilsenrath, J. and Klein, M., "Tables of Thermodynamic Properties of Air in Chemical Equilibrium Including Second Virial Corrections from 1500°K to 15,000°K," AEDC-TR-65-58 and related publications, Arnold Engineering Development Center, Air Force Systems Command, Arnold Air Force Station, Tennessee, March 1965.

7. Gilmore, F. R., "Thermal Radiation Phenomena. The Equilibrium Thermodynamic Properties of High Temperature Air," DASA 1971-1, 3-27-67-1, Vol. 1, May 1967.

8. Schreiber, P. W., Hunter, A. M., II, and Benedetto, K. R., "Measurement of Nitrogen Plasma Transport Properties," AIAA Journal, Vol. 10, No. 5, May 1972, pp. 670-674.

9. Hermann, W. and Schade, E., Z. Phys., Vol. 233, 1970, p. 333.

10. Morris, J. C., Rudis, R. P., and Yos, J. M., "Measurements of Electrical and Thermal Conductivity of Hydrogen, Nitrogen, and Argon at High Temperatures," The Physics of Fluids, Vol. 13, No. 3, March 1970, pp. 608-617.

11. Asinovsky, E. I., Kirillin, A. V., Pakhomov, E. P., and Shabashov, V. I., "Experimental Investigation of Transport Properties of Low-Temperature Plasma by Means of Electric Arc," Proceedings of the IEEE, Vol. 59, No. 4, April 1971, pp. 592-601.

12. Schreiber, P. W., Hunter, A. M., II, and Benedetto, K. R., "Argon and Nitrogen Plasma Viscosity Measurements," The Physics of Fluids, Vol. 14, No. 12, December 1971, pp. 2696-2702.

13. Schreiber, P. W., Hunter, A. M., II, and Benedetto, K. R., "Electrical Conductivity and Total Emission Coefficient of Air Plasma," AIAA Journal Vol. 11, No. 6, June 1973, pp. 815-821.

14. Capitelli, M. and DeVoto, R. S., "Transport Coefficients of High-Temperature Nitrogen," The Physics of Fluids, Vol. 16, No. 11, November 1973, pp. 1835-1841.

15. Sherman, M. P., "Transport Properties of Partially-Ionized Nitrogen. I. Collision Integrals. II. Method and Results," R65SD43 and R65SD44, NASA Contract NASr-32, Space Sciences Laboratory, Missile and Space Division, General Electric, July-August 1965.

16. Yos, J. M., "Transport Properties of Nitrogen, Hydrogen, and Air to 30,000°K," Technical Memorandum RAD-TM-63-7, Research and Advanced Development Division, Avco Corporation, Wilmington, Massachusetts, March 22, 1963.

17. Peng, T. C. and Pindroh, A. L., "An Improved Calculation of Gas Properties at High Temperatures: Air," Paper No. 1995-61, Fourth Biennial Gas Dynamics Symposium, American Rocket Society, Northwestern University, Evanston, Illinois, August 23-25, 1961. Also Document No. D2-11722, Category Code No. 81205, Boeing Airplane Company, Seattle, Washington, February 1962.

18. Hansen, C. F., "Approximations for the Thermodynamics and Transport Properties of High-Temperature Air." NASA TR R-50, Ames Research Center, Moffett Field, California, 1959.

19. Kendall, R. M., "An Analysis of the Coupled Chemically Reacting Boundary Layer and Charring Ablator, Part V. A General Approach to the Thermochemical Solution of Mixed Equilibrium-Nonequilibrium, Homogeneous or Heterogeneous Systems," Final Report No. 66-7, Part V, NASA Contract NAS9-4599, Aerotherm Corporation, Palo Alto, California, March 14, 1967.

20. Powars, C. A. and Kendall, R. M., "User's Manual, Aerotherm Chemical Equilibrium (ACE) Computer Program," Aerotherm Corporation, Mountain View, California, May 1969.

21. Griem, H. R., Plasma Spectroscopy. McGraw-Hill Book Company, New York, 1964, pp. 137-145.

22. Griem, H. R., "High-Density Corrections in Plasma Spectroscopy," Physical Review, Vol. 128, No. 3, November 1, 1962, pp. 997-1003.

23. Hirschfelder, J. O., Curtiss, C. F., and Bird, R. B., Molecular Theory of Gases and Liquids, John Wiley and Sons, Inc., 1954.

24. Butler, J. N. and Brokaw, R. S., "Thermal Conductivity for Gas Mixtures in Chemical Equilibrium," The Journal of Chemical Physics, Vol. 26, No. 6, June 1957, pp. 1636-1643.

25. Meador, W. E., Jr. and Staton, L. D., "Electrical and Thermal Properties of Plasmas," The Physics of Fluids, Vol. 8, No. 9, September 1965, pp. 1694-1703.

26. Fay, J. A., "Hypersonic Heat Transfer in the Air Laminar Boundary Layer," The High Temperature Aspects of Hypersonic Flow. W. C. Nelson, Ed., The Macmillan Co., New York, pp. 583-605.

27. Liboff, R. L., "Transport Coefficients Determined Using the Shielded Coulomb Potential," The Physics of Fluids, Vol. 2, No. 1, January-February 1959, pp. 40-46.

28. Knof, H., Mason, E. A., and Vanderslice, J. T., "Interaction Energies, Charge Exchange Cross Sections, and Diffusion Cross Sections for N+-N and O+-O Collisions," The Journal of Chemical Physics, Vol. 40, No. 12, June 15, 1964, pp. 3548-3553.

29. Spitzer, L., Jr. and Härm, R., "Transport Phenomena in a Completely Ionized Gas," Physical Review, Vol. 89, No. 5, March 1, 1953, pp. 977-981.

30. Kendall, R. M., Rubesin, M. W., Dahm, T. J., and Mendenhall, M. R., "Mass, Momentum, and Heat Transfer Within a Turbulent Boundary Layer with Foreign Gas Mass Transfer at the Surface," Office of Naval Research and Advanced Research Projects Agency, Washington, D.C., February 1, 1964.

31. Van Driest, E. R., "On Turbulent Flow Near a Wall," Journal of the Aeronautical Sciences, Volume 23, Number 11, November 1956, p. 1007.

32. Bankston, C. A. and McEligot, D. M., "Turbulent and Laminar Heat Transfer to Gases with Varying Properties in the Entry Region of Circular Ducts," International Journal of Heat and Mass Transfer, Volume 13, No. 2, February 1970, pp. 319-344.

33. Graves, R. A. and Wells, W. L., "Preliminary Study of a Wall-Stabilized Constricted Arc," NASA Technical Memorandum X-2700, February 1973.

34. Launder, B. E. and Spalding, D. B., Mathematical Models of Turbulence, Academic Press, London, 1972.

35. Rotta, J. C., "Turbulent Boundary Layers in Incompressible Flow," in Progress in Aeronautical Sciences, Volume 2 (edited by A. Ferri, D. Kuchemann, and L. H. G. Sterne), The Macmillan Company, New York, 1962.

36. Spalding, D. B., Launder, B. E., Morse, A. P., and Maples, G., "Combustion of Hydrogen-Air Jets in Local Chemical Equilibrium," NASA Contractor Report CR-2407, June 1974.

37. Winovich, W., "On the Equilibrium Sonic-Flow Method for Evaluating Electric-Arc Air-Heater Performance," NASA TN D-2132, March 1964.

APPENDICES

APPENDIX A

NONGRAY, NONHOMOGENEOUS RADIATIVE TRANSFER IN A CONSTRICTOR ARC

The ability to predict the local radiative heat flux is important in the design and operation of a wall-stabilized constrictor arc. Such a prediction is doubly complicated due to the nongray nature of the radiating medium and due to the geometry. Further complications are encountered when the participating medium considered is nonhomogeneous. Several simplifying assumptions which are unrealistic at high pressure were introduced in the earlier analyses (References A-1, A-2). The medium was considered to be:

- Optically thin so that the interlayer absorption could be neglected
- Gray so that spectral dependency of the radiative properties could be ignored.

In this analysis the nongray nature of the radiating medium is taken into account and also the radiative properties are allowed to vary spatially. Moreover, this analysis is not limited either to optically thin or optically thick conditions. The local radiant heat flux equations are derived from basic principles. An exponential kernel approximation is introduced which simplifies the radiant flux equations, and the resulting equations are then cast in terms of an optical depth parameter. A brief description of the numerical scheme is given and the results obtained are compared with other investigations.

ANALYSIS

The governing equation for radiative transfer in an absorbing and emitting medium is the equation of transfer, i.e.,

$$\frac{dI_\nu}{ds} = \kappa_\nu (B_\nu - I_\nu) \qquad \text{(A-1)}$$

where B_ν is the Planck black body spectral intensity, I_ν is the spectral intensity traveling along a ray s and κ_ν is the spectral mass absorption coefficient corrected for induced emission.

The spectral radiative flux $q_\nu(r)$ at any radial location r may be expressed as:

$$q_\nu(r) = \int_\Omega I_\nu \cos\theta \, d\Omega \tag{A-2}$$

where θ is the angle between the ray and the outward normal to the cylindrical surface and Ω is the solid angle. The cylindrical geometry and coordinate system are shown in Figure A-1.

Equation (A-1) may be formally integrated and substituted into Equation (A-2) to yield for $q_\nu(r)$ (References A-3, A-4)

$$q_\nu(r) = 4\int_0^{\pi/2} \cos\gamma \Bigg\{ B_\nu(R) D_3 \Bigg(\int_0^{(R^2-r^2\sin^2\gamma)^{1/2}} \mu(y)dy + \int_0^{r\cos\gamma} \mu(y)dy \Bigg)$$

$$+ \int_0^{(R^2-r^2\sin^2\gamma)^{1/2}} B_\nu(y)\mu(y) D_2 \Bigg(\int_0^{y} \mu(y')dy' + \int_0^{r\cos\gamma} \mu(y)dy \Bigg) dy$$

$$+ \int_0^{r\cos\gamma} B_\nu(y)\mu(y) D_2 \Bigg(\int_y^{r\cos\gamma} \mu(y')dy' \Bigg) dy \Bigg\} d\gamma$$

$$- 4\int_0^{\pi/2} \cos\gamma \Bigg\{ B_\nu(R) D_3 \Bigg(\int_{r\cos\gamma}^{(R^2-r^2\sin^2\gamma)^{1/2}} \mu(y)dy \Bigg)$$

$$+ \int_{r\cos\gamma}^{(R^2-r^2\sin^2\gamma)^{1/2}} B_\nu(y)\mu(y) D_2 \Bigg(\int_{r\cos\gamma}^{y} \mu(y')dy' \Bigg) dy \Bigg\} d\gamma \tag{A-3}$$

where

$$y = (r'^2 - r^2\sin^2\gamma)^{1/2} \tag{A-4}$$

$$y' = (r''^2 - r^2\sin^2\gamma)^{1/2} \tag{A-5}$$

and

$$D_n(x) = \int_0^1 \frac{z^{n-1}}{\sqrt{1 - z^2}} \exp\left(- \frac{x}{z}\right) dz \tag{A-6}$$

In arriving at Equation A-3, it is assumed that the nonscattering medium is bounded by a black surface and is in local thermodynamic equilibrium. Further, it is assumed that axial variation of temperature is small and can be neglected. This approximation is consistent with the boundary-layer simplifications adopted in this report.

The $D_n(x)$ functions defined above are known as exponential integral functions and are peculiar to the cylindrical geometry. The $D_n(x)$ functions have the following properties:

$$\frac{d}{dx} D_n(x) = - D_{n-1}(x) \ , \ n > 1 \tag{A-7}$$

and

$$D_{n+1}(x) = \int_x^\infty D_n(x) dx \tag{A-8}$$

It is common practice in radiation analyses involving either plane-parallel geometry or cylindrical geometry to introduce the exponential kernel approximation. Accordingly, following References A-4 and A-5, we have

$$D_3(x) \doteq a \ e^{-bx} \tag{A-9}$$

where the constants a and b are selected such that they best fit Equation (A-6) for n = 3. In this study, numerical values to a and b are assigned to be

$$a = 1/4 \tag{A-10}$$

and

$$b = 5/4 \tag{A-11}$$

The local spectral radiant heat flux $q_\nu(r)$ is written as

$$q_\nu(r) = q_\nu^+(r) - q_\nu^-(r) \tag{A-12}$$

where $q_\nu^+(r)$ is the radiant flux directed away from the location r and $q_\nu^-(r)$ is the radiant flux directed towards the location r.

The approximate form of the directional spectral fluxes may be written, in terms of angular directional fluxes $G(r,\gamma)$, i.e.,

$$q_\nu^\pm(r) = \int_0^{\pi/2} \cos\gamma \; G^\pm(r,\gamma)\, d\gamma \tag{A-13}$$

where

$$G^+(r,\gamma) = E_\nu(R) \exp\left\{-\left[\tau\left((R^2 - r^2\sin^2\gamma)^{1/2}\right) + \tau(r\cos\gamma)\right]\right\}$$

$$+ \int_0^{\tau\left((R^2-r^2\sin^2\gamma)^{1/2}\right)} E_\nu(t) \exp\left\{-\left(t + \tau(r\cos\gamma)\right)\right\} dt$$

$$+ \int_0^{\tau(r\cos\gamma)} E_\nu(t) \exp\left\{-\left(\tau(r\cos\gamma) - t\right)\right\} dt \tag{A-14}$$

$$G^-(r,\gamma) = E_\nu(R) \exp\left\{-\left[\tau\left((R^2 - r^2\sin^2\gamma)^{1/2}\right) - \tau(r\cos\gamma)\right]\right\}$$

$$+ \int_{\tau(r\cos\gamma)}^{\tau\left[(R^2-r^2\sin^2\gamma)^{1/2}\right]} E_\nu(t) \exp\left\{-\left(t - \tau(r\cos\gamma)\right)\right\} dt \tag{A-15}$$

where $\tau(y)$ is the optical depth defined as

$$\tau(y) = b\int_0^y \omega(y')\,dy' \tag{A-16}$$

and

$$E_\nu(y) = \pi B_\nu(y) \qquad \text{(A-17)}$$

is the black body emissive power.

Equations (A-12) to (A-17) complete the formulation of the spectral radiant flux equations for a nonhomogeneous medium enclosed in a black-walled constrictor. It is of interest to examine the physical meaning of individual terms in Equations (A-14) or (A-15). The first term in Equation (A-14) is the wall emission that has been attenuated by the gas medium as the radiation passes through Points B and C (see Figure A-1). The second term represents the emission by the gas between Points B and E attenuated as the radiation passes from the point of emission to Point C. Radiant energy emitted by the gas volume between Points E and C, attenuated as it passes from the point of emission to Point C is given by the third term of Equation (A-14).

Analytical solutions to the above equations are difficult to obtain. Hence, a numerical scheme was devised, which is simple, computationally fast, and yet accurate. In the following, the numerical method used is described.

EVALUATION OF RADIANT FLUX INTEGRALS

Let the radius of the constrictor be divided into N-1 radial subdivisions. The wall is located at $r_{i=N} = R$ and the axis of the constrictor at $r_{i=1} = 0$. As shown in Figure A-2, consider the plane perpendicular to the axis of the constrictor. Let j and i be the indices on the radial mesh points along the axis and perpendicular to the axis of the constrictor respectively.

To evaluate the angular directional fluxes $G^+(r,\psi)$, $G^-(r,\psi)$, and optical depth τ the following procedure is adopted. Consider the plane perpendicular to the radius vector at any r_j. As shown in Figure A-2, let $\theta_{i,j}$ be the angle between the radius r_i and the plane. In evaluating the optical depth τ, following Nicolet (Reference A-6), it is assumed that the spectral mass absorption coefficient κ at any value of y may be written as

$$\kappa(y) = \kappa(y_{i,j}) \left[\frac{\kappa(y_{i+1,j})}{\kappa(y_{i,j})} \right]^{\frac{y - y_{i,j}}{y_{i+1,j} - y_{i,j}}} \qquad \text{(A-18)}$$

where the quantities $Y_{i,j}$ and $Y_{i+1,j}$ are given by

$$Y_{i,j} = (r_i^2 - r_j^2)^{1/2} \tag{A-19a}$$

$$Y_{i+1,j} = (r_{i+1}^2 - r_j^2)^{1/2} \tag{A-19b}$$

At any value of j, the optical depth increment is, from Equations (A-16) and (A-18)

$$\tau_{i+1,j} - \tau_{i,j} = \Delta\tau_{i+1,i,j} = b\omega(Y_{i,j})(Y_{i+1,j} - Y_{i,j}) \times \frac{\left[\dfrac{\omega(Y_{i+1,j})}{\omega(Y_{i,j})} - 1\right]}{\ln \dfrac{\omega(Y_{i+1,j})}{\omega(Y_{i,j})}} \tag{A-20}$$

Combining Equations (A-20), (A-14), (A-15), and employing a logarithmic interpolation in terms of optical depth for the black body emissive power distribution, the following recursion relations are obtained for the angular directional fluxes. At any value of j

$$G_{i,j}^{+} = e^{-\Delta\tau_{i,i-1,j}} \left\{ G_{i-1,j}^{+} + \frac{\Delta\tau_{i,i-1,j}\left(E_{i,j}\, e^{\Delta\tau_{i,i-1,j}} - E_{i-1,j}\right)}{\Delta\tau_{i,i-1,j} + \ln \dfrac{E_{i,j}}{E_{i-1,j}}} \right\} \tag{A-21}$$

and

$$G_{i-1,j}^{-} = e^{-\Delta\tau_{i,i-1,j}} \left\{ G_{i,j}^{-} - \frac{\Delta\tau_{i,i-1,j}\left(E_{i,j} - E_{i-1,j}\, e^{\Delta\tau_{i,i-1,j}}\right)}{\Delta\tau_{i,i-1,j} - \ln \dfrac{E_{i,j}}{E_{i-1,j}}} \right\} \tag{A-22}$$

Starting at the wall, $i=N$, from the known boundary condition, values of $G_{i,j}^{-}$ can be calculated. To evaluate $G_{i,j}^{+}$ the cylindrical symmetry condition is invoked. Equations (A-21) and (A-22) may be substituted into Equation (A-1) to yield the following equation for the directional spectral fluxes:

$$q_\nu^+(r_i) = \sum_{j=2}^{j=N} \left(\frac{G^+_{i,j} + G^+_{i,j-1}}{2} \right) (\sin \gamma_{i,j} - \sin \gamma_{i,j-1}) \qquad \text{(A-23)}$$

RADIATIVE PROPERTIES OF HIGH TEMPERATURE AIR

Radiation properties of high temperature air are complex due to the strong variation of spectral absorption coefficient with wavelength over the spectrum. The variations in the spectral absorption coefficient are due to bound-free, bound-bound, and free-free transitions.

Detailed calculations of the spectral absorption coefficient are not warranted for this study since they complicate the calculation scheme and also increase the computing time involved considerably. A simple band model approach was adopted to characterize the variation of the absorption coefficient with wavelength.

The spectrum (0 to 100 ev) is divided into two gray bands; one band covers the range from 0 to 10.5 ev, and the other band extends from 10.5 ev to 100 ev. Within each band the absorption coefficient is, then, invariant with wavelength.

Values of absorption coefficient for various pressures and temperatures are obtained from several sources. The Rosseland mean free paths from Johnston and Platas (Reference A-7) are used for the low frequency band. Continuum absorption coefficient values are obtained from Reference (A-8) for the high frequency band. For the temperature range from 4000°K to 10,000°K values of absorption coefficient are extracted from emissivity data reported by Faberman and Mnatsakanjan (Reference A-9). Figures A-3 and A-4 show the variation of absorption coefficient for the two bands with temperature for different pressures.

Once the band model is selected and the radiative properties are available, calculation of total radiative flux is simple. Total radiative flux at any radius r is obtained by integrating Equation (A-23) over the frequency, i.e.

$$q_R(r) = \int_0^\infty q_\nu(r)\, d\nu \qquad \text{(A-24)}$$

Under the band model assumption the total radiative flux may be written as

$$q_R(r) = \sum_{i=1}^{m} q_i(r) \qquad \text{(A-25)}$$

where m is the total number of bands (in this study m = 2) and $q_i(r)$ is the radiant flux contribution from the i^{th} band to the total flux which is given by

$$q_i(r) = \int_{\Delta\nu_i} q_\nu(r)\, d\nu \qquad \text{(A-26)}$$

where $\Delta\nu_i$ is the band-width for the i^{th} band.

Let $W_i(r)$ be the local band weighting function and defined by

$$W_i(r) = \int_{\Delta\nu_i} E_\nu(r)\, d\nu / \sigma T^4(r) \qquad \text{(A-27)}$$

Equation (A-27) may be re-written in terms of a fractional function of the first kind (Reference A-10) once the band limits of the i^{th} band are specified. Note that the local band weighting function $W_i(r)$ has numerical values between 0 and 1. Combining Equations (A-27), (A-18), and (A-15) and substituting into Equation (A-26) leads to the necessary equation for the flux from the i^{th} band.

RESULTS AND DISCUSSION

Radiant heat flux distributions in a cylindrical medium are calculated for the case of a gray gas with a single band. The temperature distribution is assumed to be linear with radius and the absorption coefficient of the medium is assumed to be uniform. The calculated radial radiant heat flux distributions are shown in Figure A-1, and are compared with exact calculations of Keston (Reference A-1). Keston employed a numerical integration scheme to evaluate the exponential integral functions $E_n(x)$, whereas, in the present calculational scheme, as mentioned earlier, an exponential kernel approximation is used. Figure A-4 compares the results of the present scheme with the results

of Keston (Reference A-3) and Chiba (Reference A-11). Chiba used a value of $a = 1$ and $b = 5/4$ in the exponential kernel approximation for $D_2(x)$, whereas, in the present study $a = 5\pi/16$ and $b = 5/4$ are assigned. It is seen that the results obtained by the present calculational method compare favorably with the approximate results of Chiba and the results are in good agreement with the exact calculations of Keston (Reference A-3).

One of the inherent weaknesses in the present method is that the predicted flux near the axis of the constrictor is less accurate. One way to increase the accuracy is to have a finer radial mesh near the axis of the constrictor. The advantage of the present computational scheme is that the use of recursion relations is much superior compared to directly evaluating the radiant flux equations by, say, a numerical integration scheme. The computational algorithm is made simple by eliminating the integrations required over the angular and radial coordinates.

The strength of the present approach lies in the fact that it can be used to predict radial radiative heat fluxes for all optical conditions of interest. This method can be used to determine the effect of "self-absorption" of the cold gas near the wall. The present method can be easily extended to include multi-band gases and mixtures of gases as well.

REFERENCES FOR APPENDIX A

A-1. Watson, V. R. and Pegot, E. B., "Numerical Calculations for the Characteristics of a Gas Flowing Axially Through a Constricted Arc," NASA TN D-4042, June 1967.

A-2. Graves, R. A. and Wells, W. L., "Preliminary Study of a Wall-Stabilized Constricted Arc," NASA TM X-2700, February 1973.

A-3. Keston, A. S., "Radiant Heat Flux Distribution in a Cylindrically Symmetric Nonisothermal Gas with Temperature Dependent Absorption Coefficient," Journal of Quantitative Spectroscopic and Radiative Transfer, Vol. 8, 1968, pp. 419-434.

A-4. Wassel, A. T. and Edwards, D. K., "Molecular Gas Band Radiation in Cylinders," Journal of Heat Transfer, Transactions of ASME, Vol. 96, 1974, pp. 21-26.

A-5. Habib, I. S. and Greif, R., "Nongray Radiative Transport in a Cylindrical Medium," Journal of Heat Transfer, Transactions of ASME, Vol. 92, 1970, pp. 28-32.

A-6. Nicolet, W. E., "Methods for the Prediction of Stagnation Point Heating in the Hypervelocity Entry Environment," Submitted for publication.

A-7. Johnston, R. R. and Platas, O. R., "Atomic Line Transitions and Radiation from High Temperature Air," LMSC Final Report N-3L-70-2, Lockheed Palo Alto Research Laboratory, December 1970.

A-8. Johnston, R. R. and Platas, O. R., "Atomic Line Transitions and Radiation from High Temperature Air," LMSC Technical Report N-3L-69-1, Lockheed Palo Alto Research Laboratory, July 1969.

A-9. Biberman, L. M. and Mnatsakanyan, A. Kh., "Optical Properties of Air in the Temperature Range 4000°K to 10,000°K," Translated from Teplofizika Vysokikh Temperatur, Vol. 4, pp. 148-159, 1966.

A-10. Edwards, D. K., Denny, V. E., and Mills, A. F., Transport Processes, Holt, Rinehart and Winston, New York, 1973, pp. 175-176.

A-11. Chiba, Z., The Study of Heat Transfer with Radiation to Gases in Turbulent Flow within Tubes, Ph.D. Thesis in Engineering, University of California, Berkeley, September 1972.

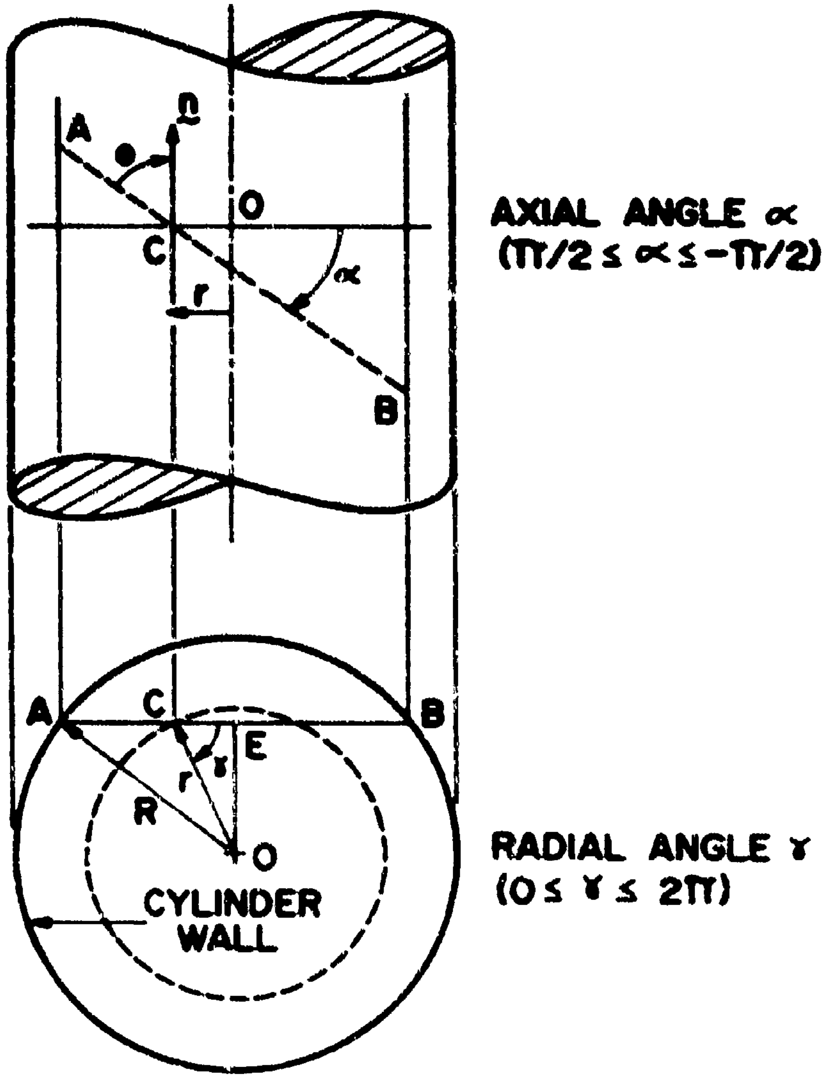

Figure A-1. Cylindrical geometry and coordinate system

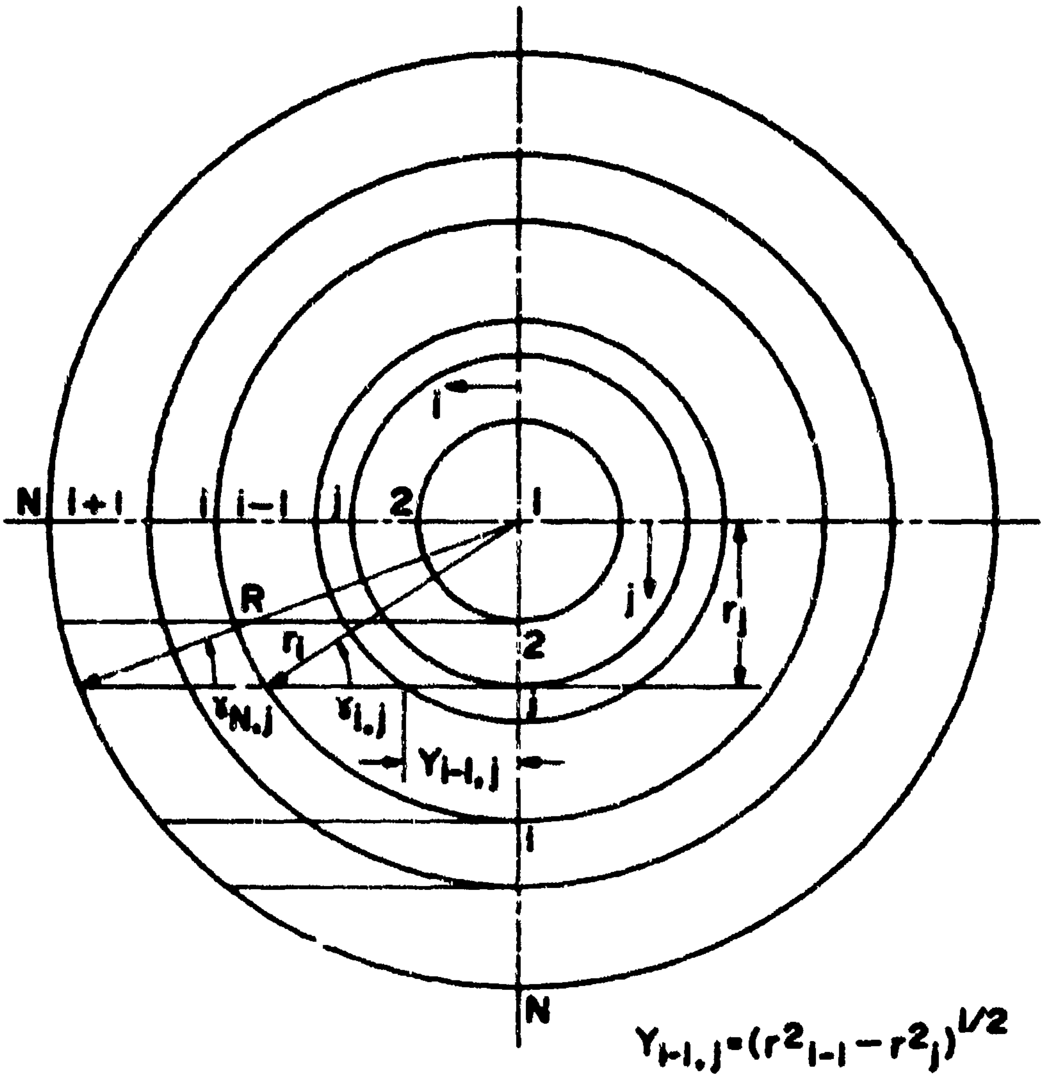

Figure A-2. Radial mesh distribution

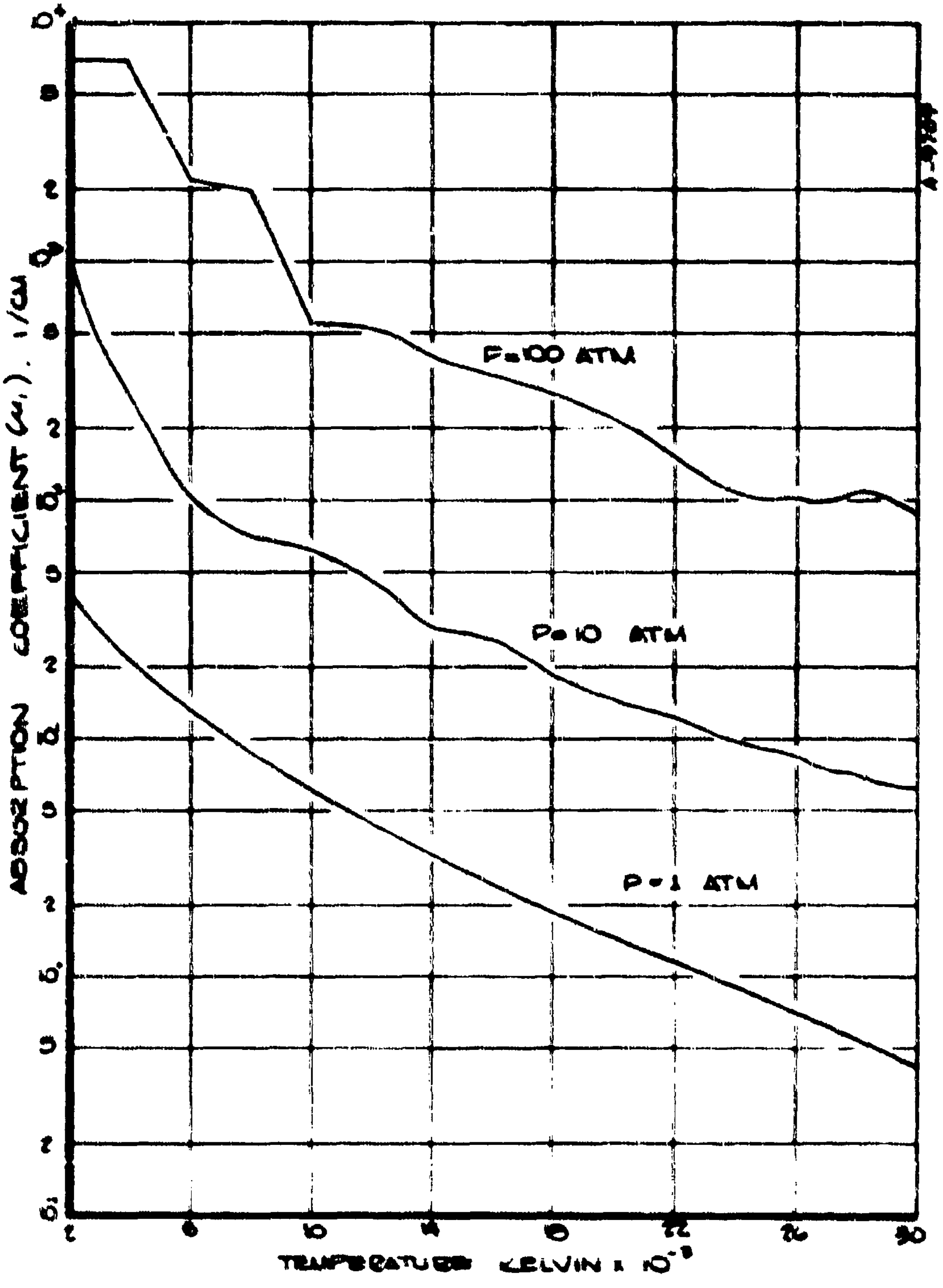

Figure 4-3. High frequency band (10.5 ev - 100 ev) absorption coefficient

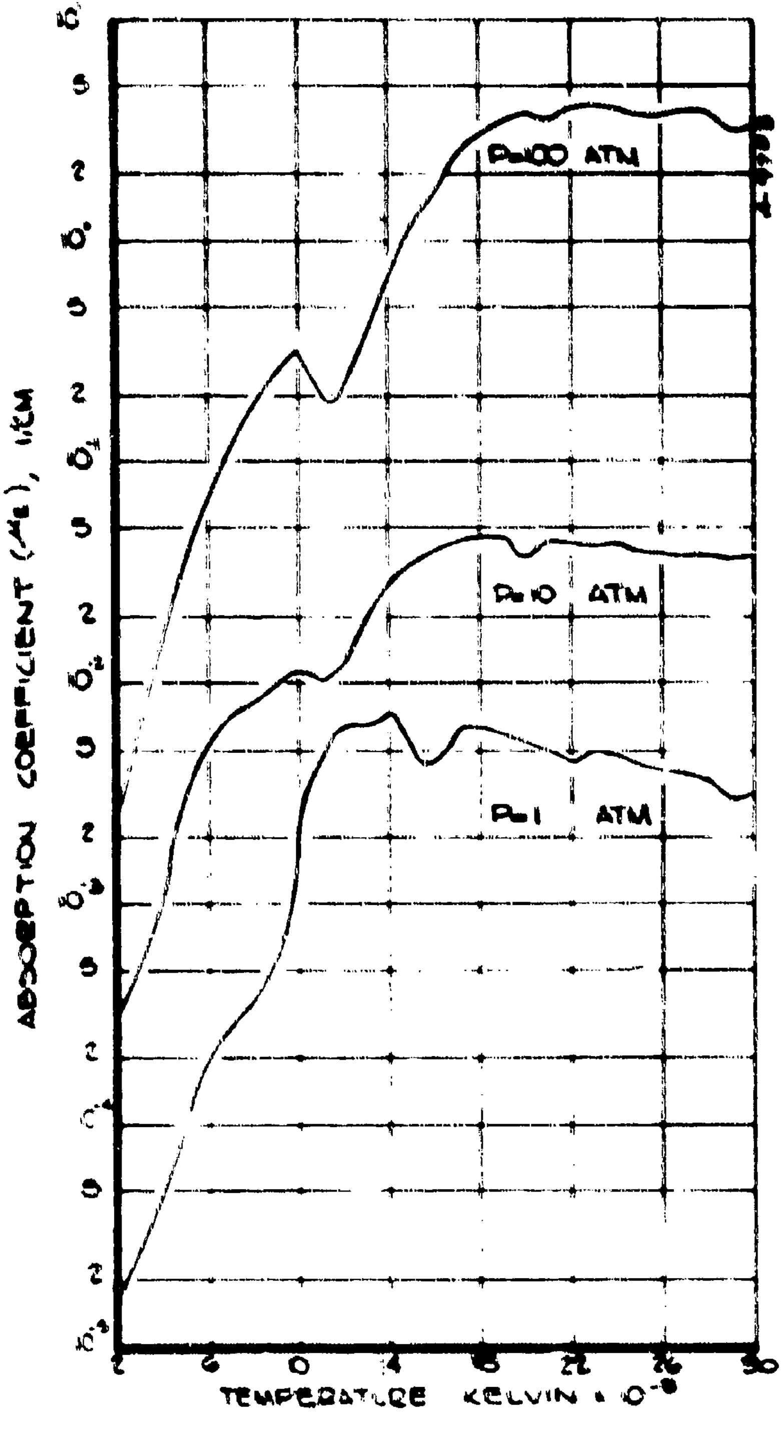

Figure 3-8. Low frequency band ([illegible] ev - 10.5 ev) absorption coefficient

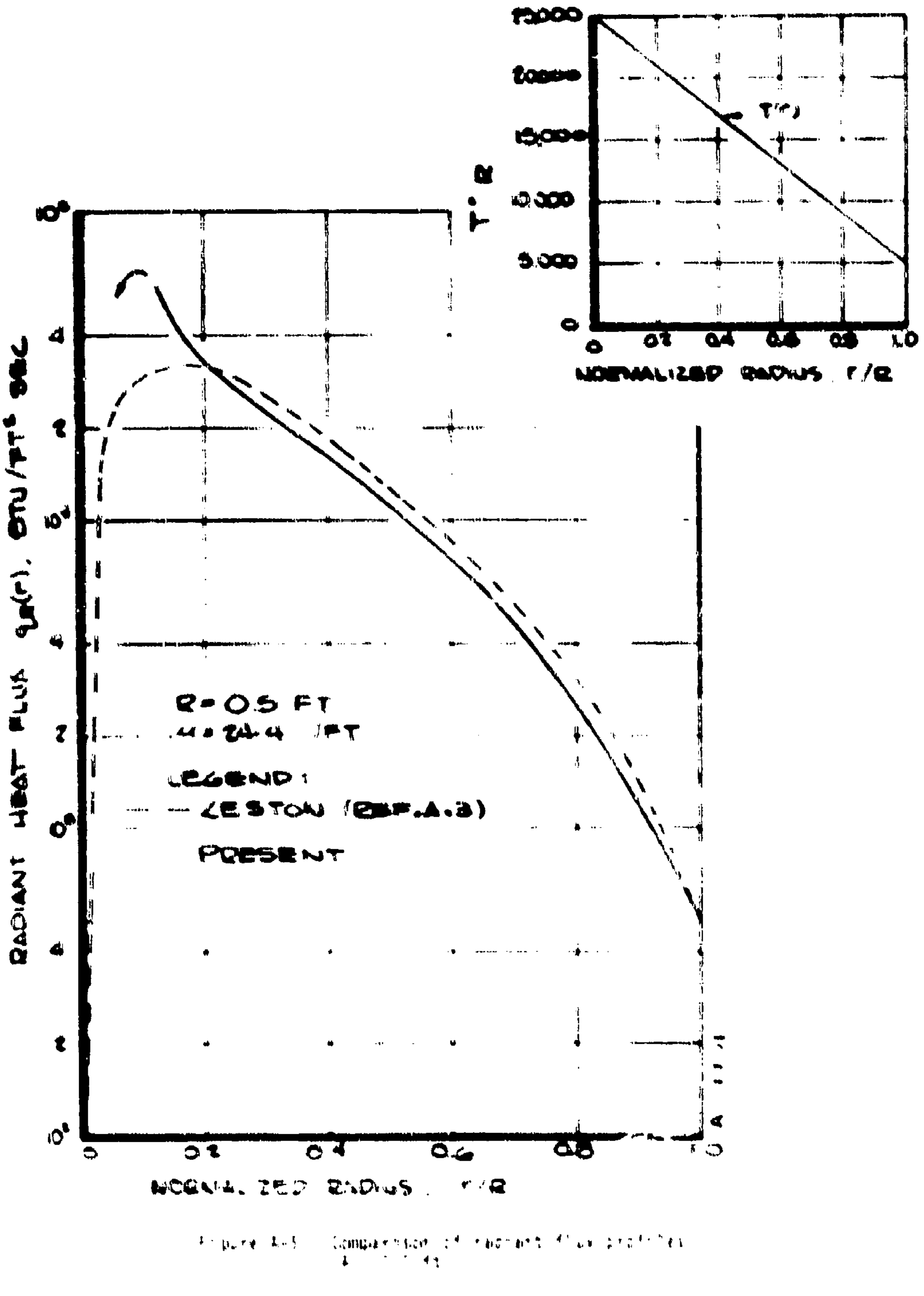

Figure A-5. Comparison of radiant flux profiles [illegible]

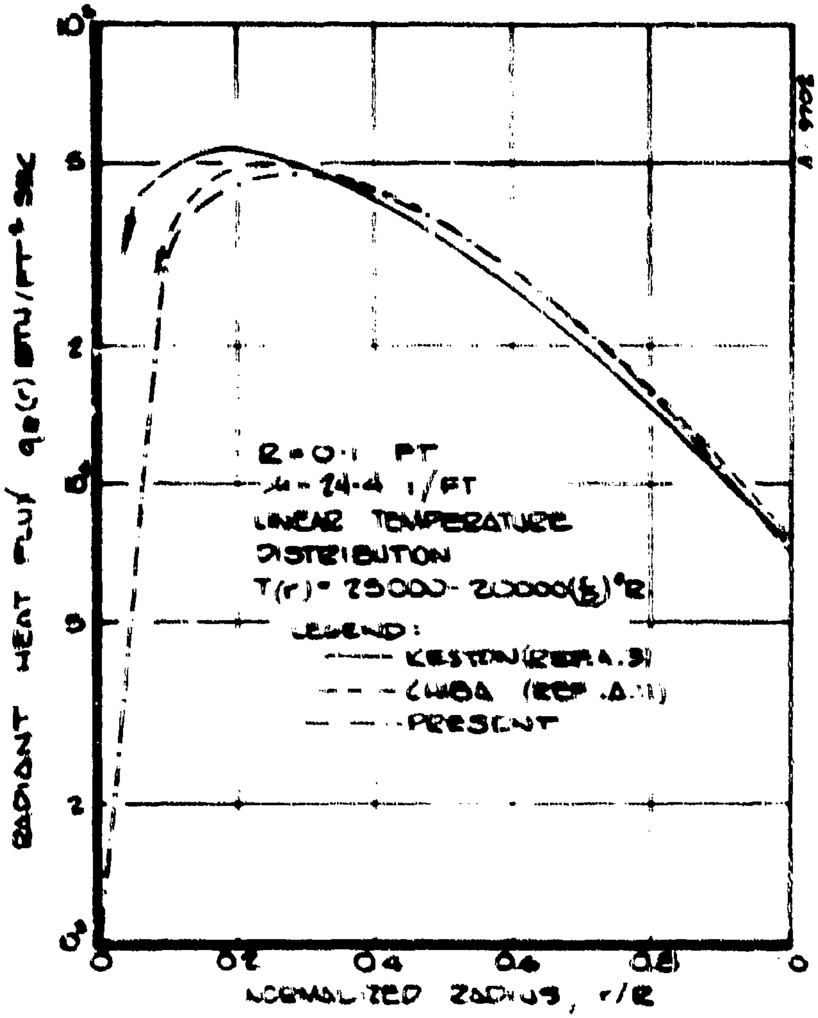

Figure A-6. Comparison of radiant flux profiles (R = 0.1 ft)

APPENDIX B

THERMODYNAMIC AND TRANSPORT PROPERTIES

Both Versions 1 and 2 of the ARCFLO code require input of thermodynamic and transport properties in tabular format, with pressure and temperature as the independent variables. The property tables are arranged in constant-pressure groups, with each subtable for a given pressure extending over a wide range of temperatures. Version 1 accepts data at only two pressures, and in the original work of Watson and Pegot (Reference B-1) pressures of 1 and 10 atm were considered. Version 2 of the code accepts up to six constant-pressure tables, and in this work pressures of 1, 10, 50, 100, 150, and 200 atm were considered, over the temperature range 1000°K $\leq T \leq$ 30,000°K. This appendix discusses in detail the methods used to generate the property tables for the six pressures of interest.

B.1 THERMODYNAMIC PROPERTIES

The thermodynamic properties ρ, h, and X_i are calculated using the Aerotherm Chemical Equilibrium (ACE) computer program (References B-2, B-3), modified to include the Debye-Huckel correction. This subsection presents a brief summary of the ACE formulation for equilibrium gas mixtures. Also, incorporation of the Debye-Huckel corrections into the ACE formulation is described. Finally, the resulting predictions for ρ, h, and X_i as a function of p and T are compared with values available in the literature.

First, the unmodified ACE treatment is summarized. Consider a gas mixture comprised of J species N_j, $j = 1, 2, \ldots, J$. In this system there will exist, in the general case, I set of independent equilibrium reactions. The number of such reactions is usually equal to the total number of species less the number of elements. For computational purposes, a set of species in the system is preselected and the formation reactions of all other species from this base set represent the independent set of equilibrium reactions:

$$\sum_{j=1}^{J} \nu_{ij} N_j \rightleftharpoons N_i \qquad \text{(B-1)}$$

where the summation is over the I base species M_i, $i = 1, 2, \ldots, I$, and the ν_{ji} are stoichiometric coefficients of the formation reactions. The number of base species, I, is equal to the number of elements in the system. The number of independent reactions is then equal to J-I, where $j = I+1, I+2, \ldots, J$. Note that $I \leq J$.

The most stable (equilibrium) state of this system, if it is maintained at constant temperature and pressure, is one for which the Gibbs free energy of the system is at a minimum (Reference B-4). Therefore, associated with the general formation reaction of Equation (B-1) is the equilibrium constraint

$$\bar{G}_j = \sum_{i=1}^{I} \nu_{ji} \bar{G}_i \tag{B-2}$$

If the gas mixture is ideal and each species subgas follows the perfect gas thermal equation of state, then the partial molal Gibbs free energy (chemical potential) for species j in the mixture is given by

$$\bar{G}_j = \bar{G}_j^{o} + R_u T \ln p_j \tag{B-3}$$

Equations (B-2) and (B-3) can be combined to give an expression for the equilibrium constant for each independent reaction specified by Equation (B-1):

$$\ln K_{p_j} = \ln p_j - \sum_{i=1}^{I} \nu_{ji} \ln p_i \tag{B-4}$$

where

$$\ln K_{p_j}(T) = \frac{1}{R_u T} \left(-\bar{G}_j^{o} + \sum_{i=1}^{I} \nu_{ji} \bar{G}_i^{o} \right) \tag{B-5}$$

Equation (B-4) can be written for each of the J-I independent reactions, giving J-I equations in the J unknown specie partial pressures.

An additional equation relating the partial pressures is the requirement that their sum equal the total system pressure.

$$p = \sum_{j=1}^{J} p_j \tag{B-6}$$

The remaining I-1 equations required to complete the formulation for closed-system gas mixtures are obtained from element conservation equations.

The equilibrium formulation just described is based on the assumption that the various molecules are noninteracting except for brief binary encounters which are required to establish chemical and thermal equilibrium. That is, for a given particle the time between collisions is much greater than the time involved in collisions. From another point of view, the particle interaction potentials are small relative to their mean thermal energies. These restrictions are applicable to a low-density gas mixture comprised of electrically neutral particles (i.e., an ideal mixture of thermally perfect gases).

Particle interaction potentials become important whenever they are strong enough to influence the particle over a large portion of its trajectory. This can occur when the gas mixture is extremely dense, in which case the mean distance between particles is always so small that they are in the force field of adjacent particles. It can also occur if charged particles are present in the mixture, since the Coulomb interaction potential between two charged particles is proportional to the inverse of their separation distance and, consequently, has a much greater range than the repulsive potential between two neutral particles which typically varies as the inverse of their separation distance to the sixth or greater power. In this work, particle potential energies are important because charged particles are present. The Debye-Huckel theory described below is used to treat this phenomena. When gas densities are so high that even neutral particle interaction potentials influence the gas state, the second and higher virial corrections must be considered in the equation of state (Reference B-5). However, densities of interest here were never high enough to cause these virial corrections to be significant.

As discussed in Reference B-6, in a plasma particles with charge of one sign tend to be surrounded by particles with charge of the opposite sign due to the attractive Coulomb forces. Thus, although the plasma can be neutral on a macroscopic scale, it is polarized on a microscopic scale. Energy of [illegible] is associated with this polarization. The polarization energy is generated at the expense of the electron binding energies. In other words the ionization energies are reduced relative to their values associated with isolated particles. The energy of polarization and associated reduction of ionization energies influence all aspects of the gas mixture, including composition, pressure, and thermodynamic properties.

The reduction in ionization energy can be derived in a purely (macroscopic) thermodynamic manner by extremizing the system Helmholtz free energy with respect to ionization (Reference B-7), or (microscopically) by solving Poisson's equation for the potential in the neighborhood of an ion surrounded by electrons (Reference B-6). In either case, it is found that the reduction is a function of the temperature of the gas and the charged species number densities:

$$\Delta I_j = 2(z_j + 1)\, e^3 \left(\frac{\pi}{kT}\right)^{1/2} \left(n_e + \sum_{j=1}^{J} z_j^2 n_j\right)^{1/2} \tag{B-7}$$

Equation (B-7) is written in cgs units, and $z_j = 0$ for neutral atom j, $z_j = 1$ for singly-ionized atom j, etc.

The effect of the ionization potential lowering on mixture composition can be treated by introducing a correction factor to the equilibrium constant of Equation (B-4) when written for ionizing reactions. Equation (B-4) is then written as

$$\ln K_{p_j}^{L} = \ln K_{p_j} L_j = \ln p_j - \sum_{i=1}^{I} \nu_{ji} \ln p_i \tag{B-8}$$

Assuming the base species I are comprised of the neutral atoms and the free electron, the correction factor takes the form

$$\ln L_j = (z_j + 1)\, e^3 \left(\frac{\pi p_e}{(kT)^3}\right)^{1/2} \left(n_e + \sum_{j=1}^{J} z_j^2 n_j\right)^{1/2} \tag{B-9}$$

Equation (B-9) can be derived by starting with the Saha equation, which relates the number density of the i^{th} specie in the $(z + 1)^{st}$ ionization stage, n_i^{z+1}, to the number density of the same specie in the z^{th} ionization stage, n_i^z, and the number density of the free electrons, n_e

$$\frac{n_e n_i^{z+1}}{n_i^z} = \frac{2 Q_i^{z+1}}{Q_i^z} \left(\frac{2\pi m_e kT}{h^2}\right)^{3/2} \exp\left(-I_i^z/kT\right) \tag{B-10}$$

If it is assumed that the lowering of the ionization potentials of the j^{th} specie in the z^{th} and $(z+1)^{st}$ ionization stages has a negligible influence on their respective partition functions, then Equation (B-10) can be modified to account for the ionization potential lowering by simply replacing I_j^z with $I_j^z - \Delta I_j^z$, with ΔI_j^z given by Equation (B-7). When Equation (B-10) is generalized to the base specie formulation on which Equation (B-4) is structured, by writing

$$\frac{(n_e)^{z+1} n_j^{z+1}}{n_j^o} = \prod_z \frac{n_e n_j^{z+1}}{n_j^z} \qquad \text{(B-11)}$$

with each term on the right-hand side of Equation (B-11) given by Equation (B-10) with $I_j^z - \Delta I_j^z$ in place of I_j^z, the correction factor given by Equation (B-9) falls out.

The Debye-Hückel corrections to the remaining thermodynamic properties are derived in References B-8 and B-7. Each mixture property ϕ is assumed to be a summation of the unperturbed (uncorrected) value plus a contribution due to Coulomb interactions:

$$\phi = \phi_o + \phi_c \qquad \text{(B-12)}$$

Thus, the internal energy per unit volume is given by

$$U = U_o + U_c \qquad \text{(B-13)}$$

where

$$U_c = -e^3 \left(\frac{\pi}{kT}\right)^{1/2} \left(\frac{P_o}{kT}\right)^{3/2} \left(X_e + \sum_{j=1}^{J} z_j^2 X_j\right)^{3/2} \qquad \text{(B-14)}$$

Equation (B-14) is again obtained by solving Poisson's equation for the potential distribution in the neighborhood of a single charged particle surrounded by a spherically symmetric cloud of charged particles of opposite sign (References B-6, B-7). The Helmholtz free energy is given by

$$F = U - TS = F_o + F_c \qquad \text{(B-15)}$$

and, since

$$S = - \left.\frac{\partial F}{\partial T}\right|_{v,n_j} \tag{B-16}$$

one can write

$$F_c = U_c + T \frac{\partial F_c}{\partial T} = \frac{2}{3} U_c \tag{B-17}$$

Once F_c is known, the correction to mixture entropy can be obtained:

$$S = S_o + S_c \tag{B-18}$$

where

$$S_c = \frac{1}{T} (U_c - F_c) = \frac{1}{3} \frac{U_c}{T} \tag{B-19}$$

Also, the pressure correction is given as

$$p = p_o + \Delta p \tag{B-20}$$

where, since

$$p = - \left.\frac{\partial (Fv)}{\partial v}\right|_{T,n_j} \tag{B-21}$$

one can write

$$\Delta p = - \frac{\partial (F_c v)}{\partial v} = - F_c - v \frac{\partial F_c}{\partial v} = \frac{1}{2} F_c = \frac{1}{3} U_c \tag{B-22}$$

since F_c is proportional to $v^{-1/3}$ (see Equations (B-17) and (B-14) and note that $X_j p_o/kT = v^{-1}$). Finally, the correction to the mixture enthalpy is given as

$$H = H_o + H_c \tag{B-23}$$

where, since

$$H = U + p \tag{B-24}$$

it follows that

$$H_c = U_c + \Delta p = \frac{4}{3} U_c \tag{B-25}$$

In Equation (B-20) above, p_o is the so-called "thermal" pressure. Since Δp is directly proportional to U_c and U_c is a negative quantity, it follows that the Coulomb interactions induce a "negative" pressure which serves to make the total plasma pressure smaller than the thermal pressure. In most laboratory plasmas, however, this correction is usually quite small (Reference B-7).

Other miscellaneous relations needed to incorporate the Debye-Hückel correction into the ACE code are the mole fraction definition,

$$X_j = \frac{p_j}{p_o} \tag{B-26}$$

which requires that Equation (B-6) be rewritten as

$$p_o = \sum_{j=1}^{J} p_j \tag{B-27}$$

The mixture equation of state is

$$\frac{p_o}{\rho} = \frac{R_u}{\bar{M}} T \tag{B-28}$$

and the conversions from per-unit-volume to per-unit-mass are

$$h_c = \frac{H_c}{\rho} \; ; \; e_c = \frac{E_c}{\rho} \tag{B-29}$$

Finally, in the equation for mixture reactive thermal conductivity, Equation (B-36) below, the correction to the enthalpy of species j is required. This correction is defined in the following manner:

$$h = h_o + h_c = \frac{1}{M} \sum_{j=1}^{J} X_j \, (\tilde{h}_{j_o} + \tilde{h}_{j_c}) = \frac{1}{M} \sum_{j=1}^{J} X_j \tilde{h}_j \qquad \text{(B-30)}$$

Combination of Equations (B-29), (B-28), (B-25), and (B-14) gives

$$\tilde{h}_{j_c} = -\frac{4}{3} \frac{e^3}{k^2} \frac{(\pi \rho_o)^{1/2}}{T} \left(\sum_{j=1}^{J} z_j^2 X_j\right)^{1/2} R_u z_j^2 \qquad \text{(B-31)}$$

The above coulomb corrections have been incorporated into the ACE code. Predictions of ρ, h, and X_i from the modified ACE code were then compared with the calculations in References B-8 and B-9. In the ACE calculations, eleven species were considered:

N_2, N, N^+, N^{++}

O_2, O, O^+, O^{++}

NO, NO^+

e

Tables B-1 through B-3 present a portion of these comparisons. Table B-1 indicates good agreement between the unmodified ACE predictions and those of Hilsenrath, et al., at 2000°K and 1 atm where the effects of Coulomb interactions are essentially zero due to the low degree of ionization. Table B-2 indicates that at 15,000°K and 1 atm, the Coulomb corrections are small and good agreement with the results of Hilsenrath is obtained at this condition. Finally, Table B-3 indicates that at 15,000°K and 200 atm, inclusion of the Debye-Hückel corrections can alter the ACE-predicted charged particle number densities by as much as 20 percent, and that these corrections should be included to obtain the best agreement with the results of Hilsenrath, et al. In general, the predictions of ACE with the Coulomb corrections agree with those of Hilsenrath, et al., to within 1 percent for ρ and h and 5 percent for X_i.

Figures B-1 and B-2 present plots of ρ and h as a function of T for the six pressures of interest, as predicted by ACE with Coulomb corrections. Also included are the tabulated values at 1 and 10 atm and the extrapolated values at 200 atm used by Watson and Pegot (Reference B-11). At temperatures in the vicinity of 4000°K, the Watson and Pegot values of h are 30-40 percent below the ACE values, while at 16,000°K - 20,000°K they are 10-15 percent higher. The Watson and Pegot values of ρ at 1 and 10 atm are very close to the ACE values, but their extrapolation to 200 atm is up to 25 percent lower than the ACE values.

B.2 TRANSPORT PROPERTIES

The transport properties μ, K, and σ are calculated using the mixture rules of Yos (Reference B-10) and the species mole fractions, specific heats, and enthalpies calculated by the modified ACE code described in Section B.1. The Yos formulation requires numerous collision integrals, and the values originally used by Yos have been updated in this work through a survey of the recent literature. Also, the calculations carried out in this work have been compared extensively with other theories and experimental data available in the literature. This subsection discusses in detail the various aspects of the transport properties model developed here.

The expressions given by Yos for the transport properties of a partially-ionized gas mixture are the following (for convenience, use of the subscripts i and j here differs from their use in Section B.1):

$$\mu = \sum_{i=1}^{N}\left[m_i X_i \Big/ \left(\sum_{j=1}^{N} X_j \Delta_{ij}^{(2)}\right)\right] \tag{B-32}$$

$$K = K_{tr} + K_{int} + K_r \tag{B-33}$$

$$K_{tr} = \frac{15}{4} k \sum_{i=1}^{N}\left[X_i \Big/ \left(\sum_{j=1}^{N} \alpha_{ij} X_j \Delta_{ij}^{(2)}\right)\right] \tag{B-34}$$

$$K_{int} = k \sum_{i=1}^{N}\left[\left(\frac{C_{p_i}}{\bar{R}_u} - \frac{5}{2}\right) X_i \Big/ \left(\sum_{j=1}^{N} X_j \Delta_{ij}^{(1)}\right)\right] \tag{B-35}$$

$$K_r = k \sum_{i=1}^{L}\left(\frac{\Delta H_i}{R_u T}\right)^2 \Big/ \left[\sum_{k=1}^{N}\left(\frac{\nu_{ik}}{X_k}\right) \sum_{j=1}^{N} (\nu_{ik} X_j - \nu_{ij} X_k)\, \Delta_{kj}^{(1)}\right] \tag{B-36}$$

$$\sigma = \left(\frac{e^2}{kT}\right) X_e \Big/ \left(\sum_{j=1}^{N} X_j \Delta_{ej}^{(1)}\right) \tag{B-37}$$

where

$$\Delta_{ij}^{(q)} = C_q \left[\frac{2m_i m_j}{\pi kT(m_i + m_j)}\right]^{1/2} \pi\bar{\Omega}_{ij}^{(q,q)} \qquad \text{(B-38)}$$

$$C_1 = \frac{8}{3}\ ;\ C_2 = \frac{16}{5}$$

$$a_{ij} = 1 + \frac{(1 - m_i/m_j)(0.45 - 2.54\ m_i/m_j)}{(1 + m_i/m_j)^2} \qquad \text{(B-39)}$$

In the above expressions, N is the total number of species present (equal to J in the nomenclature of Section B.1).

The internal thermal conductivity given by Equation (B-35) is the so-called Eucken contribution which accounts for the transport of energy stored in the rotational, vibrational and electronic excited states of the various species. It is assumed that the transport of this energy is associated with the diffusion process, hence the use of Equation (B-38) with $q = 1$.

The reactive thermal conductivity given by Equation (B-36) accounts for the transport of chemical energy associated with the diffusion of reacting species in the mixture, under the constraint of chemical equilibrium. In air under the conditions of interest, three recombination reactions are the principal contributors to energy transport by diffusion (Reference B-11):

$$e + N^+ \rightarrow N$$

$$2N \rightarrow N_2$$

$$2O \rightarrow O_2$$

Equation (B-36) is based upon the formulation of Butler and Brokaw (Reference B-12), which has been shown to be valid for ambipolar diffusion in a partially-ionized gas mixture by Meador and Staton (Reference B-13).

In Equation (B-36), the summation over ℓ is a summation over all independent reactions in the mixture. Thus, comparing with the subscript convention used in Equation (B-1), the reactions $\ell = 1, 2, \ldots, L$ in this section are equivalent to the reactions $j = I+1, I+2, \ldots, J$ in Section B.1. The stoichiometric coefficients in Equation (B-36) are written for reaction ℓ in the balanced form:

$$\sum_{i=1}^{N} \nu_{\ell i} \, M_i = 0 \qquad \text{(B-40)}$$

which is equivalent to Equation (B-1) written in the form

$$\sum_{i=1}^{I} \nu_{ji} \, M_i + \nu_{jj} \, M_j = 0 \qquad \text{(B-41)}$$

where j in Equation (B-41) represents ℓ in Equation (B-40) and $\nu_{jj} = -1$. Corresponding to Equation (B-40), the heat of reaction per mole of reaction ℓ in Equation (B-36) is given by

$$\Delta H_\ell = \sum_{i=1}^{N} \nu_{\ell i} \, \hat{h}_i \qquad \text{(B-42)}$$

where $\hat{h}_i$ includes the Coulomb correction given by Equation (B-31).

In Equation (B-37), the prime on the summation sign denotes summation over all species except the electron.

In Equation (B-38), the collision integral $\pi\bar{\Omega}_{ij}^{(p,q)}$ has the physical significance of an effective cross section, with units of area, for collisions between molecules i and j. The collision integral is given formally by (Reference B-5).

$$\pi\bar{\Omega}_{ij}^{(p,q)} = \pi\sigma_{ij}^{2} \, \Omega_{ij}^{*(p,q)} \qquad \text{(B-43)}$$

where

$$\Omega_{ij}^{*(p,q)} = \frac{\Omega_{ij}^{(p,q)}}{\left(\Omega_{ij}^{(p,q)}\right)_{\text{rigid sphere}}} \qquad \text{(B-44)}$$

$$\Omega_{ij}^{(p,q)} = \sqrt{\frac{kT}{2\pi\mu_{ij}}} \int_{0}^{\infty} e^{-\gamma^{2}} \, \gamma^{2q+3} \, Q_{ij}^{(p)} \, d\gamma \qquad \text{(B-45)}$$

$$(\Omega_{ij}^{(p,q)})_{\text{rigid sphere}} = \sqrt{\frac{kT}{2\pi\mu}}\ \frac{(q+1)!}{2}\left[1 - \frac{1}{2}\ \frac{1+(-1)^p}{1+p}\right]\pi d_{ij}^2 \tag{B-46}$$

$$\gamma = \sqrt{\frac{\mu g^2}{2kT}} \tag{B-47}$$

$$\mu = \frac{m_i m_j}{m_i + m_j} \tag{B-48}$$

and the gas-kinetic cross-section is given by

$$Q_{ij}^{(p)}(g) = 2\pi \int_0^\pi (1 - \cos^p\chi)\ \sigma_{ij}\ (\chi,g)\ \sin\chi\ d\chi \tag{B-49}$$

where σ_{ij} is the differential cross-section for collisions between molecules i and j, χ is the scattering angle in the center-of-mass system, and g is the relative velocity between the colliding molecules. Equation (B-45) specifies an average of the gas-kinetic cross-section weighted by a moment of the Maxwellian velocity distribution. In Equation (B-46), d_{ij} is the mean diameter of molecules i and j assuming they are rigid spheres. With the collision integral defined in this manner (Equation (B-43)), it reduces to the collision cross-section area πd_{ij}^2 if the two particles are actually rigid spheres.

Evaluation of the gas-kinetic cross-section given by Equation (B-49) requires knowledge of the intermolecular potential between molecules i and j, since the scattering angle χ is a function of this parameter (Reference B-5). Once the intermolecular potential is known, either from experimental data or a theoretical model, Equation (B-43) can be evaluated for the collision integral. In the approximate mixture rules specified by Yos, Equations (B-32) through (B-37) in this work, only the collision integrals for p = q = 1 and p = q = 2 are required.

References B-10, B-11, B-14, B-15, B-16, B-17, and B-18 were consulted for collision integrals for the air system. Plots of the data for $\pi\bar{\Omega}_{ij}^{(q,q)}$ for all collisions except the coulomb collisions revealed that

$$\ln \pi\bar{\Omega}_{ij}^{(q,q)} = A_{ij}^q \ln\left(\frac{T}{1000}\right) + B_{ij}^q \tag{B-50}$$

to within the scatter of the data, where A^q_{ij} and B^q_{ij} are constants. For the sake of consistency, the collision integral for molecules i and j used by Yos (Reference B-10) was also used here whenever it was substantiated by the values given by the other references. However, the collision integrals for charge exchange used by Yos were found to be too high by a factor of up to four. Thus, in this work the nitrogen charge exchange integrals were taken from Capitelli and DeVoto (Reference B-14) and those for oxygen were taken from Knof, et al. (Reference B-18). Table B-4 summarizes the constants A^q_{ij} and B^q_{ij} for all but the Coulomb collisions. Constants for collisions between a neutral particle and a second ion were not considered, since the number densities for these two species are never simultaneously significant under conditions of interest.

The Yos collision integrals for Coulomb collisions were based on the Gvosdover cross-section multiplied by factors ranging from 0.3 to 12, depending on the particular pair of charged particles. The multiplicative factors were obtained by Yos through comparison with the electrical and thermal conductivities of a fully-ionized gas predicted by Spitzer and Härm (Reference B-19), but these latter results have been found to be low relative to experimental data (Reference B-14). Therefore, in this work the Coulomb collision integrals were taken from Liboff (Reference B-17), who calculated the integrals assuming an unscreened Coulomb potential with Debye-length cutoff. The Liboff expression is (cgs units)

$$\pi\bar{\Omega}^{(1,1)}_{ij} = \pi\bar{\Omega}^{(2,2)}_{ij} = \frac{\pi}{2}\Lambda^2\left[\ln\left(\frac{2h}{\Lambda}\right) - 0.577\right] \qquad \text{(B-51)}$$

where

$$\Lambda = \frac{Z_i Z_j e^2}{kT} \qquad \text{(B-52)}$$

and the Debye length is

$$h^2 = \frac{kT}{4\pi e^2 n_e} \qquad \text{(B-53)}$$

The Debye-length assuming screening by electrons only is used, as recommended by Capitelli and DeVoto (Reference B-14). The Coulomb collision integral for collisions involving an electron was corrected using a single multiplicative

factor, as outlined below. All other Coulomb collision integrals, i.e., for collisions between various ions, were obtained directly from Equation (B-51) with no modifications.

Extensive comparisons between the transport property model described above and other models and experimental data available in the literature were carried out. Table B-5 summarizes the theoretical calculations considered, and Table B-6 summarizes the experimental data considered. Note that with the exception of the Capitelli and DeVoto calculations, all of the theoretical treatments are relatively dated. On the other hand, all of the experimental data are quite recent. This confirms the appropriateness of the transport property model updating performed here.

The primary purpose in carrying out the comparisons between theories and data was to validate the property model developed in this work. The major portion of the validation procedure concentrated on comparisons at one atmosphere, since all of the experimental data and most of the theoretical calculations in the literature pertain to this condition. However, several comparisons between the present model and other theories were also performed at 100 atm.

The following facts were considered in establishing the validation procedure:

a. From a transport property point-of-view, an N_2 plasma does not differ much from an air plasma (e.g., compare the two calculations performed by Yos)

b. There are considerably more experimental transport property data for N_2 than there are for air

c. There exists a recent, thorough calculation of N_2 plasma transport properties (Capitelli and DeVoto).

Considering the above constraints, it was decided that the new transport property model should first be "tuned" to achieve optimum agreement with the theory and experimental data for the N_2 plasma (at one atmosphere). Then, using the same "tuned" formulation, the calculations of the new model were compared with the theory and data for the air plasma (at one atmosphere). Finally, it was assumed that all modifications to the new model at one atmosphere are valid also at the higher pressures of interest, and this was confirmed through comparisons between the new calculations and the other theories at 100 atm.

The "tuning" of the new model was accomplished by utilizing multiplicative constants for the various collision integrals. The constants are assumed to be independent of temperature, composition, pressure, etc. This is a fairly standard procedure for forcing agreement between theory and data for transport properties and is usually required due to the high uncertainty in many of the collision cross-sections, especially those for Coulomb collisions where the shielding process is not presently well quantified. In this work it was found that the only collision integral correction required was for the Coulomb collisions involving an electron.

Figure B-3 shows the comparisons for the transport properties of an N_2 plasma at one atmosphere. The frozen thermal conductivity is defined as K_{tr} + K_{int} (Equations (B-34) and (B-35)). The experimental data for electrical conductivity were considered to be the primary standard. The calculations of Capitelli and DeVoto were considered to be the primary theoretical standard. Note that Capitelli and DeVoto appear to agree better with the N_2 data than the other theories considered.

Four iterations of the new theory were considered:

a. Unmodified cross-sections; without O^{++} and N^{++}

b. Unmodified cross-sections; with O^{++} and N^{++}

c. All Coulomb collision integrals multiplied by 0.6; with O^{++} and N^{++}

d. Only Coulomb collision integrals involving an electron multiplied by 0.6; with O^{++} and N^{++}.

Several features of the comparisons for N_2 are evident.

a. Inclusion of N^{++} is necessary for $T > 22{,}000$°K.

b. The frozen and total thermal conductivities and the electrical conductivity are quite insensitive to Coulomb collisions involving ions, since the third and fourth iterations (c. and d. above) give essentially the same results.

c. The viscosity is quite insensitive to Coulomb collisions involving electrons, for $T \leq 16{,}000$°K, since the second and third iterations (b. and d. above) give essentially the same results.

d. It follows that a good approach for determing the multiplicative constants is to use the electrical and/or thermal conductivity comparison to back out the constant for electron-electron and electron-ion collisions, and to use the viscosity comparison to back out the constant for ion-ion collisions.

These features also are essentially valid for the air plasma comparisons.

The final iteration on the new model provides predictions that agree with the N_2 experimental electrical conductivity data to within 10 percent over the entire temperature range considered. In addition, deviations of the predictions of the new model from the N_2 total thermal conductivity data never exceed 20 percent for $T \leq 24{,}000°K$. These particular data exhibit large scatter, and the prediction usually lies within this scatter. Finally, the new model predicts N_2 viscosity within the scatter of the few data points available.

For the N_2 plasma, the new model generally compares quite closely with the rigorous kinetic theory calculations of Capitelli and DeVoto, being within 10 percent for total thermal conductivity and electrical conductivity in the range $5000°K \leq T \leq 20{,}000°K$, and within 20 percent for temperatures outside this range. The only appreciable disagreement occurs for the viscosity in the range $14{,}000°K \leq T \leq 18{,}000°K$, where the new model prediction is roughly 43 percent higher than that of Capitelli and DeVoto. However, outside this temperature range the agreement is better, generally being within 10 percent or less. Attempts to reduce the discrepancy for $14{,}000°K \leq T \leq 18{,}000°K$ were not pursued, since experimental data in this range, which could be used to substantiate either the new model or Capitelli and DeVoto, are lacking.

Figure B-4 shows the comparisons for the transport properties of an air plasma at one atmosphere. The final iteration of the new model provides electrical conductivity predictions which are within 10 percent of the experimental data for $7000°K \leq T \leq 15{,}000°K$ and within 20 percent for the only data point outside this range. The agreement with the total thermal conductivity is not as good, being within 20 percent for $7000°K \leq T \leq 14{,}000°K$ and deviating as much as 70 percent for $T < 7000°K$. However, in this case there is only one set of data with which to compare, and the new model compares with the data as well as, or better than, the other theories over the entire temperature range considered.

In comparing the theories for the air plasma, it appears that the new model and that of Peng and Pindroh are in close agreement for all properties for all temperatures below 15,000°K, with the exception of the viscosity in the range $12{,}000°K \leq T \leq 15{,}000°K$. There the new model is about 50 percent higher. Yos appears to be slightly low in predicting electrical conductivity for $T \geq 12{,}000°K$, due to his decision to determine the multiplicative constants for the Coulomb collision integrals from comparisons with the predictions of Spitzer and Harm, which are felt to be low themselves (Capitelli and DeVoto). Further, for $8000°K < T \leq 20{,}000°K$ Yos' prediction of total thermal conductivity is clearly too low, due to his use of erroneously high charge-transfer cross-sections

Finally, Yos appears to be substantially too high in his viscosity prediction for $T > 16,000°K$, again due to his method of determining the Coulomb multiplicative constants (this is also substantiated through the N_2 comparisons).

The Hansen prediction for air viscosity is lower than that of the other models for $4000°K \leq T \leq 10,000°K$. In addition, Hansen's total thermal conductivity appears to be in gross error for $T > 9000°K$.

Figure B-5 presents a comparison of the new model with the calculations of Sherman for an N_2 plasma at 100 atm. The agreement between the two viscosity calculations is excellent over the entire temperature range considered. The agreement between the two calculations for frozen and total thermal conductivity is very good for $T \leq 8000°K$, but Sherman drops below the new model for higher temperatures (although the temperature-dependent trends are identical). Recall that Sherman's calculation of N_2 frozen thermal conductivity at 1 atm appears to be low for $T > 8000°K$, relative to the other theories, including the new model and those of Yos and Capitelli and DeVoto.

Figure B-6 presents a comparison of the new model with the calculations of Hansen and Peng and Pindroh for an air plasma at 100 atm. For viscosity, the new model and Peng and Pindroh are within 13 percent for all temperatures considered, while Hansen's results are generally lower by up to 25 percent. For total thermal conductivity, the agreement between the new model and Peng and Pindroh is excellent, with deviations never exceeding 10 percent. As for the 1 atm comparisons the Hansen calculation appears again to be grossly erroneous. For electrical conductivity, the new model and Peng and Pindroh differ substantially for $T \leq 8000°K$. This is due to the fact that the new model uses a significantly larger e-N_2 collision integral than that used by Peng and Pindroh. At 8000°K and 100 atm, the mole fraction of N_2 is 0.48, so that e-N_2 collisions are dominant. At 1 atm and 8000°K, the mole fraction of N_2 is only 0.06, so the e-N_2 collisions are insignificant, thus explaining the good agreement between the new model and Peng and Pindroh at those conditions.

Figure B-7 presents viscosity, frozen and total thermal conductivity, and electrical conductivity for air under the conditions $1 \leq p \leq 200$ atm, $1000°K \leq T \leq 28,000°K$, as calculated by the new model with corrected electron-ion collision integrals. Viscosity is found to be relatively independent of pressure for $T \leq 12,000°K$, but becomes increasingly pressure dependent for greater temperatures. Frozen thermal conductivity becomes significantly pressure-dependent for $T \geq 8000°K$, while a strong pressure-dependence is exhibited by the total thermal conductivity for temperatures as low as 3000°K. Finally, electrical conductivity is a strong function of pressure for almost all temperatures.

One noteworthy observation is that for 12,000°K $\leq$ T $\leq$ 13,000°K, all four transport properties appear to be relatively insensitive to pressure variations. For all properties this is a "cross-over" region below which property values decrease with increasing pressure and above which they increase with increasing pressure.

REFERENCES FOR APPENDIX B

B-1. Watson, V. R. and Pegot, E. B., "Numerical Calculations for the Characteristics of a Gas Flowing Axially Through a Constricted Arc," NASA TN D-4042, Ames Research Center, Moffett Field, California, June 1967.

B-2. Kendall, R. M., "An Analysis of the Coupled Chemically Reacting Boundary Layer and Charring Ablator, Part V, A General Approach to the Thermochemical Solution of Mixed Equilibrium - Nonequilibrium, Homogeneous or Heterogeneous Systems," Final Report No. 66-7, Part V, NASA Contract NAS9-4599, Aerotherm Corporation, Palo Alto, California, March 14, 1967.

B-3. Powars, C. A. and Kendall, R. M., "User's Manual, Aerotherm Chemical Equilibrium (ACE) Computer Program," Aerotherm Corporation, Mountain View, California, May 1969.

B-4. Denbigh, K., The Principles of Chemical Equilibrium, Cambridge at the University Press, London, 1966, Chapter [illegible].

B-5. Hirschfelder, J. O., Curtiss, C. F., and Bird, R. B., Molecular Theory of Gases and Liquids, John Wiley and Sons, Inc., 1954.

B-6. Griem, H. R., Plasma Spectroscopy, McGraw-Hill Book Company, New York, 1964, pp. 137-140.

B-7. Griem, H. R., "High-Density Corrections in Plasma Spectroscopy," Physical Review, Vol. 128, No. 3, November 1, 1962, pp. 997-1003.

B-8. Hilsenrath, J. and Klein, M., "Tables of Thermodynamic Properties of Air in Chemical Equilibrium Including Second Virial Corrections from 1500°K to 15,000°K," AEDC-TR-65-58 and related publications, Arnold Engineering Development Center, Air Force Systems Command, Arnold Air Force Station, Tennessee, March 1965.

B-9. Gilmore, F. R., "Thermal Radiation Phenomena, The Equilibrium Thermodynamic Properties of High Temperature Air," DASA 1971-1, 3-27-67-1, Vol. 1, May 1967.

B-10. Yos, J. M., "Transport Properties of Nitrogen, Hydrogen, and Air to 30,000°K," Technical Memorandum RAD-TM-63-7, Research and Advanced Development Division, Avco Corporation, Wilmington, Massachusetts, March 22, 1963.

B-11. Peng, T. C. and Pindroh, A. L., "An Improved Calculation of Gas Properties at High Temperatures: Air," Paper No. 1995-61, Fourth Biennial Gas Dynamics Symposium, American Rocket Society, Northwestern University, Evanston, Illinois, August 23-25, 1961. Also, Document No. D2-11722, Category Code No. 01205, Boeing Airplane Company, Seattle, Washington, February 1962.

B-12. Butler, J. N. and Brokaw, R. S., "Thermal Conductivity of Gas Mixtures in Chemical Equilibrium," The Journal of Chemical Physics, Vol. 26, No. 6, June 1957, pp. 1636-164.

B-13. Meador, W. E., Jr. and Staton, L. D., "Electrical and Thermal Properties of Plasmas," The Physics of Fluids, Vol. 8, No. 9, September 1965, pp. 1694-1703.

B-14. Capitelli, M. and DeVoto, R. S., "Transport Coefficients of High-Temperature Nitrogen," The Physics of Fluids, Vol. 16, No. 11, November 1973, pp. 1835-1841.

B-15. Sherman, M. P., "Transport Properties of Partially-Ionized Nitrogen, I. The Collision Integrals, II. Method and Results," R65SD43 and R65SD44, NASA Contract NASr-32, Space Sciences Laboratory, Missile and Space Division, General Electric, July-August 1965.

B-16. Fay, J. A., "Hypersonic Heat Transfer in the Air Laminar Boundary Layer," The High Temperature Aspects of Hypersonic Flow, W. C. Nelson, Ed., The MacMillan Co., New York, pp. 583-605.

B-17. Liboff, R. L., "Transport Coefficients Determined Using the Shielded Coulomb Potential," The Physics of Fluids, Vol. 2, No. 1, January-February 1959, pp. 40-46.

B-18. Knof, H., Mason, E. A., and Vanderslice, J. T., "Interaction Energies, Charge Exchange Cross Sections, and Diffusion Cross Sections for N^+-N and O^+-O Collisions," The Journal of Chemical Physics, Vol. 40, No. 12, June 15, 1964, pp. 3548-3553.

B-19. Spitzer, L., Jr. and Härm, R., "Transport Phenomena in a Completely Ionized Gas," Physical Review, Vol. 89, No. 5, March 1, 1953, pp. 977-981.

B-20. Hansen, C. F., "Approximations for the Thermodynamic and Transport Properties of High-Temperature Air," NASA TR R-50, Ames Research Center, Moffett Field, California, 1959.

B-21. Schreiber, P. W., Hunter, A. M., II, and Benedetto, K. R., "Argon and Nitrogen Plasma Viscosity Measurements," The Physics of Fluids, Vol. 14, No. 12, December 1971, pp. 2696-2702.

B-22. Schreiber, P. W., Hunter, A. M., II, and Benedetto, K. R., "Electrical Conductivity and Total Emission Coefficient of Air Plasma," AIAA Journal, Vol. 11, No. 6, June 1973, pp. 815-821.

B-23. Schreiber, P. W., Hunter, A. M., II, and Benedetto, K. R., "Measurement of Nitrogen Plasma Transport Properties," AIAA Journal, Vol. 10, No. 5, May 1972, pp. 670-674.

B-24. Hermann, W. and Schade, E., Z. Phys., Vol. 233, 1970, p. 333.

B-25. Morris, J. C., Rudis, R. P., and Yos, J. M., "Measurements of Electrical and Thermal Conductivity of Hydrogen, Nitrogen, and Argon at High Temperatures," The Physics of Fluids, Vol. 13, No. 3, March 1970, pp. 608-617.

B-26. Asinovsky, E. I., Kirillin, A. V., Pakhomov, E. P., and Shabashov, V. I., "Experimental Investigation of Transport Properties of Low-Temperature Plasma by Means of Electric Arc," Proceedings of the IEEE, Vol. 59, No. 4, April 1971, pp. 592-601.

TABLE B-1

COMPARISON OF PRESENT CALCULATIONS WITH HILSENRATH, ET AL.

$T = 2000°K$, $p = 1$ atm

		ACE	Hilsenrath, et al.
	ρ, gm/cc	0.1764×10^{-3}	0.1762×10^{-3}
	h, cal/gm	479.1	474.1
MOLE FRACTIONS	N_2	0.78×10^{0}	0.78×10^{0}
	O_2	0.21×10^{0}	0.21×10^{0}
	NO	0.82×10^{-2}	0.83×10^{-2}
	O	0.38×10^{-3}	0.33×10^{-3}
	N	0.84×10^{-8}	--
	e	0.29×10^{-10}	--
	N^+	0.20×10^{-20}	--
	O^+	0.29×10^{-22}	--
	NO^+	0.29×10^{-10}	--

TABLE B-2

COMPARISON OF PRESENT CALCULATIONS WITH HILSENRATH, ET AL.

$T = 15,000°K$, $p = 1$ atm

		ACE With D-H Correction	ACE Without D-H Correction	Hilsenrath, et al.
	ρ, gm/cc	0.7793×10^{-5}	0.7788×10^{-5}	0.7796×10^{-5}
	h, cal/gm	27,504	27,288	27,429
MOLE FRACTIONS	N_2	0.3555×10^{-3}	0.3798×10^{-3}	--
	O_2	--	--	--
	NO	--	--	--
	O	0.8015×10^{-1}	0.8298×10^{-1}	0.74×10^{-1}
	N	0.2788	0.2344	0.19
	e	0.3465	0.3410	0.36
	N^+	0.2870	0.2828	0.30
	O^+	0.5741×10^{-1}	0.5614×10^{-1}	0.61×10^{-1}
	NO^+	0.4097×10^{-5}	0.4120×10^{-5}	--

TABLE B-3

COMPARISON OF PRESENT CALCULATIONS WITH HILSENRATH, ET AL.

$T = 15{,}000°K$, $P = 200$ atm

		ACE With D-H Correction	ACE Without D-H Correction	Hilsenrath, et al.
	ρ, gm/cc	0.2281×10^{-2}	0.2286×10^{-2}	0.2281×10^{-2}
	h, cal/gm	14,447	14,243	14,440
MOLE FRACTIONS	N_2	0.6697×10^{-2}	0.6928×10^{-2}	0.687×10^{-2}
	O_2	0.3203×10^{-4}	0.3206×10^{-4}	-
	NO	0.9241×10^{-3}	0.9520×10^{-3}	-
	O	0.1935	0.1967	0.193
	N	0.6937	0.7080	0.693
	e	0.5037×10^{-1}	0.4146×10^{-1}	0.500×10^{-1}
	N^+	0.4267×10^{-1}	0.3513×10^{-1}	0.425×10^{-1}
	O^+	0.6706×10^{-2}	0.5490×10^{-2}	0.604×10^{-2}
	NO^+	0.2934×10^{-3}	0.2439×10^{-3}	0.327×10^{-3}

TABLE B-4

CONSTANTS FOR EQUATION (B-50)
(ASSUMING $\pi\bar{\Omega}_{ij}$ IN Å^2 AND T IN °K)

Specie i	Specie j	A^1_{ij}	B^1_{ij}	A^2_{ij}	B^2_{ij}
N_2	N_2	-0.2739	3.434	-0.2613	3.097
N	N_2	-0.3120	3.262	-0.2739	3.434
N	N	-0.3098	2.956	-0.2817	3.001
e	N_2	0.2870	1.041	0.2870	1.041
e	N	0.0000	1.000	0.0000	1.000
N	N^+	-0.1010	3.970	-0.3048	3.726
O	O	-0.2001	2.955	-0.2632	3.140
O_2	O_2	-0.1503	3.296	-0.1106	3.434
O	O_2	-0.2309	3.153	-0.2219	3.314
O	O^+	-0.0060	4.158	-0.3057	3.646
e	O	0.6790	-0.5447	0.6790	-0.5447
e	O_2	0.4740	0.9083	0.4740	0.9083
N	O^+	-0.3979	4.094	-0.3999	4.007
O	N^+	-0.3978	4.094	-0.3999	4.007
N	O	-0.3424	3.091	-0.3327	3.243
N_2	O_2	-0.1949	3.367	-0.1120	3.497
O_2	NO	-0.1949	3.367	-0.1120	3.497
O	N_2	-0.2072	3.329	-0.2722	3.512
NO	NO	-0.1461	3.307	-0.1399	3.512
N_2	NO	-0.1899	3.367	-0.1383	3.497
O	NO	-0.2829	3.243	-0.2074	3.304
N	NO	-0.2048	3.219	-0.1679	3.367
NO	NO^+	-0.1269	4.291	-0.3979	3.790
e	NO	0.5322	1.308	0.5322	1.308
N_2	N^+	-0.3120	3.262	-0.2739	3.434
N_2	O^+	-0.2072	3.329	-0.2722	3.512
N_2	NO^+	-0.1899	3.367	-0.1383	3.497
N	O_2	-0.2072	3.329	-0.2722	3.512
N	NO^+	-0.2048	3.219	-0.1679	3.367
N^+	O_2	-0.3979	4.094	-0.3999	4.007
N^+	NO	-0.2048	3.219	0.1679	3.367
O_2	O^+	-0.2309	3.153	-0.2219	3.314
O_2	NO^+	-0.1949	3.367	-0.1120	3.497
O	NO^+	-0.2529	3.243	-0.2074	3.304
O^+	NO	-0.2529	3.243	-0.2074	3.304

TABLE B-5

THEORETICAL CALCULATIONS FOR TRANSPORT PROPERTIES AVAILABLE IN THE LITERATURE

Source	Composition	Pressure Range (atm)	Temperature Range (°K)	Date Published	Comments
Capitelli and Devoto (B-14)	Nitrogen	1	1000 - 30,000	1973	Most recent, best validated calculation available; higher order kinetic theory; accounts for I.P. lowering.
Sherman (B-15)	Nitrogen	10^{-4} - 10^{2}	1000 - 15,000	1965	No comparisons with experimental data; higher order kinetic theory; thermodynamic properties not described.
Hansen (B-20)	Air	10^{-4} - 10^{2}	1000 - 15,000	1960	Simple mixture rules; many collision integrals now outdated; does not account for I.P. lowering.
Peng and Pindroh (B-11)	Air	$10^{-3} \le \rho/\rho_0 \le 10^{1}$	1000 - 15,000	1961	Improved collision integrals relative to Hansen; higher order kinetic theory; does not account for I.P. lowering
Yos (B-10)	Air and Nitrogen	1-30	1000 - 30,000	1963	Charge transfer collision integrals too high; Coulomb collision integrals need updating; does not account for I.P. lowering; species mole fractions and thermodynamics properties taken from different sources (not consistent)

TABLE B-6

EXPERIMENTAL DATA FOR TRANSPORT PROPERTIES
AVAILABLE IN THE LITERATURE

Source	Property Measured	Composition	Pressure Range (atm)	Temperature Range (°K)	Date Published
Schreiber, et al. (B-21)	μ	Nitrogen	1	10,500-12,200	1971
Schreiber, et al. (B-23)	κ, σ	Nitrogen	1	10,000-1[illegible],200	1972
Hermann and Schade (B-26)	κ, σ	Nitrogen	1	6,000-26,000	1970
Morris, et al. (B-25)	κ, σ	Nitrogen	0.5-2.0	8,000-14,000	1970
Asinovsky, et al. (B-26)	κ	Nitrogen	1	11,500-16,900	1971
Schreiber, et al. (B-22)	σ	Air	1	8,000-12,000	1973
Asinovsky, et al. (B-26)	κ, σ	Air	1	2,000-14,000	1971

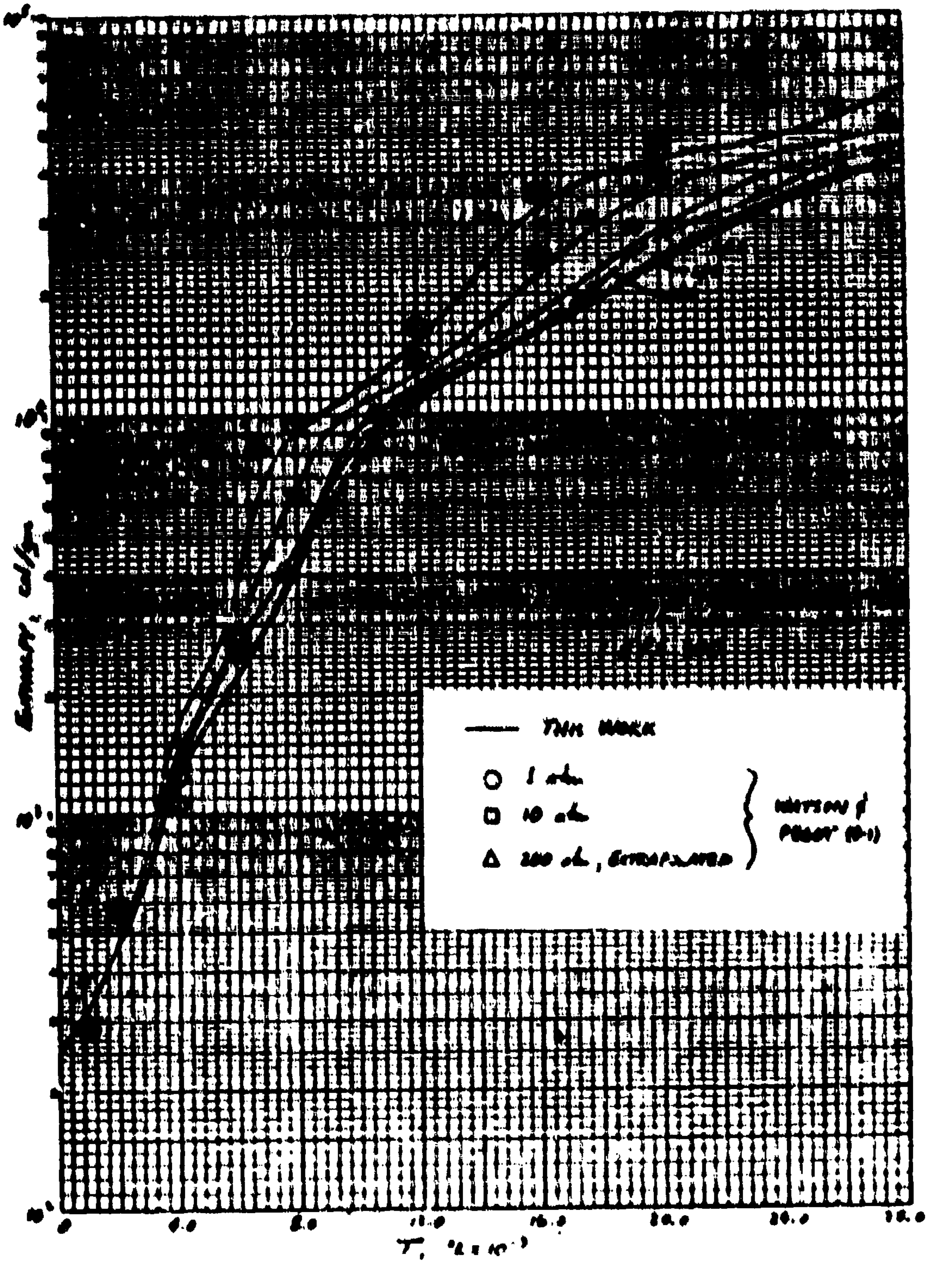

Figure B-1. Air enthalpy predictions.

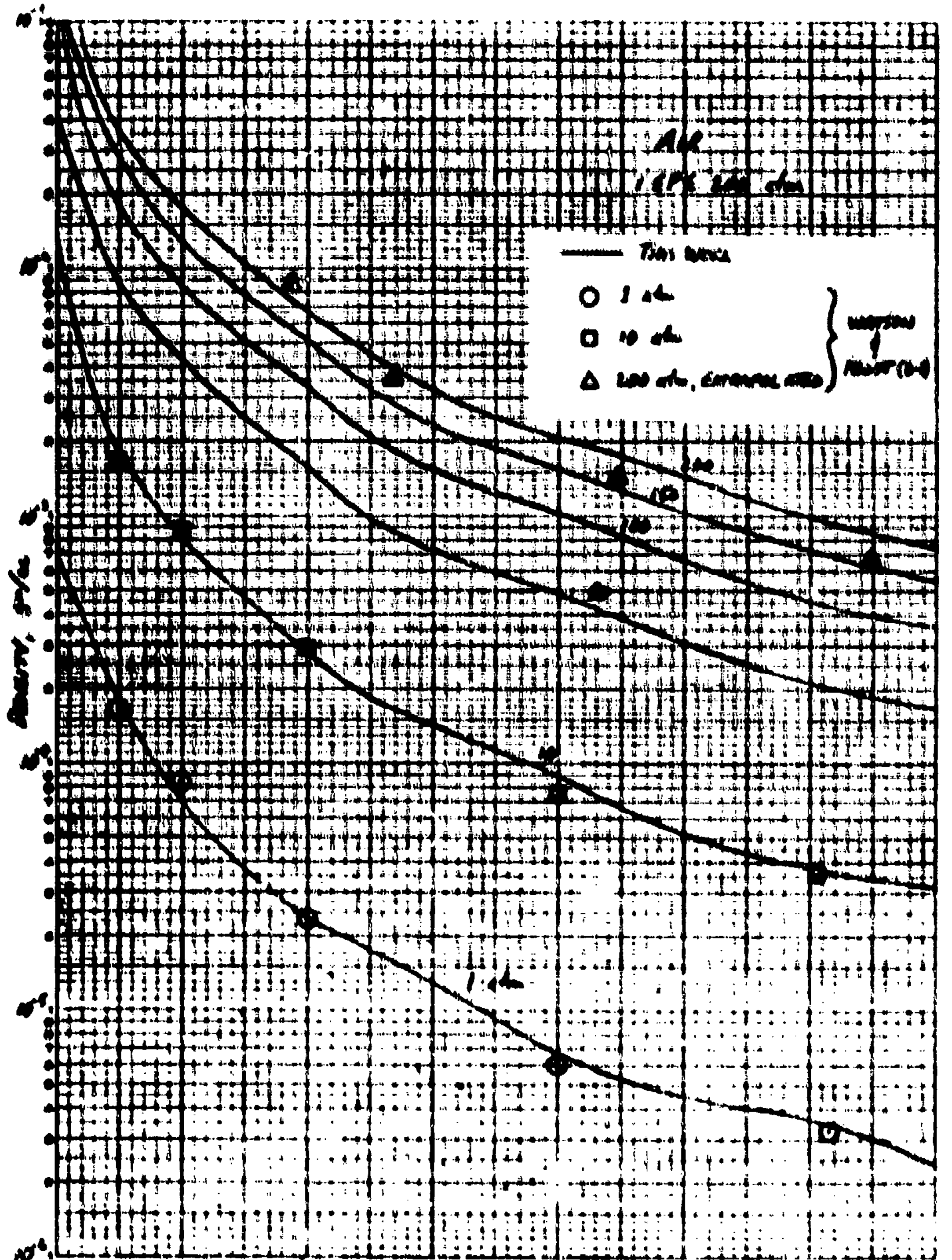

Figure B-2. Air density predictions.

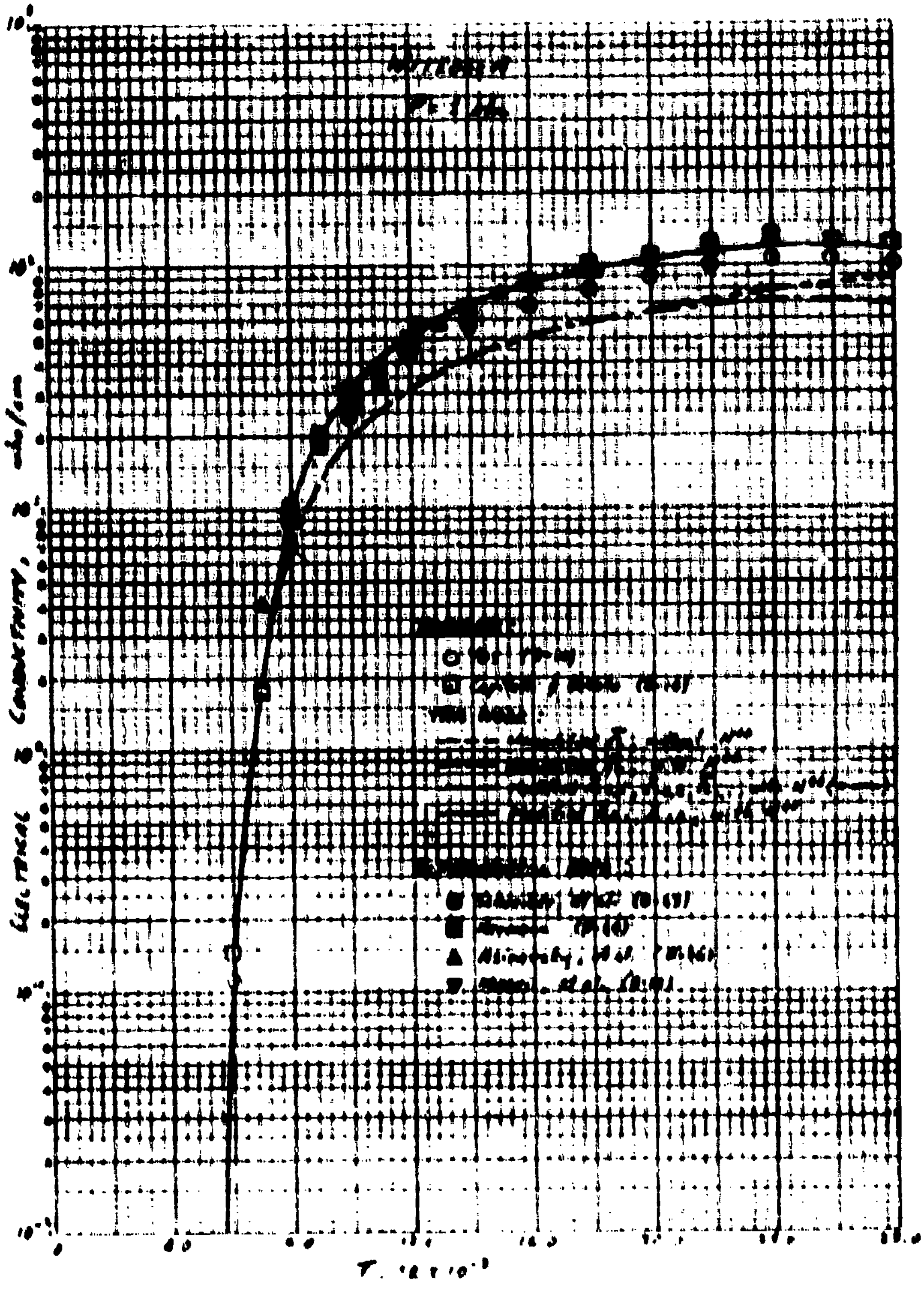

Figure B-3a. Comparisons for nitrogen transport properties at 1 atm - electrical conductivity.

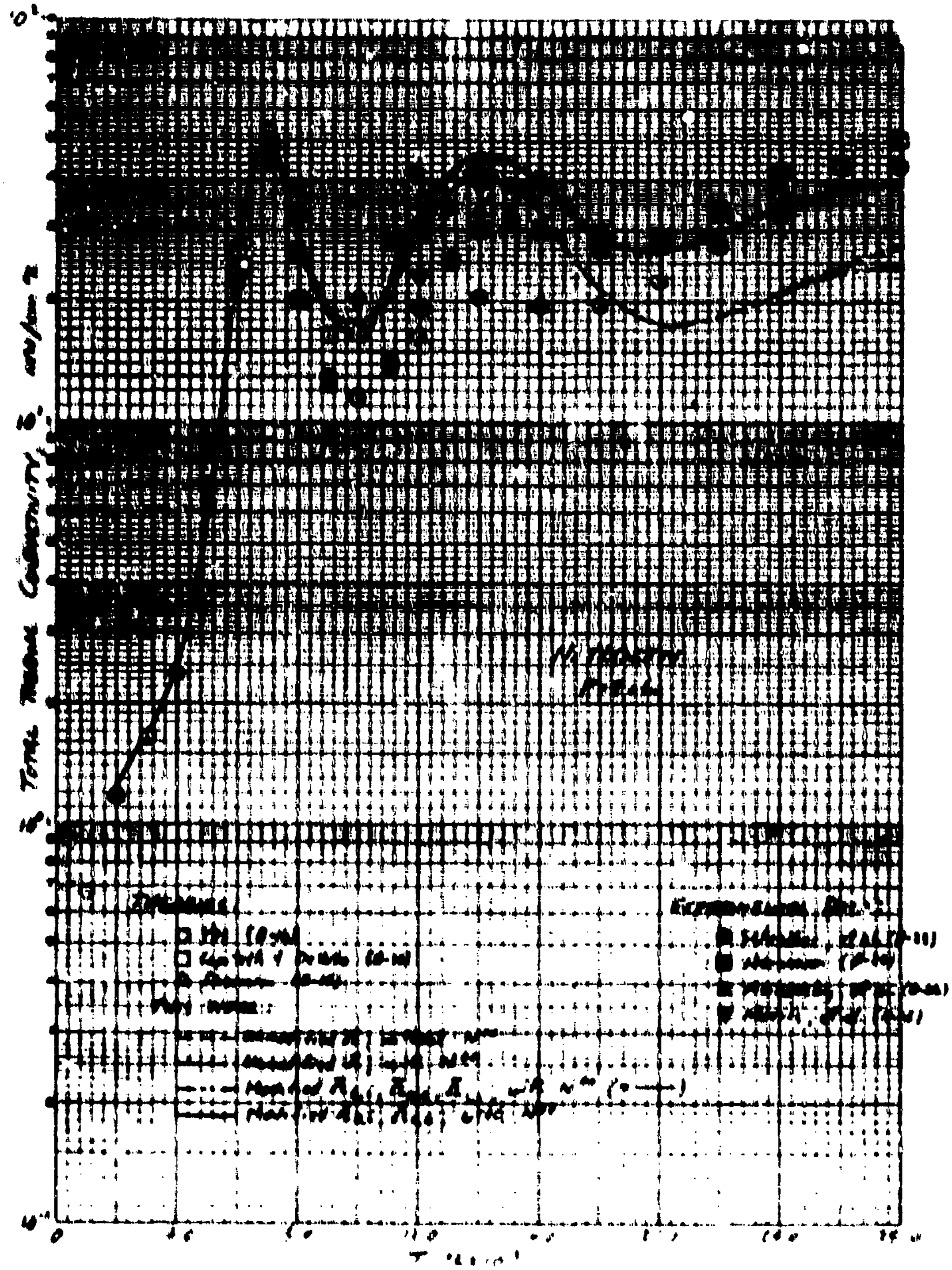

Figure B-3b. Comparisons for nitrogen transport properties at 1 atm - total thermal conductivity.

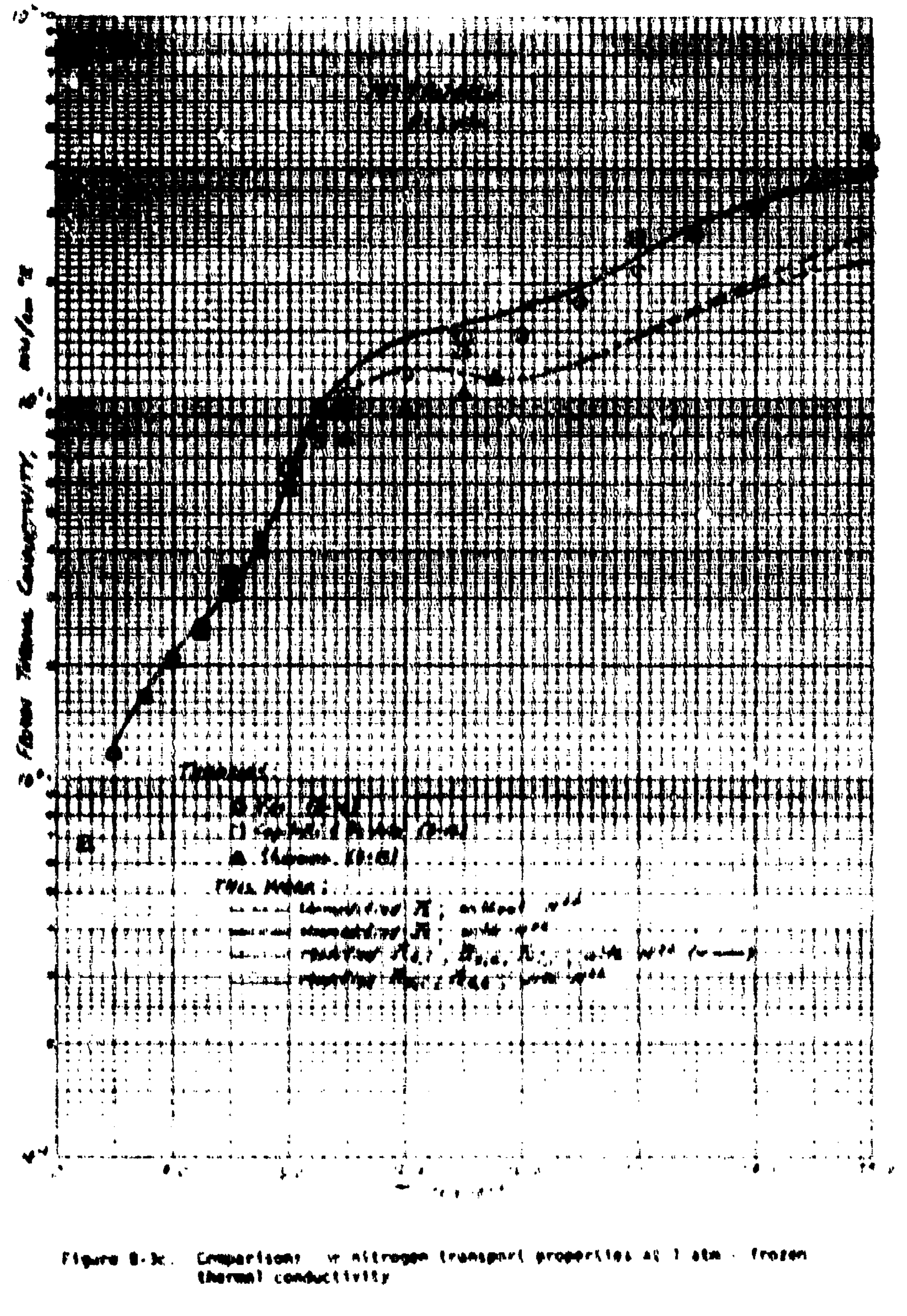

Figure B-3c. Comparisons of nitrogen transport properties at 1 atm - frozen thermal conductivity

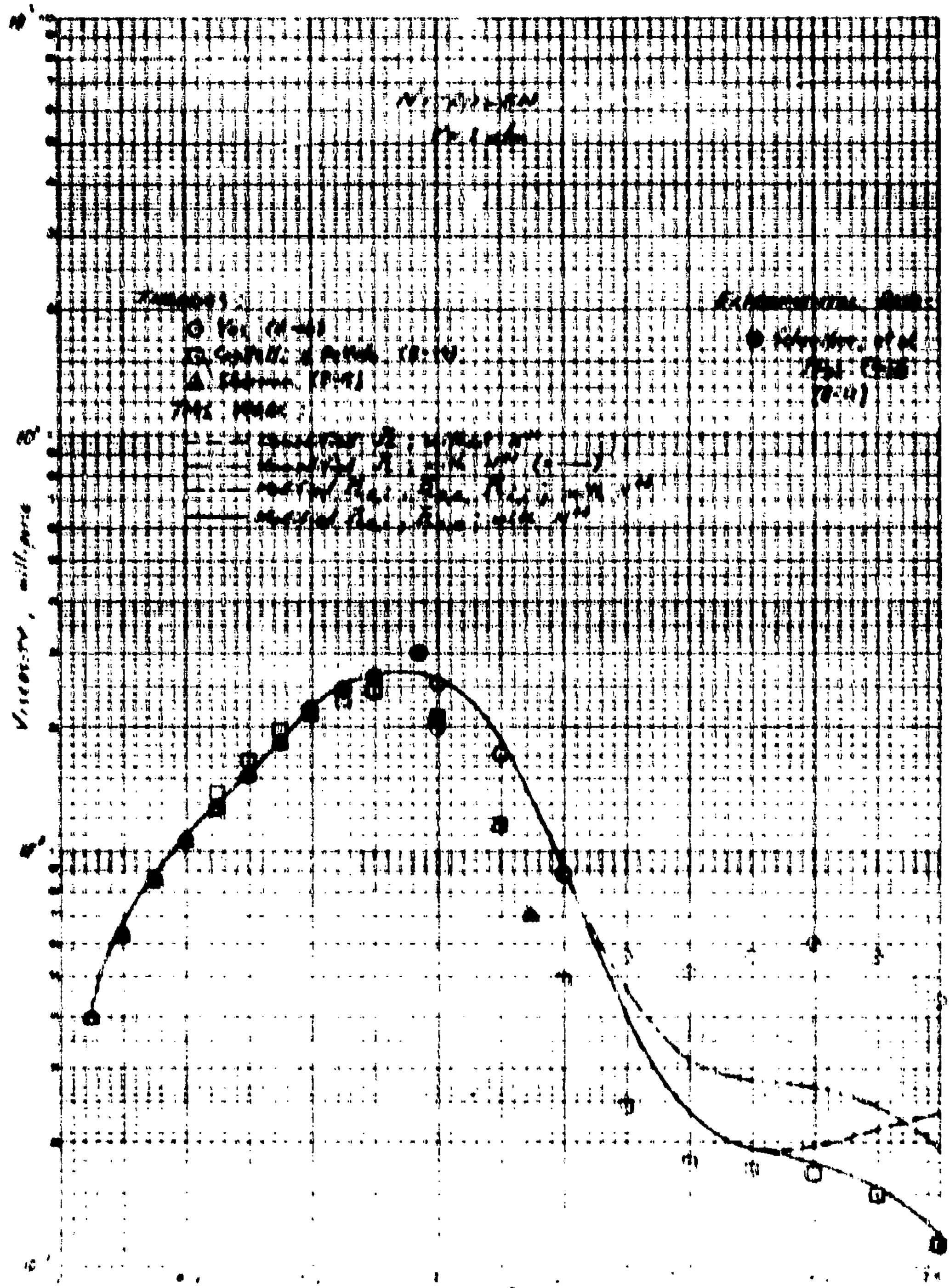

Figure B-3d. Comparisons for nitrogen transport properties at 1 atm - viscosity

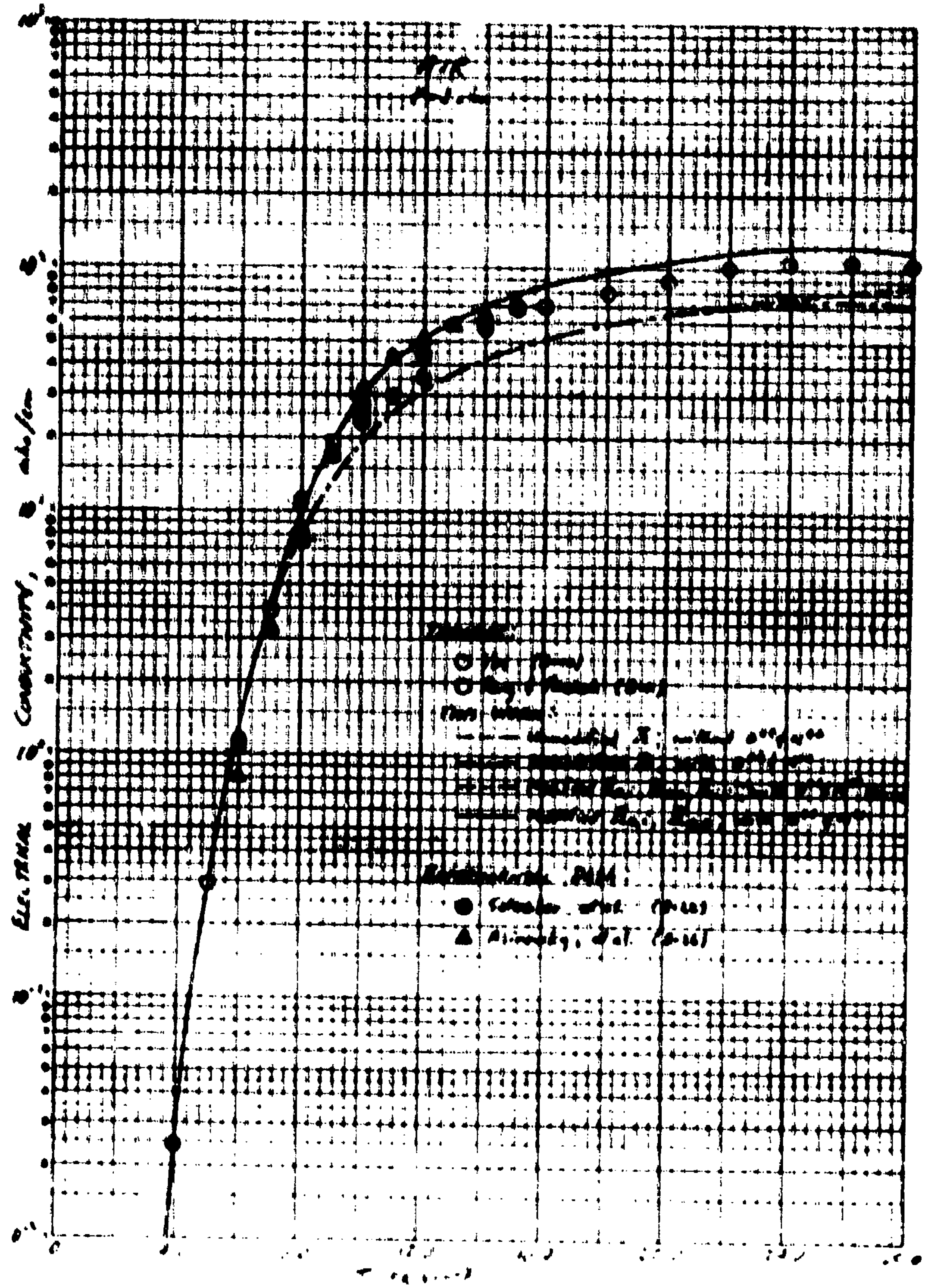

Figure B-4a. Comparisons for air transport properties at 1 atm - electrical conductivity.

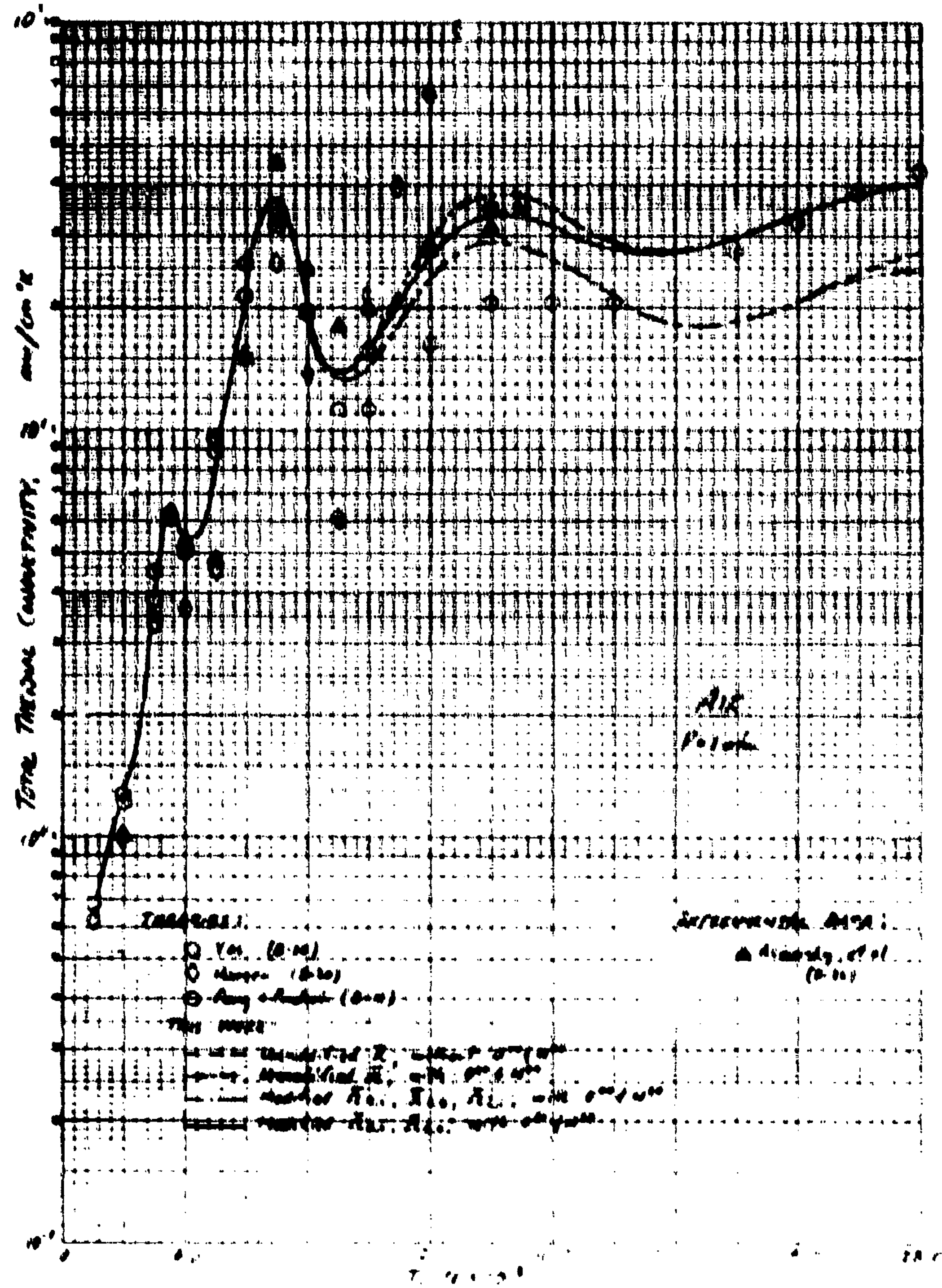

Figure B-4b. Comparisons for air transport properties at 1 atm - total thermal conductivity.

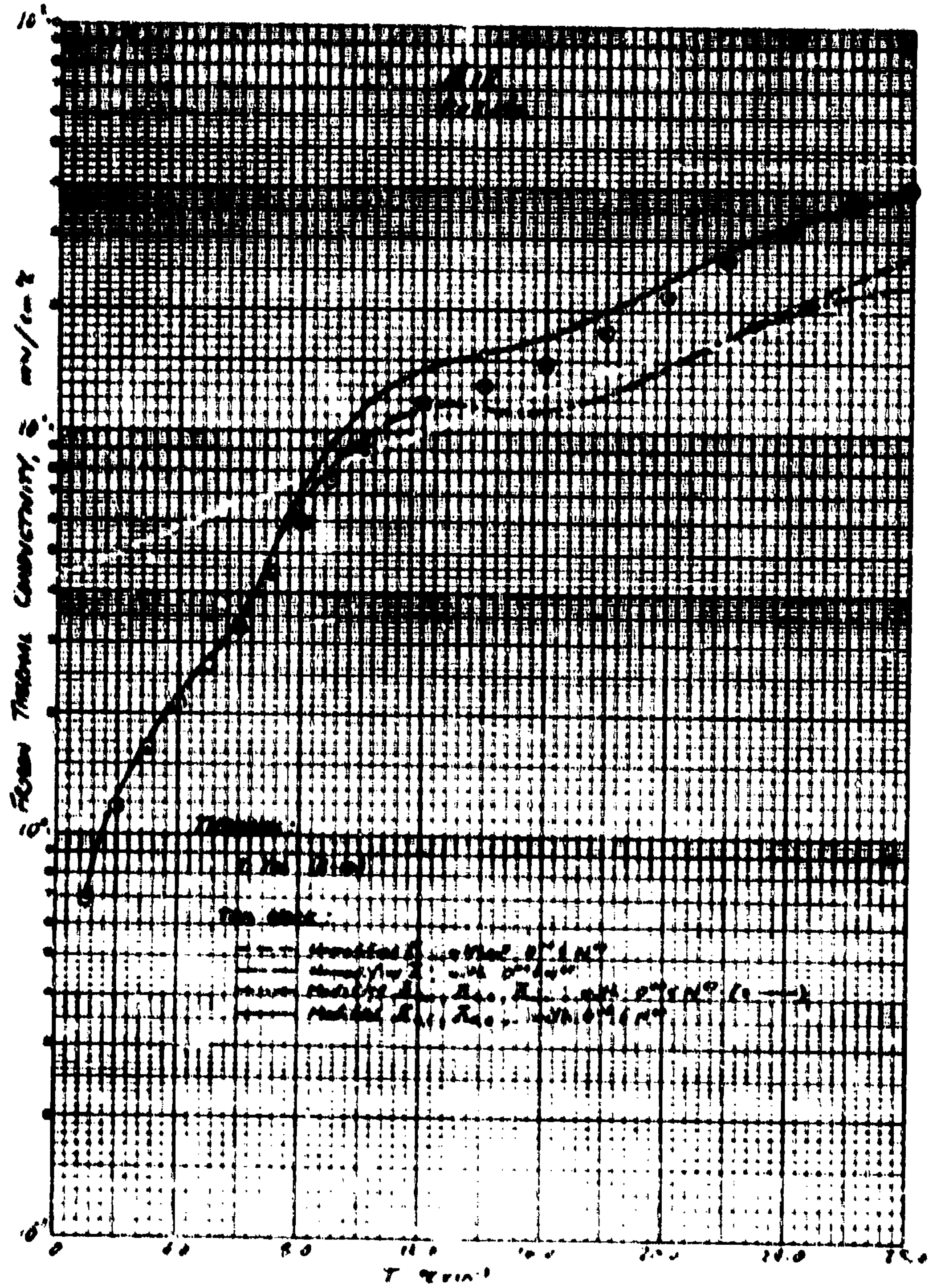

Figure B-4c. Comparisons for air transport properties at 1 atm - frozen thermal conductivity.

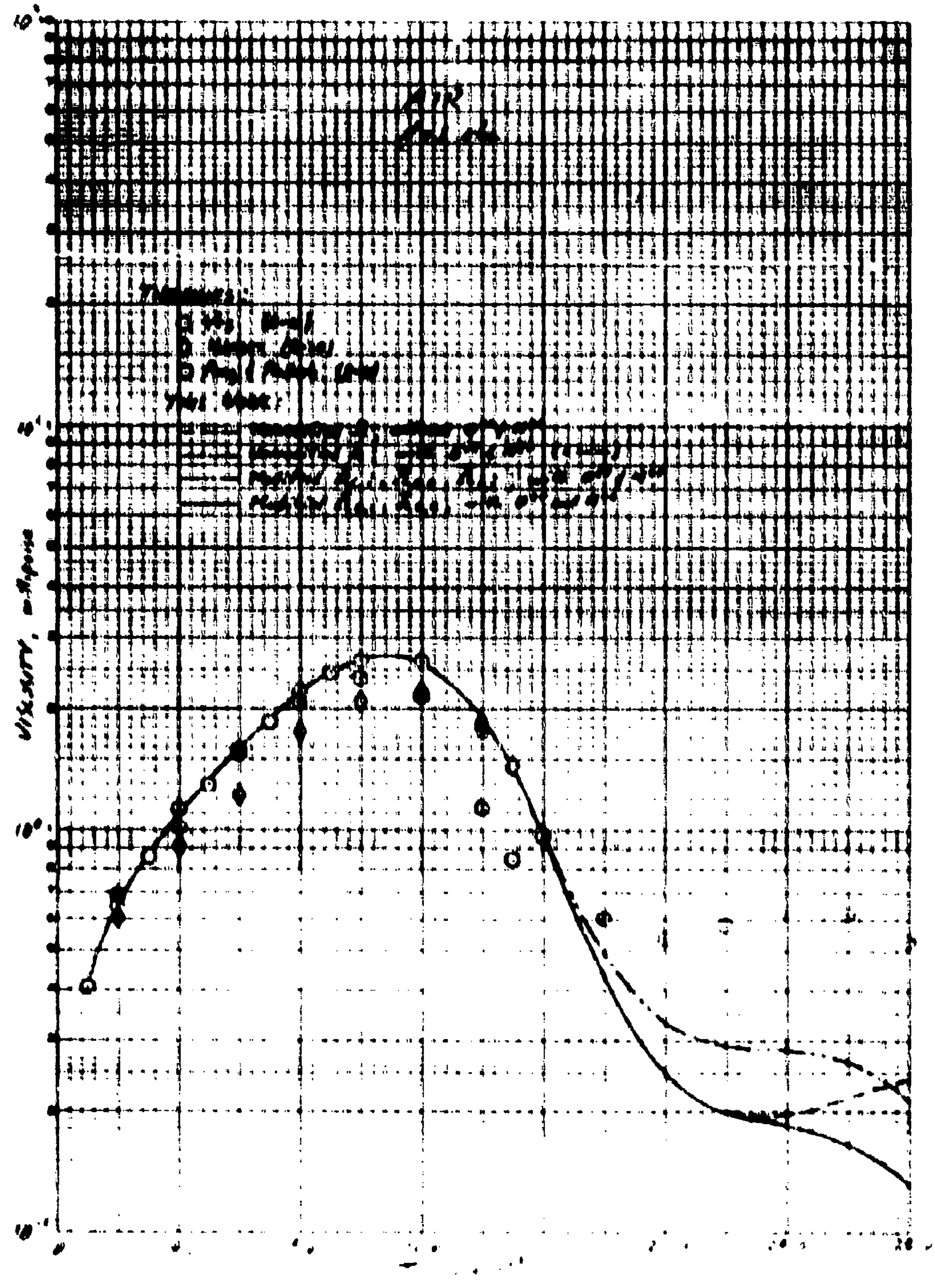

Figure B-44. Comparisons for air transport properties at 1 atm - viscosity.

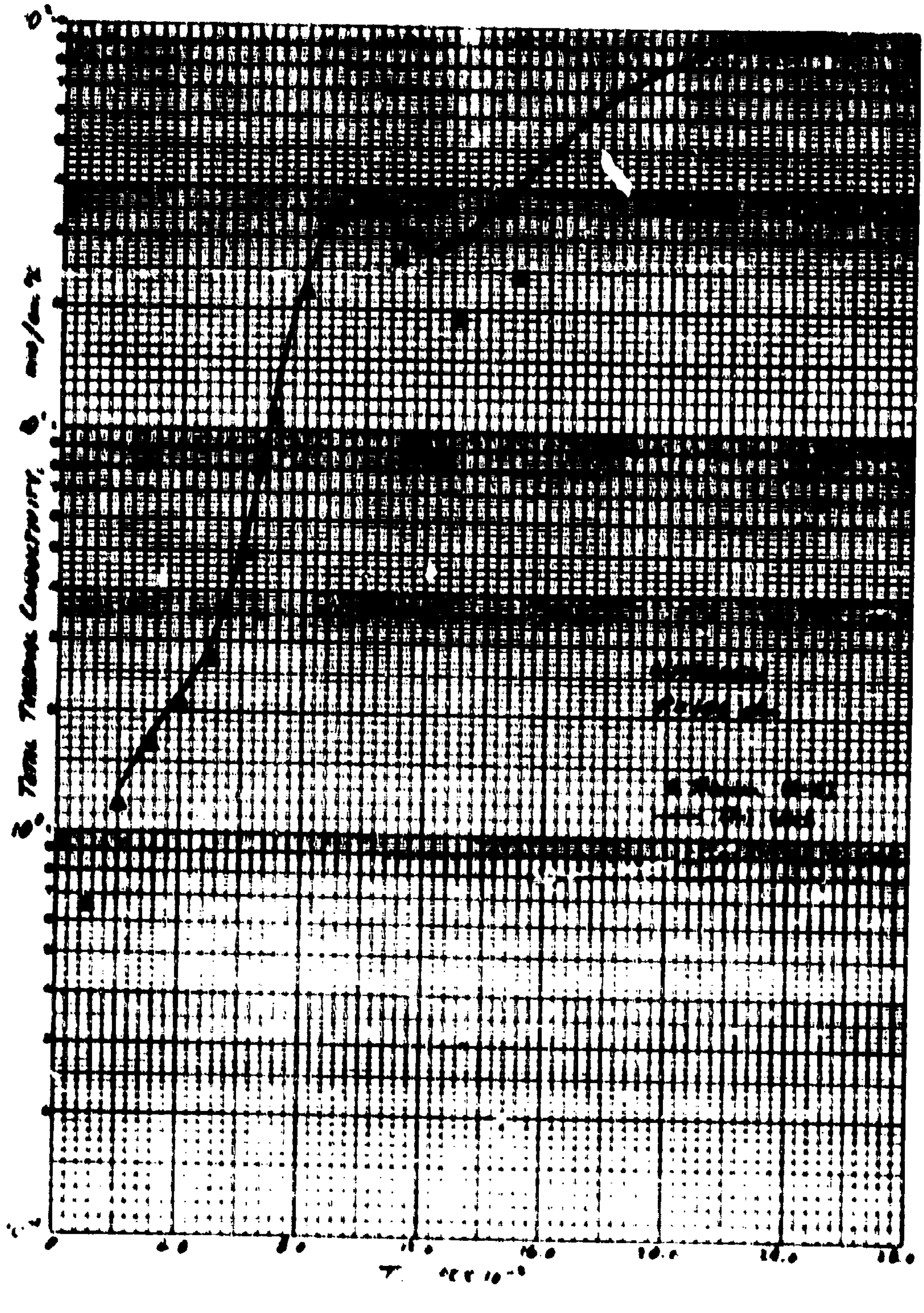

Figure B-5a. Comparisons for nitrogen transport properties at 100 atm - total thermal conductivity.

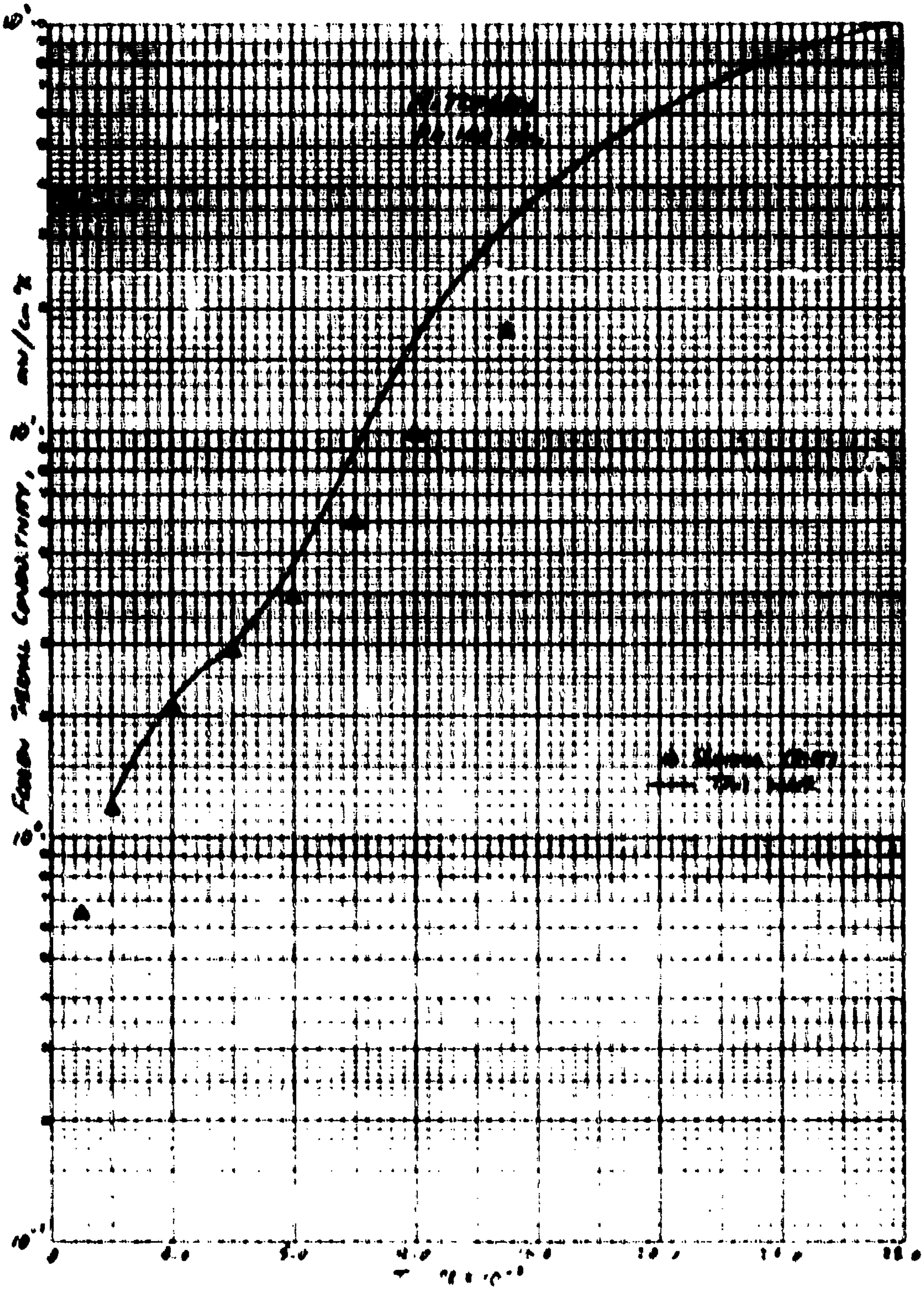

Figure B-5b. Comparisons for nitrogen transport properties at 100 atm - frozen thermal conductivity.

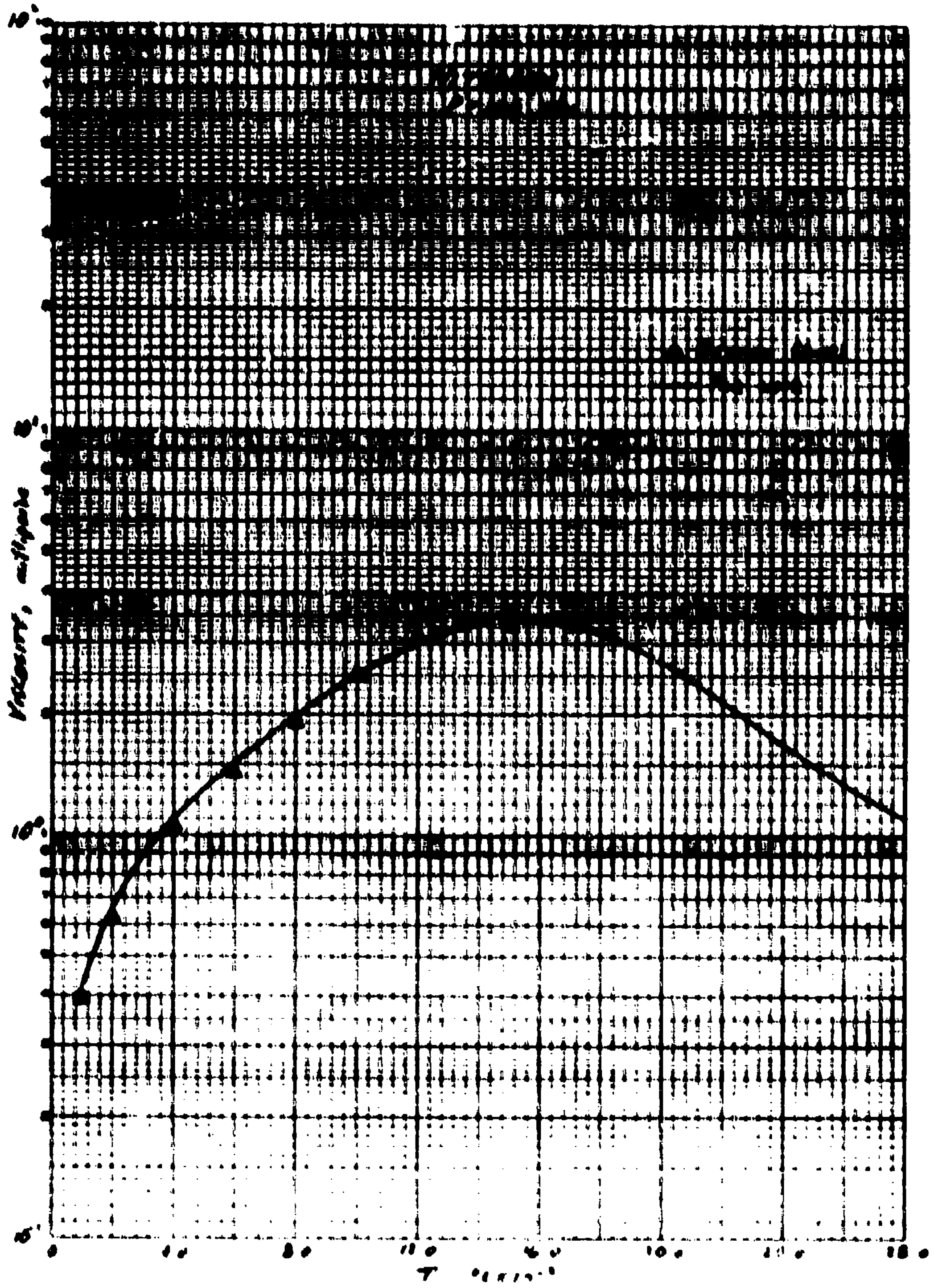

Figure B-5c. Comparisons for nitrogen transport properties at 100 atm - viscosity.

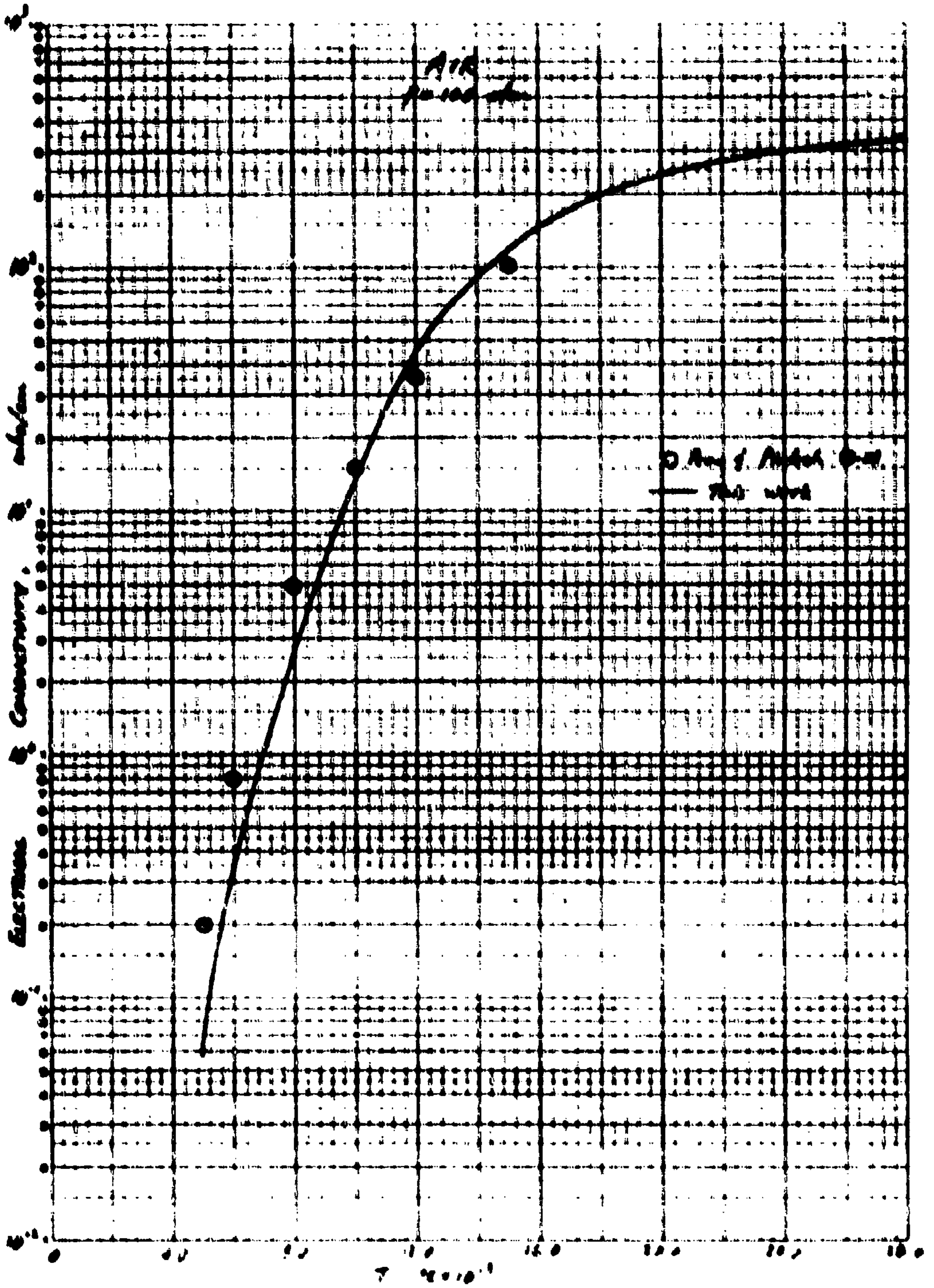

Figure B-6a. Comparisons for air transport properties at 100 atm - electrical conductivity.

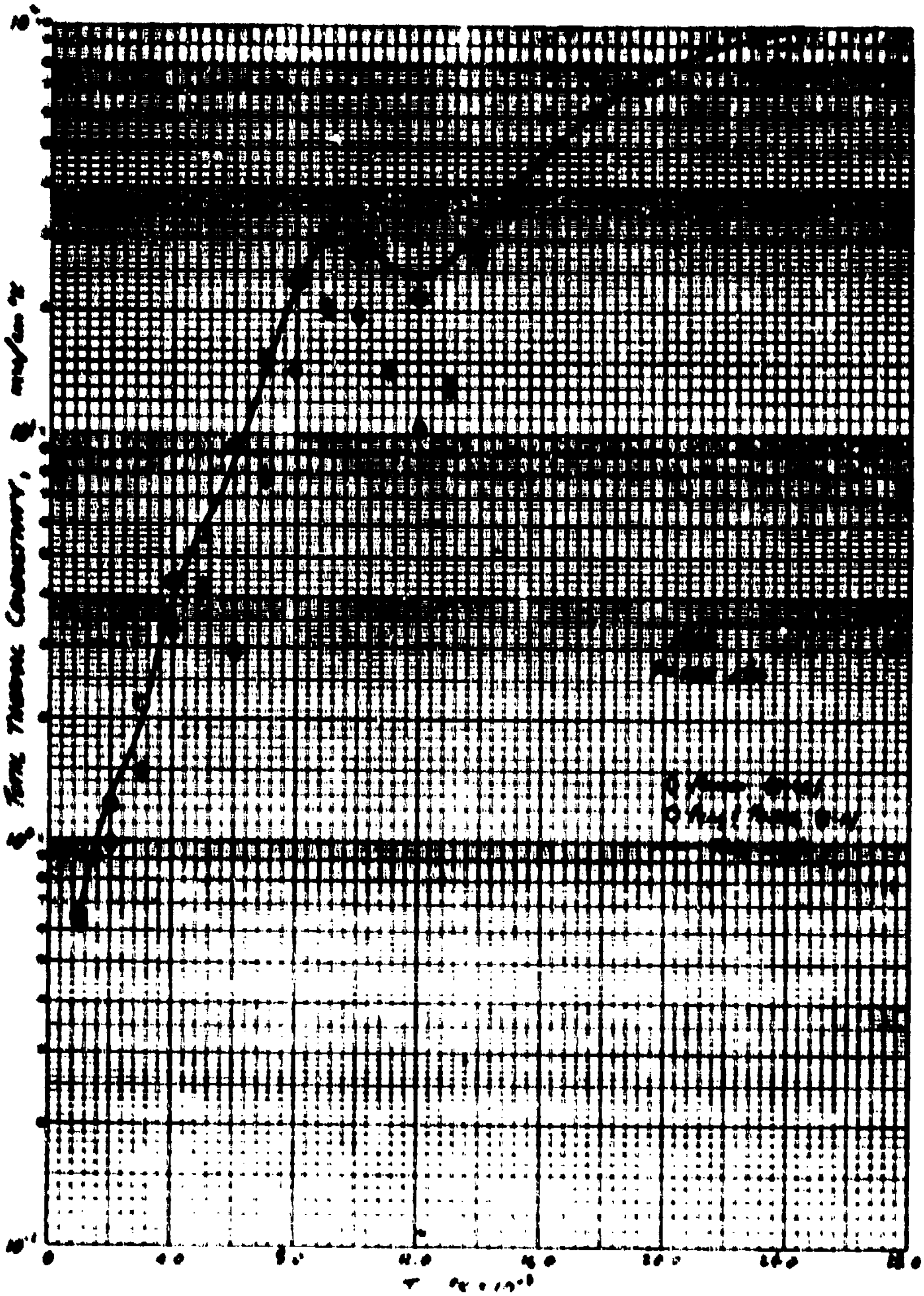

Figure B-6b. Comparisons for air transport properties at 100 atm - total thermal conductivity.

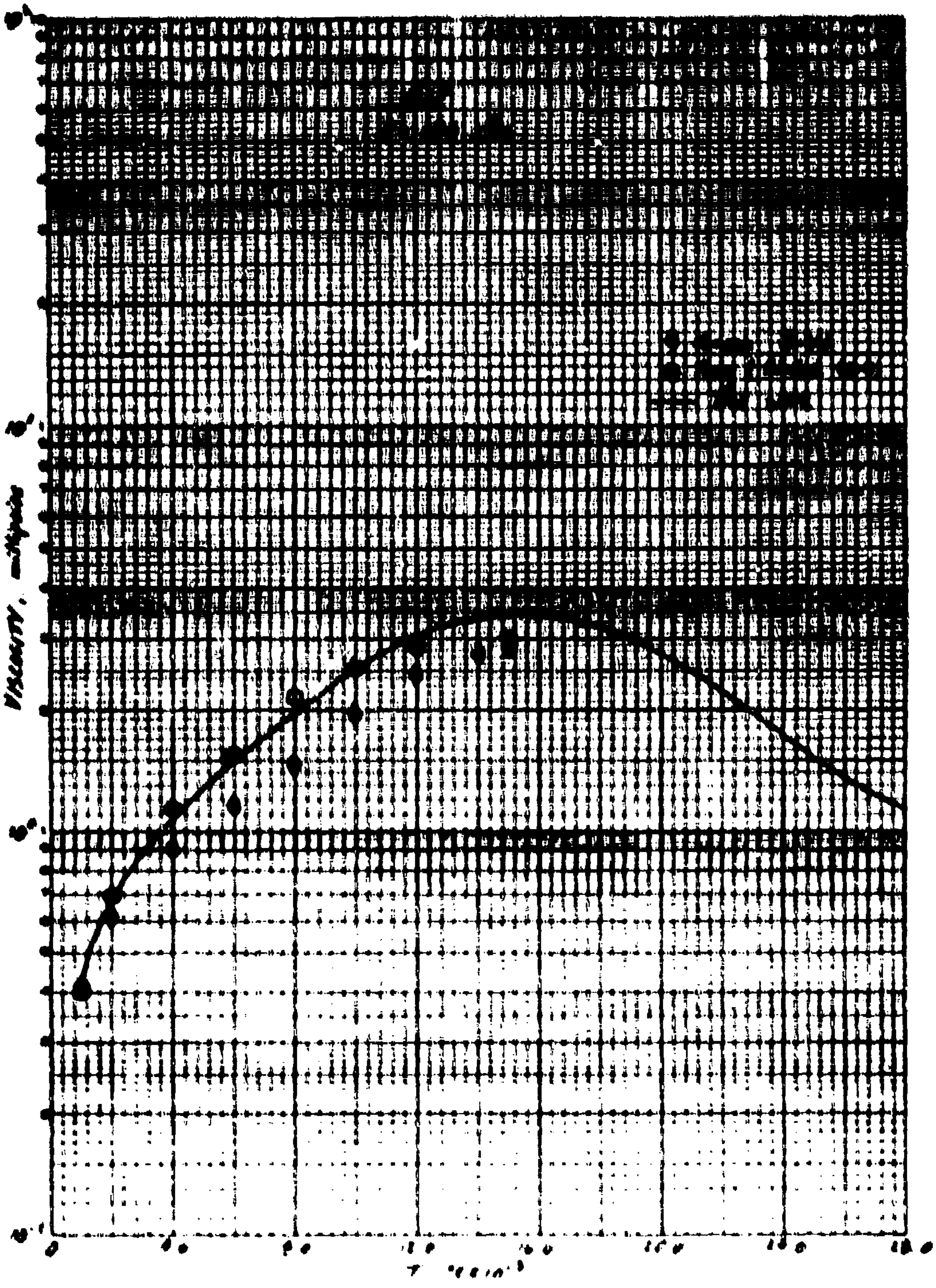

Figure B-6c. Comparisons for air transport properties at 100 atm - viscosity.

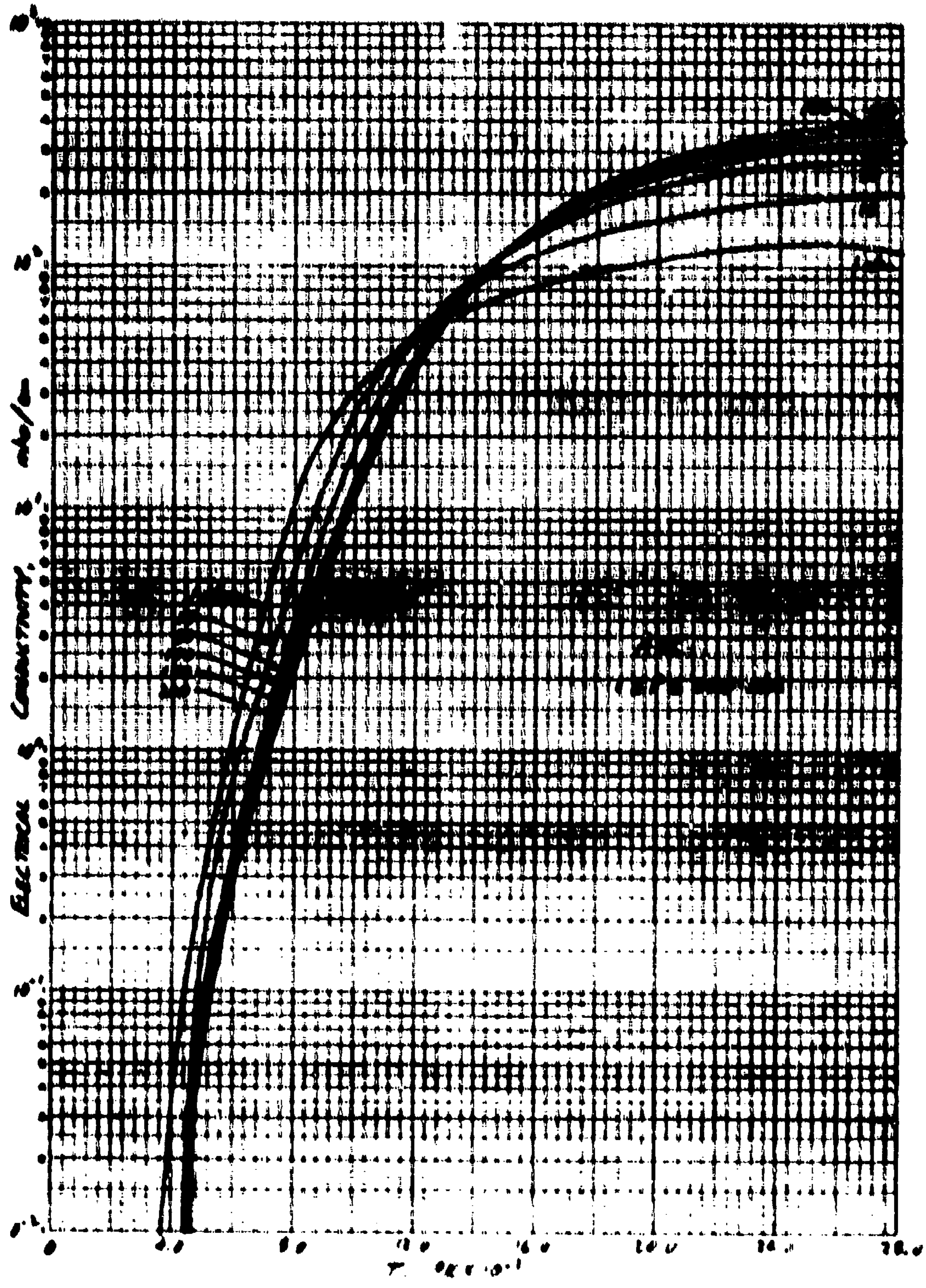

Figure 8-7a. Air transport properties predicted in this work - electrical conductivity.

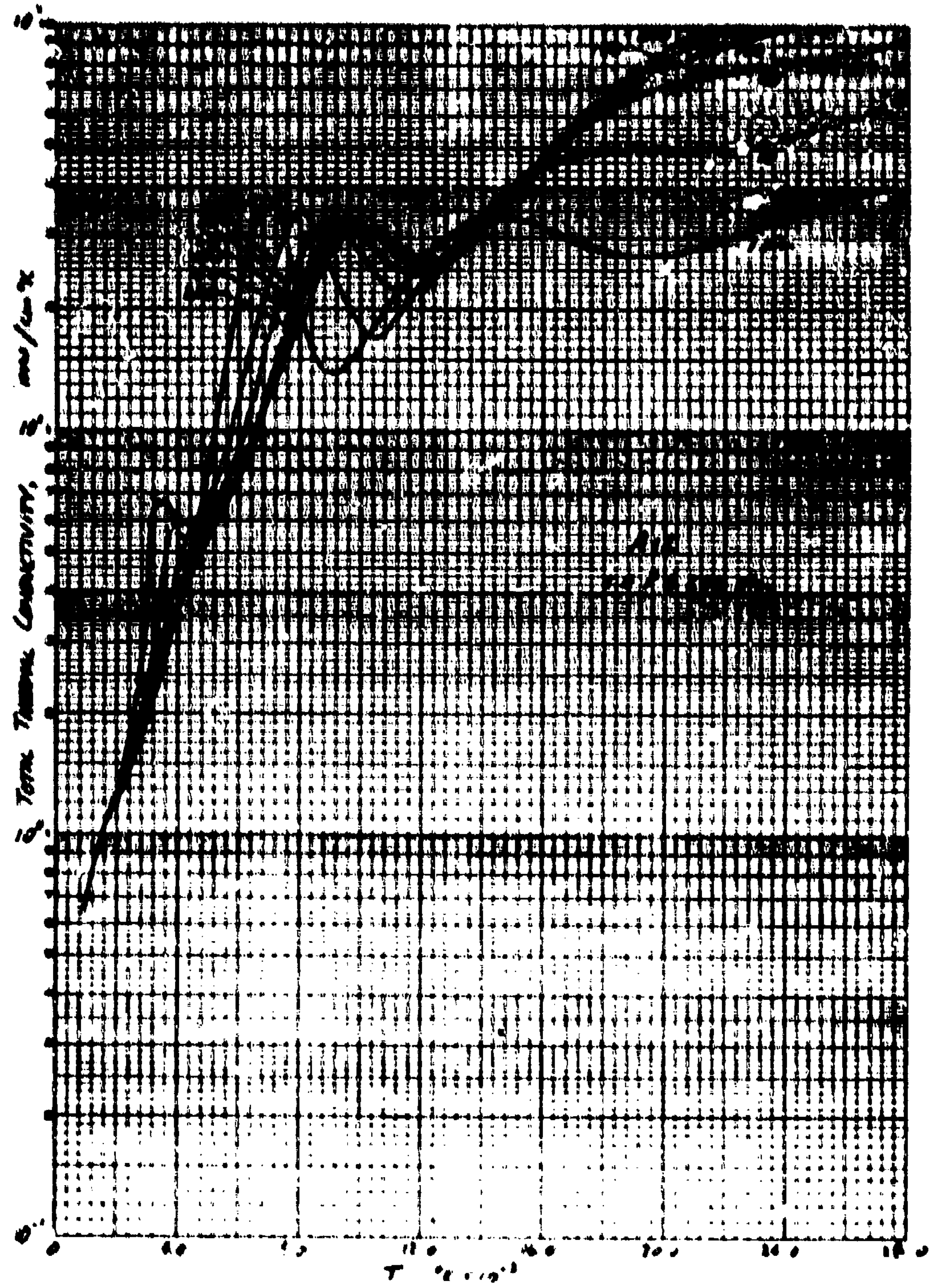

Figure B-7b. Air transport properties predicted in this work - total thermal conductivity.

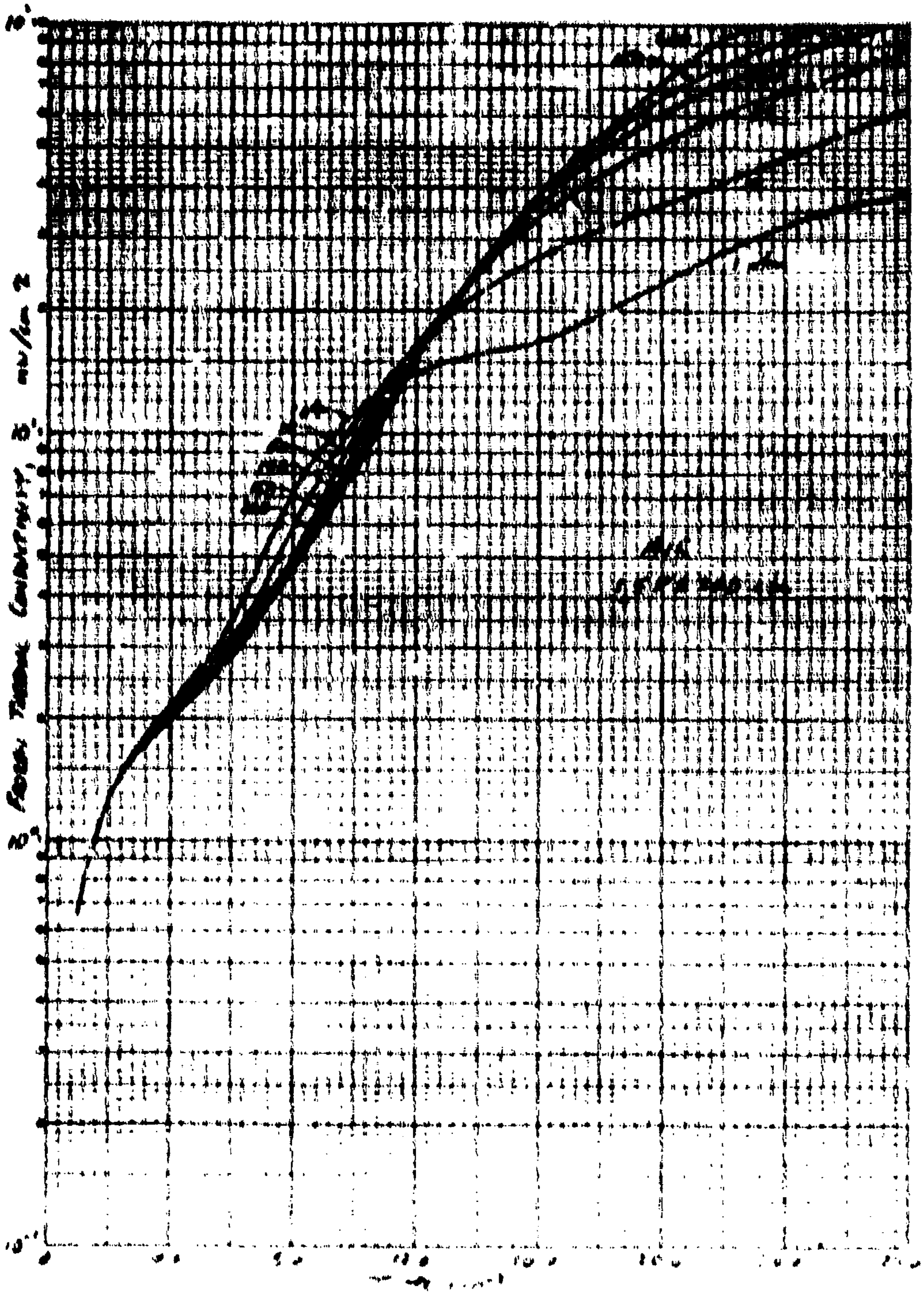

Figure B-72. Air transport properties predicted in [illegible]'s work - frozen thermal conductivity.

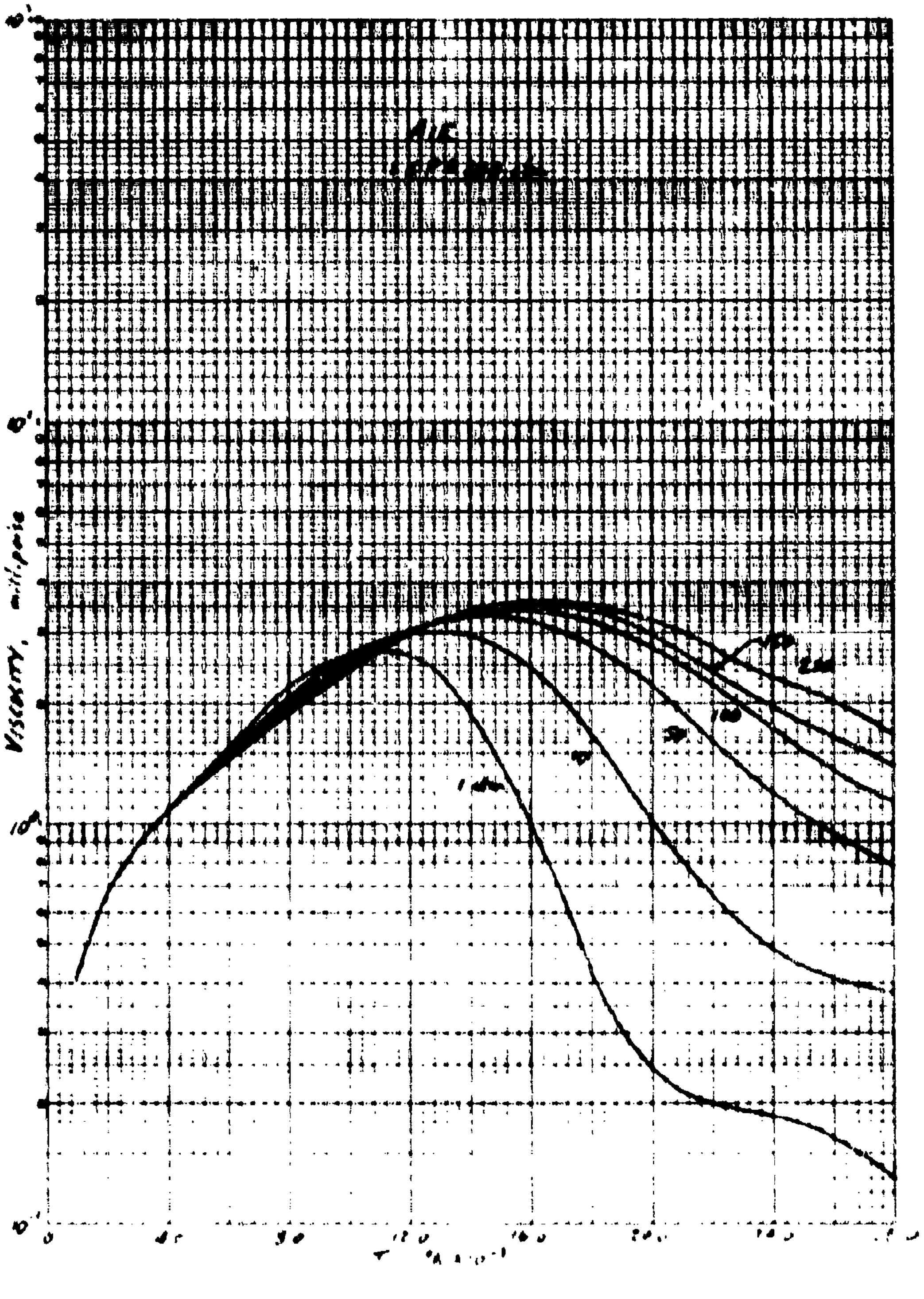

Figure B-76. Air transport properties predicted in this work - viscosity.

APPENDIX C

CALCULATION OF TURBULENT FLOW

In the calculation of turbulent flows, the shear stress τ is composed of a laminar part and a turbulent part. By defining an eddy viscosity for turbulent flow which is analogous to the kinematic viscosity of laminar flow, there results

$$\tau = \rho(\nu + \epsilon)\frac{d\bar{u}}{dy} \qquad \text{(C-1)}$$

where
- ν = kinematic viscosity
- ϵ = eddy viscosity
- ρ = fluid density
- $\frac{d\bar{u}}{dy}$ = mean velocity gradient in the direction normal to the wall

Similarly, the heat flux q is composed of laminar and turbulent contributions yielding

$$q = -\left(\frac{k}{c_p} + \frac{\rho\epsilon}{P_t}\right)\frac{d\bar{h}}{dy} \qquad \text{(C-2)}$$

where
- k = thermal conductivity
- c_p = specific heat at constant pressure
- P_t = turbulent Prandtl number
- $\frac{d\bar{h}}{dy}$ = mean enthalpy gradient in the direction normal to the wall

In the Watson and Pegot model (Reference C-2), the eddy viscosity is calculated by using Prandtl's mixing length hypothesis,

$$\epsilon = [illegible] \frac{d\bar{u}}{dy} \qquad \text{(C-3)}$$

where ℓ = mixing length. For flow in smooth pipes, the mixing length was found by Nikuradse (Reference C-1) to be independent of Reynolds number for values of $Re > 10^5$. Nikuradse's equation for mixing length is given in Equation (C-4):

$$\frac{\ell}{R} = 0.14 - 0.08\left(1 - \frac{y}{R}\right)^2 - 0.06\left(1 - \frac{y}{R}\right)^4 \qquad \text{(C-4)}$$

where

R = pipe radius

y = distance from pipe wall

In correlating data, Watson and Pegot (Reference C-2) found the Nikuradse mixing length did not provide good agreement, and reduced it by a factor of two. Thus, in the Watson and Pegot model, $\ell_W = \frac{1}{2}\,\ell_N$. This assumption gave much better correlations with low-pressure arc data.

With regards to heat flux calculations, the Watson and Pegot model assumed a turbulent Prandtl number of unity. While this is true in the vicinity of a wall, it is not true near the center of a pipe. However, no correlation prot ems in this regard were noted by Watson and Pegot. Since recent investigations have found the turbulent Prandtl number deviates considerably from unity near the axis for flow in ducts, a turbulent Prandtl number given by

$$P_t = 0.95 - 0.45\left(\frac{y}{R}\right)^2 \qquad \text{(C-5)}$$

was used in ARCFLO Version 2.

Mixing length formulations which explicitly treat the presence of a rough wall do not appear to be available in the literature. One of the principal ambiguities associated with this problem is the definition of the actual wall location as seen by the flow field when the wall is rough. A second difficulty involves determination of the equivalent sand-grain roughness height associated with a peculiar roughness geometry (such as segmented constrictor walls), a necessary step since most empirical correlations based upon experimental data for wall heat flux and shear augmentation are expressed in terms of equivalent sand-grain roughness.

Order-of-magnitude calculations carried out for the flow/wall conditions of interest here indicated that the roughness-dominated regime is approached. This means that the equivalent sand-grain roughness height is of the same order of magnitude as the laminar sublayer thickness that would exist if the wall were smooth. For this case, the friction-factor and velocity-profile data available for low-temperature, incompressible flow (see, for instance, Reference C-3), can be used to show that the mixing length at the wall, i.e., at the tops of

the roughness elements, is some fraction of the mean roughness element height. Using this result for guidance, it was decided in this work to model wall roughness effects by evaluating the van Driest mixing length formula discussed in Section 5 at "$y + K_s$" rather than "y", where y is the distance from the wall and K_s is the equivalent sand-grain roughness height. At the wall, $y = 0$, this then gives $\ell_w \leq 0.4\ K_s$ which is consistent with the aforementioned low-temperature experimental data base.

The presence of wall roughness also influences the turbulent Prandtl number near the wall. The available experimental data (e.g., References C-3 and C-4) indicate that for Reynolds numbers of 10^4 wall roughness serves to augment wall shear by a factor which is up to three times the corresponding augmentation of the wall convective heat flux. This is due to the fact that the form drag associated with the roughness elements has no heat conduction analog. This also suggests that P_{t_w} could be as large as 3. In addition, the detailed profile measurements carried out in the study described in Reference C-4 involving wall injection and suction were used to show that the Rotta correlation, Equation (C-5) above, is quite valid away from the wall. However, for $y/R < 0.05$, P_t was found to increase sharply as the wall was approached and occasionally exceeded even 3.0. Based upon the calculations described in Section 6 for air arcs, in which rough wall effects were studied parametrically, the recommended value for P_{t_w} was determined to be 3.0. For the region $y/R < 0.05$, a linear interpolation between 3.0 and 0.949, the value given by Equation (C-5) evaluated at $y/R = 0.05$, was used.

REFERENCES FOR APPENDIX C

C-1. Nikuradse, J., "Gesetzmässigkeit der turbulenten Strömung in glatten Rohren," Forschungsheft 356 (1932).

C-2. Watson, V. R. and Pegot, E. B., "Numerical Calculations for the Characteristics of a Gas Flowing Axially Through a Constricted Arc," NASA Technical Note D-4042, June 1967.

C-3. Hinze, J. O., Turbulence - An Introduction to Its Mechanism and Theory, McGraw-Hill Book Co., Inc., New York, 1959.

C-4. Simpson, R. L., Whitten, D. G., and Moffat, R. J., "An Experimental Study of the Turbulent Prandtl Number of Air with Injection and Suction," Int. J. Heat Mass Transfer, vol. 13, 1970, pp. 125-143.

APPENDIX D

CONSTRICTOR ARC DATA

As discussed in Section 6, 270 data points were gathered from six different constrictor arcs in order to select the most appropriate data for code validation. A compilation of this data is given on the following pages along with material for the identification of each constrictor arc facility.

Arnold Engineering Development Center (AEDC)
Tullahoma, Tennessee

No.	Current, amps	Voltage, volts	Constrictor Diameter, inches	Nozzle Throat Diameter, inches	Length, inches	Air Flow Rate, lbm/sec	Mass-Average Enthalpy, Btu/lbm	Pressure, atm	Efficiency, percent
1	521	2080	0.934	0.215	18.30	0.065	6603	26.3	38.3
2	427	2080	0.934	0.215	18.50	0.088	6024	26.0	41.5
3	501	2120	0.934	0.215	18.50	0.066	6089	26.2	32.4
4	475	3390	0.934	0.215	18.50	0.120	5326	53.2	43.0
5	370	3380	0.934	0.215	18.50	0.121	4500	51.0	47.1
6	575	3300	0.934	0.215	18.50	0.116	5963	53.7	38.5
7	477	4230	0.934	0.215	18.50	0.187	4663	77.6	46.6
8	561	4465	0.934	0.215	18.50	0.192	5270	84.4	42.6
9	602	4830	0.934	0.215	18.50	0.200	4448	102.0	42.0
10	682	3544	0.934	0.215	18.50	0.136	5886	64.0	34.9
11	529	3016	0.934	0.215	18.50	0.112	5140	46.0	38.1
12	543	3286	0.934	0.215	18.50	0.123	5084	52.9	37.0
13	635	3050	0.934	0.215	18.50	0.100	6340	43.9	34.5
14	525	3460	0.934	0.215	18.50	0.120	6025	58.4	42.0
15	584	4980	0.934	0.215	18.50	0.253	4256	101.5	41.2

Air Force Flight Dynamics Laboratory (AFFDL)
Wright-Patterson Air Force Base, Ohio

No.	Current, amps	Voltage, volts	Constrictor Diameter, inches	Nozzle Throat Diameter, inches	Length,* inches	Air Flow Rate, lbm/sec	Mass-Average Enthalpy, Btu/lbm	Pressure, atm	Efficiency, percent
1	1000	15,000	3.0	1.00	96.0	5.9	2080	97.28	53.8
2	2000	14,700	3.0	1.00	96.0	6.0	2300	103.40	49.5
3	2400	14,000	3.0	1.00	96.0	6.1	2400	106.80	46.0
4	2000	5,700	3.0	2.00	72.0	3.8	1500	25.85	54.5
5	2000	11,700	3.0	2.00	96.0	7.0	2500	48.30	56.3
6	3000	6,000	3.0	2.00	72.0	4.2	2800	31.97	57.4
7	4000	9,900	3.0	2.00	96.0	6.6	2960	56.78	51.9
8	3700	9,000	3.0	2.00	96.0	8.2	2960	59.18	49.7
9	2000	7,000	3.0	1.00	46.0	3.0	2800	54.08	56.8
10	2000	10,300	3.0	1.00	72.0	4.56	2300	77.86	53.6
11	2400	13,000	3.0	1.00	72.0	5.5	2000	103.40	52.1
12	2000	8,100	3.0	1.00	46.0	3.6	3050	65.31	51.1
13	2000	8,100	3.0	1.00	45.0	3.6	3050	65.31	51.1
14	4000	3,000	3.0	1.00	45.0	1.7	3000	34.36	56.8
15	4400	2,700	3.0	1.00	45.0	1.56	3400	31.97	46.8
16	4000	2,700	3.0	1.00	45.0	1.87	3300	36.37	50.2
17	2000	12,300	3.0	1.00	72.0	5.3	3400	95.24	56.2
18	2000	12,300	3.0	1.00	72.0	5.3	3400	95.24	56.2
19	3200	10,000	3.0	1.00	72.0	4.5	3080	83.67	46.2
20	3200	10,000	3.0	1.00	72.0	4.5	3080	83.67	46.2
21	3600	6,500	3.0	1.00	72.0	3.6	3300	67.36	53.6
22	3600	6,500	3.0	1.00	72.0	3.6	3300	67.36	53.6
23	1200	6,050	3.0	1.00	45.0	1.9	2200	28.57	60.7
24	1200	11,200	3.0	1.00	72.0	4.1	1600	61.56	51.5
25	1600	9,600	3.0	1.00	45.0	3.5	2000	57.82	67.3
26	1000	12,000	3.0	1.00	72.0	4.7	2000	74.83	51.6
27	2000	11,000	3.0	1.00	46.0	5.4	2650	93.80	60.6

*Downstream electrode length (Huels-type arc heater)

Sandia Laboratories
Albuquerque, New Mexico

No.	Current, amps	Voltage, volts	Constrictor Diameter, inches	Nozzle Throat Diameter, inches	Length, inches	Air Flow Rate, lbm/sec	Mass-Average Enthalpy, Btu/lbm	Pressure, atm	Efficiency, percent
1	709	2467	1.0	0.333	36.75	0.069	10,300	15.2	48.4
2	529	2180	1.0	0.333	36.75	0.082	9,700	11.7	46.1
3	1003	2309	1.0	0.333	36.75	0.064	12,980	14.5	37.0
4	382	2376	1.0	0.333	36.75	0.084	5,880	11.5	47.7
5	981	2427	1.0	0.333	36.75	0.065	13,970	14.3	41.1
6	960	1745	1.0	0.333	36.75	0.034	17,000	8.0	37.7
7	770	2417	1.0	0.333	36.75	0.068	12,430	13.8	46.3
8	753	1775	1.0	0.333	36.75	0.034	15,540	7.8	41.7
9	551	2427	1.0	0.333	36.75	0.065	9,290	13.3	47.6
10	946	1780	1.0	0.333	36.75	0.034	12,920	7.4	46.0
11	413	2503	1.0	0.333	36.75	0.066	8,190	12.4	54.3
12	377	1768	1.0	0.333	36.75	0.034	9,520	6.9	51.2

National Aeronautics and Space Administration - Johnson Space Center (NASA-JSC)
Houston, Texas

No.	Current, amps	Voltage, volts	Constrictor Diameter, inches	Nozzle Throat Diameter, inches	Length, inches	Air Flow Rate, lbm/sec	Mass-Average Enthalpy, Btu/lbm	Pressure, atm	Efficiency, percent
1	1984	5700	1.5	2.25	122.	0.237*	15,740	5.17	38.1
2	1960	4080	1.5	2.25	93.	0.262	15,670	5.16	43.4
3	1036	4100	1.5	2.25	93.	0.230*	11,087	3.86	36.7
4	2000	4620	1.5	2.25	93.	0.230*	15,236	4.97	41.6
5	1006	4000	1.5	2.25	93.	0.230*	12,001	4.03	46.5
6	1900	4940	1.5	2.25	93.	0.290	16,900	4.13	46.0
7	1000	5040	1.5	2.25	93.	0.290	10,900	4.90	51.5
8	1004	5790	1.5	2.25	93.	0.290	12,300	4.73	61.1
9	1900	4800	1.5	2.25	93.	0.303	13,000	5.03	43.6
10	496	5200	1.5	2.25	79.	0.499*	2,900	5.21	51.3
11	920	3930	1.5	2.25	79.	0.199	9,307	2.98	54.6
12	408	3820	1.5	2.25	79.	0.193	5,617	2.80	80.1
13	492	3430	1.5	2.25	64.	0.404*	2,233	4.16	88.9
14	500	3400	1.5	2.25	64.	0.633*	2,030	5.20	70.5
15	908	3850	1.5	2.25	64.	0.994*	3,238	5.00	92.7
16	1516	4715	1.5	2.25	64.	0.632*	6,194	6.70	57.7
17	1500	4220	1.5	2.25	64.	0.951*	4,905	6.19	48.6
18	1920	4460	1.5	2.25	64.	0.620*	5,706	6.86	44.7
19	496	3380	1.5	2.25	64.	0.627*	1,774	3.76	70.0
20	996	3900	1.5	2.25	64.	0.982*	3,387	5.10	92.2
21	470	3540	1.5	2.25	64.	0.620*	1,940	4.01	76.6
22	940	4010	1.5	2.25	64.	0.980*	3,872	5.44	62.8
23	1004	4500	1.5	2.25	64.	0.400	6,790	5.24	63.4
24	1956	4700	1.5	2.25	64.	0.390	12,200	6.80	54.6
25	500	3580	1.5	2.25	64.	0.304	2,576	3.74	58.4
26	1000	4170	1.5	2.25	64.	0.304	6,067	5.17	90.0
27	1504	4250	1.5	2.25	64.	0.304	8,583	6.01	84.4
28	2000	4440	1.5	2.25	64.	0.302	11,071	6.70	90.4
29	1850	4400	1.5	2.25	64.	0.336	12,877	6.49	98.2
30	1940	4365	1.5	2.25	64.	0.330	12,694	6.33	52.0
31	1380	3630	1.5	2.25	64.	0.256	13,867	4.05	76.3
32	1810	3490	1.5	2.25	64.	0.251	12,506	4.41	52.4
33	940	3300	1.5	2.25	64.	0.251	9,960	3.94	86.0

*Flow indicated is that through arc heater alone. Total flow through nozzle is higher due to additional gas injection in plenum.

NASA-JSC (Continued)

No.	Current, amps	Voltage, volts	Constrictor Diameter, inches	Nozzle Throat Diameter, inches	Length, inches	Air Flow Rate, lbm/sec	Mass-Average Enthalpy, Btu/lbm	Pressure, atm	Efficiency, percent
34	1465	2750	1.5	2.25	57.5	0.332*	6,664	3.61	57.0
35	800	3140	1.5	2.25	57.5	0.250*	2,730	3.23	30.4
36	1560	3640	1.5	2.25	57.5	0.405	8,002	5.92	65.1
37	1980	3070	1.5	2.25	57.5	0.242	13,460	4.83	56.6
38	1542	3070	1.5	2.25	57.5	0.241	11,983	4.38	64.6
39	1258	3000	1.5	2.25	57.5	0.240	10,086	4.03	67.9
40	1562	2650	1.5	2.25	57.5	0.220*	12,011	3.14	67.3
41	1044	2630	1.5	2.25	57.5	0.220*	8,007	3.06	67.6
42	1966	2620	1.5	2.25	57.5	0.215*	15,100	3.40	66.8
43	634	2450	1.5	2.25	57.5	0.210*	4,983	2.14	71.1
44	408	2200	1.5	2.25	57.5	0.147	6,066	2.07	68.0
45	906	2235	1.5	2.25	57.5	0.147	7,888	2.34	60.8
46	1214	2480	1.5	2.25	57.5	0.147	12,583	2.82	66.0
47	900	2450	1.5	2.25	57.5	0.147	9,989	2.58	70.2
48	1210	2310	1.5	2.25	57.5	0.147	9,531	2.38	52.9
49	1240	2460	1.5	2.25	57.5	0.147	12,[illegible]51	2.81	64.4
50	900	2180	1.5	2.25	57.5	0.146	7,283	2.11	57.4
51	1212	2320	1.5	2.25	57.5	0.144	10,925	2.29	58.3
52	448	2000	1.5	2.25	57.5	0.144	4,379	1.65	74.3
53	2000	2290	1.5	2.25	57.5	0.143	14,884	2.71	49.1
54	972	3560	1.5	2.25	50.0	0.220*	9,158	6.19	63.7
55	546	2910	1.5	2.25	50.0	0.220*	4,579	4.18	66.8
56	900	3022	1.5	2.25	50.0	0.398	2,626	4.39	45.7
57	1960	3570	1.5	2.25	50.0	0.397	9,643	5.80	57.8
58	1400	3500	1.5	2.25	50.0	0.394	7,290	5.20	58.6
59	1226	990	1.5	2.25	36.	0.053	12,320	1.0	57.3
60	910	960	1.5	2.25	36.	0.053	10,675	0.90	68.4
61	710	930	1.5	2.25	36.	0.053	8,160	0.80	60.7
62	510	790	1.5	2.25	36.	0.040	5,601	0.16	58.7
63	508	785	1.5	2.25	36.	0.040	5,584	0.16	59.1
64	508	780	1.5	2.25	36.	0.040	6,318	0.16	67.3
65	508	782	1.5	2.25	36.	0.040	5,391	0.15	57.4
66	1500	4200	1.5	2.25	79.	0.400	10,212	5.03	68.4
67	1500	4530	1.5	2.25	79.	0.400	9,919	5.05	61.6

*Flow indicated is that through arc heater alone. Total flow through nozzle is higher due to additional gas injection in plenum

NASA-JSC (Concluded)

No.	Current, amps	Voltage, volts	Constrictor Diameter, inches	Nozzle Throat Diameter, inches	Length, inches	Air Flow Rate, lbm/sec	Mass-Average Enthalpy, Btu/lbm	Pressure, atm	Efficiency, percent
[illegible]	1510	[illegible]	1.5	2.25	79.	[illegible]*	[illegible]	5.17	[illegible]
[illegible]	[illegible]	[illegible]	1.5	2.25	79.	[illegible]*	13,701	5.44	[illegible]
70	[illegible]	[illegible]	1.5	2.25	79.	[illegible]*	[illegible]	5.07	[illegible]
71	[illegible]	[illegible]	1.5	2.25	79.	[illegible]*	16,419	6.15	[illegible]
72	[illegible]	4700	1.5	2.25	79.	[illegible]*	[illegible]	6.22	47.5
73	[illegible]	[illegible]	1.5	2.25	79.	[illegible]*	[illegible]	6.53	[illegible]
74	[illegible]	[illegible]	1.5	2.25	79.	0.351*	[illegible]	6.67	47.0
75	[illegible]	5100	1.5	2.25	79.	0.411*	[illegible]	[illegible]	53.0
76	[illegible]	5700	1.5	2.25	93.3	[illegible]*	[illegible]	6.29	53.9
77	[illegible]	[illegible]	1.5	2.25	93.3	[illegible]*	[illegible]	6.06	47.3
78	[illegible]	[illegible]	1.5	2.25	93.3	[illegible]*	14,306	[illegible]	46.1
79	[illegible]	[illegible]	1.5	2.25	93.3	0.239	[illegible]	5.94	51.6
[illegible]	[illegible]	4670	1.5	2.25	93.3	0.241	18,740	5.64	[illegible]
81	1512	4870	1.5	2.25	93.3	0.241	[illegible]	5.20	54.9
[illegible]	[illegible]	5100	1.5	2.25	93.3	0.241	12,936	4.78	[illegible]
[illegible]	[illegible]	5725	1.5	2.25	93.3	0.372	18,070	6.94	[illegible]
[illegible]	[illegible]	[illegible]	1.5	2.25	93.3	[illegible]*	15,301	6.37	46.7
[illegible]	[illegible]	5300	1.5	2.25	93.3	[illegible]*	15,706	[illegible]	44.2
[illegible]	[illegible]	5300	1.5	2.25	93.3	[illegible]*	15,330	6.05	43.1
87	[illegible]	5440	1.5	2.25	93.3	[illegible]*	15,430	6.10	42.9
[illegible]	1904	5400	1.5	2.25	93.3	0.300*	15,043	6.12	46.3
[illegible]	1906	5430	1.5	2.25	93.3	0.304*	16,200	6.49	46.7
90	[illegible]	4700	1.5	2.25	93.3	0.241	17,430	7.54	48.1

*Flow indicated is that through arc heater alone. Total flow through nozzle is higher due to additional gas injection in plenum.

National Aeronautics and Space Administration - Ames Research Center (NASA Ames, 6 cm)
Moffett Field, California

No.	Current, amps	Voltage, volts	Constrictor Diameter, inches	Nozzle Throat Diameter, inches	Length, inches	Air Flow Rate, lbm/sec	Mass-Average Enthalpy, Btu/lbm	Pressure, atm	Efficiency, percent
1	1047	1856	2.362	1.50	47.0	0.833	1,600	4.44	41.1
2	3050	2597	2.362	1.50	47.0	0.828	4,000	6.90	37.3
3	3006	2873	2.362	1.50	47.0	0.811	4,700	8.90	37.9
4	3000	2513	2.362	1.50	47.0	0.770	4,600	6.73	43.3
5	1771	1750	2.362	1.50	47.0	0.700	1,000	4.15	30.2
6	3050	2005	2.363	1.50	47.0	0.610	6,000	7.61	40.5
7	3300	2306	2.362	1.50	47.0	0.586	4,000	5.04	37.9
8	3519	2444	2.362	1.50	47.0	0.500	5,605	6.51	38.1
9	3311	2307	2.362	1.50	47.0	0.514	5,900	4.80	41.9
10	3006	2304	2.362	1.50	47.0	0.496	6,700	5.06	42.5
11	4007	2727	2.362	1.50	47.0	0.470	9,000	6.75	30.8
12	3773	2296	2.362	1.50	47.0	0.460	7,400	4.53	41.5
13	3005	2423	2.362	1.50	47.0	0.418	9,500	4.76	47.0
14	4154	2447	2.362	1.50	47.0	0.402	9,800	5.76	41.4
15	4023	2251	2.362	1.50	47.0	0.300	10,100	5.04	30.8
16	4430	2194	2.362	1.50	47.0	0.197	11,000	3.01	38.4
17	6002	1802	2.362	1.50	47.0	0.290	10,300	3.70	33.7
18	6104	1521	2.362	1.50	47.0	0.205	16,500	1.82	46.5
19	6432	1639	2.362	1.50	47.0	0.266	17,400	1.83	46.6
20	5620	1614	2.362	1.50	47.0	0.181	14,700	2.25	30.9
21	1020	2070	2.362	1.12	93.7	0.103	6,175	1.94	31.8
22	976	2040	2.362	1.12	93.7	0.179	6,300	3.36	40.1
23	954	3017	2.362	1.12	93.7	0.262	5,057	4.63	44.5
24	974	2705	2.362	1.12	93.7	0.160	6,030	2.04	37.3
25	1500	1957	2.362	1.12	93.7	0.104	7,005	2.06	30.7
26	1640	3310	2.362	1.12	93.7	0.239	7,200	4.90	30.1
27	1600	3770	2.362	1.12	93.7	0.293	6,900	5.61	30.6
28	1443	4326	2.362	1.12	93.7	0.357	6,640	6.80	40.3
29	1439	4930	2.362	1.12	93.7	0.445	6,170	8.42	41.1
30	1650	1895	2.362	1.12	93.7	0.100	6,970	2.05	23.5
31	1617	2700	2.362	1.12	93.7	0.180	7,160	3.57	30.6
32	1605	4126	2.362	1.12	93.7	0.331	7,320	6.76	35.0
33	1670	5350	2.362	1.12	93.7	0.491	6,640	9.00	39.7
34	605	2700	2.362	1.12	93.7	0.103	4,460	1.01	34.6
35	613	3050	2.362	1.12	93.7	0.184	4,830	3.12	44.3
36	596	4430	2.362	1.12	93.7	0.265	4,000	4.41	47.4
37	587	5400	2.362	1.12	93.7	0.330	4,700	5.51	52.9
38	391	1657	2.362	1.12	93.7	0.050	3,170	1.19	28.0
39	540	1700	2.362	1.12	93.7	0.066	4,050	1.15	29.7
40	611	1640	2.362	1.12	93.7	0.071	4,000	1.20	27.5

[illegible] Runs, 6 cm (Continued)

No.	Current, amps	Voltage, volts	Constrictor Diameter, inches	Nozzle Throat Diameter, inches	Length, inches	Air Flow Rate, lbm/sec	Mass-Average Enthalpy, Btu/lbm	Pressure, atm	Efficiency, percent
41	1112	1627	2.362	1.12	93.7	0.073	4,986	1.37	22.8
42	1404	1900	2.362	1.12	93.7	0.073	5,010	1.43	25.0
43	1775	1473	2.362	1.12	93.7	0.070	3,730	1.46	20.6
44	2000	1900	2.362	1.12	93.7	0.074	4,000	1.52	16.3
45	2263	1524	2.362	1.12	93.7	0.073	4,170	1.56	9.6
46	651	1611	2.362	1.12	93.7	0.072	3,371	1.33	66.3
47	777	1004	2.362	1.12	93.7	0.073	3,916	1.35	71.1
48	800	1003	2.362	1.12	93.7	0.073	3,961	1.36	71.4
49	604	2400	2.362	1.12	93.7	0.195	6,579	3.00	46.7
50	538	2436	2.362	1.12	93.7	0.206	6,067	3.42	47.5
51	501	2642	2.362	1.12	93.7	0.212	6,262	3.92	43.8
52	606	2606	2.362	1.12	93.7	0.208	6,216	3.00	46.0
53	700	2882	2.362	1.12	93.7	0.217	4,921	3.90	40.6
54	770	2720	2.362	1.12	93.7	0.219	5,411	4.02	43.1
55	706	2638	2.362	1.12	93.7	0.224	5,667	4.06	46.2
56	770	2664	2.362	1.12	93.7	0.227	6,006	4.40	46.3
57	1070	2006	2.362	1.12	93.7	0.201	7,173	3.02	43.5
58	1006	3304	2.362	1.12	93.7	0.218	7,362	4.07	44.8
59	1003	3400	2.362	1.12	93.7	0.217	7,400	4.13	45.4
60	1046	3601	2.362	1.12	93.7	0.228	7,127	4.23	46.1
61	1010	3602	2.362	1.12	93.7	0.225	7,666	4.27	46.0
62	2009	4362	2.362	1.12	93.7	0.414	7,998	8.62	27.6
63	906	2202	2.362	1.12	93.7	0.107	5,762	2.09	29.7
64	1647	2075	2.362	1.12	93.7	0.110	7,676	2.30	26.2
65	2041	2003	2.362	1.12	93.7	0.100	7,300	2.08	19.6
66	517	2061	2.362	1.12	93.7	0.101	4,037	1.77	26.9
67	1003	2707	2.362	1.12	93.7	0.150	7,652	1.90	37.2
68	1466	2657	2.362	1.12	93.7	0.100	7,909	2.19	30.0
69	1904	2029	2.362	1.12	93.7	0.100	9,702	1.79	26.4
70	2006	1973	2.362	1.12	93.7	0.109	8,763	2.36	20.7
71	2900	2075	2.362	1.12	93.7	0.117	10,007	2.43	26.5
72	2904	2000	2.362	1.12	93.7	0.206	10,250	4.47	26.2
73	2643	2024	2.362	1.12	93.7	0.206	9,131	4.37	27.0
74	2056	2002	2.362	1.12	93.7	0.205	9,000	4.29	31.9
75	1536	3124	2.362	1.12	93.7	0.205	7,053	4.10	35.5
76	1066	3366	2.362	1.12	93.7	0.205	6,700	3.09	40.8
77	537	4019	2.362	1.12	93.7	0.204	4,643	3.01	44.7
78	609	5122	2.362	1.12	93.7	0.310	5,302	5.27	53.0
79	1079	4430	2.362	1.12	93.7	0.311	6,004	5.79	47.6
80	1401	3972	2.362	1.12	93.7	0.299	8,377	5.01	44.3
81	1970	3804	2.362	1.12	93.7	0.290	8,350	6.16	36.9

NASA Ames, 6 cm (Continued)

No.	Current, amps	Voltage, volts	Constrictor Diameter, inches	Nozzle Throat Diameter, inches	Length, inches	Air Flow Rate, lbm/sec	Mass-Average Enthalpy, Btu/lbm	Pressure, atm	Efficiency, percent
82	1636	3730	2.362	1.12	93.7	0.300	8,901	0.33	30.7
83	2020	3680	2.362	1.12	93.7	0.300	9,110	0.52	26.8
84	2000	4733	2.362	1.12	93.7	0.391	11,214	0.41	36.9
85	2005	4416	2.362	1.12	93.7	0.391	8,165	0.38	32.2
86	1995	4341	2.362	1.12	93.7	0.391	7,098	0.05	36.4
87	2520	4042	2.362	1.12	93.7	0.505	8,457	10.97	30.3
88	509	1972	2.362	3.36	92.5	0.066	2,410	0.85	26.4
89	510	2036	2.362	3.36	92.5	0.116	2,981	1.20	38.3
90	490	2001	2.362	3.36	92.5	0.154	2,260	1.28	23.2
91	1012	2103	2.362	3.36	92.5	0.126	4,218	1.46	25.2
92	1552	2300	2.362	3.36	92.5	0.120	5,190	1.55	22.9
93	1518	2037	2.362	3.36	92.5	0.126	5,379	1.56	27.4
94	771	2215	2.362	3.36	92.5	0.114	4,196	1.25	29.5
95	1010	2091	2.362	3.36	92.5	0.116	4,680	1.33	27.0
96	1513	1967	2.362	3.36	92.5	0.118	5,964	1.43	25.0
97	2003	2070	2.362	3.36	92.5	0.131	7,252	1.66	25.1
98	2514	2032	2.362	3.36	92.5	0.135	7,865	1.76	19.6
99	2576	2712	2.362	3.36	92.5	0.216	7,080	2.70	25.5
100	2001	2756	2.362	3.36	92.5	0.210	6,465	2.70	26.6
101	1500	2905	2.362	3.36	92.5	0.210	5,614	2.60	29.8
102	1027	3121	2.362	3.36	92.5	0.210	4,376	2.42	31.5
103	767	3279	2.362	3.36	92.5	0.210	3,474	2.29	31.8
104	373	4258	2.362	3.36	92.5	0.303	4,000	3.23	40.6
105	1003	3807	2.362	3.36	92.5	0.303	4,502	3.44	37.6
106	1500	3400	2.362	3.36	92.5	0.300	5,914	3.36	32.7
107	2010	3390	2.362	3.36	92.5	0.308	6,621	3.61	31.6
108	2505	3266	2.362	3.36	92.5	0.300	7,336	3.07	30.2
109	2002	3716	2.362	3.36	92.5	0.404	6,330	4.12	30.6
110	2002	4010	2.362	3.36	92.5	0.402	6,178	4.94	32.4
111	1511	4166	2.362	3.36	92.5	0.406	5,088	4.77	36.4
112	766	2266	2.362	3.36	92.5	0.176	3,614	1.31	26.3
113	1515	2802	2.362	3.36	92.5	0.210	5,567	2.54	30.2
114	1512	2871	2.362	3.36	92.5	0.218	5,575	2.54	29.5
115	1502	2910	2.362	3.36	92.5	0.217	5,021	2.54	27.5
116	1519	2823	2.362	3.36	92.5	0.117	5,300	2.12	30.1
117	1510	3000	2.362	3.36	92.5	0.300	5,322	3.49	32.2
118	1515	2579	2.362	3.36	92.5	0.311	5,555	1.60	41.9
119	1516	3094	2.362	3.36	92.5	0.314	5,515	3.66	33.5
120	1512	3063	2.362	3.36	92.5	0.314	5,306	3.67	32.6
121	760	3476	2.362	3.36	92.5	0.135	4,035	1.49	37.7
122	[illegible]	1967	2.362	3.36	92.5	0.142	5,991	1.64	33.0

[illegible] Amps, 6 cm (Concluded)

No.	Current, amps	Voltage, volts	Constrictor Diameter, inches	Nozzle Throat Diameter, inches	Length, inches	Air Flow Rate, lbm/sec	Mass-Average Enthalpy, Btu/lbm	Pressure, atm	Efficiency, percent
123	1988	2244	2.362	3.36	92.5	0.142	6,312	1.70	28.9
124	2012	2084	2.362	3.36	92.5	0.130	6,244	1.74	22.0
125	2005	1734	2.362	3.36	92.5	0.109	5,566	1.30	14.0
126	2070	1708	2.362	3.36	92.5	0.109	6,067	1.03	14.6
127	777	2364	2.362	3.36	92.6	0.132	3,435	1.02	26.0
128	1611	3572	2.362	3.36	92.5	0.312	5,502	3.70	34.1
129	1603	3570	2.362	3.36	92.5	0.310	5,500	3.63	33.5
130	1509	3544	2.362	3.36	92.5	0.310	5,416	3.65	33.1
131	1507	3549	2.362	3.36	92.5	0.310	5,400	3.63	33.1
132	1515	3563	2.362	3.36	92.5	0.306	5,541	3.65	33.4
133	1506	3582	2.362	3.36	92.5	0.300	5,605	3.64	33.9
134	1605	3579	2.362	3.36	92.5	0.300	5,619	3.62	33.9
135	1510	3580	2.362	3.36	92.5	0.300	5,675	3.64	33.0

Martin Marietta Corporation, Denver Division (MMC)
Denver, Colorado

No.	Current, amps	Voltage, volts	Constrictor Diameter, inches	Nozzle Throat Diameter, inches	Length, inches	Air Flow Rate, lbm/sec	Mass-Average Enthalpy, Btu/lbm	Pressure, atm	Efficiency, percent
1	350	263	1.0	0.397	6.55	0.011	4,920	1.07	62.0
2	530	4160	1.0	0.397	35.48	0.198	5,134	25.6	48.6
3	800	5507	1.0	0.397	49.85	0.190	8,127	29.9	37.0
4	900	6176	1.0	0.397	64.15	0.147	10,037	24.76	28.0
5	1600	1295	1.0	0.397	28.33	0.030	14,200	5.24	21.7
6	1200	243	1.0	0.397	6.50	0.006	11,206	0.95	24.3
7	400	492	1.0	0.397	13.95	0.065	2,020	0.345	70.4
8	1000	375	1.0	0.397	13.95	0.009	15,175	0.065	38.4
9	1350	2658	1.0	0.397	57.00	0.082	14,572	0.833	35.1
10	650	5511	1.0	0.397	57.00	0.264	7,367	2.29	57.4
11	700	4255	1.0	0.397	57.00	0.141*	8,420	3.63	42.1

*Total flow 0.560 lbm/sec; 0.141 lbm/sec through arc, balance introduced in plenum.

APPENDIX E

USER'S MANUAL FOR ARCFLO, VERSION 2

This appendix provides the information required to operate the ARCFLO Version 2 computer program. Sections E.1 and E.2 provide input instructions and output descriptions, respectively. Section E.3 provides a global flow diagram and FORTRAN listing of the code. Section E.4 presents a sample problem (the NMC test point discussed in Section 6) which was run on a CDC 7600 computer. For the sample problem, a listing of the input decks and a few typical pages of the output are included.

E.1 INPUT INSTRUCTIONS

Input to ARCFLO consists of two decks, Deck A and Deck B. Deck B contains thermodynamic, transport, and radiative property data of air at six different pressures. Deck B is to be viewed as a permanent deck and no changes are to be made.

The following are instructions to assemble Deck A.

DECK A (Called from Routine BOUNDC)

Card 1: FORMAT (12A6) TITLE

Title for the particular run, used for identification of printed output. Columns 1-72 are punched with the desired title (alphanumeric).

Card 2: FORMAT (3I4) KMAX, KINC, KTAB

Field 1 (Columns 1-4, RIGHT JUSTIFIED)

KMAX - Maximum number of axial stations (should not exceed 5000)

Field 2 (Columns 5-8, RIGHT JUSTIFIED)

KINC - Axial station interval for printing output, usually set to a value in the range 30 to 120.

Field 3 (Columns 9-12, RIGHT JUSTIFIED)

KTAB - Flag to print out input property tables (Deck B) and corresponding internally-generated tables with finer resolution, leave blank for no output, set to 1 for output

Card 3: FORMAT (2I4) NMESH

Field 1 (Columns 1-4, RIGHT JUSTIFIED)

NMESH - Number of radial increments from center to wall, usually set to either 13 or 25

Card 4: FORMAT (I4) ITURB

Field 1 (Columns 1-4, RIGHT JUSTIFIED)

ITURB - Flag for selecting turbulence model, set to 0 for Watson and Pegot model, set to 1 for model described in Section 5 of this report

Card 5: FORMAT (I4) ISTART

Field 1 (Columns 1-4, RIGHT JUSTIFIED)

ISTART - Flag reserved for restart option (currently not used, leave blank)

Card 6: FORMAT (4F10.0) AMPS, WS, TRCL, P(1)

Field 1 (Columns 1-10)

AMPS - Input current in amps

Field 2 (Columns 11-20)

WS - Inlet mass flow rate in kg/sec

Field 3 (Columns 21-30)

TRCL - Transpiration cooling flow rate in kg/sec-m^2

Field 4 (Columns 31-40)

P(1) - Inlet pressure in atm

Card 7: FORMAT (7F10.0) DIA, THETA, HW, ZCRIT, ZMAX, RKS, TPRW

Field 1 (Columns 1-10)

DIA - Diameter of the constrictor in meters

Field 2 (Columns 11-20)

THETA - Nozzle divergence angle in degrees

Field 3 (Columns 21-30)

HW - Wall enthalpy in joules/kg

Field 4 (Columns 31-40)

ZCRIT - Axial distance after which current is turned off (i.e., AMPS = 0) in meters

Field 5 (Columns 41-50)

ZMAX - Maximum axial distance in meters for which solution is desired

Field 6 (Columns 51-60)

RKS - Equivalent sand-grain roughness height for constrictor wall in meters (0.0000889 m for the NMC arc, 0.000127 m for AEDC arc)

Field 7 (Columns 61-70)

TPRW - Turbulent Prandtl number at the constrictor wall, generally set equal to 1.0 for high-pressure arcs

Card 8: FORMAT (4F10.0) FZO, EX, EXX, EPS

Field 1 (Columns 1-10)

FBO - Length of first axial increment divided by the characteristic length ZO, usually set to FBO = 0.0001 (multiplied internally by 1.0E-06)

Field 2 (Columns 11-20)

EX - Axial distance increment factor, usually set to EX = 1.05

Field 3 (Columns 21-30)

EXX - Stability factor, usually set to EXX = 0.16

Field 4 (Columns 31-40)

EPS - Maximum allowable relative discrepancy of the mass flow rate, usually set to EPA = 1.0 (multiplied internally by 1.0E-04)

Card 9: FORMAT (6F10.0) ZZ1, ZZ2, ZZ3, ZZ4, DD2, DD3

These parameters are associated with a code option designed to treat variable-area constrictors. This option has not been checked out and should not be utilized. Set all ZZ's equal to ZMAX and set all DD's equal to DIA.

Card (set) 10: FORMAT (8F10.0) H(1,J), J = 1, NNNRN

Field 1 (Columns 1-10), Field 2 (Columns 11-20), etc., eight to a card

H(1,J) - Inlet total enthalpy profile in joules/kg (multiplied internally by 1.0E+07)

Card (set) 11: FORMAT (8F10.0) U(1,J), J = 1, NNNRN

Field 1 (Columns 1-10), Field 2 (Columns 11-20), etc., eight to a card

U(1,J) - Inlet axial velocity profile in meters/sec (relative values only, corrected to satisfy global mass continuity)

DECK B (Called from Routine WTAB)

Permanent deck cards continue.

E.3 OUTPUT DESCRIPTION

The ARCFLO Version 2 code prints a detailed output block for each of the first three axial stations. Then, as the axial marching is continued, additional output blocks are provided at every KINCth axial station. Note that KINC is an input parameter.

Each output block occupies two pages and contains both input parameters and quantities which are calculated for the current axial station. The top of the output block contains the title of the problem which is supplied by the user for identification purposes. Various input parameters then follow, including diameter, current, flow rate, wall injection rate, number of radial nodes, and axial stepsize and stability parameters. The various calculated quantities appear next. These include global parameters, such as bulk enthalpy, and local

parameters, such as the enthalpy, velocity, and mass flux at each point in the flow field where a node is located. In general, the value of each parameter is provided in both English and SI units.

The quantities LOC and DM shown on the output require some explanation. The quantity LOC is the number of pressure iterations required to satisfy the total mass flow rate at each axial station. The quantity DM is the error in the total mass balance, i.e.,

$$DM = \frac{\dot{m}_{calc} - \dot{m}_{input}}{\dot{m}_{input}}$$

where $\dot{m}$ is the mass flow rate.

Towards the bottom of the first page of the output block, the current axial distance, mass average enthalpy, wall heat transfer rates by molecular and turbulent conduction and radiation, voltage, and efficiency are printed out.

In one version of the code, a set of diagnostic information is included as the next to last entry on the first page of the output block. The code authors at Aerotherm should be consulted for interpretation of this information.

The final line of output on the first page contains the input wall turbulent Prandtl number and equivalent sand-grain roughness height, and the calculated wall radiation fluxes for the two individual wavelength bands described in Section 3.

The second page of the output block contains radial distributions of temperature, TEMPERATURE; mean absorption coefficients for the two bands, K1 and K2; emissive power, SEE; heat flux potential, PHI ($= \int K\, dT$); electrical conductivity, SIGMA; gas density, DENSITY; viscosity, VISCOSITY; mixing length, MIXL; divergence of the radiative heat flux, DIVQR ($= -\frac{1}{r}\frac{\partial}{\partial r}(rq_r)$); divergence of the molecular conduction heat flux, DIVQC ($= -\frac{1}{r}\frac{\partial}{\partial r}(rq_c)$); divergence of the turbulent conduction heat flux, DIVQCT ($= -\frac{1}{r}\frac{\partial}{\partial r}(rq_t)$); radial convection, RADCON ($= \rho v \frac{\partial H}{\partial r}$); axial convection, AXCON ($= \rho u \frac{\partial H}{\partial z}$); ohmic heating, OHMIC HTG ($= \sigma E_z^2$); and radial mass flux, RHOV ($= \rho v$).

E.3 FLOW DIAGRAM AND CODE LISTING

Figure E-1 presents the flow diagram of the ARCFLO Version 2 code. The functions of the various subroutines are briefly described on the flow chart. A Fortran listing of the code is presented in Figure E-2. The Fortran variables list is given in Reference 1 and hence is not reproduced here.

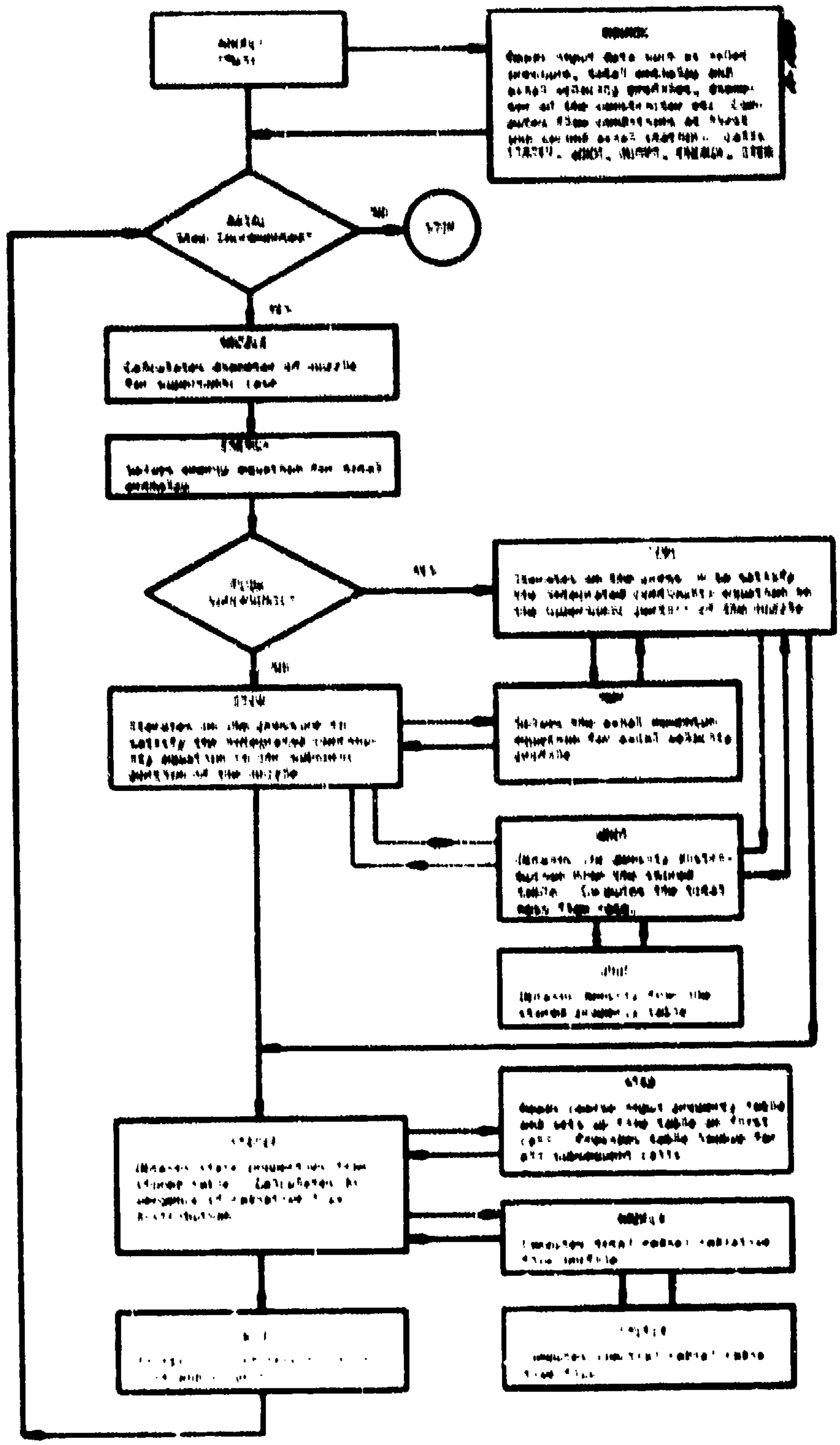

Figure I-1. Flow diagram of the ARCFIT code, version 2

```
C SET INITIAL CONDITIONS AND COMPUTE FIRST AXIAL STEP
C MAIN LOOP FOR COMPUTING EACH AXIAL STEP
C READ TITLE CARD
```

Figure C-2. FORTRAN listing of ARCFLO Version 2.

```
C
C INCREASE IN FLOW RATE FROM TRANSPIRATION COOLING
      [illegible]
C
C ALTERNATING STORAGE LOCATION FOR AXIAL STATIONS
      [illegible]
C
C EVALUATION OF THE ENTHALPY AT NEXT AXIAL STATION FROM ENERGY EQUATION
      CALL [illegible]
      [illegible]
  ... CONTINUE
C
C CHECK FOR SUPERSONIC OR SUBSONIC FLOW
      IF([illegible]) [illegible]
C
C CALCULATION OF VELOCITY AT NEXT STA THRU ITERATION - SUBSONIC FLOW
      CALL [illegible]
      GO TO [illegible]
C
C CALCULATION OF VELOCITY AT NEXT STA THRU ITERATION - SUPERSONIC FLOW
      CALL [illegible]
C
C CHECK FOR CHOKED FLOW
C   IF CHOKED AND SUBSONIC, START DIVERGING NOZZLE
C   IF CHOKED AND SUPERSONIC, GIVE ERROR READING AND EXIT
      [illegible]
      CALL OUTPUT
      [illegible]
      CALL [illegible]
      [illegible]
      CALL [illegible]
      [illegible]
   [illegible] CONTINUE
C
C IF PRESSURE TOO LOW FOR GAS TABLES, EXIT
      IF([illegible]) [illegible]
      CALL OUTPUT
      GO TO [illegible]
C
C WRITE OUT VALUES FOR EVERY [illegible] AXIAL STATION
      [illegible]
      CALL OUTPUT
      [illegible]
C
C     THIS SET OF STATEMENTS IS FOR CHANGING UNITS
```

Figure C-2. Continued.

```
[illegible]
```

Figure E-2. Continued.

[illegible]

Figure E-2. Continued.

```
      [illegible]
      [illegible]
      CALL OUTPUT
C
C CALCULATE THE PROPERTIES FOR THE SECOND AXIAL STATION
      [illegible]
      CALL [illegible]
      [illegible]
      CALL [illegible]
      CALL [illegible]
      CALL STATE
      CALL OUTPUT
C 100 FORMAT([illegible])
C 101 FORMAT([illegible])
C 102 FORMAT([illegible])
      GO TO 999
  900 CONTINUE
C     CALL [illegible]
  999 CONTINUE
      [illegible]
      RETURN
      END
```

```
      SUBROUTINE ENERGY
      [illegible]
C
C CALCULATE THE ENTHALPY AT THE NEXT AXIAL STATION
      [illegible]
      DO 9 [illegible]
      [illegible]
      DO 60 [illegible]
      [illegible]
 1000 [illegible]
      GO TO 3000
 2000 [illegible]
 3000 CONTINUE
      [illegible] GO TO 110
      [illegible]
   60 [illegible]
      [illegible]
```

Figure E-2. Continued.

```
[illegible]
```

Figure E-2. Continued.

Figure E-2. Continued.

```
      SUBROUTINE [illegible]
      COMMON/COM1/ [illegible], LOC, L, [illegible]
     1[illegible]
      COMMON/COM2/ [illegible]
      COMMON/COM3/ [illegible]
      COMMON/COM4/ [illegible]
      COMMON/COM5/ [illegible]
      COMMON/MPL1/ [illegible]
      DIMENSION [illegible]
     ,[illegible]
     ,[illegible]
C
C EVALUATION OF THE FLOW RATE, AVERAGE DENSITY, AND ENERGY FLUX
      FIRST = 1.0
      [illegible]
      DO [illegible]
          CALL [illegible]
          [illegible]
          IF(J-1) [illegible]
 31       [illegible]
          [illegible]
 31 CONTINUE
      [illegible]
      CALL [illegible]
      LAST = 1
      RETURN
      END
```

```
      SUBROUTINE ITER
      COMMON/COM1/ [illegible], LOC, L, [illegible]
     1[illegible]
      COMMON/COM2/ [illegible]
      COMMON/COM3/ [illegible]
      COMMON/COM4/ [illegible]
      COMMON/COM5/ [illegible]
      DIMENSION [illegible]
     ,[illegible]
     ,[illegible]
C
C ITERATION TO CALCULATE THE VELOCITY AT THE NEXT AXIAL STATION - SUBSONIC
C     VELOCITY IS FROM MOMENTUM EQUATION
C     ITERATE UNTIL THE MASS FLOW IS CONSERVED
      FIRST = 1.0
      IND = 0
      [illegible]
      DPINT = DP
      [illegible]
      IF(ABS(DP)-.001) 21,21,22
   21 [illegible]
   22 CONTINUE
      P(K) = P(K-1) + DP
      LOC = 0
      [illegible]
      DO 15 [illegible]
          [illegible]
          CALL [illegible]
          [illegible]
          CALL [illegible]
          [illegible]
          IF(ABS [illegible]
    1         IF([illegible]
    3             IF(IND) [illegible]
    5                 [illegible]
    7                 DP = DP - [illegible]
                      P(K) = P(K-1) + DP
                      IF(P(K)) 17,17,15
    6             CONTINUE
                  DP = DP + [illegible]
                  P(K) = P(K-1) + DP
              IND = 1
   15 CONTINUE
   17 [illegible] = 1
      DP = DPINT
      LAST = 1
   30 CONTINUE
      RETURN
      END
```

Figure E-2. Continued.

```
      SUBROUTINE ITER
      [illegible]
C
C ITERATION TO CALCULATE THE VELOCITY AT THE NEXT AXIAL STATION - SUPERSONIC
C     VELOCITY IS FROM MOMENTUM EQUATION
C     ITERATE UNTIL THE MASS FLOW IS CONSERVED
      [illegible]
   15 CONTINUE
      [illegible]
   21 CONTINUE
      RETURN
      END
```

```
      SUBROUTINE [illegible]
      [illegible]
C
C CALCULATE THE VELOCITY AT THE NEXT AXIAL STATION
      [illegible]
C
C CORRECTION FOR RADIAL CONVECTION
      [illegible]
```

Figure E-2. Continued.

```
[illegible]
50 CONTINUE
[illegible]
LAST = 1
RETURN
END
```

Figure E-2. Continued.

Figure C-2. Continued.

[illegible]

Figure E-2. Continued.

```
[illegible]
C     SET UP DEPENDENT VARIABLE TEMPERATURE, PRESSURE/DENSITY, VISCOSITY,
C     THERMAL CONDUCTIVITY, ELECTRICAL CONDUCTIVITY, AND HEAT FLUX
C     POTENTIAL ARRAYS
[illegible]
C     SET UP DEPENDENT VARIABLE RADIATION PARAMETER ARRAYS
[illegible]
C     LINEAR INTERPOLATION ON LOG OF PRESSURE
[illegible]
```

Figure E-2. Continued.

```
[illegible]
[illegible]
      GO TO [illegible]
[illegible]
[illegible]
      GO TO [illegible]
[illegible]
[illegible]
C     [illegible]
[illegible]
[illegible]
      GO TO [illegible]
[illegible]
[illegible]
[illegible]
[illegible]
[illegible]
[illegible]
[illegible]
[illegible]
      RETURN
[illegible]
[illegible]
[illegible]
      GO TO [illegible]
   [illegible] CONTINUE
[illegible]
[illegible]
[illegible]
[illegible]
[illegible]
[illegible]
[illegible]
[illegible]
[illegible]
[illegible]
[illegible]
[illegible]
[illegible]
[illegible]
[illegible]
[illegible]
[illegible]
[illegible]
[illegible]
      RETURN
      END
```

```
      SUBROUTINE [illegible]
[illegible]
[illegible]
[illegible]
[illegible]
[illegible]
[illegible]
[illegible]
[illegible]
[illegible]
[illegible]
[illegible]
[illegible]
[illegible]
[illegible]
[illegible]
[illegible]
[illegible]
      DO [illegible]
[illegible]
[illegible]
[illegible]
[illegible]
[illegible]
[illegible]
[illegible]
[illegible]
[illegible]
[illegible]
[illegible]
[illegible]
[illegible]
[illegible]
 [illegible] CONTINUE
      RETURN
      END
```

Figure E-2. Continued.

Figure E-2. Continued.

Figure E-2. Continued.

```
[illegible]
```

Figure E-2. Concluded.

E.4 SAMPLE PROBLEM

This sample problem is the solution provided by ARCFLO, Version 2, for NMC Test Point 80b (Run 16 of Section 6). A listing of the input cards for this problem is shown first. Included are both Deck A, as described in Section E.1, and Deck B, which is the permanent properties deck for air. Then follows several pages of sample output. Output is illustrated for the first three stations and, in addition, for station 483 (z = 10.89 inches) and station 1683 (z = 67.12 inches). The solution was carried out to station 2500 (z > 100 inches), and the total computer time requirement for a CDC 7600 computer was 31 seconds (compilation plus execution).

INPUT - SAMPLE PROBLEM

[illegible]

.0000000 1.0

.25 .125 .15

67.37 50.53 21.66

[illegible]

INPUT – SAMPLE PROBLEM (Continued)

INPUT - SAMPLE PROBLEM (Continued)

INPUT - SAMPLE PROBLEM (Continued)

[illegible]

INPUT – SAMPLE PROBLEM (Concluded)

[illegible]

OUTPUT — SAMPLE PROBLEM

[illegible]

[illegible]

OUTPUT – SAMPLE PROBLEM (Continued)

[illegible]

OUTPUT – SAMPLE PROBLEM (Continued)

OUTPUT – SAMPLE PROBLEM (Concluded)

[illegible]

OUTPUT - SAMPLE PROBLEM 1

Sample Problem 1 P = 150 atm I = 1500 amps Dia. = 1.75 inch

AXIAL STATION = 1   DC THERMAL ARC WITH AXIAL GAS FLOW

AXIAL DIST = 0.000 METERS
0.000 INCHES
VOLTAGE GRAD = [illegible] VOLTS/M
[illegible] VOLTS/INCH
WALL HEAT FLUX = [illegible] WATTS/M**2
[illegible] BTU/FT2-SEC
RADIATION LOSS = [illegible] PERCENT

PRESSURE = 1.500+02 ATMOS
LOC = [illegible]
[illegible] = [illegible]
[illegible] = [illegible]
THETA = .0 DEG

DIAMETER = [illegible] METERS
1.750+00 INCHES
CURRENT = 1.500+03 AMPS
FLOW RATE = [illegible] KG/SEC
[illegible] LB/SEC
TRANS COOLING = 0.000 KG/SEC-M**2
0.000 LB/FT2-SEC
WALL ENTHALPY = [illegible] JOULES/KG
[illegible] BTU/LB
[illegible] = [illegible]
[illegible] = [illegible]
[illegible] = [illegible]
[illegible] = [illegible]
[illegible] = [illegible]

SPACE AVERAGE ENTHALPY = [illegible] JOULES/KG OR [illegible] BTU/LB
MASS AVERAGE ENTHALPY = [illegible] JOULES/KG OR [illegible] BTU/LB
AVERAGE ENERGY DENSITY = [illegible] JOULES/M**3 OR .00000 BTU/INCH**3
TOTAL ENTHALPY M.AVG. = [illegible] JOULES/KG OR [illegible] BTU/LB

RADIUS METERS	RADIUS INCH	ENTHALPY JOULES/KG	ENTHALPY BTU/LB	VELOCITY M/S	VELOCITY FT/SEC	MASS FLUX KG/S M**2	MASS FLUX LB/FT2-SEC
.00000	.00000	[illegible]	[illegible]	[illegible]	[illegible]	[illegible]	[illegible]
[illegible]	[illegible]	[illegible]	[illegible]	[illegible]	[illegible]	[illegible]	[illegible]
[illegible]	[illegible]	[illegible]	[illegible]	[illegible]	[illegible]	[illegible]	[illegible]
[illegible]	[illegible]	[illegible]	[illegible]	[illegible]	[illegible]	[illegible]	[illegible]
[illegible]	[illegible]	[illegible]	[illegible]	[illegible]	[illegible]	[illegible]	[illegible]
[illegible]	[illegible]	[illegible]	[illegible]	[illegible]	[illegible]	[illegible]	[illegible]
[illegible]	[illegible]	[illegible]	[illegible]	[illegible]	[illegible]	[illegible]	[illegible]
[illegible]	[illegible]	[illegible]	[illegible]	[illegible]	[illegible]	[illegible]	[illegible]
[illegible]	[illegible]	[illegible]	[illegible]	[illegible]	[illegible]	[illegible]	[illegible]
[illegible]	[illegible]	[illegible]	[illegible]	[illegible]	[illegible]	[illegible]	[illegible]
[illegible]	[illegible]	[illegible]	[illegible]	[illegible]	[illegible]	[illegible]	[illegible]
[illegible]	[illegible]	[illegible]	[illegible]	[illegible]	[illegible]	[illegible]	[illegible]
[illegible]	[illegible]	[illegible]	[illegible]	[illegible]	[illegible]	[illegible]	[illegible]
[illegible]	[illegible]	[illegible]	[illegible]	[illegible]	[illegible]	[illegible]	[illegible]
[illegible]	[illegible]	[illegible]	[illegible]	[illegible]	[illegible]	[illegible]	[illegible]
[illegible]	[illegible]	[illegible]	[illegible]	[illegible]	[illegible]	[illegible]	[illegible]
[illegible]	[illegible]	[illegible]	[illegible]	[illegible]	[illegible]	[illegible]	[illegible]
[illegible]	[illegible]	[illegible]	[illegible]	[illegible]	[illegible]	[illegible]	[illegible]
[illegible]	[illegible]	[illegible]	[illegible]	[illegible]	[illegible]	[illegible]	[illegible]
[illegible]	[illegible]	[illegible]	[illegible]	[illegible]	[illegible]	[illegible]	[illegible]
[illegible]	[illegible]	[illegible]	[illegible]	[illegible]	[illegible]	[illegible]	[illegible]
[illegible]	[illegible]	[illegible]	[illegible]	[illegible]	[illegible]	[illegible]	[illegible]
[illegible]	[illegible]	[illegible]	[illegible]	[illegible]	[illegible]	[illegible]	[illegible]
[illegible]	[illegible]	[illegible]	[illegible]	[illegible]	[illegible]	[illegible]	[illegible]
[illegible]	[illegible]	[illegible]	[illegible]	[illegible]	[illegible]	[illegible]	[illegible]
[illegible]	[illegible]	[illegible]	[illegible]	[illegible]	[illegible]	[illegible]	[illegible]
[illegible]	[illegible]	[illegible]	[illegible]	.00000	.00000	.00000	.00000

OUTPUT - SAMPLE PROBLEM 1 (Continued)

Sample Problem 1 P = 150 atm I = 1500 amps Dia. = 1.75 inch

AXIAL STATION = [illegible]	DC THERMAL ARC WITH AXIAL GAS FLOW	DIAMETER =	[illegible] METERS
AXIAL DIST =	[illegible] METERS		1.750+00 INCHES
	[illegible] INCHES	CURRENT =	[illegible] AMPS
VOLTAGE GRAD =	[illegible] VOLTS/M	FLOW RATE =	[illegible] KG/SEC
	[illegible] VOLTS/INCH		[illegible] LB/SEC
WALL HEAT FLUX =	[illegible] WATTS/M2	TRANS COOLING =	[illegible] KG/SEC-M2
	[illegible] BTU/FT2-SEC		[illegible] LB/FT2-SEC
RADIATION LOSS =	[illegible] PERCENT	WALL ENTHALPY =	[illegible] JOULES/KG
			[illegible] BTU/LB
PRESSURE =	[illegible] ATMOS	[illegible] =	[illegible]
[illegible] =	[illegible]	[illegible] =	[illegible]
[illegible] =	[illegible]	[illegible] =	[illegible]
[illegible] =	[illegible]	[illegible] =	[illegible]
THETA =	.0 DEG	[illegible] =	[illegible]

SPACE AVERAGE ENTHALPY =	[illegible] JOULES/KG	OR	[illegible] BTU/LB
MASS AVERAGE ENTHALPY =	[illegible] JOULES/KG	OR	[illegible] BTU/LB
AVERAGE ENERGY DENSITY =	[illegible] JOULES/(M**3)	OR	[illegible] BTU/(INCH**3)
TOTAL ENTHALPY M.AVG. =	[illegible] JOULES/KG	OR	[illegible] BTU/LB

RADIUS METERS	RADIUS INCH	ENTHALPY JOULES/KG	ENTHALPY BTU/LB	VELOCITY M/S	VELOCITY FT/SEC	MASS FLUX KG/S M**2	MASS FLUX LB/FT2-SEC
.00000	.00000	[illegible]	[illegible]	[illegible]	[illegible]	[illegible]	[illegible]
[illegible]	[illegible]	[illegible]	[illegible]	[illegible]	[illegible]	[illegible]	[illegible]
[illegible]	[illegible]	[illegible]	[illegible]	[illegible]	[illegible]	[illegible]	[illegible]
[illegible]	[illegible]	[illegible]	[illegible]	[illegible]	[illegible]	[illegible]	[illegible]
[illegible]	[illegible]	[illegible]	[illegible]	[illegible]	[illegible]	[illegible]	[illegible]
[illegible]	[illegible]	[illegible]	[illegible]	[illegible]	[illegible]	[illegible]	[illegible]
[illegible]	[illegible]	[illegible]	[illegible]	[illegible]	[illegible]	[illegible]	[illegible]
[illegible]	[illegible]	[illegible]	[illegible]	[illegible]	[illegible]	[illegible]	[illegible]
[illegible]	[illegible]	[illegible]	[illegible]	[illegible]	[illegible]	[illegible]	[illegible]
[illegible]	[illegible]	[illegible]	[illegible]	[illegible]	[illegible]	[illegible]	[illegible]
[illegible]	[illegible]	[illegible]	[illegible]	[illegible]	[illegible]	[illegible]	[illegible]
[illegible]	[illegible]	[illegible]	[illegible]	[illegible]	[illegible]	[illegible]	[illegible]
[illegible]	[illegible]	[illegible]	[illegible]	[illegible]	[illegible]	[illegible]	[illegible]
[illegible]	[illegible]	[illegible]	[illegible]	[illegible]	[illegible]	[illegible]	[illegible]
[illegible]	[illegible]	[illegible]	[illegible]	[illegible]	[illegible]	[illegible]	[illegible]
[illegible]	[illegible]	[illegible]	[illegible]	[illegible]	[illegible]	[illegible]	[illegible]
[illegible]	[illegible]	[illegible]	[illegible]	[illegible]	[illegible]	[illegible]	[illegible]
[illegible]	[illegible]	[illegible]	[illegible]	[illegible]	[illegible]	[illegible]	[illegible]
[illegible]	[illegible]	[illegible]	[illegible]	[illegible]	[illegible]	[illegible]	[illegible]
[illegible]	[illegible]	[illegible]	[illegible]	[illegible]	[illegible]	[illegible]	[illegible]
[illegible]	[illegible]	[illegible]	[illegible]	[illegible]	[illegible]	[illegible]	[illegible]
[illegible]	[illegible]	[illegible]	[illegible]	[illegible]	[illegible]	[illegible]	[illegible]
[illegible]	[illegible]	[illegible]	[illegible]	[illegible]	[illegible]	[illegible]	[illegible]
[illegible]	[illegible]	[illegible]	[illegible]	[illegible]	[illegible]	[illegible]	[illegible]
[illegible]	[illegible]	[illegible]	[illegible]	[illegible]	[illegible]	[illegible]	[illegible]
[illegible]	[illegible]	[illegible]	[illegible]	.00000	.00000	.00000	.00000

OUTPUT - SAMPLE PROBLEM 1 (Continued)

TEMPERATURE	[illegible]	[illegible]	[illegible]	QRAD	[illegible]	[illegible]
[illegible]	1/CM	1/CM	WATTS/M**2	WATTS/M**3	WATTS/M**3	WATTS/M**2
[illegible]	[illegible]	[illegible]	[illegible]	[illegible]	[illegible]	[illegible]
[illegible]	[illegible]	[illegible]	[illegible]	[illegible]	[illegible]	[illegible]
[illegible]	[illegible]	[illegible]	[illegible]	[illegible]	[illegible]	[illegible]
[illegible]	[illegible]	[illegible]	[illegible]	[illegible]	[illegible]	[illegible]
[illegible]	[illegible]	[illegible]	[illegible]	[illegible]	[illegible]	[illegible]
[illegible]	[illegible]	[illegible]	[illegible]	[illegible]	[illegible]	[illegible]
[illegible]	[illegible]	[illegible]	[illegible]	[illegible]	[illegible]	[illegible]
[illegible]	[illegible]	[illegible]	[illegible]	[illegible]	[illegible]	[illegible]
[illegible]	[illegible]	[illegible]	[illegible]	[illegible]	[illegible]	[illegible]
[illegible]	[illegible]	[illegible]	[illegible]	[illegible]	[illegible]	[illegible]
[illegible]	[illegible]	[illegible]	[illegible]	[illegible]	[illegible]	[illegible]
[illegible]	[illegible]	[illegible]	[illegible]	[illegible]	[illegible]	[illegible]
[illegible]	[illegible]	[illegible]	[illegible]	[illegible]	[illegible]	[illegible]
[illegible]	[illegible]	[illegible]	[illegible]	[illegible]	[illegible]	[illegible]
[illegible]	[illegible]	[illegible]	[illegible]	[illegible]	[illegible]	[illegible]
[illegible]	[illegible]	[illegible]	[illegible]	[illegible]	[illegible]	[illegible]
[illegible]	[illegible]	[illegible]	[illegible]	[illegible]	[illegible]	[illegible]
[illegible]	[illegible]	[illegible]	[illegible]	[illegible]	[illegible]	[illegible]
[illegible]	[illegible]	[illegible]	[illegible]	[illegible]	[illegible]	[illegible]
[illegible]	[illegible]	[illegible]	[illegible]	[illegible]	[illegible]	[illegible]
[illegible]	[illegible]	[illegible]	[illegible]	[illegible]	[illegible]	[illegible]
[illegible]	[illegible]	[illegible]	[illegible]	[illegible]	[illegible]	[illegible]
[illegible]	[illegible]	[illegible]	[illegible]	[illegible]	[illegible]	[illegible]
[illegible]	[illegible]	[illegible]	[illegible]	[illegible]	[illegible]	[illegible]
[illegible]	[illegible]	[illegible]	[illegible]	[illegible]	[illegible]	[illegible]
[illegible]	[illegible]	[illegible]	[illegible]	[illegible]	[illegible]	[illegible]

OUTPUT - SAMPLE PROBLEM 1 (Continued)

Sample Problem 1 P = 150 atm I = 1500 amps Dia. = 1.75 inch

AXIAL STATION = [illegible]   DC THERMAL ARC WITH AXIAL GAS FLOW

AXIAL DIST	=	[illegible]	METERS
		[illegible]	INCHES
VOLTAGE GRAD	=	[illegible]	VOLTS/M
		[illegible]	VOLTS/INCH
WALL HEAT FLUX	=	[illegible]	WATTS/M**2
		[illegible]	BTU/FT2-SEC
RADIATION LOSS	=	[illegible]	PERCENT
PRESSURE	=	[illegible]	ATMOS
LOC	=	[illegible]	
PR	=	[illegible]	
[illegible]	=	[illegible]	
THETA	=	.0	DEG

DIAMETER	=	[illegible]	METERS
		1.750+00	INCHES
CURRENT	=	1.500+03	AMPS
FLOW RATE	=	[illegible]	KG/SEC
		[illegible]	LB/SEC
TRANS COOLING	=	0.000	KG/SEC-M**2
		0.000	LB/FT2-SEC
WALL ENTHALPY	=	[illegible]	JOULES/KG
		[illegible]	BTU/LB
[illegible]	=	[illegible]	
[illegible]	=	[illegible]	
[illegible]	=	[illegible]	
[illegible]	=	[illegible]	
[illegible]	=	[illegible]	

SPACE AVERAGE ENTHALPY	=	[illegible]	JOULES/KG	OR	[illegible] BTU/LB
MASS AVERAGE ENTHALPY	=	[illegible]	JOULES/KG	OR	[illegible] BTU/LB
AVERAGE ENERGY DENSITY	=	[illegible]	JOULES/M**3	OR	[illegible] BTU/INCH**3
TOTAL ENTHALPY M.AVG.	=	[illegible]	JOULES/KG	OR	[illegible] BTU/LB

RADIUS METERS	RADIUS INCH	ENTHALPY JOULES/KG	ENTHALPY BTU/LB	VELOCITY M/S	VELOCITY FT/SEC	MASS FLOW KG/S M**2	MASS FLOW LB/FT2-SEC
[illegible]	[illegible]	[illegible]	[illegible]	[illegible]	[illegible]	[illegible]	[illegible]
[illegible]	[illegible]	[illegible]	[illegible]	[illegible]	[illegible]	[illegible]	[illegible]
[illegible]	[illegible]	[illegible]	[illegible]	[illegible]	[illegible]	[illegible]	[illegible]
[illegible]	[illegible]	[illegible]	[illegible]	[illegible]	[illegible]	[illegible]	[illegible]
[illegible]	[illegible]	[illegible]	[illegible]	[illegible]	[illegible]	[illegible]	[illegible]
[illegible]	[illegible]	[illegible]	[illegible]	[illegible]	[illegible]	[illegible]	[illegible]
[illegible]	[illegible]	[illegible]	[illegible]	[illegible]	[illegible]	[illegible]	[illegible]
[illegible]	[illegible]	[illegible]	[illegible]	[illegible]	[illegible]	[illegible]	[illegible]
[illegible]	[illegible]	[illegible]	[illegible]	[illegible]	[illegible]	[illegible]	[illegible]
[illegible]	[illegible]	[illegible]	[illegible]	[illegible]	[illegible]	[illegible]	[illegible]
[illegible]	[illegible]	[illegible]	[illegible]	[illegible]	[illegible]	[illegible]	[illegible]
[illegible]	[illegible]	[illegible]	[illegible]	[illegible]	[illegible]	[illegible]	[illegible]
[illegible]	[illegible]	[illegible]	[illegible]	[illegible]	[illegible]	[illegible]	[illegible]
[illegible]	[illegible]	[illegible]	[illegible]	[illegible]	[illegible]	[illegible]	[illegible]
[illegible]	[illegible]	[illegible]	[illegible]	[illegible]	[illegible]	[illegible]	[illegible]
[illegible]	[illegible]	[illegible]	[illegible]	[illegible]	[illegible]	[illegible]	[illegible]
[illegible]	[illegible]	[illegible]	[illegible]	[illegible]	[illegible]	[illegible]	[illegible]
[illegible]	[illegible]	[illegible]	[illegible]	[illegible]	[illegible]	[illegible]	[illegible]
[illegible]	[illegible]	[illegible]	[illegible]	[illegible]	[illegible]	[illegible]	[illegible]
[illegible]	[illegible]	[illegible]	[illegible]	[illegible]	[illegible]	[illegible]	[illegible]
[illegible]	[illegible]	[illegible]	[illegible]	[illegible]	[illegible]	[illegible]	[illegible]
[illegible]	[illegible]	[illegible]	[illegible]	[illegible]	[illegible]	[illegible]	[illegible]
[illegible]	[illegible]	[illegible]	[illegible]	[illegible]	[illegible]	[illegible]	[illegible]
[illegible]	[illegible]	[illegible]	[illegible]	[illegible]	[illegible]	[illegible]	[illegible]
[illegible]	[illegible]	[illegible]	[illegible]	.00000	.00000	.00000	.00000

AXIAL DIST METER	AXIAL DIST INCH	AVERAGE ENTHALPY JOULE/KG	AVERAGE ENTHALPY BTU/LB	HTR - COND WATTS/M**2	HTR - COND BTU/FT2-SEC	HTR - RAD WATTS/M**2	HTR - RAD BTU/FT2-SEC	VOLTAGE VOLTS	EFF
[illegible]	[illegible]	[illegible]	[illegible]	[illegible]	[illegible]	[illegible]	[illegible]	770.117	.790

OUTPUT - SAMPLE PROBLEM 1 (Continued)

TEMPERATURE KELVIN	K1 1/CM	K2 1/CM	BEE WATTS/M**3	QRAD WATTS/M**3	DIVQR WATTS/M**3	QCOND WATTS/M**3
[illegible]	[illegible]	[illegible]	[illegible]	.0000	[illegible]	[illegible]
[illegible]	[illegible]	[illegible]	[illegible]	[illegible]	[illegible]	[illegible]
[illegible]	[illegible]	[illegible]	[illegible]	[illegible]	[illegible]	[illegible]
[illegible]	[illegible]	[illegible]	[illegible]	[illegible]	[illegible]	[illegible]
[illegible]	[illegible]	[illegible]	[illegible]	[illegible]	[illegible]	[illegible]
[illegible]	[illegible]	[illegible]	[illegible]	[illegible]	[illegible]	[illegible]
[illegible]	[illegible]	[illegible]	[illegible]	[illegible]	[illegible]	[illegible]
[illegible]	[illegible]	[illegible]	[illegible]	[illegible]	[illegible]	[illegible]
[illegible]	[illegible]	[illegible]	[illegible]	[illegible]	[illegible]	[illegible]
[illegible]	[illegible]	[illegible]	[illegible]	[illegible]	[illegible]	[illegible]
[illegible]	[illegible]	[illegible]	[illegible]	[illegible]	[illegible]	[illegible]
[illegible]	[illegible]	[illegible]	[illegible]	[illegible]	[illegible]	[illegible]
[illegible]	[illegible]	[illegible]	[illegible]	[illegible]	[illegible]	[illegible]
[illegible]	[illegible]	[illegible]	[illegible]	[illegible]	[illegible]	[illegible]
[illegible]	[illegible]	[illegible]	[illegible]	[illegible]	[illegible]	[illegible]
[illegible]	[illegible]	[illegible]	[illegible]	[illegible]	[illegible]	[illegible]
[illegible]	[illegible]	[illegible]	[illegible]	[illegible]	[illegible]	[illegible]
[illegible]	[illegible]	[illegible]	[illegible]	[illegible]	[illegible]	[illegible]
[illegible]	[illegible]	[illegible]	[illegible]	[illegible]	[illegible]	[illegible]
[illegible]	[illegible]	[illegible]	[illegible]	[illegible]	[illegible]	[illegible]
[illegible]	[illegible]	[illegible]	[illegible]	[illegible]	[illegible]	[illegible]
[illegible]	[illegible]	[illegible]	[illegible]	[illegible]	[illegible]	[illegible]
[illegible]	[illegible]	[illegible]	[illegible]	[illegible]	[illegible]	[illegible]
[illegible]	[illegible]	[illegible]	[illegible]	[illegible]	[illegible]	[illegible]
[illegible]	[illegible]	[illegible]	[illegible]	[illegible]	[illegible]	[illegible]
[illegible]	[illegible]	[illegible]	[illegible]	[illegible]	[illegible]	[illegible]

SIGMA 1/OHM-CM	DENSITY KG/M**3	VISCOSITY N SEC/M**2	OHMIC LOSS WATTS/M**3
[illegible]	[illegible]	[illegible]	[illegible]
[illegible]	[illegible]	[illegible]	[illegible]
[illegible]	[illegible]	[illegible]	[illegible]
[illegible]	[illegible]	[illegible]	[illegible]
[illegible]	[illegible]	[illegible]	[illegible]
[illegible]	[illegible]	[illegible]	[illegible]
[illegible]	[illegible]	[illegible]	[illegible]
[illegible]	[illegible]	[illegible]	[illegible]
[illegible]	[illegible]	[illegible]	[illegible]
[illegible]	[illegible]	[illegible]	[illegible]
[illegible]	[illegible]	[illegible]	[illegible]
[illegible]	[illegible]	[illegible]	[illegible]
[illegible]	[illegible]	[illegible]	[illegible]
[illegible]	[illegible]	[illegible]	[illegible]
[illegible]	[illegible]	[illegible]	[illegible]
[illegible]	[illegible]	[illegible]	[illegible]
[illegible]	[illegible]	[illegible]	[illegible]
[illegible]	[illegible]	[illegible]	[illegible]

OUTPUT - SAMPLE PROBLEM 1 (Concluded)

[illegible]	[illegible]	[illegible]	[illegible]
[illegible]	[illegible]	[illegible]	[illegible]
[illegible]	[illegible]	[illegible]	[illegible]
[illegible]	[illegible]	[illegible]	[illegible]
[illegible]	[illegible]	[illegible]	[illegible]
[illegible]	[illegible]	[illegible]	[illegible]
[illegible]	[illegible]	[illegible]	[illegible]
[illegible]	[illegible]	[illegible]	[illegible]

K.5 SAMPLE PROBLEM 2

The second sample problem presented is identical to the first sample problem except that the distributed mass flow (transpiration cooling) option is utilized. A transpiration cooling rate (TRCL) of 1.00 lbm/ft^2sec is assumed. Other operating conditions being equal, comparison with the previous run shows the effect of distributed mass addition on the enthalpy and velocity profiles. At an axial distance of 1.695 inches away from the entrance, the efficiency of the arc increases from 0.729 to 0.791 due to mass addition, and the center line temperature is reduced by about 365 degrees Kelvin.

INPUT - SAMPLE PROBLEM 2
(Deck A Only)

[illegible]

OUTPUT - SAMPLE PROBLEM 2

Sample Problem 2 P = 150 atm I = 1500 amps Dia. = 1.75 inch

AXIAL STATION = 1   DC THERMAL ARC WITH AXIAL GAS FLOW

AXIAL DIST	=	[illegible] METERS		DIAMETER	=	[illegible] METERS
		[illegible] INCHES				[illegible] INCHES
VOLTAGE GRAD	=	[illegible] VOLTS/M		CURRENT	=	[illegible] AMPS
		[illegible] VOLTS/INCH		FLOW RATE	=	[illegible] KG/SEC
WALL HEAT FLUX	=	[illegible] WATTS/M**2				[illegible] LB/SEC
		[illegible] BTU/FT2-SEC		TRANS COOLING	=	[illegible] KG/SEC(M**2)
RADIATION LOSS	=	[illegible] PERCENT				[illegible] LB/FT2-SEC
				WALL ENTHALPY	=	[illegible] JOULES/KG
						[illegible] BTU/LB
PRESSURE	=	[illegible] ATMOS		NMESH	=	[illegible]
INC	=	[illegible]		FZO	=	[illegible]
DH	=	[illegible]		FMS	=	[illegible]
KINC	=	[illegible]		EX	=	[illegible]
THETA	=	.0 DEG		EXX	=	[illegible]

SPACE AVERAGE ENTHALPY	=	[illegible]	JOULES/KG	OR	[illegible] BTU/LB
MASS AVERAGE ENTHALPY	=	[illegible]	JOULES/KG	OR	[illegible] BTU/LB
AVERAGE ENERGY DENSITY	=	[illegible]	JOULES/M**3	OR	[illegible] BTU/INCH**3
TOTAL ENTHALPY M.AVG.	=	[illegible]	JOULES/KG	OR	[illegible] BTU/LB

RADIUS METERS	RADIUS INCH	ENTHALPY JOULES/KG	ENTHALPY BTU/LB	VELOCITY M/S	VELOCITY FT/SEC	MASS FLUX KG/S M**2	MASS FLUX LB/FT2-SEC
.00000	.00000	[illegible]	[illegible]	[illegible]	[illegible]	[illegible]	[illegible]
[illegible]	[illegible]	[illegible]	[illegible]	[illegible]	[illegible]	[illegible]	[illegible]
[illegible]	[illegible]	[illegible]	[illegible]	[illegible]	[illegible]	[illegible]	[illegible]
[illegible]	[illegible]	[illegible]	[illegible]	[illegible]	[illegible]	[illegible]	[illegible]
[illegible]	[illegible]	[illegible]	[illegible]	[illegible]	[illegible]	[illegible]	[illegible]
[illegible]	[illegible]	[illegible]	[illegible]	[illegible]	[illegible]	[illegible]	[illegible]
[illegible]	[illegible]	[illegible]	[illegible]	[illegible]	[illegible]	[illegible]	[illegible]
[illegible]	[illegible]	[illegible]	[illegible]	[illegible]	[illegible]	[illegible]	[illegible]
[illegible]	[illegible]	[illegible]	[illegible]	[illegible]	[illegible]	[illegible]	[illegible]
[illegible]	[illegible]	[illegible]	[illegible]	[illegible]	[illegible]	[illegible]	[illegible]
[illegible]	[illegible]	[illegible]	[illegible]	[illegible]	[illegible]	[illegible]	[illegible]
[illegible]	[illegible]	[illegible]	[illegible]	[illegible]	[illegible]	[illegible]	[illegible]
[illegible]	[illegible]	[illegible]	[illegible]	[illegible]	[illegible]	[illegible]	[illegible]
[illegible]	[illegible]	[illegible]	[illegible]	[illegible]	[illegible]	[illegible]	[illegible]
[illegible]	[illegible]	[illegible]	[illegible]	[illegible]	[illegible]	[illegible]	[illegible]
[illegible]	[illegible]	[illegible]	[illegible]	[illegible]	[illegible]	[illegible]	[illegible]
[illegible]	[illegible]	[illegible]	[illegible]	[illegible]	[illegible]	[illegible]	[illegible]
[illegible]	[illegible]	[illegible]	[illegible]	[illegible]	[illegible]	[illegible]	[illegible]
[illegible]	[illegible]	[illegible]	[illegible]	[illegible]	[illegible]	[illegible]	[illegible]
[illegible]	[illegible]	[illegible]	[illegible]	[illegible]	[illegible]	[illegible]	[illegible]
[illegible]	[illegible]	[illegible]	[illegible]	[illegible]	[illegible]	[illegible]	[illegible]
[illegible]	[illegible]	[illegible]	[illegible]	[illegible]	[illegible]	[illegible]	[illegible]
[illegible]	[illegible]	[illegible]	[illegible]	[illegible]	[illegible]	[illegible]	[illegible]
[illegible]	[illegible]	[illegible]	[illegible]	[illegible]	[illegible]	[illegible]	[illegible]
[illegible]	[illegible]	[illegible]	[illegible]	[illegible]	[illegible]	[illegible]	[illegible]
[illegible]	[illegible]	[illegible]	[illegible]	[illegible]	[illegible]	[illegible]	[illegible]
[illegible]	[illegible]	[illegible]	[illegible]	.00000	.00000	.00000	[illegible]

OUTPUT - SAMPLE PROBLEM 2 (Continued)

Sample Problem 2 P = 150 atm I = 1500 amps Dia. = 1.75 inch

DC THERMAL ARC WITH AXIAL GAS FLOW

AXIAL STATION	=	2	DIAMETER	=	4.445e-02 METERS
					1.750e00 INCHES
AXIAL DIST	=	1.433e-01 METERS	CURRENT	=	1.500e03 AMPS
		5.642e00 INCHES			
VOLTAGE GRAD	=	1.594e04 VOLTS/M	FLOW RATE	=	1.362e00 KG/SEC
		4.050e02 VOLTS/INCH			3.003e00 LB/SEC
WALL HEAT FLUX	=	9.357e07 WATTS/M2	TRANS COOLING	=	4.887e00 KG/SEC-M2
		8.729e03 BTU/FT2-SEC			1.001e00 LB/FT2-SEC
RADIATION LOSS	=	00.0000 PERCENT	WALL ENTHALPY	=	6.290e05 JOULES/KG
					3.000e02 BTU/LB
PRESSURE	=	1.583e02 ATMOS	NMESH	=	25
LTC	=	1	FZO	=	1.000e00
Ae	=	-1.301e-05	EPS	=	0.400e-01
MINC	=	30	EE	=	1.100e00
THETA	=	.0 DEG	EEI	=	1.000e01

SPACE AVERAGE ENTHALPY = .3424e07 JOULES/KG OR .14734e04 BTU/LB
MASS AVERAGE ENTHALPY = .1851e07 JOULES/KG OR .7964e03 BTU/LB
AVERAGE ENERGY DENSITY = .4915e08 JOULES/M3 OR .1320e00 BTU/INCH3
TOTAL ENTHALPY M.AVG. = .1852e07 JOULES/KG OR .7969e03 BTU/LB

RADIUS METERS	INCH	ENTHALPY JOULES/KG	BTU/LB	VELOCITY M/S	FT/SEC	MASS FLUX KG/S M2	LB/FT2-SEC
.00000	.00000	.30003e08	.12908e05	.11273e03	.36979e03	.18827e01	.7701e02
.88132e-03	.10220e-01	.30035e08	.12918e05	.11271e03	.36978e03	.18977e01	.7061e02
.13891e-02	.54647e-01	.30006e08	.12929e05	.10817e03	.34179e03	.15913e01	.73591e02
.23151e-02	.91100e-01	.30160e08	.12932e05	.90001e02	.32971e03	.16932e01	.0.887e02
.32411e-02	.12760e00	.30597e08	.12919e05	.93920e02	.20631e03	.11363e01	.04752e02
.41672e-02	.16076e00	.29971e08	.12894e05	.80585e02	.27760e03	.29190e01	.59701e02
.50932e-02	.20452e00	.28112e08	.12213e05	.75975e02	.26077e03	.29013e01	.59618e02
.60193e-02	.23698e00	.22132e08	.95291e04	.71856e02	.23110e03	.34330e01	.62127e02
.69453e-02	.27344e00	.11340e08	.48809e04	.42173e02	.20199e03	.41042e01	.80749e02
.78710e-02	.30990e00	.96991e06	.41720e03	.50330e02	.16485e03	.25477e00	.52177e01
.87970e-02	.34635e00	.93938e06	.40400e03	.49220e02	.14151e03	.22930e00	.46961e01
.97230e-02	.38291e00	.93933e06	.40400e03	.42200e02	.13867e03	.19807e00	.40124e01
.10640e-01	.41927e00	.93330e06	.40200e03	.35000e02	.11367e03	.16110e00	.33452e01
.11570e-01	.45573e00	.93300e06	.40100e03	.20251e02	.92699e02	.11161e00	.24991e01
.12502e-01	.49219e00	.93200e06	.40090e03	.25701e02	.84522e02	.12300e00	.24917e01
.13428e-01	.52866e00	.93130e06	.40080e03	.23079e02	.77735e02	.10917e00	.22300e01
.14354e-01	.56510e00	.93340e06	.40150e03	.10792e02	.60534e02	.92197e-01	.18882e01
.15280e-01	.60158e00	.93300e06	.40000e03	.18802e02	.61690e02	.87542e-01	.17937e01
.16206e-01	.63802e00	.93800e06	.40800e03	.17742e02	.58211e02	.86114e-01	.10640e01
.17132e-01	.67448e00	.93000e06	.40000e03	.15470e02	.51400e02	.71317e-01	.14957e01
.18058e-01	.71094e00	.93000e06	.40000e03	.14117e02	.46317e02	.65790e-01	.13467e01
.18984e-01	.74710e00	.93000e06	.43330e03	.12566e02	.41229e02	.58595e-01	.11982e01
.19910e-01	.78145e00	.93040e06	.40390e03	.11773e02	.38627e02	.54900e-01	.11231e01
.20836e-01	.82011e00	.93000e06	.40000e03	.15985e02	.36434e02	.51172e-01	.10484e01
.21762e-01	.85677e00	.93000e06	.40000e03	.55373e01	.18168e02	.25798e-01	.52820e00
.22225e-01	.87500e00	.92900e06	.39991e03	.00000	.00000	.00000	.00000

OUTPUT - SAMPLE PROBLEM 2 (Continued)

TEMPERATURE	K1	K2	[illegible]	[illegible]	[illegible]	[illegible]
KELVIN	1/CM	1/CM	WATTS/M**2	WATTS/M**2	WATTS/M**2	WATTS/M**2
[illegible]	[illegible]	[illegible]	[illegible]	[illegible]	[illegible]	[illegible]
[illegible]	[illegible]	[illegible]	[illegible]	[illegible]	[illegible]	[illegible]
[illegible]	[illegible]	[illegible]	[illegible]	[illegible]	[illegible]	[illegible]
[illegible]	[illegible]	[illegible]	[illegible]	[illegible]	[illegible]	[illegible]
[illegible]	[illegible]	[illegible]	[illegible]	[illegible]	[illegible]	[illegible]
[illegible]	[illegible]	[illegible]	[illegible]	[illegible]	[illegible]	[illegible]
[illegible]	[illegible]	[illegible]	[illegible]	[illegible]	[illegible]	[illegible]
[illegible]	[illegible]	[illegible]	[illegible]	[illegible]	[illegible]	[illegible]
[illegible]	[illegible]	[illegible]	[illegible]	[illegible]	[illegible]	[illegible]
[illegible]	[illegible]	[illegible]	[illegible]	[illegible]	[illegible]	[illegible]
[illegible]	[illegible]	[illegible]	[illegible]	[illegible]	[illegible]	[illegible]
[illegible]	[illegible]	[illegible]	[illegible]	[illegible]	[illegible]	[illegible]
[illegible]	[illegible]	[illegible]	[illegible]	[illegible]	[illegible]	[illegible]
[illegible]	[illegible]	[illegible]	[illegible]	[illegible]	[illegible]	[illegible]
[illegible]	[illegible]	[illegible]	[illegible]	[illegible]	[illegible]	[illegible]
[illegible]	[illegible]	[illegible]	[illegible]	[illegible]	[illegible]	[illegible]
[illegible]	[illegible]	[illegible]	[illegible]	[illegible]	[illegible]	[illegible]
[illegible]	[illegible]	[illegible]	[illegible]	[illegible]	[illegible]	[illegible]
[illegible]	[illegible]	[illegible]	[illegible]	[illegible]	[illegible]	[illegible]
[illegible]	[illegible]	[illegible]	[illegible]	[illegible]	[illegible]	[illegible]
[illegible]	[illegible]	[illegible]	[illegible]	[illegible]	[illegible]	[illegible]
[illegible]	[illegible]	[illegible]	[illegible]	[illegible]	[illegible]	[illegible]
[illegible]	[illegible]	[illegible]	[illegible]	[illegible]	[illegible]	[illegible]
[illegible]	[illegible]	[illegible]	[illegible]	[illegible]	[illegible]	[illegible]
[illegible]	[illegible]	[illegible]	[illegible]	[illegible]	[illegible]	[illegible]
[illegible]	[illegible]	[illegible]	[illegible]	[illegible]	[illegible]	[illegible]

OUTPUT - SAMPLE PROBLEM 2 (Continued)

Sample Problem 2 P = 150 atm I = 1500 amps Dia. = 1.75 inch

AXIAL STATION = 121 DC THERMAL ARC WITH AXIAL GAS FLOW

AXIAL DIST = [illegible] METERS [illegible] INCHES		DIAMETER = [illegible] METERS [illegible] INCHES	
VOLTAGE GRAD = [illegible] VOLTS/M [illegible] VOLTS/INCH		CURRENT = [illegible] AMPS	
WALL HEAT FLUX = [illegible] WATTS/M**2 [illegible] BTU/FT2-SEC		FLOW RATE = [illegible] KG/SEC [illegible] LB/SEC	
RADIATION LOSS = [illegible] PERCENT		TRANS COOLING = [illegible] KG/SEC-M**2 [illegible] LB/FT2-SEC	
		RAIL ENTHALPY = [illegible] JOULES/KG [illegible] BTU/LB	
PRESSURE = [illegible] ATMS		[illegible] = [illegible]	
[illegible] = [illegible]		[illegible] = [illegible]	
[illegible] = [illegible]		[illegible] = [illegible]	
[illegible] = [illegible]		[illegible] = [illegible]	
THETA = [illegible] DEG		[illegible] = [illegible]	

SPACE AVERAGE ENTHALPY =	[illegible] JOULES/KG	OR	[illegible] BTU/LB
MASS AVERAGE ENTHALPY =	[illegible] JOULES/KG	OR	[illegible] BTU/LB
AVERAGE ENERGY DENSITY =	[illegible] JOULES/M**3	OR	[illegible] BTU/INCH**3
TOTAL ENTHALPY [illegible] =	[illegible] JOULES/KG	OR	[illegible] BTU/LB

RADIUS METERS	RADIUS INCH	ENTHALPY JOULES/KG	ENTHALPY BTU/LB	VELOCITY M/S	VELOCITY FT/SEC	MASS FLUX KG/M**2	MASS FLUX LB/FT2-SEC
[illegible]	[illegible]	[illegible]	[illegible]	[illegible]	[illegible]	[illegible]	[illegible]
[illegible]	[illegible]	[illegible]	[illegible]	[illegible]	[illegible]	[illegible]	[illegible]
[illegible]	[illegible]	[illegible]	[illegible]	[illegible]	[illegible]	[illegible]	[illegible]
[illegible]	[illegible]	[illegible]	[illegible]	[illegible]	[illegible]	[illegible]	[illegible]
[illegible]	[illegible]	[illegible]	[illegible]	[illegible]	[illegible]	[illegible]	[illegible]
[illegible]	[illegible]	[illegible]	[illegible]	[illegible]	[illegible]	[illegible]	[illegible]
[illegible]	[illegible]	[illegible]	[illegible]	[illegible]	[illegible]	[illegible]	[illegible]
[illegible]	[illegible]	[illegible]	[illegible]	[illegible]	[illegible]	[illegible]	[illegible]
[illegible]	[illegible]	[illegible]	[illegible]	[illegible]	[illegible]	[illegible]	[illegible]
[illegible]	[illegible]	[illegible]	[illegible]	[illegible]	[illegible]	[illegible]	[illegible]
[illegible]	[illegible]	[illegible]	[illegible]	[illegible]	[illegible]	[illegible]	[illegible]
[illegible]	[illegible]	[illegible]	[illegible]	[illegible]	[illegible]	[illegible]	[illegible]
[illegible]	[illegible]	[illegible]	[illegible]	[illegible]	[illegible]	[illegible]	[illegible]
[illegible]	[illegible]	[illegible]	[illegible]	[illegible]	[illegible]	[illegible]	[illegible]
[illegible]	[illegible]	[illegible]	[illegible]	[illegible]	[illegible]	[illegible]	[illegible]
[illegible]	[illegible]	[illegible]	[illegible]	[illegible]	[illegible]	[illegible]	[illegible]
[illegible]	[illegible]	[illegible]	[illegible]	[illegible]	[illegible]	[illegible]	[illegible]
[illegible]	[illegible]	[illegible]	[illegible]	[illegible]	[illegible]	[illegible]	[illegible]
[illegible]	[illegible]	[illegible]	[illegible]	[illegible]	[illegible]	[illegible]	[illegible]
[illegible]	[illegible]	[illegible]	[illegible]	[illegible]	[illegible]	[illegible]	[illegible]
[illegible]	[illegible]	[illegible]	[illegible]	[illegible]	[illegible]	[illegible]	[illegible]
[illegible]	[illegible]	[illegible]	[illegible]	[illegible]	[illegible]	[illegible]	[illegible]
[illegible]	[illegible]	[illegible]	[illegible]	[illegible]	[illegible]	[illegible]	[illegible]
[illegible]	[illegible]	[illegible]	[illegible]	[illegible]	[illegible]	[illegible]	[illegible]
[illegible]	[illegible]	[illegible]	[illegible]	[illegible]	[illegible]	[illegible]	[illegible]
[illegible]	[illegible]	[illegible]	[illegible]	[illegible]	[illegible]	[illegible]	[illegible]

AXIAL DIST METER	AXIAL DIST INCH	AVERAGE ENTHALPY JOULE/KG	AVERAGE ENTHALPY BTU/LB	HTR - COND WATTS/M**2	HTR - COND BTU/FT2-SEC	HTR - RAD WATTS/M**2	HTR - RAD BTU/FT2-SEC	VOLTAGE VOLTS	EFF
[illegible]	[illegible]	[illegible]	[illegible]	[illegible]	[illegible]	[illegible]	[illegible]	[illegible]	[illegible]

OUTPUT - SAMPLE PROBLEM 2 (Continued)

[illegible]	[illegible]	[illegible]	[illegible]	[illegible]	[illegible]	[illegible]
[illegible]	[illegible]	[illegible]	[illegible]	[illegible]	[illegible]	[illegible]
[illegible]	[illegible]	[illegible]	[illegible]	[illegible]	[illegible]	[illegible]
[illegible]	[illegible]	[illegible]	[illegible]	[illegible]	[illegible]	[illegible]
[illegible]	[illegible]	[illegible]	[illegible]	[illegible]	[illegible]	[illegible]
[illegible]	[illegible]	[illegible]	[illegible]	[illegible]	[illegible]	[illegible]
[illegible]	[illegible]	[illegible]	[illegible]	[illegible]	[illegible]	[illegible]
[illegible]	[illegible]	[illegible]	[illegible]	[illegible]	[illegible]	[illegible]
[illegible]	[illegible]	[illegible]	[illegible]	[illegible]	[illegible]	[illegible]
[illegible]	[illegible]	[illegible]	[illegible]	[illegible]	[illegible]	[illegible]
[illegible]	[illegible]	[illegible]	[illegible]	[illegible]	[illegible]	[illegible]
[illegible]	[illegible]	[illegible]	[illegible]	[illegible]	[illegible]	[illegible]
[illegible]	[illegible]	[illegible]	[illegible]	[illegible]	[illegible]	[illegible]
[illegible]	[illegible]	[illegible]	[illegible]	[illegible]	[illegible]	[illegible]
[illegible]	[illegible]	[illegible]	[illegible]	[illegible]	[illegible]	[illegible]
[illegible]	[illegible]	[illegible]	[illegible]	[illegible]	[illegible]	[illegible]
[illegible]	[illegible]	[illegible]	[illegible]	[illegible]	[illegible]	[illegible]
[illegible]	[illegible]	[illegible]	[illegible]	[illegible]	[illegible]	[illegible]
[illegible]	[illegible]	[illegible]	[illegible]	[illegible]	[illegible]	[illegible]
[illegible]	[illegible]	[illegible]	[illegible]	[illegible]	[illegible]	[illegible]
[illegible]	[illegible]	[illegible]	[illegible]	[illegible]	[illegible]	[illegible]
[illegible]	[illegible]	[illegible]	[illegible]	[illegible]	[illegible]	[illegible]
[illegible]	[illegible]	[illegible]	[illegible]	[illegible]	[illegible]	[illegible]
[illegible]	[illegible]	[illegible]	[illegible]	[illegible]	[illegible]	[illegible]
[illegible]	[illegible]	[illegible]	[illegible]	[illegible]	[illegible]	[illegible]
[illegible]	[illegible]	[illegible]	[illegible]	[illegible]	[illegible]	[illegible]

[illegible]	[illegible]	[illegible]	[illegible]
[illegible]	[illegible]	[illegible]	[illegible]
[illegible]	[illegible]	[illegible]	[illegible]
[illegible]	[illegible]	[illegible]	[illegible]
[illegible]	[illegible]	[illegible]	[illegible]
[illegible]	[illegible]	[illegible]	[illegible]
[illegible]	[illegible]	[illegible]	[illegible]
[illegible]	[illegible]	[illegible]	[illegible]
[illegible]	[illegible]	[illegible]	[illegible]
[illegible]	[illegible]	[illegible]	[illegible]
[illegible]	[illegible]	[illegible]	[illegible]
[illegible]	[illegible]	[illegible]	[illegible]
[illegible]	[illegible]	[illegible]	[illegible]
[illegible]	[illegible]	[illegible]	[illegible]
[illegible]	[illegible]	[illegible]	[illegible]
[illegible]	[illegible]	[illegible]	[illegible]
[illegible]	[illegible]	[illegible]	[illegible]
[illegible]	[illegible]	[illegible]	[illegible]

OUTPUT - SAMPLE PROBLEM [illegible] (Concluded)

[illegible]	[illegible]	[illegible]	[illegible]
[illegible]	[illegible]	[illegible]	[illegible]
[illegible]	[illegible]	[illegible]	[illegible]
[illegible]	[illegible]	[illegible]	[illegible]
[illegible]	[illegible]	[illegible]	[illegible]
[illegible]	[illegible]	[illegible]	[illegible]
[illegible]	[illegible]	[illegible]	[illegible]
[illegible]	[illegible]	[illegible]	[illegible]

a	constant used in the exponential kernel approximation, $a = 4$
A^*	throat area
b	constant used in the exponential kernel approximation, $b = 1.25$
c_p	specific heat at constant pressure
d	constrictor diameter
D	constrictor diameter
D_2	cylindrical exponential integral function of order 2
E	emissive power
g_c	universal constant = 32.174 ft-lbm/lbf-sec^2
G	angular directional radiative flux
h	mixture enthalpy per unit mass (Section 4)
h	heat transfer coefficient (Section 8)
$\bar{h}$	mean enthalpy per unit mass
$H_{avg}, \bar{H}$	mass-average enthalpy per unit mass
H_∞	asymptotic mass-average enthalpy per unit mass
H_{cl}	centerline enthalpy per unit mass
H_{corr}	correlation enthalpy per unit mass
H_{sf}	sonic-flow enthalpy per unit mass
i	radial index
I	current

LIST OF SYMBOLS (Continued)

I_ν	spectral intensity of radiation
j	radial index
K	mixture total thermal conductivity
ℓ	mixing length
L	constrictor length
$\dot{m}$	fluid mass flow rate
N	total number of radial nodes
P	constrictor pressure
P_t	turbulent Prandtl number
$\dot{q}$	wall heat flux
q_R	wall radiant heat flux
q	spectral radiative flux
r	local radius
R	constrictor radius
t	thickness of constrictor disk
T	temperature
u	mean fluid velocity in axial direction
V	voltage
V_{corr}	correlation voltage
w	wall condition
x_i	mole fraction of species i in mixture

LIST OF SYMBOLS (Concluded)

y	path length along projected line of sight (Section 3)
y	distance from constrictor wall (Section 5)
z	distance along constrictor axis

<u>Greek</u>

[illegible]	angle between line of sight and plane perpendicular to the axis of the cylinder measured in plane parallel to cylinder axis
[illegible]	angle in cross-sectional plane from radial direction to projected line of sight
ε	eddy viscosity
C	axial voltage gradient
η	efficiency
θ	angle
κ	spectral absorption coefficient (Section 3)
μ	mixture viscosity
	kinematic viscosity
ρ	mixture density
σ	mixture electrical conductivity
τ	optical depth (Section 3)
τ	shear stress (Section 5)
$\Delta\tau$	incremental optical depth
Ω	solid angle

LIST OF SYMBOLS FOR APPENDICES

APPENDIX A

a	constant used in the exponential kernel approximation, $a = \pi/4$
b	constant used in the exponential kernel approximation, $b = 1.25$
B_λ	Planck black body spectral intensity
D_n	cylindrical exponential integral function of order n
E	emissive power
G	angular directional radiative flux
i	radial index
I_λ	spectral intensity of radiation
j	radial index
k	index on the spectral band
n	total number of bands
N	total number of radial nodes
p	pressure
q	spectral radiative flux
r, r', r''	local radius
R	constrictor radius
s	path length along the line of sight
w	local band weighting function
y	path length along the projected line of sight

APPENDIX A NOMENCLATURE

Greek

δ	angle between line of sight and a plane perpendicular to the axis of the cylinder measured in a plane parallel to the cylinder axis
γ	angle in the cross-sectional plane from the radial direction to the projected line of sight
κ_ν	spectral absorption coefficient
ν	wave number
$\Delta\nu$	band width
π	3.1415927...
σ	Stefan-Boltzman constant
τ	optical depth
$\Delta\tau$	incremental optical depth
Ω	solid angle

APPENDIX B

A_{ij}^q	constant in Equation (B-50)
B_{ij}^q	constant in Equation (B-50)
c_{p_i}	molar specific heat of species i
d_{ij}	mean diameter for hard-sphere molecules i and j
e	electronic charge
F	mixture Helmholtz free energy, Equation (B-15)

[illegible]

$\bar{G}_j$	partial molal Gibbs free energy (chemical potential) of species j in mixture
G_j^0	Gibbs free energy of pure species j at standard state (1 atm)
g	relative velocity between colliding molecules
H	mixture enthalpy per unit volume
ΔH_i	heat of reaction per mole of reaction i, Equation (B-42)
h	mixture enthalpy per unit mass; Planck's constant
h_j	molar enthalpy of species j
I	total number of base species i
I_j^s	ionization energy of specie j in s^{th} ionization stage
ΔI_j	reduction in ionization energy of specie j, Equation (B-7)
i	base specie index in Section B.1; general specie index in Section B.2
J	total number of base and nonbase species j
j	nonbase specie index in Section B.2
K	mixture total thermal conductivity, Equation [illegible]
K_{tr}	mixture translational thermal conductivity, Equation [illegible]
K_{int}	mixture internal thermal conductivity, Equation [illegible]
K_r	mixture reactive thermal conductivity, Equation [illegible]
K_{p_j}	equilibrium constant for reaction forming specie j, Equation [illegible]

APPENDIX B (Continued)

k	Boltzman constant
L	total number of independent reactions in mixture
L_j	correction factor for equilibrium constant to account for lowering of ionization potential of specie j, Equation (B-9)
ℓ	independent reaction index
$\mathcal{M}$	mixture molecular weight
m_j	mass of molecule j
N	represents molecule in Section B.1; total number of species in Section B.2
n_j	number density of species j in mixture
p	mixture total pressure, Equations (B-6) and (B-20)
p_θ	mixture thermal pressure, Equations (B-20) and (B-27)
p_j	partial pressure of species j in mixture, Equation (B-26)
Δp_e	pressure correction due to Coulomb interactions, Equation (B-22)
Q_j^z	partition function for specie j in z^{th} ionization stage
r_u	universal gas constant
S	mixture entropy per unit volume
s	mixture entropy per unit mass
T	temperature
U	mixture internal energy per unit volume

APPENDIX B (Concluded)

V	mixture total volume
v	mixture specific volume per unit mass
x_j	mole fraction of species j in mixture
z_j	charge number for species j: 0 for neutral atom, 1 for singly-ionized atom, 2 for doubly-ionized atom, etc.

<u>Greek</u>

α_{ij}	constant depending on ratio of masses of molecules i and j, Equation (B-39)
$\Delta_{ij}^{(q)}$	collision integral parameter, Equation (B-38)
μ	mixture viscosity, Equation (B-32); reduced mass, Equation (B-48)
ρ	mixture mass density
σ	mixture electrical conductivity, Equation (B-37)
$\pi\Omega_{ij}^{(p,q)}$	collision integral for collisions between molecules i and j, Equation (B-43)

APPENDIX C

c_p	specific heat at constant pressure
$\bar{h}$	mean enthalpy
k	thermal conductivity of the fluid
ℓ	mixing length
ℓ_N	Nikuradse mixing length

APPENDIX C (Concluded)

ℓ_W	Watson and [illegible] mixing length = 1/2 ℓ_M
P_t	turbulent Prandtl number
q	wall heat flux
R	constrictor radius
$\bar{u}$	mean velocity in axial direction
y	distance from constrictor wall

Greek

ϵ	eddy viscosity
ν	kinematic viscosity
ρ	fluid density
τ	shear stress